Loan Copy #2

NEUTRON ECONOMY IN FUSION REACTOR BLANKET ASSEMBLIES

ALBERT J. IMPINK, JR.

TECHNICAL REPORT 434

JUNE 22, 1965

MASSACHUSETTS INSTITUTE OF TECHNOLOGY
RESEARCH LABORATORY OF ELECTRONICS
CAMBRIDGE, MASSACHUSETTS

The Research Laboratory of Electronics is an interdepartmental laboratory in which faculty members and graduate students from numerous academic departments conduct research.

The research reported in this document was made possible in part by support extended the Massachusetts Institute of Technology, Research Laboratory of Electronics, by the JOINT SERVICES ELECTRONICS PROGRAMS (U.S. Army, U.S. Navy, and U.S. Air Force) under Contract No. DA36-039-AMC-03200(E); additional support was received from the National Science Foundation (Grant GK-57).

MASSACHUSETTS INSTITUTE OF TECHNOLOGY

RESEARCH LABORATORY OF ELECTRONICS

Technical Report 434 June 22, 1965

NEUTRON ECONOMY IN FUSION REACTOR BLANKET ASSEMBLIES

Albert J. Impink, Jr.

This report is based on a thesis submitted to the Department of Nuclear Engineering, M.I.T., January 7, 1963, in partial fulfillment of the requirements for the degree of Doctor of Philosophy.

(Manuscript received March 31, 1965)

Abstract

The conceptual design of a blanket assembly for a hypothesized fusion power reactor is considered from the point of view of neutron economy. Containment of a steady-state thermonuclear plasma composed of equal parts of deuterium and tritium in a cylindrical configuration is assumed.

Requirements and limitations imposed on the blanket by the plasma and by other components of the reactor system are analyzed, and the conceptual arrangement of a suitable blanket utilizing a refractory metal first wall and fused-salt cooling is presented.

Neutron transport and scattering models are compared in terms of applicability to the present problem. Multigroup, multiregion formulations for neutron transport and scattering in various energy regimes are developed; solutions are obtained by a combination of analytical and numerical methods. A multigroup treatment of resonance absorption and scattering is outlined, and a method of calculating approximate absorption cross sections in the resonance energy region is derived.

Comparison of theoretical predictions with published experimental measurements in several test cases has been made to determine the adequacy of the models and computational procedures.

Calculated tritium breeding ratios and neutron-induced reaction rates in a variety of permutations on the basic blanket configuration are summarized and compared. It is shown that the proposed blanket design is adequate from the point of view of neutron economy. A reasonable degree of flexibility for satisfying other requirements imposed on the blanket is indicated when suitable combinations of nuclides are exploited.

Consideration is given also to several shielding configurations and to the potential merits of various materials, including certain fissile nuclides, not treated in this study.

PREFACE

This is the first in a series of five reports on Fusion Blanket research. Taken together, this series completes the initial phase of this work.

Appendix B of this report explains two sets of digital computer codes that were developed in this study and written in the IBM Fortran II language. The actual code * listings are omitted but are available on application to the Research Laboratory of Electronics, Massachusetts Institute of Technology, Cambridge, Massachusetts, 02139.

A list of the authors and titles of the four succeeding reports in this series follows.

Technical Report 435	William G. Homeyer, "Thermal and Chemical Properties of the Thermonuclear Blanket Problem"
Technical Report 436	Laszlo N. Lontai, "Study of a Thermonuclear Reactor Blanket with Fissile Nuclides"
Technical Report 437	Patrick S. Spangler, "Fusion Reactor Blanket Experiment"
Technical Report 438	Lester M. Petrie, Jr., "Gamma-Ray Spectra in Fusion Blanket Mock-ups"

*

A xerox copy of the code listings can be made from the Impink thesis which is at Hayden Library.

(The listings are not in our copy of this thesis.)

TABLE OF CONTENTS

CONTENTS

I. INTRODUCTION

A study has been made of several aspects of the basic problem of making a first estimate of the feasibility and practicality of blanket assemblies for proposed thermonuclear power reactors. The investigation was motivated by the following premises:

1. Containment of a thermonuclear plasma of interest from the point of view of useful power production by nuclear fusion is possible and will soon be accomplished.

2. The energy liberated in the fusion reaction will appear as kinetic energy of lightweight nuclear particles. The larger part of this kinetic energy will be recovered as useful thermal energy through the intermediary process of slowing down neutral particles in a solid or liquid medium, for instance, in a blanket surrounding the fusion reaction region.

3. The physical limitations unavoidably associated with any practical blanket assembly may well impress severe restrictions on the properties of the thermonuclear plasma and on the amount of useful power that can be recovered. It is conceivable that inability to develop a practical blanket assembly satisfying all of the requirements imposed upon it might present an insuperable barrier to the attainment of commercial power from thermonuclear fusion.

4. Present understanding of plasma physics is sufficiently far advanced that the general outlines of a potentially useful power-generating fusion reactor may be sketched. Critical characteristics of such a machine can be estimated (although with some uncertainty).

With these points in mind, the goals of the study, of which the work reported here represents a part, were the following.

1. To analyse the nature and implications of the restrictions imposed on blanket assemblies by other components of the fusion reactor system, in particular by the plasma.

2. To develop the conceptual design of a blanket assembly capable of meeting the several imposed requirements.

3. To weigh the feasibility of the blanket design and, by implication, to estimate the ultimate feasibility and practicality of fusion power reactors from the point of view of the blanket problem.

Related goals are those of compiling physical and nuclear data of importance in blanket design, developing appropriate computational methods, and carrying through the necessary calculations to permit drawing of reasonably reliable conclusions.

In the work reported here we do not presume to treat the entire problem of fusion reactor blanket assemblies. Rather, the intent is to study those aspects of the problem dealing with the multiplication, transport, and ultimate utilization of fusion-born neutrons. The immediate goals of this portion of the over-all study are to provide information relating to neutron economy and to the distribution and magnitude of the several neutron-induced reaction rates of interest. The results, considered in conjunction with

those from related studies, will permit drawing more general conclusions concerning the feasibility and practicality of fusion reactor blankets. To the extent that neutronic considerations are the determining factor, more general conclusions will be drawn in this report.

The conceptual design is the result of the combined efforts of David J. Rose, Irving Kaplan, William G. Homeyer, Patrick S. Spangler and the author. The area of primary interest to the author has been that of neutron economy. Matters relating to materials and to nuclear heating will form the substance of a concurrent work by Homeyer.[1] Spangler[2] is developing experimental techniques that will permit testing of the neutron scattering and transport calculations in systems approximating the hypothesized designs.

In general, the current studies have excluded nuclear fission as a constituent neutron-induced reaction in the blanket, a consideration also neglected in all eariler studies with very few exceptions.[3,4] This somewhat artificial limitation will be preserved here with the exception of occasional parenthetical observations. Recently, Lontai[5] has undertaken an investigation closely paralleling those of Homeyer and the author to determine the advantages to be derived by introducing fissile nuclides into power-producing fusion reactor blankets.

The rest of this work will be organized in the following manner: Consideration will be given first to developing the over-all problem, outlining the general characteristics of a fusion power reactor, delineating the requirements and limitations imposed on the blanket, and summarizing earlier studies on the problem. Succeeding sections will be devoted to discussions concerning the theoretical methods employed to treat neutron scattering and neutron transport, the calculation of certain effective neutron cross sections, the development of necessary numerical procedures, and a comparison of theoretical predictions with experimental results. The results of neutronic calculations made on a variety of proposed blanket assemblies will be summarized and compared, appropriate conclusions will be drawn, and recommendations for the future course of these studies will be made. Finally, in appendices details of the digital computer codes that were used and of the neutron cross sections that were employed will be presented.

Every effort has been made to preserve a consistent scheme of notation throughout. In those cases in which usage dictates inconsistencies in the notation employed in treating unrelated problems, the generally accepted notation will be given preference.

II. DEVELOPMENT OF A CONCEPTUAL BLANKET DESIGN

2.1 DELINEATION OF THE PROBLEM

Sufficient work has been done in the past, notably by Rose[6,7] and Post,[8] that the broad outline of a potentially practical fusion reactor system for generating commercial electric power can be sketched. The following characteristics of such a system may be cited.

1. The basic thermonuclear reaction will be the fusion of a deuteron and a triton to yield a neutron, an alpha particle and approximately 17.6 Mev in particle kinetic energy.

$$ {}_1H^2 + {}_1H^3 \rightarrow {}_0n^1 + {}_2He^4 \cdot (+17.58\ \text{Mev}). \qquad (1) $$

2. The total power output of the device must be large and energy densities high if competitive costs are to be obtained. Thermal power outputs of the order of a million kilowatts per reactor are indicated.

3. The system will be run on a steady-state or quasi steady-state basis and will utilize, for plasma confinement, magnetic fields generated by superconducting coils located outside of the blanket.

4. The general configuration of the reacting plasma will be cylindrical; for the sake of this discussion, both mirror devices and stellarators are construed to be "cylindrical."

Consider now the implications of these characteristics of a hypothesized fusion reactor in terms of the requirements that they impose on the blanket. The use of tritium as a fuel for the fusion reaction is significant on two counts. First, tritium is not found in nature; hence, the blanket must breed tritium. Furthermore, since the tritium burnup per injection into the plasma will certainly be less than unity, tritium recycling and repeated re-injection, with inevitable losses, appears unavoidable. It has been estimated by Rose et al.[7] that tritium-breeding ratios as high as 1.15 tritons generated per triton burned may be necessary to compensate for losses resulting from recycling, chemical recovery, and radioactive decay.

Second, neutrons, which are the only potential source of tritium through nuclear reactions, are available initially only at 14 Mev. Although there is a large number of neutron-induced reactions that yield tritons as reaction products, only the reactions

$$ Li^6 + n \rightarrow H^3 + He^4 \qquad (2a) $$

and

$$ Li^7 + n \rightarrow H^3 + n + He^4 \qquad (2b) $$

appear to offer any real hope for tritium regeneration. Figure 1 shows the tritium production cross sections in natural lithium which are due to the lithium 6 and 7 isotopes as a function of incident neutron energy in the high-energy region. The lithium 6 cross

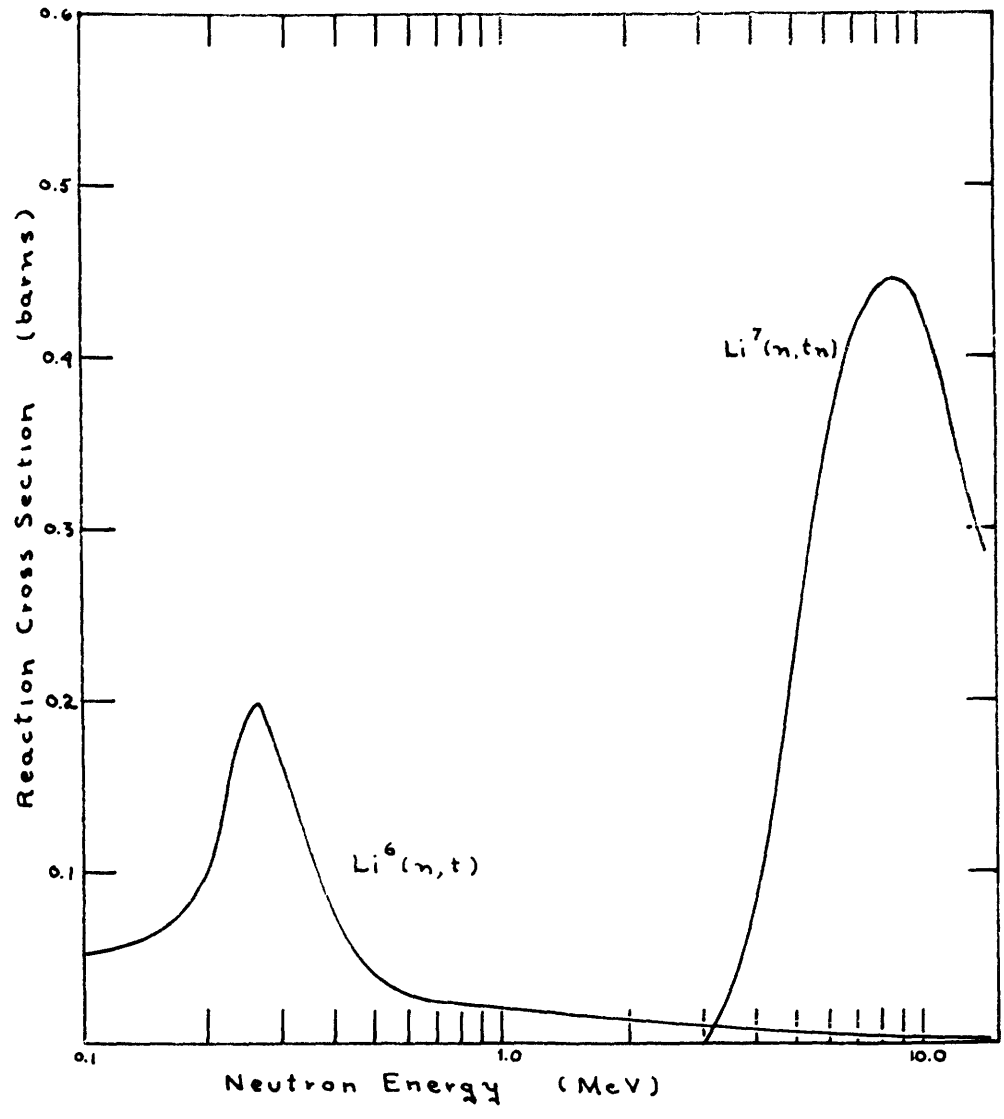

Fig. 1. Tritium yielding reaction cross sections in natural lithium.

section gradually assumes a v^{-1} dependence at lower energies and reaches a value of 71 barns at 0.025 ev.

The contribution of lithium 7 is limited by competitive down-scattering reactions in any practical system so that the basic reaction for tritium production, that involving lithium 6, is prominent only near thermal energies. It is evident that large-scale tritium breeding with 14 Mev neutrons requires that the neutrons be slowed down at least to epithermal energies, with some consequent unavoidable loss of neutrons, because of parasitic absorption and leakage. Since the D-T fusion reaction yields but one neutron per triton consumed, provision must be made in the blanket for neutron multiplication, to compensate for neutron losses and to meet the tritium-breeding requirement.

Three classes of neutron multiplying reactions are available for exploitation. These include (n, 2n) reactions in the weakly bound light nuclides, (n, 2n) reactions in the heavier nuclides, and fission reactions in the very heavy nuclides. Figure 2 is a comparison of the multiplication cross sections for (n, 2n) reactions in beryllium, molybdenum, and uranium 238 with that attributable to fission in uranium 238. The term "multiplication cross section" is defined as the product of reaction microscopic cross section and net neutron yield per reaction.

The second characteristic of the proposed fusion reactor, that of large thermal power output coupled with high energy densities in the plasma, imposes additional restrictions and requirements on the blanket, particularly with respect to materials. Of immediate concern is the first surface seen by plasma-born particles and radiation. We shall assume that a large fraction of the charged α-particles emitted in the fusion reaction are kept away from the walls and deposited safely in some region removed from the blanket under study. Both the neutrons and the plasma radiation (Bremsstrahlung and cyclotron radiation) will impinge on the first wall. The Bremsstrahlung consists of x-rays in the spectral range of tens of kilovolts; the cyclotron radiation lies in the millimeter and submillimeter wavelength region. The penetration depth of these emissions in any material suitable for a vacuum wall is negligible. Since the radiation absorbed may amount to from 10 to 20 per cent of the total output, heating in the first wall is expected to constitute a severe problem. Also, the 14-Mev neutrons will suffer energy loss in penetrating the first wall. These considerations plus those of structural integrity and sputtering on the first surface dictate the use of a refractory metal for the first wall.

Cooling the blanket, especially the first-wall region, poses an equally serious problem. Investigations have shown[6, 9, 10] that only ionic-bonded fused salts appear to be suitable for use as coolants at the high temperatures that are necessary if reasonable thermal efficiencies are to be achieved.

The third characteristic of the fusion reactor, that of obtaining plasma confinement by the use of steady-state magnetic fields generated by superconducting coils, imposes still another requirement on the blanket. Superconductivity occurs only at temperatures of the order of a few degrees Kelvin. Thus energy deposited in the coils by neutron scattering and capture and by gamma attenuation, as well as by direct thermal leakage, must

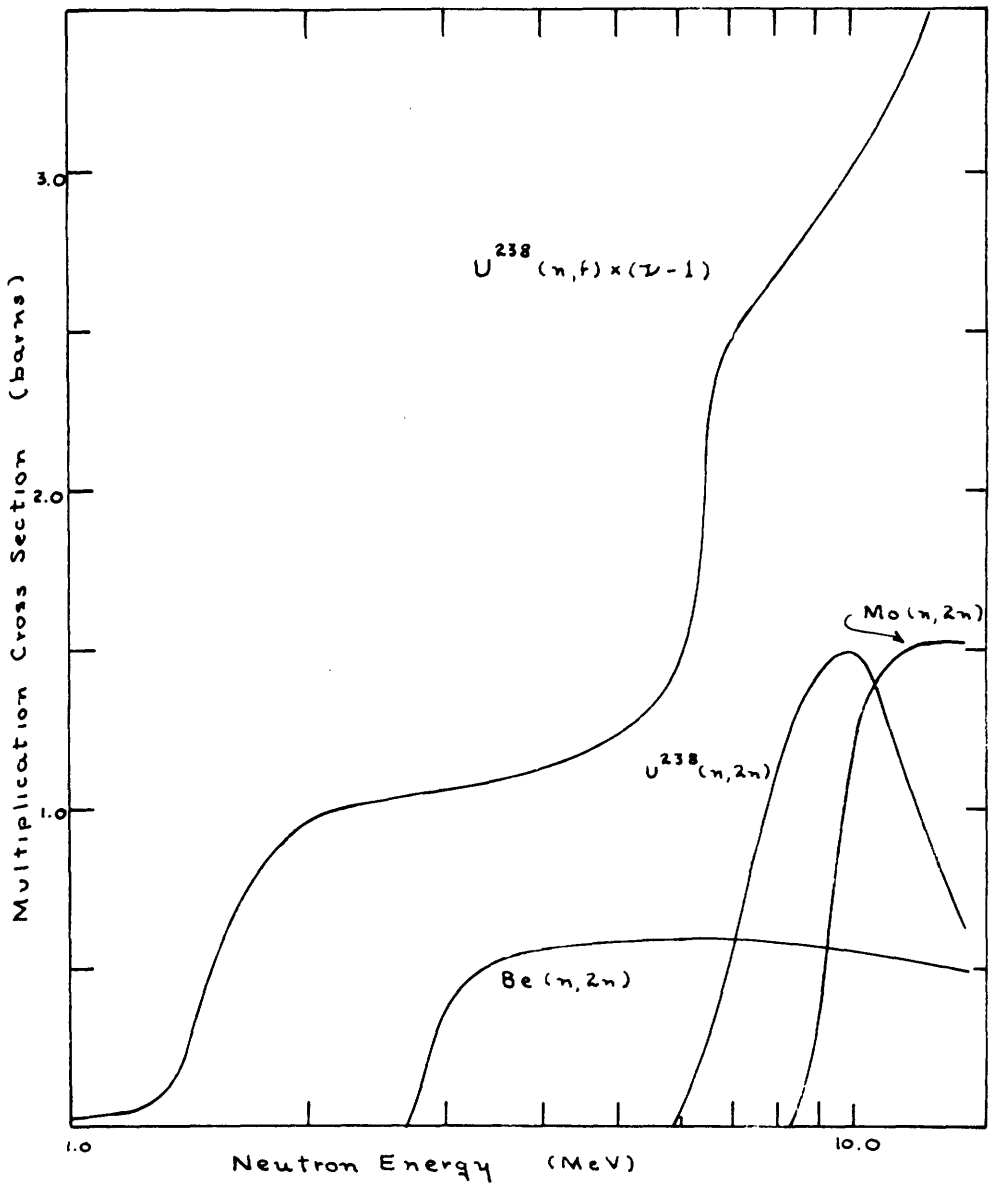

Fig. 2. Multiplication cross sections.

be extracted against a temperature differential of approximately 300°C with the attendant expenditure of large amounts of energy. Hence, the blanket must also serve as a neutron and gamma attenuator and as a thermal barrier, separating the plasma at 10^8°K with a power density of perhaps 10 Mw per cubic meter from the coils at approximately 4°K, with an absorbed power density of 100 watts per square meter of coil area facing the blanket representing a comfortable upper limit.

2.2 EARLIER STUDIES

It is interesting to note that although there is general agreement among the investigators who have studied the problem concerning the characteristics of a potentially useful fusion reactor, agreement does not obtain about what constitutes a suitable blanket design. In the earliest consideration of the problem, Spitzer et al.[11] suggested a system in which lithium metal contained in stainless-steel tubes served as the tritium-fertile material, and separately contained water supplied neutron moderation and cooling. Johnson[12] proposed that fused lithium nitrite would be a more suitable lithium source and would serve as a coolant as well, thereby supporting the separately contained water system of earlier designs. Christofilos et al.[13] have incorporated a similar moderator-coolant-lithium source system into their analyses and include a separately cooled Bremsstrahlung shield necessitated by the particular confinement system proposed. Bell et al.[14] also utilize the Johnson proposal, although at a later point in the same report[15] the advantages of the lithium beryllium fluoride fused-salt system are indicated.

Detailed neutronic calculations were pursued in several of these earlier studies and led to the general conclusion that adequate tritium-breeding ratios could be obtained in the systems then proposed. More will be said concerning comparison of these earlier calculations with those reported here.

The present study indicates that neutron economy and heat transfer both present somewhat more serious problems than seemed to be indicated by the preliminary studies. The use of high-pressure water, contained in stainless steel or monel, as moderator and coolant seems particularly unsuitable. There also appears to be serious doubt concerning the stability of fused lithium nitrite. These considerations and concern about first-wall heating led eventually to the conceptual blanket design proposed here.

2.3 PROPOSED CONCEPTUAL DESIGN

The evolution of the design under scrutiny here has been recorded,[10, 16, 17] and need not be further considered. The major departures from earlier proposals are the following.

1. Use of a refractory, neutron multiplying first wall.
2. Use of fused salts, particularly the lithium beryllium fluoride system, as coolant, elastic moderator, and tritium-fertile material.

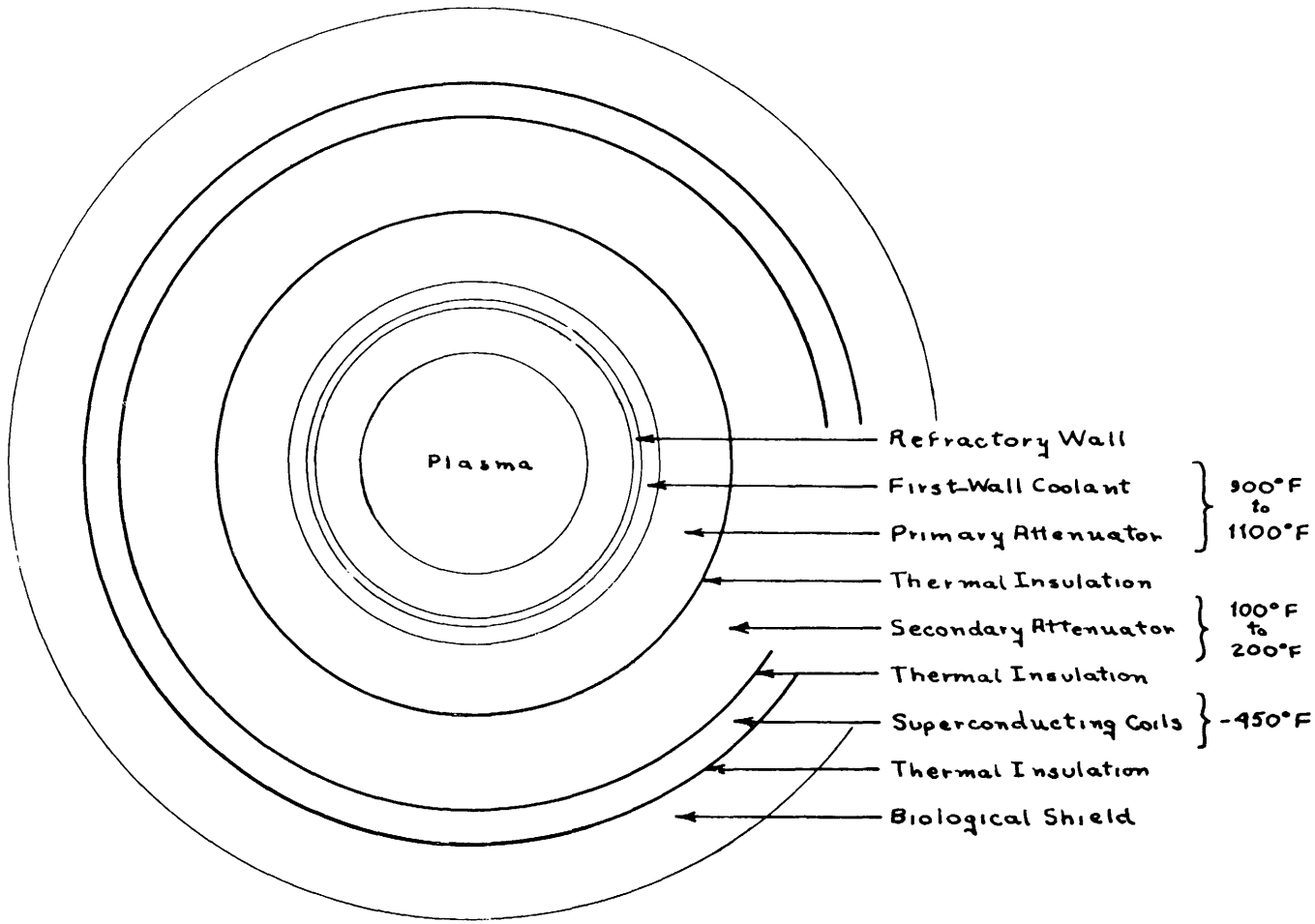

Fig. 3. Functional arrangement of proposed blanket assembly.

3. Use of a direct first-wall coolant and a separate primary attenuator that may be thermally independent of the first-wall region.

The end product of the current study is the functional arrangement sketched in Fig. 3. The refractory first wall and first-wall coolant make up the region of maximum energy density. The primary attenuator is conceived to be a graphite matrix through which a lithium-bearing fused-salt coolant is channeled. The greater part of both tritium generation and heat recovery is accomplished in this region. The lower temperature coil shield region is devoted entirely to neutron and gamma attenuation. Neutrons penetrating into this depth are considered lost to the system as sources of both tritium and useful heat.

In this report attention is devoted primarily to the inner region composed of the first wall, the first-wall coolant and the primary attenuator, since this is the region of critical interest for neutron economy and tritium regeneration. When appropriate, the calculations will be extended to include the coil shield region in order to assess nuclear heating in and near the superconducting coils. Consideration of biological shielding is beyond the scope of this work.

III. NEUTRON SCATTERING MODELS

3.1 INTRODUCTION

Before discussing neutron scattering, some remarks need be made concerning the scheme that will be used to characterize neutron energy. The neutron flux distribution in energy will be approximated by a sequence of monoenergetic fluxes corresponding to successive energy groups. The monoenergetic flux associated with a given group is an approximation to the integral of the true energy-dependent flux over the energy regime in question. Thus,

$$\phi_i(r) \approx \int_{E_L)_i}^{E_H)_i} dE\ \phi(r, E), \tag{3}$$

where the subscript i gives the group number, $E_{H)_i}$ and $E_{L)_i}$ are the higher and lower bounds, respectively, of the i^{th} group, r is the spatial variable, E the energy variable, and ϕ is the scalar flux. Since reaction rates rather than fluxes are basic in this study, the approximation given above may be replaced by the exact relationship

$$\text{Reaction Rate in } i^{th} \text{ group} = \phi_i(r)\ \Sigma_i(r)$$

$$\text{(at spatial point r)} \qquad = \int_{E_L)_i}^{E_H)_i} dE\ \phi(r, E)\ \Sigma(r, E), \tag{4}$$

where Σ is a macroscopic cross section representing a given reaction, and Σ_i is the equivalent macroscopic cross section assigned to the i^{th} group:

$$\Sigma_i(r) = \frac{\int_{E_L)_i}^{E_H)_i} dE\ \phi(r, E)\ \Sigma(r, E)}{\int_{E_L)_i}^{E_H)_i} dE\ \phi(r, E)}. \tag{5}$$

The specific group designations employed, together with the higher and lower energy bounds of the groups and the corresponding energy and lethargy widths, are summarized in Table 1.

The basic requirement of a multigroup treatment of neutron scattering is a means of expressing the probability that a neutron, initially in energy group i and having directional cosine μ, will emerge from a scattering event of a designated type in group j with directional cosine μ'. If the desired probability is represented by $P(i, \mu; j, \mu')$, the rate at which neutrons are scattered from group i to group j in reactions described by $\Sigma_i(r)$ at arbitrary point r in space is given by

$$\text{Scattering rate (at r)} = \int_{-1}^{1} d\mu\ \phi_i(r, \mu)\ \Sigma_i(r)\ P(i, \mu; j, \mu'). \tag{6}$$

Table 1. Energy group designations.

GROUP	MAXIMUM ENERGY MEV	MEAN ENERGY MEV	MINIMUM ENERGY MEV	ENERGY WIDTH MEV	LETHARGY WIDTH
01	14.930	14.200	13.470	1.460	0.1053
02	13.470	12.780	12.120	1.350	0.1053
03	12.120	11.500	10.910	1.210	0.1053
04	10.910	10.350	9.820	1.090	0.1053
05	9.820	9.310	8.830	0.990	0.1053
06	8.830	8.380	7.950	0.880	0.1053
07	7.950	7.540	7.160	0.790	0.1053
08	7.160	6.790	6.440	0.720	0.1053
09	6.440	6.110	5.800	0.640	0.1053
10	5.800	5.500	5.220	0.580	0.1053
11	5.220	4.950	4.690	0.530	0.1053
12	4.690	4.450	4.220	0.470	0.1053
13	4.220	4.010	3.800	0.420	0.1053
14	3.800	3.610	3.420	0.380	0.1053
15	3.420	3.250	3.080	0.340	0.1053
16	3.080	2.920	2.770	0.310	0.1053
17	2.770	2.630	2.490	0.280	0.1053
18	2.490	2.370	2.240	0.250	0.1053
19	2.240	2.130	2.020	0.220	0.1053
20	2.020	1.917	1.818	0.202	0.1053
21	1.818	1.725	1.636	0.182	0.1053
22	1.636	1.553	1.473	0.163	0.1053
23	1.473	1.397	1.325	0.148	0.1053
24	1.325	1.258	1.193	0.132	0.1053
25	1.193	1.132	1.073	0.120	0.1053
26	1.073	1.019	0.966	0.107	0.1053
27	0.966	0.917	0.869	0.097	0.1053
28	0.869	0.825	0.782	0.087	0.1053
29	0.782	0.742	0.704	0.078	0.1053
30	0.704	0.668	0.634	0.070	0.1053
31	0.634	0.601	0.570	0.064	0.1053
32	0.570	0.541	0.513	0.057	0.1053
33	0.513	0.487	0.462	0.051	0.1053
34	0.462	0.440	0.420	0.042	0.1053
35	0.420000	0.364000	0.320000	0.100000	0.2719
36	0.320000	0.265000	0.220000	0.100000	0.3747
37	0.220000	0.162000	0.120000	0.100000	0.6061
38	0.120000	0.091600	0.070000	0.050000	0.5390
39	0.070000	0.045800	0.030000	0.040000	0.8473
40	0.030000	0.017300	0.010000	0.020000	1.0986
41	0.010000	0.006813	0.004641	0.005359	0.7677
42	0.004641	0.003162	0.002154	0.002487	0.7677
43	0.002154	0.001468	0.001000	0.001154	0.7677
44	0.001000	0.000681	0.000464	0.000536	0.7677
45	0.000464	0.000316	0.000215	0.000249	0.7677
46	0.000215	0.000147	0.000100	0.000115	0.7677
47	0.000100	0.000068	0.000046	0.000054	0.7677
48	0.000046	0.000032	0.000021	0.000025	0.7677
49	0.000021	0.000015	0.000010	0.000011	0.7677
50	0.000010	0.000003	THERMAL	0.000010	5.9915

The transport models to be described consider only the two extremes of angular correlation. These are straight ahead scattering in which the directional characteristic of a transporting neutron is unaffected by a scattering event (although the energy may be changed due to the collision), and isotropic scattering in which the directional characteristic of a transporting neutron is lost completely in the scattering process. In these two cases the scattering probability, $P(i, \mu; j, \mu')$, may be replaced by $P(i, j)$ or, more simply, by P_{ij}. The rate of transfer of neutrons from group i to group j at the point r is then given in the straight-ahead case by

$$\text{Transfer rate} = \int_{-1}^{1} d\mu \, \phi_i(r, \mu) \, \Sigma_i(r) \, P_{ij} \tag{7a}$$

and in the isotropic case by

$$\text{Transfer rate} = \phi_i(r) \, \Sigma_i(r) \, P_{ij}. \tag{7b}$$

Neutron scattering is frequently divided into two classes, elastic and inelastic or, more properly, nonelastic scattering. While this distinction is somewhat artificial, especially in view of the observations already made concerning angular correlations, it is convenient to retain it here in discussing the several scattering models used in this study. The rest of this section is devoted to developing, first, an elastic scattering model, and then three different models for treating nonelastic scattering in various distinguishable energy regimes. In each case group transfer functions based on the models are derived. Finally, some remarks will be made concerning models appropriate to angular correlations in the several types of scattering.

3.2 ELASTIC–SCATTERING MODELS

a. Generalized Model

Consider the case of elastic scattering. For all but the lightest scatterers, the maximum energy that a neutron can lose in a single scattering event is relatively small. Furthermore, the energy with which the neutron emerges from an elastic scattering is related to the energy of incidence and the scattering angle by the relation

$$E' = \left\{ \frac{1 + A^2 + 2A\nu}{(1+A)^2} \right\} E, \tag{8}$$

where E and E' are incident and emergent neutron energies, respectively, in the laboratory system, A is the mass number of the scattering nucleus, and ν is the cosine of the scattering angle in the center of mass coordinates. Since the multigroup model is based on lethargy, it is more convenient to express the energy loss in the form

$$\frac{E'}{E} = \frac{1 + A^2 + 2A\nu}{(1+A)^2}. \tag{9}$$

This relation may be solved for ν to yield

$$\nu\left(\frac{E'}{E}\right) = \frac{(1+A)^2}{2A}\,\frac{E'}{E} - \frac{(1+A^2)}{2A}. \tag{10}$$

The probability, Q, that the ratio E'/E have a given value may be given in terms of the probability, π, of occurrence of the corresponding value of ν in the form

$$Q\left(\frac{E'}{E}\right) d\left(\frac{E'}{E}\right) = \pi\left\{\nu\left(\frac{E'}{E}\right)\right\} d\nu \tag{11a}$$

or

$$Q\left(\frac{E'}{E}\right) = \pi\left\{\nu\left(\frac{E'}{E}\right)\right\} \frac{(1+A)^2}{2A}. \tag{11b}$$

The minimum value of the energy ratio E'/E is commonly designated α, and is given by

$$\alpha = \left\{\frac{A-1}{A+1}\right\}^2. \tag{12}$$

On substituting this relation, Eq. 11b takes the form

$$Q\left(\frac{E'}{E}\right) = \pi\left\{\nu\left(\frac{E'}{E}\right)\right\} \frac{2}{1-\alpha}. \tag{13}$$

The group transfer probability P_{ij} may now be defined in the form

$$P_{ij} = \frac{\displaystyle\int_{E_L)_i}^{E_H)_i} dE \int_{\frac{E_L)_j}{E}}^{\frac{E_H)_j}{E}} d\left(\frac{E'}{E}\right) Q\left(\frac{E'}{E}\right)}{\displaystyle\int_{E_L)_i}^{E_H)_i} dE} \tag{14}$$

or, in terms of the scattering angle probability,

$$P_{ij} = \frac{1}{\Delta E)_i} \int_{E_L)_i}^{E_H)_i} dE \int_{\nu\left(\frac{E_L)_j}{E}\right)}^{\nu\left(\frac{E_H)_j}{E}\right)} d\nu\, \pi\left\{\nu\left(\frac{E'}{E}\right)\right\}. \tag{15}$$

The distribution of the cosine of the scattering angle can be obtained either by direct measurement or by calculation using the optical model of the nucleus. In this study the distributions for anisotropic elastic scattering given by Buckingham, Parker, and Pendlebury[18] were used whenever possible because their data are presented in a particularly useful and convenient graphical form from which the required group transfer probabilities can be calculated by simple numerical methods.

b. Isotropic Model

When elastic scatterings are isotropic in the center-of-mass system, the cosine probability, π, becomes simply 0.5 and the energy ratio probability, Q, reduces to

$$Q\left(\frac{E'}{E}\right) = \frac{1}{2}\left\{\frac{2}{1-\alpha}\right\} = \frac{1}{1-\alpha}. \tag{16}$$

In this case the group transfer probabilities can be evaluated directly. The following notation is used:

P_{ii} is the probability that a neutron initially in group i will remain in group i after a scattering event;

P_{ij} is the probability that a neutron scattered in group i will by-pass j-i groups and emerge in group j;

P_{iJ} is the probability that a neutron scattered in group i will by-pass J-i groups, emerging in the last permitted group, J;

$\Delta E)_i$ is the energy width of group i; and

$\Delta u)_i$ is the lethargy width of group i.

The fraction of the energy width of a source group represented by a differential element of energy is given by $dE/\Delta E)_i$. The minimum energy that a neutron of incident energy E may have after an elastic collision is αE, and the total energy span available to the scattered neutron is $E(1-\alpha)$. Furthermore, as shown in (16), the probability that a neutron scattered from energy E emerges in energy increment $\delta E'$ in the span $E(1-\alpha)$ is simply $\delta E'/E(1-\alpha)$; the probability is independent of the fractional energy loss within the allowed limits.

It is desirable to distinguish four cases in terms of the relative magnitudes of group energy widths and allowable energy losses.

1. Incident neutrons may have energies sufficiently far above the lower energy limit of the source group that none can be scattered into lower groups in a single elastic collision. The probability that such neutrons emerge from an elastic scattering in the source group is simply unity.

2. Incident neutrons may lie sufficiently close to the lower energy limit of the source group that the probability of removal from the source group by a single elastic collision is nonzero. The probability that these neutrons remain in the source group is $[E-E_L)_i]/E(1-\alpha)$.

3. Incident neutrons in source group i may have a sufficiently large allowed energy loss compared with group width that all energies in lower energy group j are accessible after a single elastic collision. The probability that the scattered neutrons emerge in group j is then $\Delta E)_i/E(1-\alpha)$.

4. Incident neutrons may have an allowed energy loss such that only the upper portion of a specified lower energy group is accessible after a single elastic collision. The probability that the emergent neutron appear in this portion of group j, the specified group, is given by $[E_H)_j-\alpha E]/E(1-\alpha)$. Group transfer probabilities of interest here may

represent either a single case or a combination of two of the cases distinguished above, determined by the relative magnitudes of group width and maximum allowable energy loss.

(i) Probability of Retention in Source Group

When the allowable energy loss is comparatively small $[\alpha E_{H)_i} > E_{L)_i}]$, only a fraction of the neutrons in the source group are within reach of lower groups, and the transfer probability for retention in the initial group is given by the relation

$$P_{ii} = \int_{E_{L)_i}}^{\frac{E_{H)_i}}{\alpha}} \frac{dE}{\Delta E)_i} \left[\frac{E - E_{L)_i}}{E(1-\alpha)}\right] + \int_{\frac{E_{L)_i}}{\alpha}}^{E_{H)_i}} \frac{dE}{\Delta E)_i} \tag{17a}$$

$$= \frac{E_{H)_i}}{\Delta E)_i} - \frac{E_{L)_i}}{\Delta E)_i} \left\{\frac{1}{1-\alpha} \ln \frac{1}{\alpha}\right\}. \tag{17b}$$

In Eq. 17a the first term accounts for those neutrons that can be removed from the group, the second, the remainder. When all neutrons in the source group can reach a lower group $[\alpha E_{H)_i} < E_{L)_i}]$, the second term disappears and the transfer probability takes the form

$$P_{ii} = \int_{E_{L)_i}}^{E_{H)_i}} \frac{dE}{\Delta E)_i} \left[\frac{E - E_{L)_i}}{E(1-\alpha)}\right] \tag{18a}$$

$$= \frac{1}{1-\alpha} \left\{1 - \frac{E_{L)_i}}{\Delta E)_i} \Delta u)_i\right\}. \tag{18b}$$

(ii) Probability of Scattering to an Intermediate Group

In this case three distinct possibilities must be considered. First, the allowable energy loss may be so small compared with group widths $[\alpha E_{H)_i} > E_{H)_i}]$ that not all neutrons in the source group can reach the object group. Of those that can reach the object group at least some are limited to the upper portion of the lower group. The transfer probability has the form

$$P_{ij} = \int_{E_{L)_i}}^{\frac{E_{L)_j}}{\alpha}} \frac{dE}{\Delta E)_i} \frac{\Delta E)_j}{E(1-\alpha)} + \int_{\frac{E_{L)_j}}{\alpha}}^{\frac{E_{H)_j}}{\alpha}} \frac{dE}{\Delta E)_i} \left\{\frac{E_{H)_j} - \alpha E}{E(1-\alpha)}\right\} \tag{19a}$$

$$= \frac{\Delta E)_j}{\Delta E_i(1-\alpha)} \ln \left\{\frac{E_{L)_j}}{\alpha E_{L)_i}}\right\} + \frac{E_{H)_j} \Delta u)_j}{\Delta E)_i(1-\alpha)} + \frac{\Delta E)_j}{\Delta E)_i(1-\alpha)}. \tag{19b}$$

Second, if the allowable energy loss is somewhat larger $[E_{H'})_j > \alpha E_{H'})_i > E_{L'})_j]$, all neutrons in the source group have access to the object group, although some are still limited to the upper portion of the object group. In this event,

$$P_{ij} = \int_{E_{L'})_i}^{\frac{E_{L'})_j}{\alpha}} \frac{dE}{\Delta E)_i} \frac{\Delta E)_j}{E(1-\alpha)} + \int_{\frac{E_{L'})_j}{\alpha}}^{E_{H'})_i} \frac{dE}{\Delta E)_i} \left\{ \frac{E_{H'})_j - \alpha E}{E(1-\alpha)} \right\} \tag{20a}$$

$$= \frac{\Delta E)_j}{\Delta E)_i (1-\alpha)} \ln \left\{ \frac{E_{L'})_j}{\alpha E_{L'})_j} \right\} + \frac{E_{H'})_j}{\Delta E)_i (1-\alpha)} \ln \left\{ \frac{\alpha E_{H'})_i}{E_{L'})_j} \right\} - \frac{1}{\Delta E)_i (1-\alpha)} \{\alpha E_{H'})_i - E_{L'})_j\}. \tag{20b}$$

Finally, when the allowable energy loss is comparatively large $[E_{L'})_j > \alpha E_{H'})_i]$, all neutrons in the source group have full access to the lower group and the transfer probability takes the form

$$P_{ij} = \int_{E_{L'})_i}^{E_{H'})_i} \frac{dE}{\Delta E)_i} \frac{\Delta E)_j}{E(1-\alpha)} \tag{21a}$$

$$= \frac{\Delta E)_j}{\Delta E)_i} \frac{\Delta u)_i}{(1-\alpha)}. \tag{21b}$$

(iii) Probability of Scattering to Lowest Permitted Group

As before, when the allowed energy loss is comparatively small $[\alpha E_{H'})_i > E_{H'})_J]$, only neutrons in the lower energy portion of the source group have access to the lowest object group. Also, by the definition of the "lowest permitted group," no neutrons scattered from the source group have access to the full width of the object group. In this case the group transfer probability is given by

$$P_{iJ} = \int_{E_{L'})_i}^{\frac{E_{H'})_J}{\alpha}} \frac{dE}{\Delta E)_i} \left\{ \frac{E_{H'})_J - \alpha E}{E(1-\alpha)} \right\} \tag{22a}$$

$$= \frac{E_{H'})_J}{\Delta E)_i (1-\alpha)} \left\{ \ln \left[\frac{E_{H'})_J}{\alpha E_{L'})_i} \right] - 1 + \frac{\alpha E_{L'})_i}{E_{H'})_J} \right. . \tag{22b}$$

In the special case when $J = i + 1$,

$$P_{iJ} = \frac{E_{L'})_i}{\Delta E)_i} \left\{ \frac{1}{1-\alpha} \ln \frac{1}{\alpha} - 1 \right\}. \tag{22c}$$

Alternatively, when the allowed energy loss is comparatively large $[E_{H'})_J > \alpha E_{H'})_i]$, all neutrons in the source group have access to some portion of the lowest permitted object

group, and the group transfer probability takes the form

$$P_{iJ} = \int_{E_L)_i}^{E_H)_i} \frac{dE}{\Delta E)_i} \left\{ \frac{E_H)_J - \alpha E}{E(1-\alpha)} \right\} \tag{23a}$$

$$= \frac{1}{1-\alpha} \left\{ E_H)_J \frac{\Delta u)_i}{\Delta E)_i} - \alpha \right\}. \tag{23b}$$

Again, when $J = i + 1$,

$$P_{iJ} = \frac{1}{1-\alpha} \left\{ E_L)_i \frac{\Delta u)_i}{\Delta E)_i} - \alpha \right\}. \tag{23c}$$

3.3 NONELASTIC SCATTERING MODELS

a. Distinguishable Energy Regimes

The treatment of nonelastic scattering is more complicated. Below ~1 Mev in the heavier nuclides, and over most of the energy range of interest in the light nuclides, the level spacings are sufficiently wide that individual levels can be distinguished. In such cases the energy lost by a neutron in exciting a particular level in a scatterer is the energy corresponding to the level plus the recoil energy of the scatterer; when the level excitation functions either are known or can be estimated, the group transfer probabilities can be calculated.

Above 2-3 Mev in the heavier nuclides, the level spacings are very close and tend to overlap to form a continuum. In such cases neutron nonelastic scattering becomes a statistical process and, in general, is amenable to treatment in terms of the statistical model of the nucleus.

At high energies in the lighter elements, and at intermediate energies (approximately a few Mev) in the heavy elements, the levels are sufficiently far apart that a true continuum is not yet established. On the other hand, the levels are too closely spaced to permit measurement of excitation functions for individual levels. In this region an empirical treatment is utilized to calculate approximate group-transfer functions.

b. Isolated-Level Model

In those cases in which individual levels can be distinguished and level excitation functions measured, development of group-transfer probabilities is straightforward. The energy of a neutron emerging from an inelastic scattering event may be calculated by successively transforming into center-of-mass coordinates, accounting for energy loss by level excitation and recoil, and transforming back to laboratory coordinates. Following the procedure outlined in Appendix A, we obtain

$$E' = \left\{ \left(\frac{A}{A+1} \right)^2 \left[1 + \frac{1}{A^2} - \frac{A+1}{A} \frac{E_\lambda}{E} - \frac{2}{A} \sqrt{1 - \frac{A+1}{A} \frac{E_\lambda}{E}} \nu \right] \right\} E, \tag{24}$$

where E_λ is the energy of the level excited, and all other symbols have their previous definitions.

Invoking the assumption that nonelastic scatterings are isotropic, we see that the average value of ν, the cosine of the scattering angle, is zero. Hence, the average value of the emergent neutron energy is given by the expressions

$$E' = \left\{ \frac{A^2 + 1}{(A+1)^2} - \frac{A}{A+1} \frac{E_\lambda}{E} \right\} E \tag{25a}$$

$$= \bar{o}\,[E, E_\lambda, A]E. \tag{25b}$$

The operator indicated in Eq. 25b is the multiplier within the brackets in Eq. 25a, and is introduced simply for convenience. The group transfer probabilities for this form of scattering depend on whether scattered source group neutrons have access to only the lower energy region of an object group or to the whole of the group, or to only the higher energy portion. For these cases the transfer probabilities have the respective forms

$$P_{ij} = \frac{1}{\Delta E)_i} [\bar{o}\, E_H)_i - E_L)_j] \qquad \bar{o}\, E_H)_i < E_H)_j \tag{26a}$$

$$P_{ij} = \frac{\Delta E)_j}{\Delta E)_i} \qquad \begin{matrix} \bar{o}\, E_H)_i > E_H)_j \\ \bar{o}\, E_L)_i < E_L)_j \end{matrix} \tag{26b}$$

$$P_{ij} = \frac{1}{\Delta E)_i} [E_H)_j - \bar{o}\, E_L)_i] \qquad \bar{o}\, E_L)_i > E_L)_j. \tag{26c}$$

c. Statistical Model

(i) Theoretical Basis

The statistical model of the nucleus was first formulated by Weisskopf[19] on the basis of a suggestion attributed to Frenkel.[20] The basic premise of the statistical model, in Weisskopf's words, is that "the individual properties of the separate nuclear quantum states are ... of no interest on account of the extremely small distance between the energy levels of highly excited heavy nuclei; it is then possible to obtain statistical information on the behavior of these nuclei by averaging over many quantum states of approximately the same energy."

Pursuing Frenkel's analogy between particle emission from highly excited nuclei and low-energy thermodynamic evaporation, Weisskopf was able to obtain expressions describing both the energy spectrum of neutrons emitted from highly excited heavy nuclei and, in later collaboration with Ewing,[21] the absolute magnitudes of cross sections such as that of the (n, 2n) reaction. The original work showed that the spectrum of emergent neutron energies depends strongly on the nature of the level distribution in the residual

nucleus. If the nucleus is assumed to be characterized by the Fermi degenerate gas model, the spectrum of the first emitted neutron is Maxwellian in form and is given by

$$n(E')\,dE' = c'\sigma_c(E')\,\frac{E'}{\tau}\,e^{-E'/\tau}\,\frac{dE'}{\tau}. \tag{27a}$$

The quantity c' is a normalization factor, E' is the energy of the emergent particle, $\sigma_c(E')$ is the cross section for formation of the compound nucleus, and τ is the nuclear temperature of the residual nucleus. The factor $\sigma_c(E')$ is usually taken to be constant, yielding a distribution of the form

$$n(E')\,dE' = C\,\frac{E'}{\tau}\,e^{-E'/\tau}\,\frac{dE'}{\tau}. \tag{27b}$$

In the original formulation the concept of an average level density was used in deriving the nuclear temperature and yielded

$$\tau \propto \sqrt{\frac{U}{\beta}}. \tag{28}$$

In (28) U is the excitation energy of the residual nucleus, and, in general, is given by

$$U \approx (E+BE)_{\substack{\text{incident}\\\text{particle}}} - (BE+2\tau)_{\substack{\text{emitted}\\\text{particle}}}. \tag{29}$$

(Note that τ is equivalent to the quantity kT, where k is the Boltzmann constant, and T is true thermodynamic temperature.) Here, BE signifies binding energy; the parameter β is a measure of the entropy of the residual nucleus and is predicted to be directly dependent on mass number and independent of excitation energy.

Implicit in the Weisskopf approach is the hypothesis that, if multiple-particle emission is energetically permitted (as, for example, in (n, 2n) reactions), the energy spectrum of the second emitted particle will also be Maxwellian. It will, however, be characterized by a somewhat lower temperature reflecting a decrease in available energy equal to the kinetic energy of the first particle and the separation energy of the second. Weisskopf and Ewing make the observation that the emission, from an excited nucleus, of charged particles with energies below the Coulomb barrier should be strongly inhibited, with an attendent distortion of the emission energy spectrum.

In a later reconsideration of the bases of the statistical model, Feld, Feshbach, Goldberger, Goldstein, and Weisskopf[22] concluded, in 1951, that the experimental evidence then available indicated that the level densities could be treated as constant for several Mev above the ground state, with a subsequent exponential rise in keeping with the Fermi degenerate gas model. This treatment yields an energy distribution of the form

$$n(E')\,dE' \propto E'\sigma_c(E')\,e^{2\left[\sqrt{\beta E'}-\sqrt{\beta E_o}\right]}\,e^{-\left[\sqrt{\beta/E}\right]E'}\,dE', \tag{30}$$

as compared with the original formulation expressed by Feld et al.[5] in the form

$$n(E')\,dE' \propto E'\sigma_c(E')\,e^{-\sqrt{\beta/E}\,E'}\,dE'. \tag{31}$$

In these expressions E is the incident neutron energy, and E_o is the energy characterizing the transition from constant level densities to densities varying exponentially. For energies appreciably below the transition point, the emergent energy spectrum is predicted to be pronouncedly non-Maxwellian. Feld et al.[22] also demonstrate theoretically that, according to the statistical model, the angular distribution of the nonelastically scattered neutrons should be isotropic.

More or less concurrently with the re-examination by Feld et al., Le Couteur independently,[23] and later with Lang,[24] undertook an analysis of the statistical model in which the average level-density method of Weisskopf was replaced by a treatment permitting statistical fluctuations in level density. The inclusion of statistical fluctuations reflects the incomplete rigidity of the nucleus and the effects of surface oscillations. The equations of state derived by Le Couteur and Lang were independent of the model chosen for the nucleus; Lang[25] has observed, however, that the Fermi gas model is in agreement with experimental results.

The Le Couteur-Lang treatment, with a few simplifying assumptions, yields for the emergent energy spectrum

$$n_1(E')\,dE' = C_1 \frac{E'}{\tau} e^{-E'/\tau} \frac{dE'}{\tau} \tag{32}$$

in cases involving single-particle emission, and

$$n_2(E')\,dE' = C_2\left(\frac{E'}{\tau^*}\right)^{5/11} e^{-E'/\tau^*} \frac{dE'}{\tau^*} \tag{33a}$$

$$\tau^* = \frac{11}{12}\sqrt{\frac{U}{\beta}} \tag{33b}$$

when emission of two successive particles is permitted. In the last case the excitation energy, U, is given by

$$U \approx (E+BE)_{\substack{\text{incident}\\\text{particle}}} - (BE+\tau)_{\substack{\text{first}\\\text{particle}}} - (BE+\tau^*)_{\substack{\text{second}\\\text{particle}}}. \tag{34}$$

It is interesting to note that Le Couteur and Lang use the quantity τ, the most probable energy of the Maxwellian, as the mean kinetic energy carried off by emergent particles, while Weisskopf used 2τ, the average energy (see Eq. 29). In either case the expression for the excitation energy is an approximation.

(ii) Validity of the model

The validity of the statistical model in terms of both the emergent particle energy distribution and the absolute cross section formulations has been investigated experimentally by a number of authors. Graves and Rosen,[26] Zamyatnin et al.,[27] and Prud'homme et al.,[28] to cite a few, have measured the spectra of emergent neutrons

arising from nonelastic collisions of 14-Mev neutrons with a wide variety of nuclides. The experimental spectra show good agreement with statistical model predictions in the range 0.5 Mev to 3 or 4 Mev, but tend to show more particles at higher energies than predicted by the model. Gugelot[29] demonstrates correspondingly good agreement for neutron spectra arising from (p, n) reactions initiated in a number of elements by 16-Mev protons. The accuracy of the experiments does not allow a clear choice among the Weisskopf, Feld et al., and Le Couteur-Lang formulations.

Allen[30-32] and Colli et al.[33] have investigated the energy spectra of protons from (n, p) interactions induced by 14-Mev neutrons in medium weight nuclei. In such reactions the Coulomb barrier exerts a strong influence on the emergent energy spectra. In general, reasonable agreement of the measured spectra with statistical model predictions is obtained at energies in the vicinity of the Coulomb barrier height. When (n, p) and (n, np) reactions are expected to be in competition, the experimental spectra can frequently be resolved into two Maxwellian distributions characterized by nuclear temperatures corresponding to first-particle emission and second-particle emission.

The measured spectra in all cases show pronounced deficiencies in population compared with a simple Maxwellian at energies appreciably below the Coulomb barrier height. At energies well above the barrier, Allen observes well-spaced groups of protons in excess of, and in direct disagreement with, the predictions of the statistical model. These strong high-energy contributions, together with the definite anisotropy in proton distributions, are attributed to so-called direct, instantaneous or local boiling interactions in which the incident particle interacts with only a few nucleons within the nucleus before a particle is ejected. The relative likelihood of direct interactions, which are observed to a lesser extent in reactions involving neutron emission, is increased by the suppressing effect of the Coulomb barrier on low-energy particle emission when the emitted particle is charged.

Although the absolute cross-section formulations derived on the bases of the statistical model are of little direct interest in this study, some comment on their experimental verification is in order, since the validity of these formulations implies, at least in part, the validity of the basic model. Comparison of measured cross sections with statistical model predictions has been attempted by a number of researchers. Weigold and Glover[34] have compared measured and theoretical (n, 2n) cross sections for a number of elements and find reasonably good agreement in all cases. Strohal, Cindro, and Eman[35] also observe that (n, 2n) reaction cross-sections are well described by the statistical model with reasonable nuclear temperatures and radii. Strohal et al.[35] point out, however, that consideration must be given to the influence of closed shells in "magic" nuclei if agreement is to be obtained over wide ranges of target mass numbers.

Allen[32] and Strohal et al.[35] have investigated the agreement between theory and experiment obtained in the case of the (n, p) cross sections at 14 Mev. Allen, in particular, concludes that the Le Couteur-Lang level density model, with appropriate allowances for pairing energies and shell effects, yields theoretical (n, p) cross sections

remarkably close to measured values. The pairing energies included by Allen were based on independent measurements, a fact that strongly re-enforces the apparent validity of the statistical model. Strohal et al., using a less refined calculation of the theoretical cross sections, obtain somewhat poorer agreement between theory and experiment.

A major source of difficulty in the statistical model is that of obtaining a suitable value for the entropy parameter, β. A number of investigators have attempted, both theoretically and experimentally, to develop either analytical or empirical expressions for the value of the β parameter. The results of these efforts are generally in poor agreement. Independent studies of given nuclides at a specific excitation energy show on occasion serious disagreements; see, for example, Graves,[26] Zamyatnin et al.,[27] and Prud'homme et al.[28] The study of individual nuclides over a range of excitation energies[36] shows definite but inconsistent dependence of β on excitation. The generally good agreement cited above between predicted and measured spectra derives, at least in part, from the use of empirical β values in a limited range of nuclide mass numbers, and also from the relative insensitivity of the spectra to the value of the entropy parameter.

(iii) Development of transfer probabilities

In the present study, in cases in which the statistical model is expected to be applicable, neutron group transfer probabilities were calculated by using the Le Couteur-Lang multiple-particle formulation when ejection of two successive particles was permitted by energetics, and the original Weisskopf formulation when single-particle emission occurred. The appropriate normalization constants are given for the single particle case by

$$C_1 = \left\{ \int_0^{E_{max}} n_1(E')\, dE' \right\}^{-1} = \left\{ 1 - \left(1 + \frac{E_{max}}{\tau} \right) e^{-E_{max}/\tau} \right\}^{-1} ; \tag{35}$$

and for the double particle case by

$$C_2 = \left\{ \frac{\int_0^{E_{max}} n_2(E')\, dE'}{2 \int_0^{E_1} C_1 n_1(E')\, dE' + \int_{E_1}^{E_{max}} C_1 n_1(E')\, dE'} \right\}^{-1} \tag{36a}$$

$$C_2 \approx \left\{ \frac{\Gamma\left(\frac{16}{11}\right)}{2 - \left(1 + \frac{E_1}{\tau} \right) e^{-E_1/\tau} - \left(1 + \frac{E_{max}}{\tau} \right) e^{-E_{max}/\tau}} \right\}. \tag{36b}$$

In (36) Γ signifies the gamma function tabulated, for example, by Hildebrand,[37] and represents the value of the integral over the spectrum. The denominator allows for

the presence of a second particle whenever the emission of that particle is permitted. The parameter E_1 defines the maximum kinetic energy that can be carried off by the first particle if second-particle ejection occurs, and is given empirically as

$$E_1 = E - BE - 0.5. \tag{37}$$

In both cases E_{max} sets the upper limit of the range of energies into which the particle is assumed to be nonelastically scattered.

Experimentally derived values of the entropy parameter and of neutron emission cross sections were used whenever available. A theoretical value of the ratio $\sigma_{(n, 2n)}/\sigma_{nonelastic}$ is implicit in the multiple-particle formulation and is used as such. In the few cases in which measured (n, 2n) excitation functions are available for comparison, the calculated (n, 2n) cross sections are in good agreement.

The final group-transfer functions derived from the statistical model take the forms:

For single-particle emission:

$$P_{ij} = \Delta E)_j \frac{E_j}{(\tau_i)^2} e^{-E_j/\tau_i} \left\{ \frac{1}{1 - \left[1 + 0.656 \frac{E_i}{\tau_i}\right] e^{-0.656 E_i/\tau_i}} \right\} \tag{37a}$$

with

$$\tau_i = \sqrt{\frac{E_i}{\beta_1}}. \tag{37b}$$

For double-particle emission:

$$P_{ij} = \frac{\Delta E)_j \left[\frac{E_j}{\tau_i^*}\right]^{5/11} \frac{1}{\tau_i^*} e^{-E_j/\tau_i^*}}{\left\{1 - \left(1 + 0.656 \frac{E_i}{\tau_i}\right) e^{-0.656 E_i/\tau_i}\right\} \Gamma\left(\frac{16}{11}\right)} \cdot \left\{2 - \left[1 - \frac{E_i)_1}{\tau_i}\right] e^{-E_i)_1/\tau_i} - \left(1 + 0.656 \frac{E_i}{\tau_i}\right) e^{-0.656 E_i/\tau_i}\right\} \tag{38a}$$

with

$$E_i)_1 = E_i - BE - 0.5 \tag{38b}$$

and

$$\tau_i^* = \frac{11}{12} \sqrt{\frac{E_i}{\beta_2}}. \tag{38c}$$

As before, the subscripts i and j denote source group and object group, respectively.

The parameters β_1 and β_2 are the single- and double-particle entropy parameters, respectively.

(iv) Empirical model

Below the regime of validity of the statistical model of the nucleus there is, for most nuclides of interest, a second energy region characterized by

1. more or less uniform level densities, and
2. level spacings too narrow to permit experimental measurement of the excitation functions of the individual levels, but so broad as to preclude treatment in terms of a continuum of levels.

Since in this energy region there are available neither experimental measurements nor readily utilized nuclear models on which inelastic scattering calculations can be based, estimates of the group transfer probabilities are developed here by using an empirical scattering model. The nature of the model and the mechanics of calculating the group-transfer probabilities will next be outlined.

Two assumptions underlie the model:

1. The neutron population in a given source group is uniform in energy.
2. The relative excitation functions of all levels affecting the inelastic scattering of neutrons in the energy region in question are identical in shape and can be approximated by a simple mathematical function.

A slightly modified Gaussian function has been selected to characterize the shape of the unmeasured excitation functions. The choice of the Gaussian was based in part on the fact that among the functions considered, it most nearly approached the shape of the few measured excitation functions available and in part on convenience and simplicity of treatment. The particular chosen function has the form

$$\epsilon(E^{**}) = K\, e^{-\{a(E^{**}-b)\}^2}, \tag{39a}$$

where

$$E^{**} = \frac{A}{A+1} E - E_\lambda. \tag{39b}$$

The ancillary condition

$$c \leq E^{**} \leq 2b - c, \tag{39c}$$

is imposed. In this formulation, ϵ is the excitation function, E is the incident energy, E_λ is the energy of the level excited. E^{**} is the excess energy available in the center of mass system, and K provides normalization. The adjustable parameters a, b, and c establish the shape of the Gaussian, the location of the function with respect to the energy of the level to be excited, and the span of the symmetrically truncated function, respectively. A typical approximate excitation function is sketched in Figure 4.

Consider now a collision in which a neutron of energy E excites a level at energy E_λ

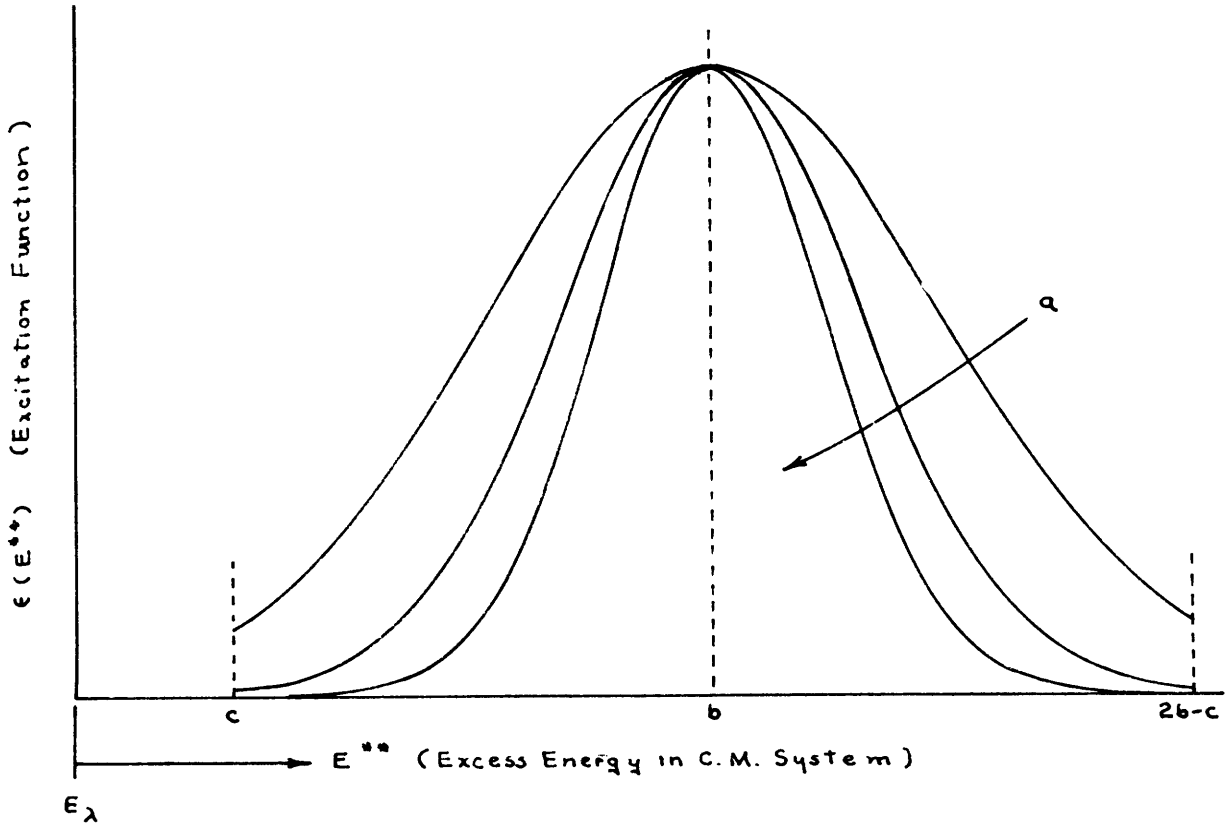

Fig. 4. Typical approximate excitation functions.

in a target nucleus. It is shown in Appendix A that the emergent energy, E', of the neutron is given by

$$E' = \left\{ \left(\frac{A}{A+1}\right)^2 \left[1 + \frac{1}{A^2} - \frac{(A+1)}{A} \frac{E_\lambda}{E} - \frac{2}{A} \sqrt{1 - \frac{(A+1)}{A} \frac{E_\lambda}{E}}\, \nu \right] \right\} E. \tag{40a}$$

It is also shown in the Appendix that if the scattering is isotropic (an assumption well supported by measurement), the average emergent energy, $\bar{E}'$, is given by

$$\bar{E}' = \left\{ \frac{A}{(A+1)^2} \left[1 + \frac{1}{A^2} - \frac{(A+1)}{A} \frac{E_\lambda}{E} \right] \right\} E \tag{40b}$$

or, more simply,

$$\bar{E}' = \left\{ \frac{A^2 + 1}{(A+1)^2} - \frac{A}{A+1} \frac{E_\lambda}{E} \right\} E. \tag{40c}$$

This expression may be solved for E_λ in terms of $\bar{E}'$ and E to yield

$$E_\lambda(E, \bar{E}') = \frac{A^2 + 1}{A(A+1)} E - \frac{(A+1)}{A} \bar{E}'. \tag{41}$$

The probability, $\pi(\bar{E}')$, that a neutron emerges with average energy $\bar{E}'$ from a collision induced by a neutron in group i is

$$\pi(\bar{E}') = \int_{E_i)_L}^{E_i)_H} dE'' \int_{E_{\lambda\,min}}^{E_{\lambda\,max}} dE''_\lambda \; P(E'')\, Q(E''_\lambda)\, \epsilon\left[\frac{A}{A+1} E'' - E''_\lambda\right], \tag{42}$$

where P(E") is the probability that the incident neutron has energy E"; $Q(E''_\lambda)$ is the distribution in energy of excitable levels in the scatterer; and ϵ is the level excitation function.

The integral over E''_λ has the effect of considering all allowed levels accessible to neutrons in group i, $Q(E''_\lambda)$ being a set of Dirac delta functions locating the levels. Assume, for the present, that

$$Q(E''_\lambda) = \delta(E''_\lambda - E_\lambda), \tag{43a}$$

which is to say that excitation is limited to a single level at E_λ. The assumption has already been made that the neutron population in the source group is uniform in energy. Hence, on a unit neutron basis

$$P(E'') = \frac{1}{\Delta E)_i}. \tag{43b}$$

Substituting in succession (43a), (43b), and (41) in (42) yields, in turn,

$$\pi(\bar{E}') = \int_{E_L)_i}^{E_H)_i} dE'' \; P(E'')\, \epsilon\left[\frac{A}{A+1} E'' - E_\lambda\right] \tag{44a}$$

$$\pi(\bar{E}') = \frac{1}{\Delta E)_i} \int_{E_L)_i}^{E_H)_i} dE'' \; \epsilon\left[\frac{A}{A+1} E'' - E_\lambda\right] \tag{44b}$$

$$\pi(\bar{E}') = \frac{1}{\Delta E)_i} \int_{E_L)_i}^{E_H)_i} dE'' \; \epsilon\left[\frac{A+1}{A} \bar{E}' - \frac{1}{A(A+1)} E''\right]. \tag{44c}$$

Observe that in the argument of the excitation function, $\bar{E}'$ is weighted by (A+1)/A, while E" is weighted by $1/(A^2+A)$. For nuclides of interest in these calculations, $A \geq 10$ so that the weighting of $\bar{E}'$ is of the order of unity, while that of E" is two orders of magnitude smaller. For values of $\bar{E}'$ and E" in the range of application of this model, ($\bar{E}' \geq 0.2$, $E'' \sim 2$); the term in E" may be safely neglected, at least to first approximation. Thus

$$\pi(\bar{E}') \approx \frac{1}{\Delta E)_i} \int_{E_L)_i}^{E_H)_i} dE'' \; \epsilon\left[\frac{A+1}{A} \bar{E}'\right], \tag{45}$$

and finally

$$\pi(\bar{E}') \approx \epsilon\left[\frac{A+1}{A} \bar{E}'\right], \tag{46a}$$

where

$$c \leq \frac{A+1}{A}\bar{E}' \leq 2b - c. \tag{46b}$$

The effect of the preceding manipulations has been to express the emission energy spectrum in terms of the emission energy itself rather than in terms of excess energy before collision. Thus, within the approximation of neglecting a second-order term, $E''/A(A+1)$, the empirical model developed here predicts that the energy spectrum of inelastically scattered neutrons is identical in shape to the assumed level-excitation function, but is independent of both the incident energy and the energy of the level excited.

The assumption already made that all levels have the same excitation function allows extension of the result just obtained for excitation of a single level to the general case in which a number of levels may be excited by neutrons in a given source group. Indeed, it will be seen that the shape of the spectrum of emergent neutrons is unaffected by the excitation of additional levels.

If more than one level can be excited by neutrons in a given source group, the excitation function for each level is given by

$$\epsilon_\eta(E^{**}) = \frac{1}{\eta} K\, e^{-\{a(E^{**}-b)\}^2}, \tag{47a}$$

where

$$c \leq E^{**} \leq 2b - c. \tag{47b}$$

Here, η is the number of allowed levels. The emergent neutron spectrum is then given by

$$\pi(\bar{E}') \approx \eta\epsilon_\eta\left[\frac{A+1}{A}\bar{E}'\right]. \tag{48}$$

Since the spectrum of inelastically scattered neutrons is not dependent on the energy of the incident neutron, the group-transfer probabilities are simply the probabilities that the scattered neutron appear in the several allowed object groups, and are given to good approximation by

$$P_{ij} = \pi(E_j)\frac{\Delta E)_j}{2(b-c)}, \tag{49}$$

where E_j is the characteristic energy of group j.

Finally, since the macroscopic cross section for excitation of all levels allowed for incident neutrons in group i is identically $\Sigma_{n,n'})_i$, the specific rate of transfer of neutrons from i to group j by inelastic collisions is given by

$$\text{Rate} = \phi_i\Sigma_{n,n'})_i\,\pi(E_j)\frac{\Delta E)_j}{2(b-c)}. \tag{50}$$

Throughout the foregoing discussion the assumption has been made implicitly that all neutrons in a given source group may excite, on the average, the same number of levels, and that the level distribution is approximately uniform. It is now necessary to consider briefly the case in which the source group lies close enough to the threshold for inelastic scattering so that

$$\frac{A}{A+1} E - E_\lambda)_{min} < 2b - c. \tag{51}$$

Since the low-lying levels whose excitation corresponds to emission of relatively high-energy secondary neutrons do not exist for incident neutrons of energy less than $\frac{A+1}{A}[E_\lambda)_{min}+(2b-c)]$, emission of scattered neutrons having energies in the upper end of the emission spectrum is impossible. The net effect is the truncation of the spectrum at energy $\overline{E}'_{max}$, where

$$\overline{E}'_{max} = \frac{A^2}{(A+1)^2} E - \frac{A}{A+1} E_\lambda)_{min}. \tag{52}$$

The spectrum is then given by

$$\pi(\overline{E}') = \epsilon\left[\frac{A+1}{A}\overline{E}'\right], \tag{53a}$$

where

$$c \leq \frac{A+1}{A}\overline{E}' \leq \frac{A}{A+1} E - E_\lambda)_{min}. \tag{53b}$$

Normalization of the emergent neutron spectrum to unity consists in setting

$$K^{-1} = \int_{\overline{E}'_{min}}^{\overline{E}'_{max}} dE' \, \pi(\overline{E}'). \tag{54a}$$

Substituting from Eq. 46a,

$$K^{-1} = \int_{\overline{E}'_{min}}^{\overline{E}'_{max}} d\overline{E}' \, e^{-\left\{a\left(\frac{A+1}{A}\overline{E}'-b\right)\right\}^2}. \tag{54b}$$

It is convenient to make the substitution

$$\mathscr{E} = \frac{A+1}{A}\overline{E}' \tag{55}$$

which leads to

$$K^{-1} = \frac{A}{A+1}\int_c^{2b-c} d\mathscr{E} \, e^{-\{a(\mathscr{E}-b)\}^2} \tag{56}$$

when the spectrum is not truncated. Carrying out the integration, we have

$$K^{-1} = \frac{A}{A+1}\frac{\sqrt{\pi}}{a}\,\mathrm{erf}\{a(b-c)\}. \tag{57a}$$

The function erf(x) is the error function or probability integral of argument x as defined, for example, by Peirce.[38] In the truncated case the normalization constant is given by

$$K^{-1} = \frac{A}{A+1}\frac{\sqrt{\pi}}{2a}\,\mathrm{erf}\left\{a\left[\frac{A}{A+1}E - E_\lambda)_{min}\right]\right\} + \mathrm{erf}\{a[b-c]\}. \tag{57b}$$

The parameters a, b, c, and $E_\lambda)_{min}$ may be expected to be characteristic of the target nuclide. When one or more level excitation functions of a particular scatterer have been measured, appropriate values of the parameters a, b, and c may be derived by empirically fitting the general excitation function to the measured results. For most nuclides of interest in this study, measured excitation functions are not available. Accordingly, the values

$$a = 3, \quad b = 0.8, \quad c = 0.2$$

were used for all nuclides considered. These values were derived from measured excitation functions for lead, and give reasonably good fits to the few other excitation functions available. With these parameters the group-transfer probabilities assume the final forms

$$P_{ij} = 1.711\,\frac{A+1}{A}\,\Delta E)_j \exp\left[-\left\{3\left(\frac{A+1}{A}E_j - 0.8\right)\right\}^2\right], \tag{58a}$$

for the normal (untruncated) case, and

$$P_{ij} = 2.821\,\frac{A+1}{A}\,\Delta E)_j \exp\left[-\left\{3\left(\frac{A+1}{A}E_j - 0.8\right)\right\}^2\right] \cdot \mathrm{erf}\left[3\left\{\frac{A}{A+1}E - E_\lambda)_{min}\right\}\right] + 0.98909 \tag{58b}$$

for the truncated case.

3.4 ANGULAR CORRELATION MODELS

Before considering the problem of neutron transport between collisions, it is appropriate to make some remarks regarding angular correlations in the several scattering reactions. Examination of differential elastic scattering cross sections, obtained either by direct measurements (as tabulated by Hughes and Carter[39] and Gerardo,[40] for example) or by optical model calculations (e.g., by Bjorklund and Fernbach[41,42]), indicates that neutrons of high angular momenta become important in elastic scattering reactions at incident energies above a few Mev. As the incident energy increases, the influence of the high angular momentum events becomes more pronounced and elastic scatterings become correspondingly more nearly straight ahead. Furthermore, the ratio of p-wave and higher neutrons to s-wave particles increases directly, although not linearly, with the atomic mass of the scattering centers, as well as with the energy of the

incident neutrons. The result is that in the heavier scatterers nearly all neutrons having energies greater than ~5 Mev emerge from elastic events with only slight changes in direction. In lighter scatterers the anisotropy at corresponding neutron energies is somewhat less pronounced but is still significant. For incident energies below ~5 Mev the lighter scatterers tend to yield more nearly isotropically distributed neutrons as a result of elastic events, while the heavier scatterers still yield a fairly straight-ahead distribution.

In an attempt to approximate the effects of neutrons of higher angular momenta without unduly complicating the treatment of the problem, the following assumptions regarding elastic collisions will be made.

1. Above 5 Mev all elastic scatterings are straight ahead, regardless of the atomic mass of the scatterer.

2. Below 5 Mev elastic scatterings in the lighter nuclides are isotropic.

3. Below 5 Mev elastic scatterings in the heavier nuclides are treated as a mixture of straight-ahead and isotropic scattering.

Classifying nuclides as light or heavy is justified in that no nuclides of interest, with the possible exception of nickel, are in the range $20 < A < 90$. The selection of 5 Mev as the boundary between pure straight-ahead scattering and mixed or pure isotropic scattering is, of course, somewhat arbitrary. The particular value chosen represents a compromise based on the individual characteristics of the various nuclides of interest. The calculated fluxes and reaction rates are expected to be rather insensitive to the value chosen for the transition energy, since the neutron population in the energy region above a few Mev, but below fusion source energies, will be small in any practical system, owing to nonelastic scattering effects. A discussion will be given later when theory and experiments are compared.

Nonelastic scatterings in nuclides of interest proceed almost without exception via an intermediate compound nucleus. Since the basic premise of the compund-nucleus concept is a complete separation of the mechanisms of excitation and de-excitation, all such collisions are isotropic in the center of mass system. Experimental measurement bears this out rather well. In a few cases direct experimental measurement has shown that a sizable fraction of certain nonelastic events, notably those involving light scatterers or charged-particle emission, by-pass formation of a compound nucleus and yield anisotropic emergent neutron distributions. With one exception these events are of sufficiently minor importance so that anisotropy can be safely disregarded; the single exception involving carbon is amenable to treatment as a pseudo-elastic scattering. Accordingly, it is assumed that all nonelastic scatterings are isotropic regardless of incident neutron energy or target mass number.

Two final remarks are in order. First, on considering conservation of momentum, it is evident that a neutron emerging from an elastic scattering with little loss in direction must perforce have lost only a small amount of energy compared with the total allowable energy loss. Since neither direction nor energy has been appreciably disturbed

by the event, to a first approximation, it did not occur. Hence, elastic collisions, particularly in the lighter elements, in which the neutron remains in the source group after scattering, may be disregarded without serious error. In the heavier scatterers where transfer from one energy group to another is less likely, the argument is re-enforced by the principle of detailed balance, provided the neutron flux is approximately isotropic. According to this principle, changes in direction as a result of collisions tend to cancel if the neutron population is large. In heavy scatterers this leads to little loss in direction and, coupled with little loss in energy, nonoccurrence of the collisions.

Second, in view of the neutron spectra predicted by the statistical model, it is safe to assume that, in the high incident energy region where nearly all nonelastic scatterings follow the statistical model, all emergent neutrons appear at energies well below the incident energy. In particular, the assertion is made that all nonelastically scattered neutrons lose at least one-third of their incident energy to residual nucleus excitation. Inelastic excitation of discrete levels at low incident energies occasionally violate this assumption. Such events are adequately treated by considering them pseudo-elastic in nature.

On the basis of the foregoing remarks, three separate energy regimes may be distinguished in terms of the scattering angular correlations that characterize them. Neutrons appearing in the highest energy regime are the products of straight-ahead elastic scatterings only. In the next lower region neutrons may appear by virtue of isotropic nonelastic events or straight-ahead elastic events. In the lowest region neutrons are born isotropically, regardless of the scattering mechanism by which they result.

GLOSSARY

Symbol	Definition	Units
A	Mass number	
BE	Nucleon binding energy	Mev
C, C', C_1, C_2, K	Constants	
E	Neutron energy at incidence	Mev
E'	Neutron energy after scattering	Mev
$\bar{E}'$	Average neutron energy after scattering	Mev
E_H	Higher bound of energy group	Mev
E_L	Lower bound of energy group	Mev
$E_{subscript}$	Characteristic group energy	Mev
ΔE	Width of energy group	Mev
E_o	Transition energy	Mev
E_1	Maximum energy of first particle in double particle emission	Mev
E^{**}	Residual energy in C. M. system after inelastic scattering	Mev
E_λ	Energy of nuclear level	Mev
$E'', E''_\lambda, \mathscr{E}$	Variables of integration	Mev
P, Q	Probabilities	
$P_{i,j}$	Group transfer probability	
U	Residual nucleus excitation energy	Mev
a, b, c	Parameters in empirical model	
n	Energy spectrum distribution	Mev^{-1}
r	Spatial coordinate	cm
u	Lethargy	
Δu	Lethargy width of energy group	
α	Limiting value of the ratio E'/E in elastic collisions	
β	Entropy parameter	Mev^{-1}
Δ	Excess energy in empirical model	Mev

GLOSSARY (continued)

Symbol	Definition	Units
ϵ	Excitation function for inelastic scattering	cm^2
η	Number of allowed levels	
μ, μ'	Directional cosines	
ν	Scattering angle cosine	
π	Probability	
σ_c	Microscopic cross section for compound nucleus formation	cm^2
Σ	Macroscopic cross section	cm^{-1}
τ, τ^*	Nuclear temperature	Mev
$\phi(r, E)$	Scalar flux	cm^{-1} sec^{-1} Mev^{-1}
$\phi(r)$	Scalar flux integrated over energy	cm^{-1} sec^{-1}

Subscripts	Reference
i	Source group
j	Object group
J	Lowest energy object group permitted in elastic scattering
max	Maximum value
min	Minimum value
1	Single-particle emission
2	Double-particle emission

IV. NEUTRON TRANSPORT MODELS

4.1 INTRODUCTION

Neutron transport can be treated by three basic methods: integral transport, differential transport, and diffusion models. Each formulation has advantages that recommend its use in some applications and disadvantages limiting its values in others. We shall now explore each formulation, with particular emphasis on those aspects of the models that are relevant to the present problem. There is only one case in which a nontrivial analytic solution to a multigroup, multiregion problem is readily derived. We shall develop this solution for a number of configurations of interest. Solution of all other cases can be obtained by numerical methods, the nature of which will be the subject of Section V.

We have made a general assumption that the several geometric configurations to be considered are all one-dimensional in space. Scalar neutron fluxes and neutron-induced reaction rates in each configuration are assumed to be dependent only on energy and on a single spatial coordinate measuring distance from the first wall. The assumption has also been made that the external boundaries of all systems considered are perfectly absorbing. No neutrons, having once left the system, return.

4.2 INTEGRAL MODEL

a. Defining Equations for Integral Transport Theory

The integral transport formulation expresses the vector flux at a given spatial point in terms of the sum of all possible sources in the system, each source being weighted by the probability that a neutron born at the source point will contribute to the directional flux at the point in question:

$$\phi(r,\mu,\nu) = \int_{\substack{\text{all}\\ \text{space}}} dr'\, S(r',\mu',\nu')\, T(r',\mu',\nu';\, r,\mu,\nu), \tag{59}$$

where $\phi(r,\mu,\nu)$ is the directional flux at spatial coordinate r characterized by directional cosines μ and ν with respect to the axes of the coordinate system. $S(r',\mu',\nu')$ is the source strength of neutrons born at position r' with directional cosines μ' and ν', and $T(r',\mu',\nu';\, r,\mu,\nu)$ is the probability that a neutron born at r' with initial direction specified by μ' and ν' will eventually contribute without an intervening collision to the directional flux $\phi(r,\mu,\nu)$.

The formulation of the probability factor or, more properly, the transport kernel, may be illustrated by considering the describing equation in a system composed of two identical opposing slabs finite in depth only and separated by a slab void. This system is a first approximation to the infinitely long annular cylinder representing the

hypothetical thermonuclear reactor. In the slab arrangement symmetry obtains so that a single directional cosine defined with respect to a normal to the slab surface suffices

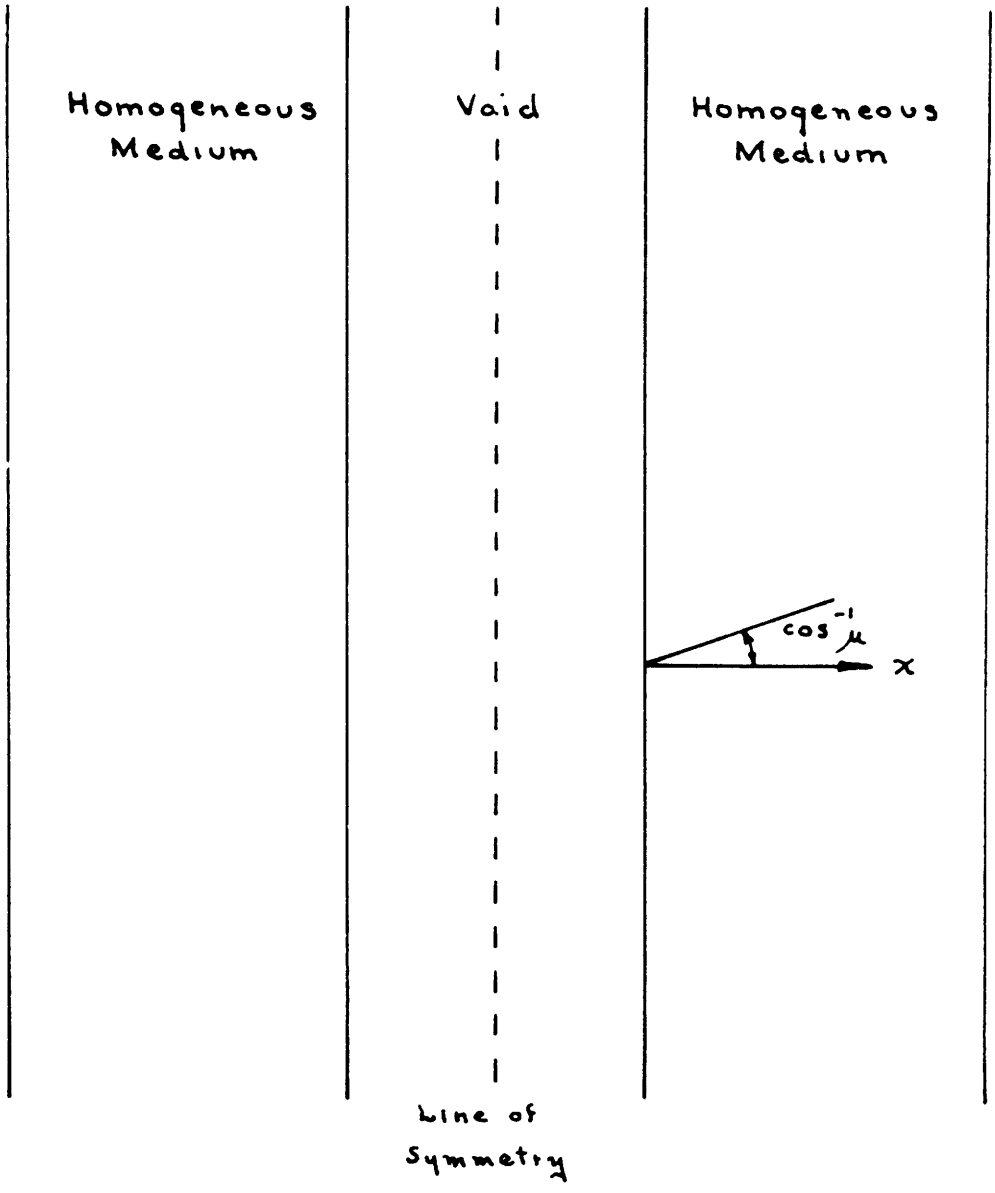

Fig. 5. Slab configuration.

to specify the direction of the vector flux. The system is sketched in Fig. 5. In this system the directional flux, $\phi(x,\mu)$, is given for the monoenergetic case by

$$\phi(x,\mu) = u^{+}(\mu)\int_0^x \frac{dx'}{\mu} S(x',\mu)\exp\left[-\frac{\Sigma_r}{\mu}(x-x')\right] + u^{+}(\mu)\int_0^X \frac{dx'}{\mu} S(x',-\mu)\exp\left[-\frac{\Sigma_r}{\mu}(x+x')\right]$$
$$+ u^{-}(\mu)\int_x^X \frac{dx'}{|\mu|} S(x',-|\mu|)\exp\left[-\frac{\Sigma_r}{|\mu|}(x'-x)\right], \qquad (60a)$$

where the functions $u^+(\mu)$ and $u^-(\mu)$ are so defined that

$$u^+(\mu) = 1, \quad u^-(\mu) = 0 \qquad \text{when } \mu > 0$$
$$u^+(\mu) = 0, \quad u^-(\mu) = 1 \qquad \text{when } \mu < 0. \tag{60b}$$

The corresponding scalar flux is given by

$$\phi(x) = \int_{-1}^{1} d\mu\, \phi(x, \mu). \tag{61}$$

The first two terms on the right-hand side of (60a) evaluate the contributions to the forward-going flux (in the increasing x sense) because of sources in the right- and left-hand slabs, respectively. The third term gives the contribution to the backward-going flux caused by sources in the right-hand slab. As is evident from the presence of factors of the form dx/μ, the integrations are in effect summations along lines of flight of the

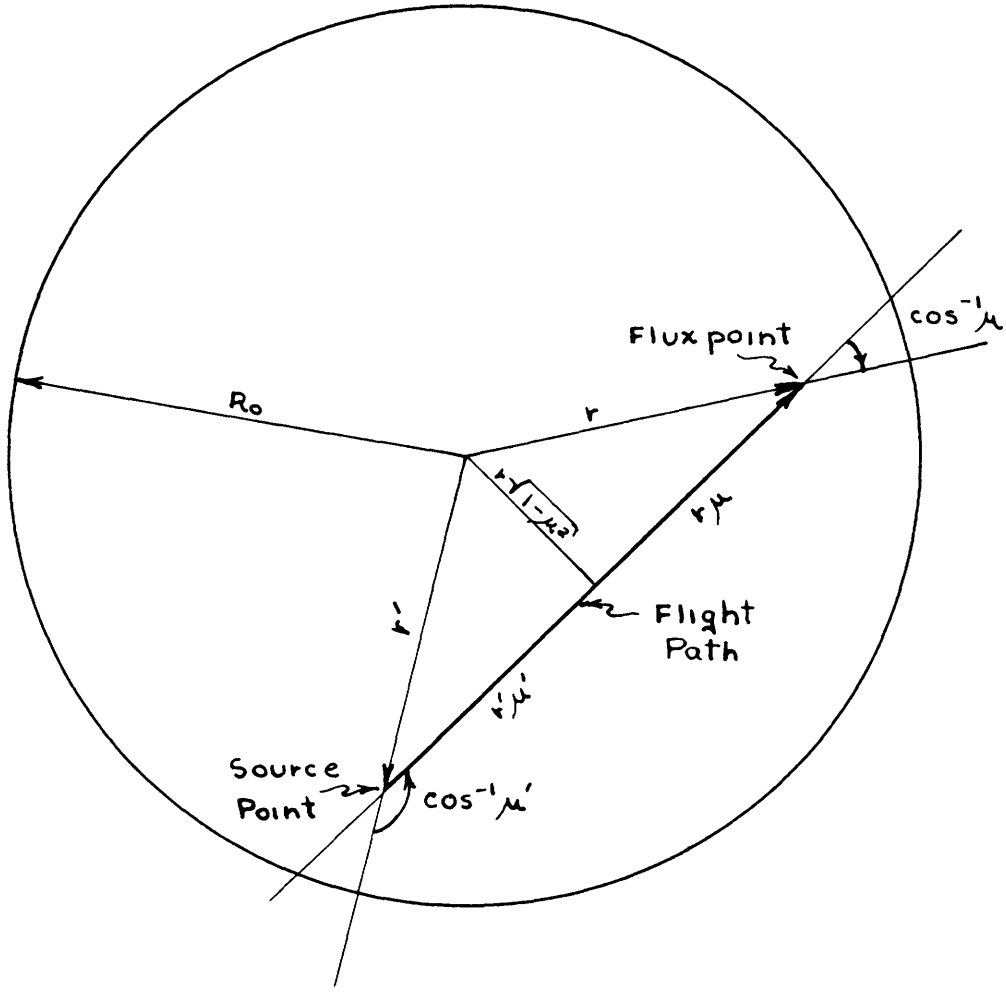

Fig. 6. Diametral plane in spherical configuration.

neutrons. In this formulation a neutron scattered in angle, with the probability of such an event given by Σ_r, is considered lost as far as its contribution to directional fluxes at more remote points on its initial line of flight is concerned. The scattering event does constitute, however, a source that will contribute to vector fluxes of the appropriate direction along a new flight path. Thus the collateral source equation in the monoenergetic case is simply

$$S(r,\mu) = \int_{-1}^{1} d\mu' \, \phi(r,\mu') \, \Sigma_r \, \pi(\mu';\mu), \tag{62}$$

where the quantity $\pi(\mu';\mu)$ describes the angular correlation appropriate to the scattering event.

Observe that the directional cosine characterizing a neutron during its flight from source to sink is invariant with respect to the position of the neutron along its flight path; that is, a neutron appearing as a source neutron at (r,μ) contributes to directional flux at (r,μ). This property is characteristic of the slab configuration and is the basis for an important simplification in the general problem of neutron transport when the problem is formulated in the slab. In the more general case the directional cosine describing the orientation of the neutron velocity vector with respect to the local radius vector varies continuously with position along the neutron flight path, and the solution of the integral transport equation is more difficult.

Consider as an illustration the monoenergetic problem formulated in a spherical shell. As in the slab, a radial coordinate and a single directional cosine suffice to specify position and direction. Details of the configuration in a diametral plane containing the neutron flight path are shown in Fig. 6. The directional flux is now given by

$$\begin{aligned}\phi(r,\mu) = {} & u^+(\mu) \int_{r\sqrt{1-\mu^2}}^{r} \frac{dr'}{\mu'} S(r',\mu') \, e^{-\Sigma_r(r\mu - r'\mu')} \left(\frac{r'}{r}\right)^2 \\ & + u^+(\mu) \int_{r\sqrt{1-\mu^2}}^{R_o} \frac{dr'}{\mu'} S(r',-\mu') \, e^{-\Sigma_r(r\mu + r'\mu')} \left(\frac{r'}{r}\right)^2 \\ & + u^-(\mu) \int_{r}^{R_o} \frac{dr'}{|\mu'|} S(r',\mu') \, e^{-\Sigma_r(r'|\mu'| - r\mu)} \left(\frac{r'}{r}\right)^2 .\end{aligned} \tag{63a}$$

The directional cosine μ' collateral with the flight path at radial position r', and yielding directional cosine μ at point r, can be expressed in the form

$$\mu' = \sqrt{1 - \left(\frac{r}{r'}\right)^2 (1-\mu^2)} \, . \tag{63b}$$

Integration thus proceeds along flight paths whose orientation with respect to the radius vector varies continuously with position.

In a cylindrical arrangement, two directional cosines, describing azimuthal and elevational orientation, are required. If these cosines are designated μ and ν, respectively, and symmetry in the elevational direction is invoked, the directional flux in the cylinder is given by

$$\phi(r,\mu,\nu) = u^{+}(\mu) \int_{r\sqrt{1-\mu^2}}^{r} \frac{dr'}{\nu\mu'} S(r',\mu',\nu) \exp\left[-\frac{\Sigma_r}{\nu}(r\mu - r'\mu')\right] \left(\frac{r'}{r}\right)$$

$$+ u^{+}(\mu) \int_{r\sqrt{1-\mu^2}}^{R_o} \frac{dr'}{\nu\mu'} S(r',-\mu',\nu) \exp\left[-\frac{\Sigma_r}{\nu}(r\mu + r'\mu')\right] \left(\frac{r'}{r}\right)$$

$$+ u^{-}(\mu) \int_{r}^{R_o} \frac{dr'}{\nu|\mu'|} S(r',\mu',\nu) \exp\left[-\frac{\Sigma_r}{\nu}(r'|\mu'| - r\mu)\right] \left(\frac{r'}{r}\right). \qquad (64)$$

Although the elevational cosine, ν, is independent of position along a flight path, the dependence on position of μ' in azimuth is clearly evident, and is indeed identical to the dependence of the symmetric directional cosine on position noted in the sphere. In the cylindrical case the symmetry existent in the elevational direction allows consideration to be limited to only the positive values of the elevational directional cosine. Hence, in this case, the scalar flux is given by

$$\phi(r) = \int_0^1 d\nu \int_{-1}^{1} d\mu\, \phi(r,\mu,\nu). \qquad (65)$$

b. Merit and Demerits of the Integral Model

It should be noted that in the integral transport treatment, conservation of neutrons is obtained implicitly (rather than explicitly as in the differential methods). "Implicitly" is used here in the sense that sources and sinks are balanced over the region of computation, but a direct statement of balance in a differential volume in the region of interest is not included in the defining equation. The integral method is susceptible not only to errors arising from approximate evaluation of the integrals, as are all methods, but also to accumulation of errors in iterative solutions. The integral formulation has the decided merit, on the other hand, of making it possible to assess directly contributions to the vector flux at interior points resulting from sources exterior to the region of calculation. An illustration of the method of treating appropriate external sources, and the implications of this characteristic of the integral method, will be developed in this section.

4.3 DIFFERENTIAL MODELS

a. Defining Equations for Differential Transport Theory

The differential transport formulation expresses the vector flux at a given point in terms of a balance of currents, sources and sinks in a differential element of volume

including the point. In its general form the defining equation is given as

$$\overline{\Omega} \cdot \text{grad}_x \, \phi(r, \overline{\Omega}) + \Sigma_r \phi(r, \overline{\Omega}) = S(r, \overline{\Omega}). \tag{66}$$

In this formulation $\overline{\Omega}$ specifies the direction of the vector flux, and the operator grad_x is the gradient operating in physical space. More convenient equations in terms of the directional cosines that have been used previously can readily be formulated. Following Carlson,[43] expressions appropriate to the several configurations of interest are given as follows:

Slab

$$\mu \frac{\partial}{\partial r} \phi(r, \mu) + \Sigma_r \phi(r, \mu) = S(r, \mu); \tag{67a}$$

Sphere

$$\left\{ \mu \frac{\partial}{\partial r} + \frac{(1-\mu^2)}{r} \frac{\partial}{\partial \mu} \right\} \phi(r, \mu) + \Sigma_r \phi(r, \mu) = S(r, \mu); \tag{67b}$$

Cylinder

$$\left\{ \sqrt{1 - \nu^2} \left[\mu \frac{\partial}{\partial r} + \frac{(1-\mu^2)}{r} \frac{\partial}{\partial \mu} \right] \right\} \phi(r, \mu, \nu) + \Sigma_r \phi(r, \mu, \nu) = S(r, \mu, \nu). \tag{67c}$$

b. Defining Equations for Diffusion Theory

Diffusion theory also makes use of the concept of neutron balance in differential volumes. In fact, the essential differences between the diffusion model and differential transport theory, at least for the purposes of this study, lie only in the manner in which leakage is described and in the use of scalar flux in diffusion calculations in lieu of the directional flux of transport calculations.

The describing equation has the familiar form

$$-\nabla \cdot D \nabla \phi(r) + \Sigma_r \phi(r) = S(r), \tag{68}$$

where D is the diffusion coefficient, and ∇ the differential vector operator. Expressing the divergence of the gradient in terms of the positional coordinate in the several configurations of interest, one obtains

Slab

$$-\frac{\partial}{\partial r} D \frac{\partial}{\partial r} \phi(r) + \Sigma_r \phi(r) = S(r); \tag{69a}$$

Cylinder

$$-\frac{1}{r} \frac{\partial}{\partial r} \left\{ rD \frac{\partial}{\partial r} \phi(r) \right\} + \Sigma_r \phi(r) = S(r); \tag{69b}$$

Sphere

$$-\frac{1}{r^2}\frac{\partial}{\partial r}\left\{r^2 D \frac{\partial}{\partial r}\phi(r)\right\} + \Sigma_r \phi(r) = S(r). \tag{69c}$$

c. Merits and Demerits of the Differential Models

By comparison with the integral transport method, several important characteristics of the differential transport and diffusion models are evident.

1. These two methods have the common property of requiring neutron conservation at all points in space. Hence accumulation of errors introduced by numerical integration of the differential equations is avoided when iterative solutions are necessary.

2. In both formulations the flux at a point is dependent explicitly on sources only in the immediate vicinity. Therefore the dependence of the azimuthal or symmetric directional cosine on position along a neutron flight path, which poses a serious complication to the integral treatment of cylinders and spheres, is of no consequence in the differential transport and diffusion treatments.

3. The flux at a point is linked to sources at more remote points only by gradient operators. Hence description of the influence of sources external to the region of computation on fluxes at internal points requires the intermediate agency of boundary conditions.

4.4 GENERALIZATION OF THE MODELS

a. Multiregion Applications

All three models discussed thus far in the context of a monoenergetic problem formulated in a homogeneous medium can readily be generalized to systems involving spatial and energy dependence. In the foregoing discussions the assumption of a single homogeneous medium has been made in the interests of simplicity. When vector fluxes are being treated explicitly, generalization to a succession of individually homogenized subregions or to media whose neutron attenuation properties vary continuously with the spatial coordinate can readily be accomplished, at least in the formal sense. The constant removal cross section, Σ_r, need only be replaced by a variable, $\Sigma_r(r)$, whose magnitude depends on position. In diffusion calculations treating scalar fluxes only, the simple substitution of a variable $\Sigma_r(r)$ breaks down at boundaries, and average values of the diffusion coefficient and the removal cross section, the former based on conservation of neutron current, must be incorporated with attendant loss of accuracy.

b. Multigroup Applications

By utilizing the group transfer probabilities, P_{ij} discussed in Section III and appropriate scattering cross sections, $\Sigma_s)_i$, and by writing the source equation in the form

$$S_j(r,\mu,\nu) = \sum^{i} \int_0^1 d\nu' \int_{-1}^{1} d\mu' \, \phi_i(r,\mu',\nu') \, \Sigma_s)_i \, P_{ij}\pi(\mu',\nu';\mu,\nu) \tag{70}$$

generalization to a succession of monoenergetic cases or, for the purposes of this study, to a multigroup treatment is obtained.

In keeping with the remarks made at the end of Section III, only the purely straight-ahead and purely isotropic directional correlations, characterized in the source equation (70), by $\pi(\mu', \nu'; \mu, \nu)$, will be considered. In these limiting cases the multigroup source equation for straight-ahead scattering takes the form

$$S_j(r, \mu, \nu) = \sum^i \phi_i(r, \mu, \nu)\, \Sigma_s)_i\, P_{ij}; \tag{71}$$

and for isotropic scattering,

$$S_j(r, \mu, \nu) = \sum^i \frac{\phi_i(r)}{2} \Sigma_s)_i\, P_{ij}. \tag{72}$$

4.5 TREATMENT OF IN-GROUP SCATTERING

An interesting comparison of the several neutron transport methods may be made by considering the effect of "in-group" sources. By this is meant those sources arising from scatterings in which the incident neutron loses so little energy in scattering that it remains in the source group after the collision. Such sources are of greatest importance in media composed of heavy nuclides, particularly for energies near or below the inelastic threshold. In default of direct analytical solutions to the relevant equations, such sources can be treated explicitly only by iterative solutions. As we have pointed out, the integral transport method is subject to accumulation of errors during iteration. Thus, only single-pass solutions in which the in-group sources are ignored by virtue of the arguments cited at the conclusion of Section III are practical. The differential transport and diffusion treatments do not accumulate errors, and iteration with direct incorporation of the effects of in-group sources is entirely feasible. Diffusion theory has the additional advantage of including at least an approximate compensation for the transfer from the center-of-mass coordinates, in which collisions actually occur, to laboratory coordinates where the calculations are made. In anticipation of some later remarks, it may be noted that in blanket configurations of interest, calculations made by integral transport procedures excluding in-group sources, and by differential transport or diffusion methods including these sources, show little dependence of over-all effects such as tritium-breeding ratio on the method of calculation, at least at the higher energies. Local effects, particularly capture in heavy media, do reveal marked influence of method on result.

4.6 OUTLINE OF AN ANALYTIC SOLUTION

a. The Formulation Considered

Although solutions for various restrictive cases are known, generation of analytic solutions to any of the describing equations in a typical multigroup-multiregion problem

of practical interest is, on the whole, prohibitive. In most cases recourse is had to numerical solution of equations by utilizing various approximation techniques of which more will be said in Section V. In the specialized, but none-the-less interesting, case of pure straight-ahead scattering at high neutron incident energies, a convenient analytical solution can be obtained for multigroup-multiregion formulations of the integral transport method in all configurations of interest.

It has been observed in discussing the directional correlations appropriate to neutron transport calculations that neutrons appearing in the region of highest neutron energies are either uncollided or are the product of straight-ahead elastic scattering. It has also been stated that the integral transport method alone has the capability of treating external sources directly. Hence the one case in which an analytical solution, exact within the validity of the straight-ahead scattering approximation, is available is precisely that which permits a direct assessment of the effect of the distribution of the fusion-born primary-source neutrons on fluxes and reaction rates within the blanket assembly proper. We shall now outline the method underlying this analytical solution and summarize the results of pursuing the method in configurations of interest.

b. Method of Attack

Consider the integral formulation in terms of the external sources. The contribution to the vector flux having a prescribed orientation in a specific energy group and at a given interior point in the spatial region of computation, because of these external sources, is the product of a source integral factor and a "collision factor." The source integral is the sum of the contributions to the directional flux in question of all allowed differential source volumes in the absence of neutron attenuation by collision. The collision factor is the probability that a neutron born in the external region will experience appropriate elastic scatterings during its passage from the source to the interior point such that it arrives at the desired point in the specified energy group.

c. Development of the Collision Factor

It is convenient to discuss the details of the calculation of the two factors in reverse order. Consider a medium which, for simplicity, is homogeneous and establish a generalized space coordinate, ρ, whose exact nature depends on the configuration, to represent distance from the medium first surface to a specified interior point measured along a flight path.

Depending on the number of energy groups intervening between the source group and the object group, several different combinations of elastic scattering events involving transfers from group to group can yield a neutron in the specified group at the required point. Several such processes involving the source group and the next two lower energy groups are diagramed in Fig. 7. It is now desirable to define three probabilities: $L_i(\rho)$ is the probability that a neutron in group i will travel a distance ρ without experiencing a collision; $M_{i,j...n,p}(\rho)$ is the probability that a neutron incident on the first wall of

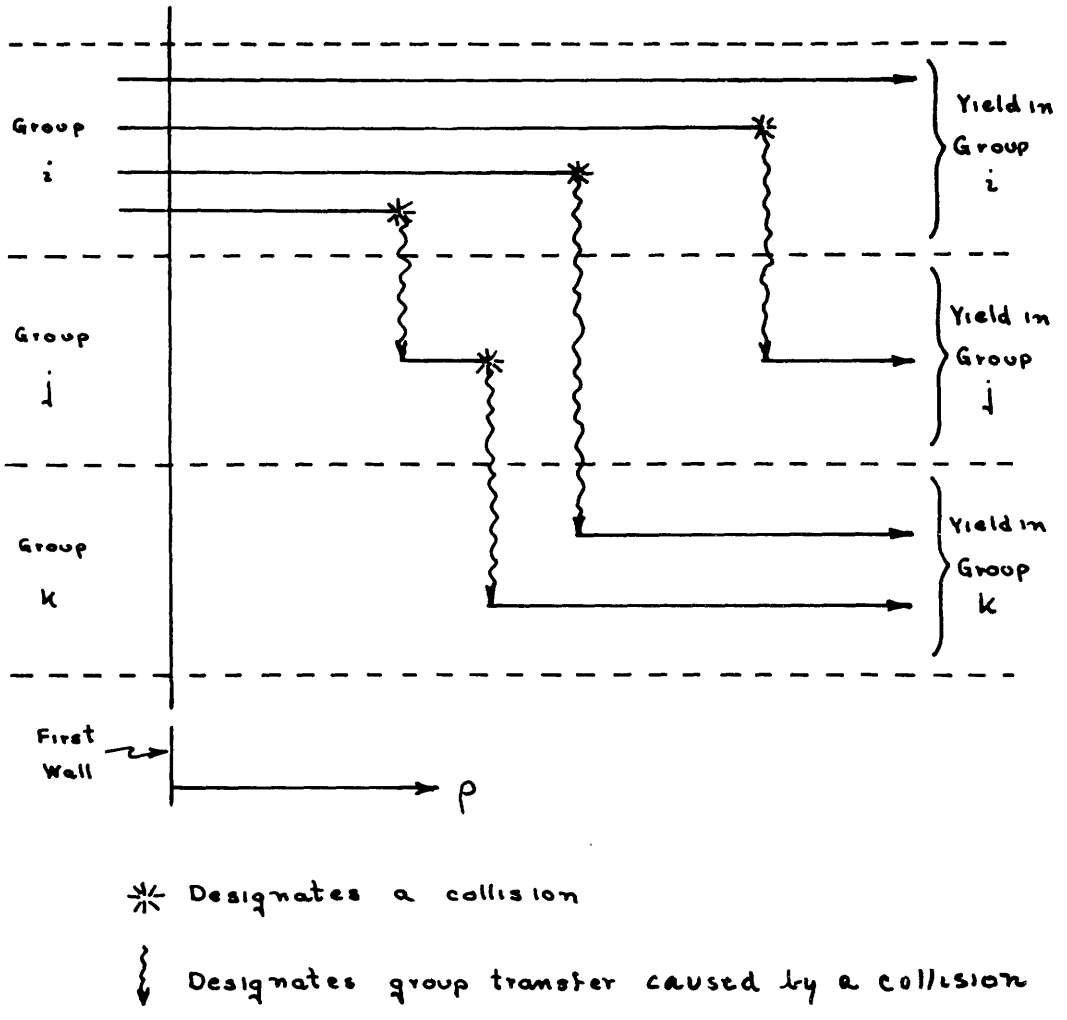

Fig. 7. Schematic life histories of primary-source neutrons in a homogeneous medium.

the medium in group i will experience successive collisions in groups i, j ... n and emerge in group p while penetrating to depth ρ; $N_{i,p}(\rho)$ is the total probability that a neutron incident on the first wall of the medium in group i will be in group p when it has penetrated to depth ρ. Applying these definitions, one may write immediately

$$N_{ii}(\rho) = L_i(\rho) \tag{73a}$$

$$N_{ij}(\rho) = M_{ij}(\rho) \tag{73b}$$

$$N_{ik}(\rho) = M_{ik}(\rho) + M_{ijk}(\rho), \tag{73c}$$

and so on. One may now proceed to evaluate the first few L and M probabilities. One obtains immediately

$$L_i(\rho) = e^{-\Sigma_r|_i \rho}, \tag{74}$$

where $\Sigma_{r|i}$ is the group removal cross section for group i. If the scattering cross section, $\Sigma_{s|i}$ is incorporated, there follows

$$M_{ij}(\rho) = \int_0^\rho d\rho' \, L_i(\rho') \, \Sigma_{s|i} \, P_{ij} L_j(\rho-\rho'). \tag{75}$$

Substituting, one obtains

$$M_{ij}(\rho) = \Sigma_{s|i} \, P_{ij} \int_0^\rho d\rho' \, e^{-\Sigma_{r|i}\rho'} \, e^{-\Sigma_{r|j}(\rho-\rho')}. \tag{76a}$$

Performing the integration yields

$$M_{ij}(\rho) = \Sigma_{s|i} \, P_{ij} \left\{ \frac{e^{-\Sigma_{r|i}\rho}}{\Sigma_{r|j} - \Sigma_{r|i}} + \frac{e^{-\Sigma_{r|j}\rho}}{\Sigma_{r|i} - \Sigma_{r|j}} \right\}. \tag{76b}$$

The procedure is readily extended to include three groups by considering

$$M_{ijk}(\rho) = \int_0^\rho d\rho' \, M_{ij}(\rho') \, \Sigma_{s|j} \, P_{ij} L_k(\rho-\rho'). \tag{77a}$$

Substituting and integrating, one gets

$$M_{ijk}(\rho) = \Sigma_{s|i} \, P_{ij} \, \Sigma_{s|j} \, P_{jk} \left\{ \frac{e^{-\Sigma_{r|i}\rho}}{(\Sigma_{r|j}-\Sigma_{r|i})(\Sigma_{r|k}-\Sigma_{r|i})} + \frac{e^{-\Sigma_{r|j}\rho}}{(\Sigma_{r|i}-\Sigma_{r|j})(\Sigma_{r|k}-\Sigma_{r|j})} + \frac{e^{-\Sigma_{r|k}\rho}}{(\Sigma_{r|i}-\Sigma_{r|k})(\Sigma_{r|j}-\Sigma_{r|k})} \right\}. \tag{77b}$$

By analogy, the probabilities for scattering chains of arbitrary length can readily be formulated.

The nondivergence of the M_{ij} probability in the limit as $\Sigma_{r|j}$ approaches $\Sigma_{r|i}$ is easily demonstrated by considering the series expansion of M_{ij}. Thus

$$M_{ij}(\rho) = \frac{\Sigma_{s|i} \, P_{ij}}{(\Sigma_{r|j}-\Sigma_{r|i})} \left\{ e^{-\Sigma_{r|i}\rho} - e^{-\Sigma_{r|j}\rho} \right\} \tag{78a}$$

which yields upon expansion

$$M_{ij}(\rho) = \frac{\Sigma_{s|i} \, P_{ij}}{(\Sigma_{r|j}-\Sigma_{r|i})} \left\{ (\Sigma_{r|j}-\Sigma_{r|i})\rho - \left(\Sigma_{r|j}^2-\Sigma_{r|i}^2\right)\frac{\rho^2}{2!} + \left(\Sigma_{r|j}^3-\Sigma_{r|i}^3\right)\frac{\rho^3}{3!} + \cdots \right\} \tag{78b}$$

and finally,

$$M_{ij}(\rho) = \Sigma_{s|i}\, P_{ij}\rho\left\{1 - (\Sigma_{r|j}+\Sigma_{r|i})\frac{\rho}{2!} + \left(\Sigma_{r|j}^2+\Sigma_{r|j}\Sigma_{r|i}+\Sigma_{r|i}^2\right)\frac{\rho^2}{3!} + \cdots\right\}. \tag{78c}$$

Consider the limiting case:

$$\underset{\Sigma_{r|j}\to\Sigma_{r|i}}{\text{Limit}}\ M_{ij} = \Sigma_{s|i}\, P_{ij}\rho\left\{1 - 2\Sigma_{r|i}\frac{\rho}{2!} + 3\Sigma_{r|i}\frac{\rho^2}{3!} + \cdots\right\} \tag{78d}$$

$$\underset{\Sigma_{r|j}\to\Sigma_{r|i}}{\text{Limit}}\ M_{ij} = \Sigma_{s|i}\, P_{ij}\left\{\rho\, e^{-\Sigma_{r|i}\rho}\right\}. \tag{78e}$$

Extending the series expansion procedure to a chain of two scatterings, and considering the limit as both $\Sigma_{r|j}$ and $\Sigma_{r|k}$ approach $\Sigma_{r|i}$, one obtains

$$\underset{\substack{\Sigma_{r|j}\to\Sigma_{r|i}\\ \Sigma_{r|k}\to\Sigma_{r|i}}}{\text{Limit}}\ M_{ijk} = \Sigma_{s|i}\, P_{ij}\, \Sigma_{s|j}\, P_{jk}\left\{\frac{\rho^2}{2} e^{-\Sigma_{r|i}\rho}\right\}. \tag{79}$$

By analogy, the nondivergence of chains of arbitrary length is demonstrable.

d. Collision Factor in Multiregion Configurations

The foregoing method of calculating group-transfer factors (as opposed to the P_{ij} probabilities) in homogeneous media may be extended to multiregion systems by assigning the requisite probabilities in each subregion and by using spatial coordinates in each subregion measured from the first surface of the subregion. The analytical expressions for the L, M, and N probabilities in the subregions are formally identical to those developed above for the single-region case. Since distances are to be defined with respect to the subregion first surfaces, the generalized spatial coordinates a and b will be used to measure penetration. Also, the superscripts A and B will be introduced to differentiate probabilities defined in terms of nuclear properties in subregions A and B, respectively, where A is the first subregion encountered by primary source neutrons.

In the straight-ahead scattering approximation with all primary sources specified to be outside of the region of computation, events occurring in subregion B have no bearing on those in subregion A if primary-source neutrons encounter A first. Thus the N^A probabilities are precisely those of a single-region problem. On the other hand, neutrons emerging from the last surface of subregion A constitute the sources for subregion B, and the N^B probabilities must, in general, include a greater variety of life histories than did the homogeneous case.

Combining appropriate probabilities in subregions A and B, and considering neutrons at penetration $\rho = A + b$, one obtains for the over-all probabilities of appearance of neutrons in the first three groups at depth ρ

$$N_{ii}(\rho) = L_i^A(A)\, L_i^B(b) \tag{80a}$$

$$N_{ij}(\rho) = L_i^A(A)\, M_{ij}^B(b) + M_{ij}^A(A)\, L_j^B(b) \tag{80b}$$

$$N_{ik}(\rho) = L_i^A(A)\, M_{ik}^B(b) + L_i^A(A)\, M_{ijk}^B(b) + M_{ik}^A(A)\, L_k^B(b) + M_{ijk}^A(A)\, L_k^B(b) + M_{ij}^A(A)\, M_{jk}^B(b). \tag{80c}$$

Obviously, the permutation of transmission and collision terms soon becomes unmanageable as the neutrons are pursued through additional groups in many-region systems, although the procedures are straightforward.

e. Development of the Source Integral

In a homogeneous slab medium, the directional flux in energy group p at true depth x along a normal, resulting from an external isotropic group i source, is

$$\phi_p(x,\omega)\, d\omega = \int_{\text{source}} \frac{d\lambda}{\cos\omega} \left\{ 2\pi \frac{(\lambda+x)^2}{\cos\omega} \tan\omega\, d\omega \right\} \left\{ \frac{S(\lambda)}{\frac{4\pi(\lambda+x)^2}{\cos^2\omega}} \right\} N_{ip}\left(\frac{x}{\cos\omega}\right). \tag{81a}$$

In this expression the variable of integration, λ, measures true depth from the first surface into the source region, the integral extending over the full depth of the region. The angle $\omega = \cos^{-1}\mu$ specifies direction. Since the group-transfer factor N_{ip} is independent of source, the equation can be written as

$$\phi_p(x,\omega)\, d\omega = N_{ip}\left(\frac{x}{\cos\omega}\right) \int_{\text{source}} \frac{d\lambda}{\cos\omega} \left\{ \frac{2\pi(\lambda+x)^2}{\cos\omega} \tan\omega\, d\omega \right\} \frac{S(\lambda)\cos^2\omega}{4\pi(\lambda+x)^2}. \tag{81b}$$

The direct coupling of exterior sources to interior fluxes is evident in the presence of the quantity $(\lambda+x)$ in the source integral.

If the assumption is made that the primary sources are uniformly distributed in a slab $\mathscr{L}$ units thick with specific source strength S, Eq. 81b reduces to

$$\phi_p(x,\omega)\, d\omega = N_{ip}\left(\frac{x}{\cos\omega}\right) \frac{S}{2} \tan\omega\, d\omega \int_0^{\mathscr{L}} d\lambda. \tag{81c}$$

On transforming to directional cosines,

$$\phi_p(x,\mu)\, d\mu = N_{ip}\left(\frac{x}{\mu}\right) \frac{S\mathscr{L}}{2\mu}\, d\mu. \tag{81d}$$

The quantity $S\mathscr{L}/2\mu$ is the unattenuated source integral desired. It is obvious that similar derivations will yield appropriate source integral factors which are, in general, functions both of the source configuration and size and of the penetration into, and configuration of, the region of computation.

f. Source Integrals in Other Configurations

A number of configurations are of immediate or potential interest within the scope of this study. Included among them are slabs with slab sources emitting neutrons either straight ahead or distributed in angle, cylinders with line or cylindrical sources, and spheres with point and spherical sources. Rather than reproduce the straight-forward but tedious derivations yielding the source integrals and the effective penetrations required by this analytical solution of the transport method in the several configurations, it is considered sufficient to tabulate these expressions for each configuration. In Table 2 the source integral and penetration distance for each of the various configurations are listed. In each case the sources are assumed to be isotropic (except in the slab/distributed source configuration) and uniform. The source strength is normalized to

Table 2. Source integrals and penetration terms for analytic solution of the integral transport formulation for straight ahead scattering.

Geometry/Source	Source Integral	Penetration
Slab/Straight Ahead (sec^{-1} cm^{-2})	1	x
Slab/Diffuse Slab (sec^{-1} cm^{-2})	$D(\mu)$ (as specified)	$\frac{x}{\mu}$
Cylinder/Line (sec^{-1} cm^{-1})	$\frac{1}{2\pi(R+r)\sqrt{1-\nu^2}}$	$\frac{r}{\nu}$
Cylinder/Cylinder (sec^{-1} cm^{-1})	$\frac{\sqrt{R_p^2-(R+r)^2(1-\mu^2)}}{\pi^2 R_p^2\sqrt{1-\mu^2}\sqrt{1-\nu^2}}$	$\frac{(R+r)\mu-\sqrt{R^2-(R+r)^2(1-\mu^2)}}{\nu}$
Sphere/Point (sec^{-1})	$\frac{1}{4\pi(R+r)^2}$	r
Sphere/Sphere (sec^{-1})	$\frac{3\sqrt{R_p^2-(R+r)^2(1-\mu^2)}}{4\pi R_p^3}$	$(R+r)\mu-\sqrt{R^2-(R+r)^2(1-\mu^2)}$

R_p is the source radius
R is the inner-wall radius
x, r are normal depths
μ, ν are directional cosines

unit neutron per unit time per unit dimension in the unbounded direction. The penetrations are measured from the first surface of the appropriate subregion.

GLOSSARY

Symbol	Reference	Unit
A	Total thickness of subregion A	cm
D	Diffusion coefficient	cm
$D(\mu)$	Source directional distribution function	
$\mathscr{L}, R_p$	Maximum dimension of source	cm
L, M, N	Group transfer factors	
p	Group transfer probability	
R	First surface radius	cm
R_o, X	Maximum dimension of attenuator	cm
$S(r, \mu, \nu)$	Directional source strength	$cm^{-3}\ sec^{-1}$
$S(r)$	Scalar source strength	$cm^{-3}\ sec^{-1}$
T	Transport kernel	
a, b, ρ, ρ'	Generalized penetration distances	cm
r, r', x, x'	Spatial coordinates in attenuator	cm
λ	Spatial coordinate in source	cm
μ, μ', ν, ν'	Directional cosines	
π	Directional correlation in scattering	
Σ_r	Macroscopic removal cross section	cm^{-1}
Σ_s	Macroscopic scattering cross section	cm^{-1}
$\phi(r, \mu, \nu)$	Directional flux	$cm^{-2}\ sec^{-1}$
$\phi(r)$	Scalar flux	$cm^{-2}\ sec^{-1}$
ω	Angle	
$\overline{\Omega}$	Unit vector	

Superscripts	Reference
A	Subregion A
B	Subregion B
i, j, k, p	Energy groups

V. METHODS OF NUMERICAL APPROXIMATION

5.1 INTRODUCTION

It has been pointed out that analytical solution of the neutron transport equations in any of the three common formulations in typical multigroup, multiregion problems is not practical except under restrictive circumstances. One such limited solution, which is directly applicable to the present problem, was developed in Section IV.

In default of direct analytical solutions to the transport equations in more general cases, we must have recourse to one of two alternatives. Either concessions must be made in the physics of the problem and simplified physical models that are amenable to analytical treatment must be utilized or approximate solutions to the more realistic (and less tractable) equations that better describe the true problem must be accepted. For the purposes of the present work, more useful answers to the problem of blanket feasibility can be obtained by pursuing the latter choice and making use of various approximate numerical equivalents to analytic operators.

Many numerical methods have been developed in recent years to expedite numerical solution of the neutron diffusion equation, especially for configurations of interest in thermal nuclear reactor applications. Representative of these various techniques are those utilized by Varga[44] and Bilodeau[45] and by Fischer.[46,47]

Of more direct interest in the present study are methods suitable for use in solving the defining equations for the differential and integral transport models. Techniques appropriate to the differential model have been developed in the past under the general title of the S_n method. This study uses the original S_n formulation of Carlson with but minor variations. Relevant details concerning approximations and procedures are to be found in the original descriptive report.[43] Efforts directed toward solving the integral transport equations have been more along the lines of introducing approximations in the physical models and developing analytic solutions to the simplified equations. The moments method developed by Spencer and Fano[48,49] and applied by Certaine,[50] among others, to problems dealing with neutral-particle transport in infinite homogeneous media, is indicative of the general method of attack.

On this account it has been necessary to develop an approximate method for solving the integral transport equations in the various configurations of interest. It is the purpose here to outline several of the numerical approximations that have been used in treating the integral transport model.

The computation of the scalar flux at a point in terms of the integral transport method involves carrying out two successive integrations. The first proceeds along a neutron flight path and sums the contribution of sources to the vector flux; the second is over direction and computes the contributions of the vector fluxes to the scalar flux. In all but the highest energy regime, in which the straight-ahead scattering approximation permits exact spatial integration, both of these integrals are evaluated approximately to

yield values of the directional and scalar flux at discrete mesh points in space and directional cosine.

5.2 SPATIAL QUADRATURE

a. Defining Equations

The spatial integration can be reduced to a series of integrations over intervals lying between successive space points. The integral over one such interval has the forms:

In the slab

$$I = \int_{x_1}^{x_2} \frac{dx'}{|\mu|} S(x', \mu) \exp\left[\frac{\sigma\Sigma}{|\mu|}(X-x')\right]; \tag{82a}$$

In the cylinder

$$I = \int_{r_1}^{r_2} \frac{dr'}{\nu} \frac{r'}{\sqrt{(r')^2 - r^2(1-\mu^2)}} S(r', \mu) \left(\frac{r'}{r}\right)$$

$$\cdot \exp\left[\frac{\sigma\Sigma}{\nu}\left\{\sqrt{(r')^2 - r^2(1-\mu^2)} - \sqrt{R^2 - r^2(1-\mu^2)}\right\}\right]; \tag{82b}$$

In the sphere

$$I = \int_{r_1}^{r_2} dr' \frac{r'}{\sqrt{(r')^2 - r^2(1-\mu^2)}} S(r', \mu') \left(\frac{r'}{r}\right)^2$$

$$\cdot \exp\left[\sigma\Sigma\left\{\sqrt{(r')^2 - r^2(1-\mu^2)} - \sqrt{R^2 - r^2(1-\mu^2)}\right\}\right]. \tag{82c}$$

In these expressions r_1 and r_2 or, alternatively, x_1 and x_2 are the spatial locations of the bounding mesh points, R or X is a reference location, Σ is the removal cross section, and σ has the value (± 1), the sign depending on the direction of neutron travel. Unprimed space and directional cosine variables refer to the directional flux that is being evaluated. It should be noted that values of the source strength, $S(r, \mu)$, are available only at mesh points.

b. Treatment of the Slab

The slab case is obviously the most tractable and will be treated first. With the substitution

$$\rho = \frac{-\sigma\Sigma x'}{|\mu|} \tag{83a}$$

Eq. 82a takes the form

$$I = \frac{e^{-\rho(X)}}{\sigma\Sigma} \int_{\rho_1}^{\rho_2} d\rho\, S(\rho,\mu)\, e^{\rho} \tag{83b}$$

The source is approximated by a linear function of path length, so that

$$S'(\rho,\mu) \approx a\rho + b \tag{84a}$$

with

$$a = \frac{S(x_1,\mu) - S(x_2,\mu)}{x_1 - x_2} \tag{84b}$$

and

$$b = \frac{x_1 S(x_2,\mu) - x_2 S(x_1,\mu)}{x_1 - x_2}. \tag{84c}$$

If Eq. 84a is substituted in Eq. 83b, analytical integration yields

$$I \approx \frac{e^{-\rho(X)}}{\sigma\Sigma} \left\{[a(\rho-1)+b]e^{\rho}\right\}\Big|_{\rho_2}^{\rho_1} \tag{85a}$$

and, finally,

$$I \approx \frac{e^{-\rho(X)}}{\sigma\Sigma} \left\{[a(\rho_1-1)+b]e^{\rho_1} - [a(\rho_2-1)+b]e^{\rho_2}\right\}. \tag{85b}$$

The quadrature expression could, of course, be expressed in terms of the original variables, but computation is simpler with the ρ variable.

c. Treatment of the Cylinder

The cylindrical integration proceeds in much the same way. With a substitution in terms of path length in the form

$$\rho = \frac{\Sigma}{\nu} \sqrt{(r')^2 - r^2(1-\mu^2)}\,, \tag{86a}$$

we obtain

$$I = \frac{\nu\, e^{-\sigma\rho(R)}}{r\Sigma^2} \int_{\rho_1}^{\rho_2} d\rho\, S'(\rho,\mu') \left\{\rho^2+\lambda^2\right\}^{1/2} e^{\sigma\rho}, \tag{86b}$$

where

$$\lambda^2 = \left\{\frac{\Sigma r\sqrt{1-\mu^2}}{\nu}\right\}^2. \tag{86c}$$

Integration is expedited by making the approximation

$$S'(\rho,\mu') \left\{\rho^2+\lambda^2\right\}^{1/2} \approx a(\rho^2+\lambda^2) + b, \tag{87a}$$

where

$$a = \frac{\nu}{\Sigma}\left\{\frac{r_2 S[r_2, \mu(r_2)] - r_1 S[r_1, \mu(r_1)]}{r_2^2 - r_1^2}\right\} \tag{87b}$$

$$b = \frac{\Sigma}{\nu} r_1 r_2 \left\{\frac{r_2 S[r_1, \mu(r_1)] - r_1 S[r_2, \mu(r_2)]}{r_2^2 - r_1^2}\right\}. \tag{87c}$$

Introducing this approximation is equivalent to stating that

$$S(r) \approx cr + \frac{d}{r}, \tag{88}$$

where the dependence of S(r) on r^{-1} is consistent with the cylindrical configuration. Then,

$$I \approx \frac{\nu e^{-\sigma\rho(R)}}{r\Sigma^2} \int_{\rho_1}^{\rho_2} d\rho \left\{a(\rho^2+\lambda^2)+b\right\} e^{\sigma\rho}. \tag{89}$$

An additional substitution

$$\epsilon = \sigma\rho \tag{90a}$$

yields

$$I \approx \frac{\sigma\nu e^{-\epsilon(R)}}{r\Sigma^2} \int_{\epsilon_1}^{\epsilon_2} d\epsilon \left\{a\epsilon^2+(a\lambda^2+b)\right\} e^{\epsilon}. \tag{90b}$$

Analytical integration yields

$$I \approx \frac{\sigma\nu e^{-\epsilon(R)}}{r\Sigma^2}\left\{a\left[\epsilon_2^2 e^{\epsilon_2} - \epsilon_1^2 e^{\epsilon_1}\right]\right.$$
$$\left. - 2a\left[\epsilon_2 e^{\epsilon_2} - \epsilon_1 e^{\epsilon_1}\right] + (2a+a\lambda^2+b)\left[e^{\epsilon_2} - e^{\epsilon_1}\right]\right\}. \tag{91}$$

Again, Eq. 91 is more tractable in ϵ variables than in r.

d. Treatment of the Sphere

Approximate evaluation of the spherical integral is similar. The substitution

$$\rho = \left\{(r')^2 - r^2(1-\mu^2)\right\}\Sigma^2 \tag{92a}$$

leads to

$$I = \frac{e^{-\sigma\sqrt{\rho(R)}}}{2r^2\Sigma^3} \int_{\rho_1}^{\rho_2} \frac{d\rho}{\sqrt{\rho}} S'(\rho, \mu') \left\{\rho^2+\lambda^2\right\} e^{\sigma\sqrt{\rho}}, \tag{92b}$$

where

$$\lambda^2 = \Sigma^2 r^2 (1-\mu^2). \tag{92c}$$

Next in order is the approximation

$$S'(\rho,\mu) \approx a\rho + b, \tag{93a}$$

where

$$a = \frac{S[r_2,\mu(r_2)] - S[r_1,\mu(r_1)]}{\Sigma^2\left(r_2^2-r_1^2\right)}, \tag{93b}$$

and

$$b = \frac{\left\{r_2^2 - r^2(1-\mu^2)\right\}\ S[r_1,\mu(r_1)] - \left\{r_1^2 - r^2(1-\mu^2)\right\}\ S[r_2,\mu(r_2)]}{r_2^2 - r_1^2}. \tag{93c}$$

The effect of the approximation in this case is to substitute for the true source distribution a quadratic function of path length, a procedure appropriate to the spherical configuration. When Eq. 93a is substituted in the integral expression, we obtain

$$I \approx \frac{e^{-\sigma\sqrt{\rho(R)}}}{2r^2\Sigma^3}\int_{\rho_1}^{\rho_2} d\rho\ \{a\rho+b\}\{\rho+\lambda^2\}\frac{e^{\sigma\sqrt{\rho}}}{\sqrt{\rho}}. \tag{94}$$

It is now convenient to define a new variable of integration in the form

$$\epsilon = \sigma\sqrt{\rho} \tag{95a}$$

to obtain, upon substitution,

$$I \approx \frac{\sigma e^{-\epsilon(R)}}{r^2\Sigma^3}\int_{\epsilon_1}^{\epsilon_2} d\epsilon\ \{a\epsilon^2+b\}\{\epsilon^2+\lambda^2\}e^{\epsilon} \tag{95b}$$

and, ultimately,

$$I \approx \frac{\sigma e^{-\epsilon(R)}}{r^2\Sigma^3}\int_{\epsilon_1}^{\epsilon_2} d\epsilon\ \{a\epsilon^4+(a\lambda^2+b)\epsilon^2+b\lambda^2\}e^{\epsilon}. \tag{95c}$$

The integration can be performed analytically to give the final result

$$\begin{aligned} I \approx \frac{\sigma e^{-\epsilon(R)}}{r^2\Sigma^3}\Bigg\{ & a\left[\epsilon_2^4 e^{\epsilon_2} - \epsilon_1^4 e^{\epsilon_1}\right] - 4a\left[\epsilon_2^3 e^{\epsilon_2} - \epsilon_1^3 e^{\epsilon_1}\right] \\ & + [a(\lambda^2+12)+b]\left[\epsilon_2^2 e^{\epsilon_2} - \epsilon_1^2 e^{\epsilon_1}\right] \\ & - 2[a(\lambda^2+12)+b]\left[\epsilon_2 e^{\epsilon_2} - \epsilon_1 e^{\epsilon_1}\right] \\ & + [2a(\lambda^2+12)+b(\lambda^2+2)]\left[e^{\epsilon_2} - e^{\epsilon_1}\right]\Bigg\}. \end{aligned} \tag{95d}$$

5.3 DIRECTIONAL QUADRATURE

a. Legendre-Gauss Methods

In slab and spherical configurations, the integrations over directional cosine required by the integral transport formulation are most conveniently effected by using the Legendre-Gauss quadrature. This procedure makes optimum use of a specified number of ordinates in those cases in which the function to be integrated is analytic and equally weighted at all points in the interval of integration. If the directional cosines to be used in establishing mesh points are those dictated by the Legendre-Gauss quadrature, the calculations required are minimized and numerical quadrature proceeds rapidly.

b. Limitations of Legendre-Gauss Quadrature

In a spherical configuration with a spherical source, not all of the directional cosine rays emanating from spatial points remote from the outer boundary of the source pass through the source. When the contribution to the scalar flux of neutrons that have not experienced at least one isotropic collision is to be evaluated under such circumstances, the Legendre-Gauss procedure tends to introduce a sizable error. The sign of the error depends on whether the ray most nearly tangent to the surface of the source lies within or outside the source, so that the calculated scalar flux as a function of position tends to oscillate about its true value. Provided at least two rays penetrate the source, the oscillatory error is largely self-compensating, and reaction rates integrated over spatial regions are relatively insensitive to the oscillation.

In the cylindrical configuration with a line source, the source integral tabulated in Section IV, when formulated in terms of elevational directional cosines, diverges as the value of the cosine approaches unity. Here, the Legendre-Gauss procedure is not applicable, and other methods must be used.

c. Quartic Quadrature

By transforming from directional cosine to angle as the variable of integration, the divergence, which is a function only of coordinate system, is eliminated. The angles corresponding to the Legendre-Gauss cosines are not, however, compatible with the Legendre-Gauss procedure.

Quadrature is effected by fitting a polynomial to the available points and integrating analytically. Owing to machine storage limitations, the number of discrete elevational angles available is four. It is physically evident, however, that at all finite depths of penetration into the attenuating cylinder, the directional flux oriented parallel to the axis is zero. Hence, a fourth-order polynomial may be fitted and integrated to yield scalar fluxes. The equivalent elevational angles and the corresponding quadrature weighting terms are listed in Table 3. The Jacobian of the transformation from directional cosine to angle has been incorporated into the weighting terms.

In the cylindrical configuration with a cylindrical source, the system of ultimate

Table 3. Angular equivalents of 4-point Legendre-Gauss cosines and corresponding quartic quadrature weights.

Angle	Quadrature Weight
0.28275705	-0.18067583
0.64903658	+0.90560425
1.01745554	-0.17579145
1.38631713	+0.20506451

interest in this study, the source integral, expressed in terms of directional cosines, diverges in both elevation and azimuth as the values of the directional cosines approach unity. The difficulty is again a consequence of the coordinate system, and is again eliminated by a transformation to angle as the variable of integration. As in the case of the line source, quadrature in elevational angle is most conveniently effected by the fourth-order polynomial fit.

d. Elliptic Quadrature

It is evident, both intuitively and mathematically, that the directional flux has a nearly elliptic dependence on azimuthal angle. Hence, the best fit to isolated ordinates to be obtained in executing a polynomial quadrature is that of an elliptic function of the form

$$\phi(r,\psi) \approx a\sqrt{1-\frac{\psi^2}{\beta^2}} = \sqrt{a^2-\gamma^2\psi^2}\,, \tag{96}$$

where ψ is the azimuthal angle. The allowed number of azimuthal ordinates available is four. In any practical configuration, however, rarely more than two of these ordinates are nonzero; hence, the actual fit of the ellipse to the calculated directional fluxes is most conveniently made in terms of the two most nearly straight-ahead angles. If we take the angles to be those corresponding to the Legendre-Gauss cosines and designate the most nearly straight-ahead angle ψ_4, the next ψ_3, then the quadrature expression assumes the form

$$\phi(r,\nu) \approx \frac{0.56632016\phi^2(r,\psi_4,\nu) - 0.10748567\phi^2(r,\psi_3,\nu)}{\sqrt{\phi^2(r,\psi_4,\nu) - \phi^2(r,\psi_3,\nu)}} \tag{97}$$

where the transformation from cosine to angle in the directional flux by way of the Jacobian has been made. No error comparable to the oscillatory error observed in the Legendre-Gauss integration for spherical sources has been detected when the elliptic

procedure is used with cylindrical sources. Analogous to this treatment of the cylindrical source, there must exist a procedure for directional integration in the spherical-source case. But this case is of least interest here, and the procedure has not been developed.

5.4 DIRECTIONAL INTERPOLATION

The expressions derived above for spatial quadrature in cylindrical and spherical configurations incorporate the dependence of source directional cosine on position along a neutron flight path. When scattering is anisotropic, the directional source is related to directional flux; for straight-ahead scattering, the relation is direct. Thus, calculated values of the directional source strength are available only at discrete values of the directional cosine, and source strengths at intermediate values of the cosines must be recovered by interpolation. Two conditions can be distinguished. If the flux is approximately isotropic, simple linear interpolation is sufficient. If the flux is strongly anisotropic, as is the flux of high-energy neutrons that have not experienced nonelastic scattering, a higher order polynomial fitting procedure is indicated. When spherical sources are involved, it is convenient to make use of a simple second-order interpolation with the two most nearly straight-ahead directional cosines and the critical cosine at which the directional flux and directional source go to zero as the three required abscissas. When the primary source is cylindrical the interpolation is more conveniently based on the elliptic fit noted above. In this case a transformation from azimuthal cosine to angle before interpolation and a reverse transformation back to cosine after interpolation is necessary to avoid the cosine induced divergence.

GLOSSARY

Symbol	Definition	Units
I	Value of an integral	as appropriate
R, X	Reference spatial positions	cm
$S(r', \mu')$	Directional source	$cm^{-3}\ sec^{-1}$
a, b, c, d	Fitting parameters for polynomials	as appropriate
r, x	Flux spatial positions	cm
r', x'	Source spatial positions	cm
α, β, γ	Fitting parameters for ellipses	as appropriate
ϵ, λ, ρ	Transformation variables	as appropriate
μ, ν	Directional cosines	

Symbol	Definition	Units
Σ	Macroscopic removal cross section	cm^{-1}
σ	Sign factor ($= \pm 1$)	
$\phi(r, \mu, \nu)$	Directional flux in cosines	$cm^{-2}\ sec^{-1}$
$\phi(r, \psi, \nu)$	Directional flux in azimuthal angle and elevational cosine $[=\phi(r, \mu, \nu) \sin(\cos^{-1} \mu)]$	$cm^{-2}\ sec^{-1}$
$\phi(r)$	Scalar flux	$cm^{-2}\ sec^{-1}$
ψ	Azimuthal angle	

Subscripts	Reference
1	Lower limit of integration
2	Upper limit of integration

VI. CALCULATION OF CERTAIN CROSS SECTIONS

6.1 INTRODUCTION

We have noted that the statistical model allows theoretical prediction of the dependence of (n, 2n) cross sections on neutron incident energy. Because the (n, 2n) excitation functions of many materials of interest have not been measured, this aspect of the statistical model is exploited whenever possible.

There are two other cases in which theoretical estimation of cross sections is necessary. These cases arise in treating multigroup resonance absorption and in calculating loss of slow neutrons to v^{-1} absorbers. Methods of generating theoretical cross sections appropriate to these two cases will be discussed here.

6.2 MULTIGROUP RESONANCE ABSORPTION CROSS SECTIONS

a. Limitations of Conventional Methods of Calculation

Wigner and his co-workers[51] have indicated that the use of average absorption cross sections in the resonance energy region can lead to serious overestimation of the resonance capture effect. In order to avoid this source of error, the approximation is often made in fission reactor calculations that the neutron flux has a simple inverse dependence on energy during slowing down. The concept of an effective resonance integral is then applicable. In blanket systems of interest the neutron absorption rate in the resonance energy region tends to be appreciably higher than in fission reactors, owing to the presence of high concentrations of resonance absorbing nuclides in the first wall and strong absorbers, particularly lithium 6, in the moderator. As a result, the flux tends to assume a more nearly linear dependence on energy and the effective resonance integral concept is not relevant. Under these circumstances, recourse must be had to a multigroup treatment of neutron slowing down and to the use of group effective absorption cross sections. A group effective absorption cross section is defined here as one such that the product of group flux and macroscopic effective cross section yields a good approximation to the true absorption rate. By following Wigner et al., resonance absorption can be conveniently separated into volume and surface absorption contributions. These will be treated in turn.

b. Volume Contribution to Resonance Capture

It is necessary to distinguish between wide and narrow resonances. A narrow resonance is one whose effective energy width (to be defined in greater detail below) is of the order of, or less than, the average energy loss experienced by a neutron in an elastic scattering collision. Thus, neutrons may be assumed to have not more than one collision, on the average, in the immediate neighborhood of a narrow resonance while slowing down past that resonance. Conversely, a wide resonance is one in which a

neutron experiences more than one collision.

Consider a neutron in the energy region immediately above a single narrow resonance. There is a probability, P, that the neutron will emerge from its next elastic scattering within the effective width of the resonance. A second probability, given by the ratio Γ_γ/Γ, is the likelihood that the subsequent collision, within the energy range of the resonance, will result in neutron capture. The quantities Γ_γ and Γ are the gamma emission level width and total level width of the resonance, respectively. The alternative ratio Γ_n/Γ, where Γ_n is the neutron emission level width, denotes the probability that the neutron is scattered in a collision within the energy range of the resonance. Values of level widths for most materials of interest have been tabulated by Hughes and Schwartz,[52] among others. The probability that a neutron, lying initially just above a resonance, is absorbed in the resonance as a result of successive scattering and capture events is, then, $P\frac{\Gamma_\gamma}{\Gamma}$. If P is generalized to describe the probability that a neutron lying at arbitrary energy within the group is scattered into the single designated resonance, the rate of absorption in the i^{th} group, because of volume effects, is given by

$$\text{Rate} = \phi_i \Sigma_{s|i} P \frac{\Gamma_\gamma}{\Gamma}. \tag{98a}$$

Here, as before, ϕ_i is group flux, and $\Sigma_{s|i}$ is group macroscopic scattering cross section. If the quantity $\Sigma_{s|i} P\frac{\Gamma_\gamma}{\Gamma}$ is replaced by an effective capture cross section, $\hat{\Sigma}_{a|i}$, the absorption rate becomes

$$\text{Rate} = \hat{\Sigma}_{a|i}\, \phi_i. \tag{98b}$$

Thus, in the narrow-resonance case the desired effective cross section is given by

$$\hat{\Sigma}_{a|i} = \Sigma_{s|i} P \frac{\Gamma_\gamma}{\Gamma}. \tag{98c}$$

If the resonance is wide, the probability that a neutron is scattered into it is still P, but the probability that a neutron, scattered into the resonance, is captured requires more elaboration. The probability that a neutron within the resonance escape capture during a single collision is Γ_n/Γ. The probability that it will survive a chain of N successive collisions in a wide resonance is $(\Gamma_n/\Gamma)^N$, and the probability that it will be captured is $[1-(\Gamma_n/\Gamma)^N]$. If $\Delta u)_r$ is the lethargy width of the resonance and ξ the logarithmic energy decrement, the number of collisions a neutron is required to make, on the average, in traversing a wide resonance is $\Delta u)_r/\xi$, and the probability of capture is $[1-(\Gamma_n/\Gamma)(\Delta u)_r/\xi)]$.

It is now necessary to specify what is meant by the energy width of a resonance. Again, following Wigner et al., the width, $\Delta E)_r$, of a resonance is defined as the distance in energy between those points on the upper and lower wings of the resonance at which

the resonance total cross section is equal in magnitude to the potential scattering cross section of the medium. The use of this characterization of resonance width, called by Wigner the "practical width," appears to be well justified by measurements.

The probability, P, of scattering into a resonance can now be readily derived in terms of the resonance width or, more conveniently, the half-width, ϵ, by using the elastic scattering formalisms developed in Section III. A narrow resonance is exactly analogous to an intermediate group with a higher energy limit, $E_H)_j$, where

$$E_H)_j = E_o + \epsilon \tag{99a}$$

and a lower limit, $E_L)_j$, where

$$E_L)_j = E_o - \epsilon. \tag{99b}$$

The resonance energy is E_o, and the resonance width, $\Delta E)_r$, is equal to 2ϵ. Substitution of Eqs. 99 in Eq. 20b yields

$$P = \frac{1}{(1-\alpha)\,\Delta E)_i}\left\{(E_o-\epsilon)\,\ln\left\{\frac{E_o+\epsilon}{E_o-\epsilon}\right\} - 2\epsilon(1+\ln\alpha)\right\}. \tag{100}$$

Correspondingly, a wide resonance is equivalent to a lowest permitted group. Substitution of Eqs. 99 in Eq. 22c gives for this case

$$P = \frac{E_o+\epsilon}{\Delta E)_i}\left\{\frac{1}{1-\alpha}\ln\frac{1}{\alpha} - 1\right\}. \tag{101}$$

In both cases $\Delta E)_i$ is the group energy width, and α is the maximum fractional energy loss per collision, as before.

c. Surface Contribution to Resonance Capture

The surface resonance effect may be treated in like manner. The group current of neutrons crossing a boundary into a medium must be considered. If the medium receiving the flow of neutrons has a single narrow resonance of width $\Delta E)_r$ within the group boundaries, the fraction of the group current that comes under the influence of the resonance upon entering the medium is simply $\Delta E)_r/\Delta E)_i$. By virtue of the large cross section of the resonance, nearly all of the neutrons entering the energy region of the resonance experience collisions close to the surface of the medium, and the fraction Γ_γ/Γ is captured. The remaining fraction, Γ_n/Γ, of those entering the resonance is scattered, loses energy, and escapes the resonance. Thus, the fraction of the entering current absorbed close to the surface of a medium having a single narrow resonance is $[\Delta E)_r/\Delta E)_i][\Gamma_\gamma/\Gamma]$.

If the resonance is wide, the fraction of the current entering the resonance is still given by $\Delta E)_r/\Delta E)_i$. The derivation of the capture probability is somewhat more complicated. It is necessary to distinguish between neutrons entering the resonance above

the resonance peak energy and those entering below this energy. A neutron entering in the higher energy half of a wide resonance will penetrate some finite distance into the medium, the amount depending on the strength of the resonance at the incident energy of the neutron. If the neutron escapes capture in its first collision in the resonance, it will be scattered down in energy, deeper into the resonance. Since the resonance cross section as seen by the neutron is now larger than that faced on entering the medium, the neutron is effectively trapped and the probability of eventual capture is given by $[1-(\Gamma_n/\Gamma)^N]$, where N is the number of collisions required for a neutron to traverse, on the average, three-fourths of the resonance practical width.

If the neutron enters the medium in the lower half of the resonance, successive noncapture collisions transfer it into energy regions of steadily decreasing resonance cross section. Hence, if isotropic scattering is assumed, the scattered neutron has approximately one chance in two of emerging from the medium before experiencing another collision in the resonance. There also remains the probability of scattering down through the resonance in successive noncapture collisions. Both of these possible modes of escape open to neutrons that have entered the medium in the lower half of a wide resonance must be taken into account in deriving the capture probability. An approximate derivation proceeds as follows: the capture probability for each collision experienced by the neutron in the resonance is $1 - \frac{\Gamma_n}{\Gamma}$. The fraction of the neutrons that survive the first collision is Γ_n/Γ. Of these, half leave the resonance absorbing medium without further collision so that only the fraction $\Gamma_n/2\Gamma$ of the initial neutrons is available for a second collision. In the second collision the fraction captured is $\frac{\Gamma_n}{2\Gamma}\left(1 - \frac{\Gamma_n}{\Gamma}\right)$; of the remainder, half, $\frac{1}{2}\left[\left(\frac{\Gamma_n}{2\Gamma}\right)\frac{\Gamma_n}{\Gamma}\right]$, escapes to the moderator to be scattered out of the region of influence of the resonance, and the other half, $\left[\frac{\Gamma_n}{2\Gamma}\right]^2$, is available for another collision.

The total capture probability in a chain of N collisions is

$$\text{Probability of capture} \approx \left\{1 - \frac{\Gamma_n}{\Gamma}\right\}\left\{1 + \frac{\Gamma_n}{2\Gamma} + \left(\frac{\Gamma_n}{2\Gamma}\right)^2 + \ldots \left(\frac{\Gamma_n}{2\Gamma}\right)^{N-1}\right\} \tag{102a}$$

$$\approx \left\{1 - \frac{\Gamma_n}{\Gamma}\right\}\left\{\frac{1 - \left(\frac{\Gamma_n}{2\Gamma}\right)^N}{1 - \left(\frac{\Gamma_n}{2\Gamma}\right)}\right\}. \tag{102b}$$

Neutrons in the lower half of a resonance must lose, on the average, energy equal to one-fourth of the resonance width in traversing the remainder of the resonance, experiencing $\Delta u)_r/4\xi$ collisions in the process. The probability of capture becomes

$$\text{Probability of capture} \approx \left\{1 - \frac{\Gamma_n}{\Gamma}\right\}\left\{\frac{1 - \left(\frac{\Gamma_n}{\Gamma}\right)^{\Delta u)_r/4\xi}}{1 - \left(\frac{\Gamma_n}{\Gamma}\right)}\right\}. \tag{102c}$$

Since neutrons are assumed to be uniformly distributed in energy in a group, the average capture probability of neutrons entering a resonance absorbing medium at energies within a single wide resonance is given by

$$\text{Probability of capture} \approx \frac{1}{2}\left\{1 - \left(\frac{\Gamma_n}{\Gamma}\right)^{3\Delta u)_r/4\xi} + \frac{\left(1 - \frac{\Gamma_n}{\Gamma}\right)}{\left(1 - \frac{\Gamma_n}{2\Gamma}\right)}\left[1 - \left(\frac{\Gamma_n}{2\Gamma}\right)^{\Delta u)_r/4\xi}\right]\right\}. \qquad (103)$$

The strength of the group current flowing across a boundary into a medium may be estimated as follows. Consider the configuration sketched in Fig. 8. The total group

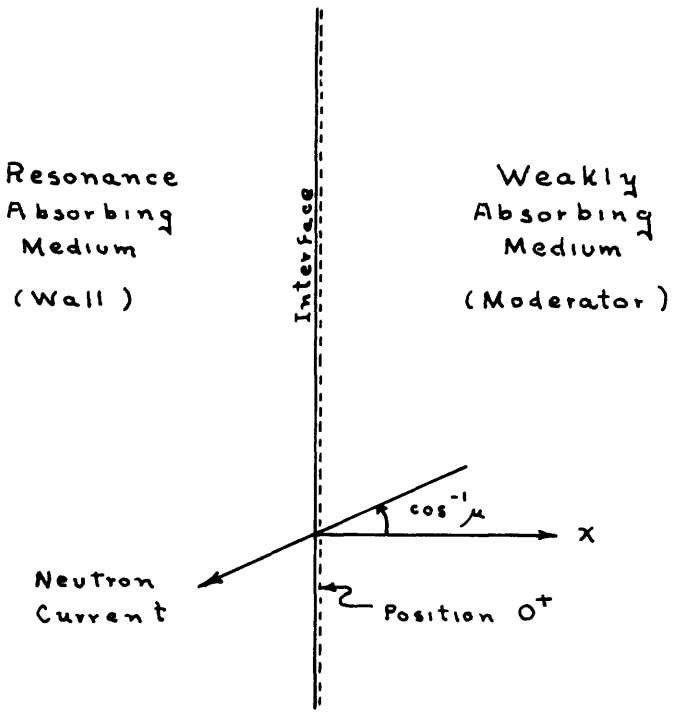

Fig. 8. Interface between resonance absorbing and weakly absorbing media.

current flowing from the moderator to the wall through the interface is given, in the integral formulation, by the expression

$$\text{Current})_i = \int_{-1}^{0} |\mu| \, d\mu \int_{\text{Mod}} \frac{dx}{|\mu|} S_i(x, \mu) \exp\left(-\frac{\Sigma_r x}{|\mu|}\right), \qquad (104)$$

where Σ_r is the macroscopic removal cross section in the moderator, $S_i(x, \mu)$ is the group directional source strength, and μ is a symmetric directional cosine. Since sources in the resonance energy region are almost purely isotropic, the approximation

$$\frac{S_i(x)}{2} \approx S_i(x, \mu) \qquad (105a)$$

is acceptable. Substitution of Eq. 105a, together with the convenient transformation

$$\mu' = -\mu \tag{105b}$$

in Eq. 104 yields

$$\text{Current})_i = \int_0^1 d\mu' \int_{\text{Mod}} dx \frac{S_i(x)}{2} \exp\left(-\frac{\Sigma_r x}{\mu'}\right), \tag{106}$$

where $S_i(x)$ is the group source strength per unit volume at x. Inversion of the order of integration gives

$$\text{Current})_i = \int_{\text{Mod}} dx \frac{S_i(x)}{2} \int_0^1 d\mu' \exp\left(-\frac{\Sigma_r x}{\mu'}\right) \tag{107a}$$

$$= \int_{\text{Mod}} dx \frac{S_i(x)}{2} E_2[\Sigma_r x], \tag{107b}$$

where $E_n[\Sigma_r x]$ signifies the n^{th}-order exponential integral

$$E_n(z) = \int_0^1 dt \frac{e^{-z/t}}{t^{n-2}}, \tag{107c}$$

tabulated by Goldstein,[53] among others. The E_2 function goes to zero rapidly with increasing argument while in cases of interest the source strength tends to vary slowly with position. Then, to a good approximation, the current becomes

$$\text{Current})_i \approx \frac{S_i(0^+)}{2} \int_{\text{Mod}} dx\, E_2[\Sigma_r x], \tag{108}$$

The spatial position 0^+ lies just to the right of the interface as shown in Fig. 8. Extending the integral over the moderator to infinity yields

$$\text{Current})_i \approx \frac{S_i(0^+)}{2} \left\{\frac{E_3(0)}{\Sigma_r}\right\} = \frac{S_i(0^+)}{4\Sigma_r}. \tag{109}$$

The loss rate caused by surface absorption is the product of current and capture probability and is given in the narrow resonance case by

$$\text{Surface loss} \approx \left\{\frac{\Delta E)_r}{\Delta E)_i} \frac{\Gamma_\gamma}{\Gamma} \frac{1}{4\Sigma_r}\right\} S_i(0^+), \tag{110a}$$

and in the wide resonance case by

$$\text{Surface loss} \approx \left\{\left[\frac{1}{2}\left\{\frac{1-\frac{\Gamma_n}{\Gamma}}{1-\frac{\Gamma_n}{2\Gamma}}\right\}\left\{1-\left(\frac{\Gamma_n}{\Gamma}\right)^{\Delta u)_r/4\xi}\right\}+\frac{1}{2}\left\{1-\left(\frac{\Gamma_n}{\Gamma}\right)^{3\Delta u)_r/4\xi}\right\}\right]\frac{1}{4\Sigma_r}\right\} S_i(0^+). \tag{110b}$$

In both equations the expression included within the outermost braces is in effect a weighting term relating the surface loss to the source strength just outside of the absorber. The surface effect may then be treated, in the differential and diffusion formulations, by assigning a sink at the point (0^+) of strength $\{\ \}\, S_2(0^+)$ or, more simply, by assigning a source of strength $[1-\{\ \}]S_i(0^+)$ in lieu of $S_i(0^+)$, where $\{\ \}$ is the weighting term enclosed in the outer braces in Eqs. 110.

d. Effects of Additional Resonances

Generalization to a succession of resonances lying within the bounds of a single energy group is simple, provided that two assumptions are made. First, it must be assumed that the resonances are sufficiently far apart in terms of neutron down-scattering that the slowing-down density above the highest resonance is re-established before each of the lower resonances is encountered. Second, it is necessary to assume that neutrons do not travel appreciable distances within the resonances. The former assumption is customary in fission reactor technology; the latter appears justified in view of the relatively large total cross sections characteristic of resonances. Within the limits of these assumptions, the volume and surface effects of the individual resonances are additive. The total group effects are the sums of the individual effects.

e. Effects of Mixtures of Nuclides

The foregoing development of the methods for calculating effective volume absorption cross sections and source weights for surface absorption presupposes the existence of an absorbing medium containing a single nuclide. The same procedures are equally applicable to media composed of mixtures of absorbing nuclides, and of mixtures of absorbers with moderator nuclides. The latter case is important when fissile nuclides are introduced into the fused-salt coolant. It is necessary, when generalization is made to mixtures, to take into account the properly weighted contributions of the various scattering nuclides in calculating the probability of scattering into a resonance. It is also necessary to consider macroscopic potential and resonance cross sections when determining practical widths and to express effective absorption cross sections on a "per atom of absorber" basis.

6.3 EPITHERMAL ABSORPTION CROSS SECTIONS

The second case which necessitates the use of calculated cross sections is that involving absorption in the lowest energy group. In groups with relatively narrow lethargy widths, the common practice is to approximate cross sections that vary slowly with energy by the value of the cross section at some suitable group mean energy. The ordering of the lethargy groups in this study provides for a last group extending from 10 ev to thermal energy, a lethargy span of nearly six units. Over these limits a (v^{-1}) absorption cross section has a range in value of more than an order of magnitude and

the use of a simple mean energy to characterize the group cross section is of doubtful validity. Instead, use is made of an effective absorption cross section so defined that the product of effective macroscopic cross section by group flux gives a good approximation to the true absorption rate. Thus

$$\hat{\Sigma}_a \int_{\text{Thermal}}^{10\text{ ev}} dE'\ \phi(x, E') = \int_{\text{Thermal}}^{10\text{ ev}} dE'\ \phi(x, E')\ \Sigma_a(E'), \tag{111a}$$

or

$$\hat{\Sigma}_a = \frac{\int_{\text{Thermal}}^{10\text{ ev}} dE'\ \phi(x, E')\ \Sigma_a(E')}{\int_{\text{Thermal}}^{10\text{ ev}} dE'\ \phi(x, E')}. \tag{111b}$$

In order to simplify the treatment, assumptions that (a) the medium in which the effective cross section is to be evaluated is infinite, and (b) the flux is spatially uniform are made. It is recognized that these assumptions are not really justified in the first wall or in the first-wall coolant in systems of interest, since these regions rarely are more than one or two mean-free paths wide. In the presence of useful amounts of lithium 6, the total neutron flux in this last group is approximately an order of magnitude smaller than that in the higher energy groups, so that errors introduced in estimating absorption cross sections are second-order effects.

According to Weinberg and Wigner,[54] the slowing down flux in an infinite, homogeneous, nonhydrogenous absorbing medium is given as a function of energy by

$$\phi(E) = \frac{S}{\xi \Sigma_r(E)\, E} \exp\left\{ - \int_E^{E_S} \frac{\Sigma_a(E')}{\xi \Sigma_T(E')} \frac{dE'}{E'} \right\}, \tag{112}$$

where $\phi(E)$ is the scalar flux at energy E, S is the slowing-down density at an elevated energy E_S, Σ_r is the macroscopic total cross section, Σ_a is the corresponding absorption cross section, and ξ is the logarithmic mean energy decrement. If the scattering cross section is assumed constant, and the absorption cross section to vary as (v^{-1}), the absorption escape probability in the range E_S-E can be shown by straightforward integration to have the form

$$\exp\left\{ \int_E^{E_S} \frac{\Sigma_a(E')\, dE'}{\xi \Sigma_s(E')\, E'} \right\} = \left[\frac{1 + \gamma\sqrt{E_S}}{\sqrt{E_S}} \right]^{2/\xi} \left[\frac{\sqrt{E}}{1 + \gamma\sqrt{E}} \right]^{2/\xi}. \tag{113}$$

The flux is then given by

$$\phi(E) = \frac{S}{\xi \Sigma_r(E)\, E} \left[\frac{1 + \gamma\sqrt{E_S}}{\sqrt{E_S}} \right]^{2/\xi} \left[\frac{\sqrt{E}}{1 + \gamma\sqrt{E}} \right]^{2/\xi}, \tag{114a}$$

and finally by

$$\phi(E) = \frac{\gamma S}{\xi \Sigma_s} \left[\frac{1 + \gamma\sqrt{E_S}}{\sqrt{E_S}} \right]^{2/\xi} \left[\frac{1}{1 + \gamma\sqrt{E}} \right]^{(2/\xi)+1} [\sqrt{E}]^{(2/\xi)-1} \tag{114b}$$

where Σ_s is the macroscopic scattering cross section and

$$\gamma = \frac{\Sigma_s}{\Sigma_a^0 \sqrt{E^0}}. \tag{114c}$$

The superscript zero indicates the appropriate values at a reference energy such as 0.025 ev. The departure of the flux from simple (E^{-1}) dependence on energy is evident in Eq. 114a.

Substitution of Eq. 114b in Eq. 111b and cancellation of appropriate factors gives

$$\hat{\Sigma}_a = \frac{\Sigma_a^0 \sqrt{E^0} \int_{\text{Thermal}}^{E_S} \frac{dE'}{E'\sqrt{E'}} \left[\frac{\sqrt{E'}}{1 + \gamma\sqrt{E'}} \right]^{(2/\xi)+1}}{\int_{\text{Thermal}}^{E_S} \frac{dE'}{E'} \left[\frac{\sqrt{E'}}{1 + \gamma\sqrt{E'}} \right]^{(2/\xi)+1}}. \tag{115}$$

No allowance has been made for thermalization; the original equation for flux, (112), is relevant only to slowing down at higher energies. But again, because of strong neutron absorption by lithium 6, few neutrons will survive to thermal energies in systems of interest. Hence, thermalization may be disregarded, and the lower limits of the integrals taken to be zero.

The numerator of (115) can be integrated exactly to give

$$\int_0^{E_S} \frac{dE'}{E'\sqrt{E'}} \left\{ \frac{\sqrt{E'}}{1 + \gamma\sqrt{E'}} \right\}^{(2/\xi)+1} = \xi \left(\frac{\omega_s}{\gamma} \right)^{r+1}, \tag{116a}$$

where

$$\omega_s = \frac{\gamma\sqrt{E_S}}{1 + \gamma\sqrt{E_S}}, \tag{116b}$$

and

$$r = \frac{2}{\xi} + 1. \tag{116c}$$

The integral in the denominator of (115) is more difficult. Making the substitution

$$\omega = \frac{\gamma\sqrt{E}}{1 + \gamma\sqrt{E}} \tag{117}$$

and introducing Eq. 116c, permits the integral to be expressed as a series in the form

$$\int_0^{E_S} \frac{dE'}{E'} \left\{ \frac{\sqrt{E'}}{1 + \gamma\sqrt{E'}} \right\}^{(2/\xi)+1} = 2\left(\frac{\omega_s}{r}\right)^r \sum_{j=0}^{\infty} \frac{(\omega_s)^j}{r+j}. \tag{118}$$

Although the series will converge rather slowly as ω_s approaches unity and as r increases, it is of a form particularly suitable for machine computation. Furthermore, it is possible to estimate the sum of the residual terms after truncation in terms of a first exponential integral function of the form

$$\sum_{j=L}^{\infty} \frac{(\omega_s)^j}{r+j} \approx \frac{1}{(\omega_s)^r} E_1\left[(r+L-\zeta) \ln \frac{1}{\omega_s} \right]. \tag{119a}$$

The parameter ζ allows adjustment of the fit of the exponential integral to the sum of the residual terms and has the approximate value

$$\zeta \approx \frac{1}{\ln\left(\frac{1}{\omega_s}\right)} \left\{ \ln \ln\left(\frac{1}{\omega_s}\right) - \ln (1-\omega_s) \right\}. \tag{119b}$$

The final expression for the effective absorption cross section then takes the form

$$\hat{\Sigma}_a \approx \frac{\Sigma_a^0 \sqrt{E^0}\, \xi \left(\frac{\omega_s}{\gamma}\right)^{r-1}}{\frac{2}{\gamma^r}\left\{ (\omega_s)^r \sum_{j=0}^{L-1} \frac{(\omega_s)^j}{r+j} + E_1\left[(r+L-\zeta) \ln \frac{1}{\omega_s} \right] \right\}}. \tag{120}$$

In media having particularly small thermal absorption cross sections, thermalization might have to be taken into account, were it not for the influence of lithium 6. In such cases the procedure outlined above would yield large absorption cross sections indicating energies well below thermal, and so is not applicable. Under these circumstances, however, no appreciable error is introduced by simply taking for the value of the effective absorption cross section in the lowest energy group the value at 0.025 ev.

GLOSSARY

Symbol	Definition	Units
E_o	Resonance energy	ev, kev
E_S	Upper reference energy	ev, kev
$\Delta E)_r$	Resonance energy width	ev, kev
P	Inscattering probability	
S(x)	Scalar source strength	cm^{-3} sec^{-1}
$S(x, \mu)$	Directional source strength	cm^{-3} sec^{-1}
$\Delta u)_r$	Resonance lethargy width	
x	Spatial position	cm
α	Maximum fractional energy loss	
Γ_γ	Resonance gamma emission width	ev, kev
Γ_n	Resonance neutron emission width	ev, kev
Γ	Resonance total width	ev, kev
ϵ	Resonance energy half width	ev, kev
μ	Directional cosine	
ξ	Logarithmic mean energy decrement	
Σ_a	Macroscopic absorption cross section	cm^{-1}
$\hat{\Sigma}_a$	Effective macroscopic absorption cross section	cm^{-1}
Σ_s	Macroscopic scattering cross section	cm^{-1}
Σ_r	Macroscopic removal cross section	cm^{-1}
Σ_T	Macroscopic total cross section	cm^{-1}
$\phi(x, E)$	Scalar flux at position x, energy E	cm^{-2} sec^{-1}
ϕ	Scalar flux	cm^{-2} sec^{-1}

Subscript	Reference
i	Group index
j	Summing index

Superscript	Reference
0	Lower reference energy (0.025 ev)

VII. COMPARISON OF THEORY AND EXPERIMENT

7.1 INTRODUCTION

No measurements seem to have been made of flux distributions or neutron-induced reaction rates in the type of large-radius cylindrical attenuator, cylindrical-source configuration of interest to this study. As we have noted, an experimental program of this kind has been started in a collateral study, but no results have yet been obtained for comparison with the present theory.

A few measurements have been made in systems that can be treated within the scope of the calculational methods outlined here. It should be emphasized that none of the known measurements are directly relevant to the present study. In default of more suitable experimental studies, an estimate of the validity of the calculational methods outlined above will be made on the basis of a comparison of theoretical predictions with the available measurements.

7.2 AREAS OF COMPARISON

a. Published Experimental Measurements

Three distinct types of measurements, suitable for purposes of comparison, have been made. The first are measurements of the spatial distribution of neutron-induced activation in threshold detectors following injection of high-energy source neutrons into spherical assemblies. Such measurements have been made in boron carbide by Belov et al.,[55] in lead by Broder et al.,[56] in iron by Ferguson,[57] in thorium by Weale,[58] and in uranium by Weale et al.[59] The second are measurements of the Fermi age to thermal energy of fast source neutrons in various homogeneous media. Relevant studies have been made in graphite by Dlougy,[60] and in water by Caswell.[61] The third measurements are concerned with the energy distribution of neutrons emerging from attenuating spherical shells following the introduction of fast neutron sources at the center of the shells. Zamyatnin et al.[62] have measured such distributions for shells of various thicknesses of iron, lead, and uranium, and Allen et al.[63] have made similar measurements in natural uranium shells.

All of these measurements were made in assemblies whose configurations closely resembled the idealized "point sources in a spherical attenuator" system, and in each case the primary source neutrons were generated by D-T fusion reactions.

b. Cases Studied Theoretically

Among the materials treated experimentally, lead, carbon, and, to a lesser extent, boron are of interest in this study. The fissile materials, while of potential value in a thermonuclear blanket, fall more properly into the area of interest of the collateral study that is being made on such materials. Iron is of no immediate interest in either study

and hydrogenous materials, including water, are not well treated by the computational methods thus far developed. Accordingly, attempts to reproduce by theoretical methods results obtained experimentally have been restricted to the cases treated by Broder (activations in lead), Belov (activations in boron carbide), Dlougy (age in graphite) and Zamyatnin (emission spectra from lead).

7.3 COMPARISON OF THEORETICAL AND EXPERIMENTAL RESULTS

a. Detector Responses in Lead

Figure 9 shows the detector response distributions obtained in a very thick lead sphere by experiment and by calculation. All responses have been normalized to unity at the inner radius of the spherical attenuator, and have been multiplied at each spatial position by the square of the radial distance to that position. The logarithms of the product of normalized response by distance squared have been plotted against radial position in each case. Comparison is to be made in terms of the shape of the curves near the origin and the asymptotic slope of the curves at points remote from the center.

It is evident that the asymptotic slopes of the measured and calculated curves in lead are in rather good agreement for the aluminum and phosphorus detectors, and in reasonable agreement for thorium. It is also evident that near the origin the slopes of the calculated response curves differ appreciably from those of the measured curves. The experimental curves at small values of radius are all characterized by slopes that are initially rather flat; the curves assume typical asymptotic attenuation shapes only at distances of a few mean-free paths from the inner surface of the sphere. In constrast, the calculated response curve for the $Al^{27}(n, p)$ reaction shows almost no change in slope throughout its entire spatial range. The $Th^{232}(n, f)$ and $P^{31}(n, p)$ curves, while showing some dependence of slope on position near the origin, have much steeper slopes at small penetration than do the corresponding experimental curves.

b. Detector Responses in Boron Carbide

Figure 10 shows the measured and calculated responses obtained in boron carbide. The logarithm of normalized response by distance squared is again plotted against radial position. In this case the agreement of predicted asymptotic slopes with measured values is somewhat poorer than that obtained in lead. Of more immediate interest, however, is the behavior of the response curves in the vicinity of the origin. Consider the measured curves first. The detectors characterized by high thresholds, $Cu^{63}(n, 2n)$ and $Sb^{121}(n, 2n)$, yield curves indicating almost pure attenuation. As the thresholds of the detectors decrease in energy, the initial slopes of the corresponding response curves become progressively less negative until finally the predominantly low-energy detectors, $B^{10}(n, \alpha)$ and $U^{235}(n, f)$, show positive initial slopes. Among the calculated responses, the detectors which respond primarily to neutrons whose energies are above a few Mev, in particular, copper, antimony, iron, and aluminum, show almost pure exponential

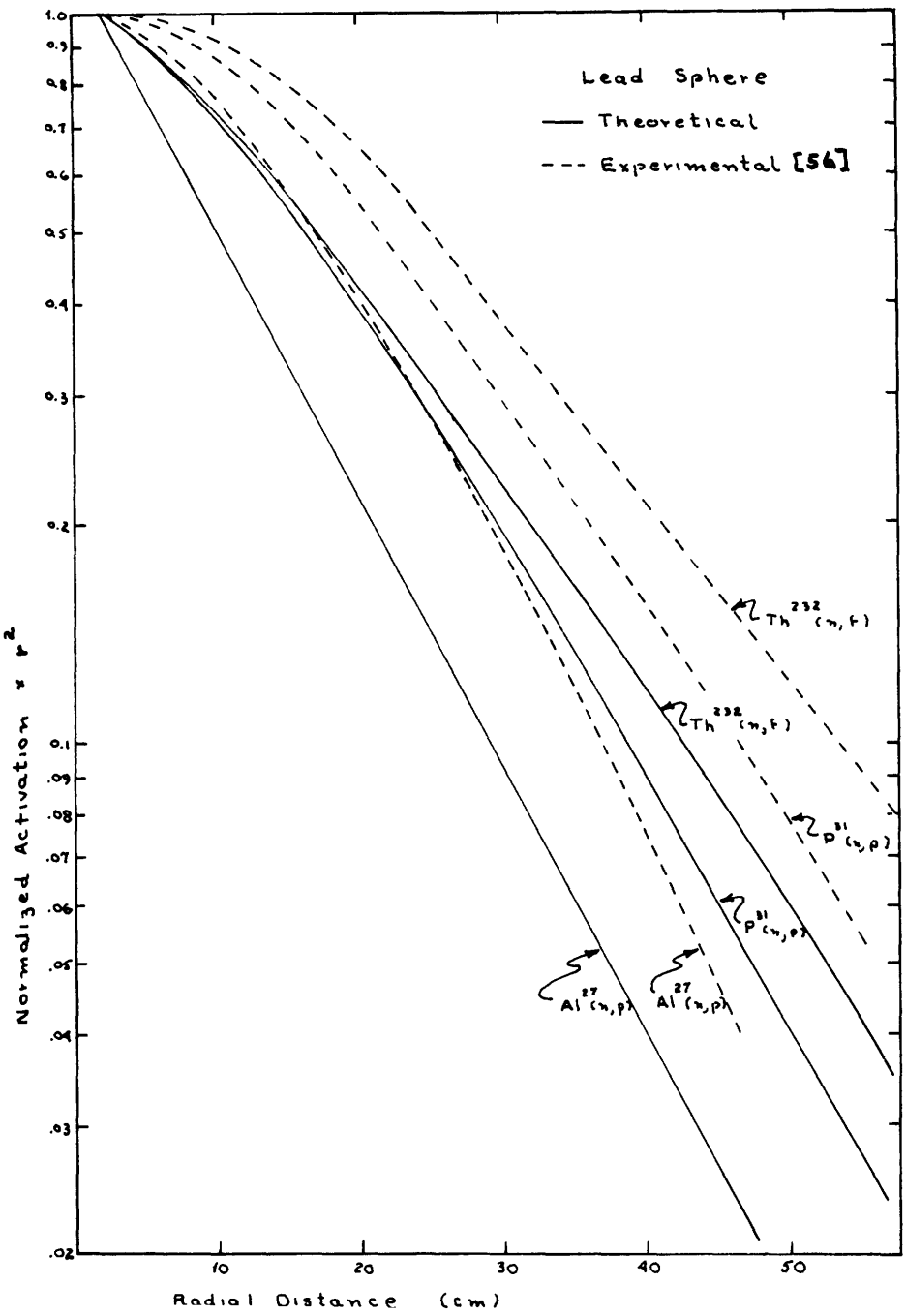

Fig. 9. Detector responses in a lead sphere.

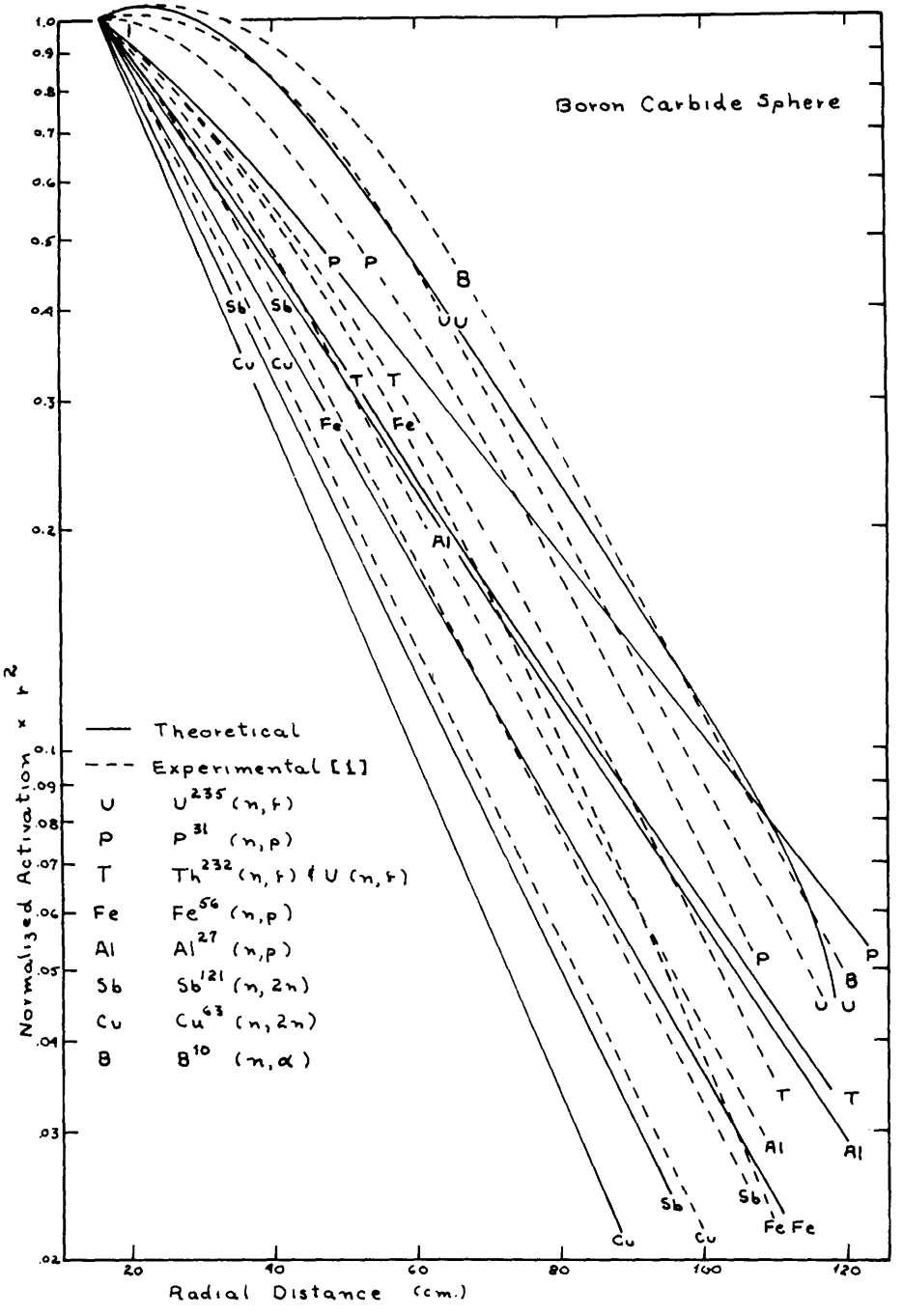

Fig. 10. Detector responses in a boron carbide sphere.

attenuation. Uranium 238, thorium, and phosphorus, whose response to lower energy neutrons (~1 Mev) is significant but not predominating, show some change in curvature near the origin, following the behavior of the measured curves but to a lesser degree. Finally, uranium 235 whose response is due almost totally to resonance and thermal neutrons reproduces fairly well the measured curve, including the initially positive slope.

Owing to limitations in the digital computer codes used in carrying out these studies, convergence of the S_n calculations could not be obtained in the last few energy groups in which the boron total cross sections are particularly large. For this reason, the calculated responses reflect flux distributions only for neutron energies above 45 ev. Since the boron detector response arises almost completely from the (v^{-1}) $B^{10}(n, \alpha)$ reaction, the calculated BF_3 responses were not considered representative of the results that would be obtained if the calculation could be carried to thermal energies, and thus are not plotted. The response of the $U^{235}(n, f)$ reaction is attributable to a large extent to resonance neutrons above 45 ev and, on this account, the calculated uranium 235 response is believed to be more nearly comparable to the experimental results.

c. Fermi Age in Graphite

Dlougy has made an experimental measurement of the Fermi age of neutrons from 14 Mev to thermal energy in graphite. On the basis of his results, Dlougy concludes that thermal neutrons characterized by three different ages exist simultaneously in a graphite assembly. The first group of neutrons, respresenting approximately 0.65 of the total population, have experienced one inelastic collision while slowing down. These have an age at thermal energies of 600 cm^2. The second group, constituting 0.25 of the population, have experienced at least two inelastic collisions and have an effective age of 240 cm^2. The third group, composed of the remaining 0.1 of the population, are characterized as having a "very small" age, and are attributed by Dlougy to neutrons slowed down only by elastic scatterings.

An attempt has been made to reproduce Dlougy's measurement theoretically, with one limitation. Since the computational methods available are not suitable for problems in which thermalization is significant, calculated flux distributions at energies of 31.5 ev and 14.5 ev, corresponding to the 48^{th} and 49^{th} lethargy groups, were used to obtain the ages of those energies. These ages were combined with corrections made according to the standard definition of the Fermi age to extend the ages from the respective higher energies to thermal energy. Figures 11 and 12 show the flux distributions in groups 48 and 49, plotted as the logarithms of flux against the square of position. The existence of at least two distinct groups of neutrons is evident in both plots. The calculated Fermi ages of these two groups based on the flux plots are tabulated in Table 4, together with Dlougy's experimental results. The differences between the results obtained with group 48 information and those obtained from group 49 are less than the uncertainties introduced in determining ages from flux plots, so that no significance is to be attached to the apparent systematic shift in calculated age with energy group.

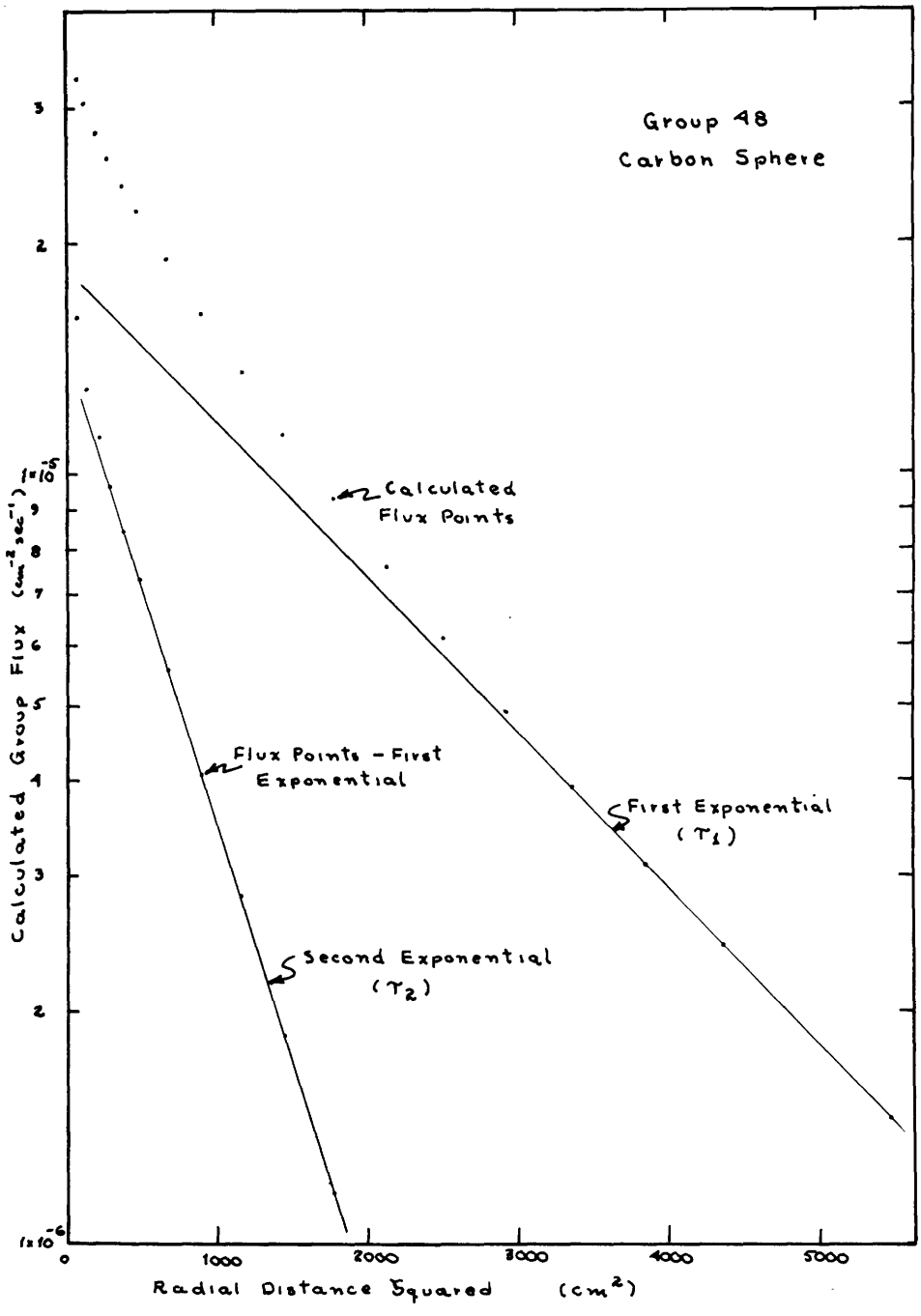

Fig. 11. Fermi age plot for group 48.

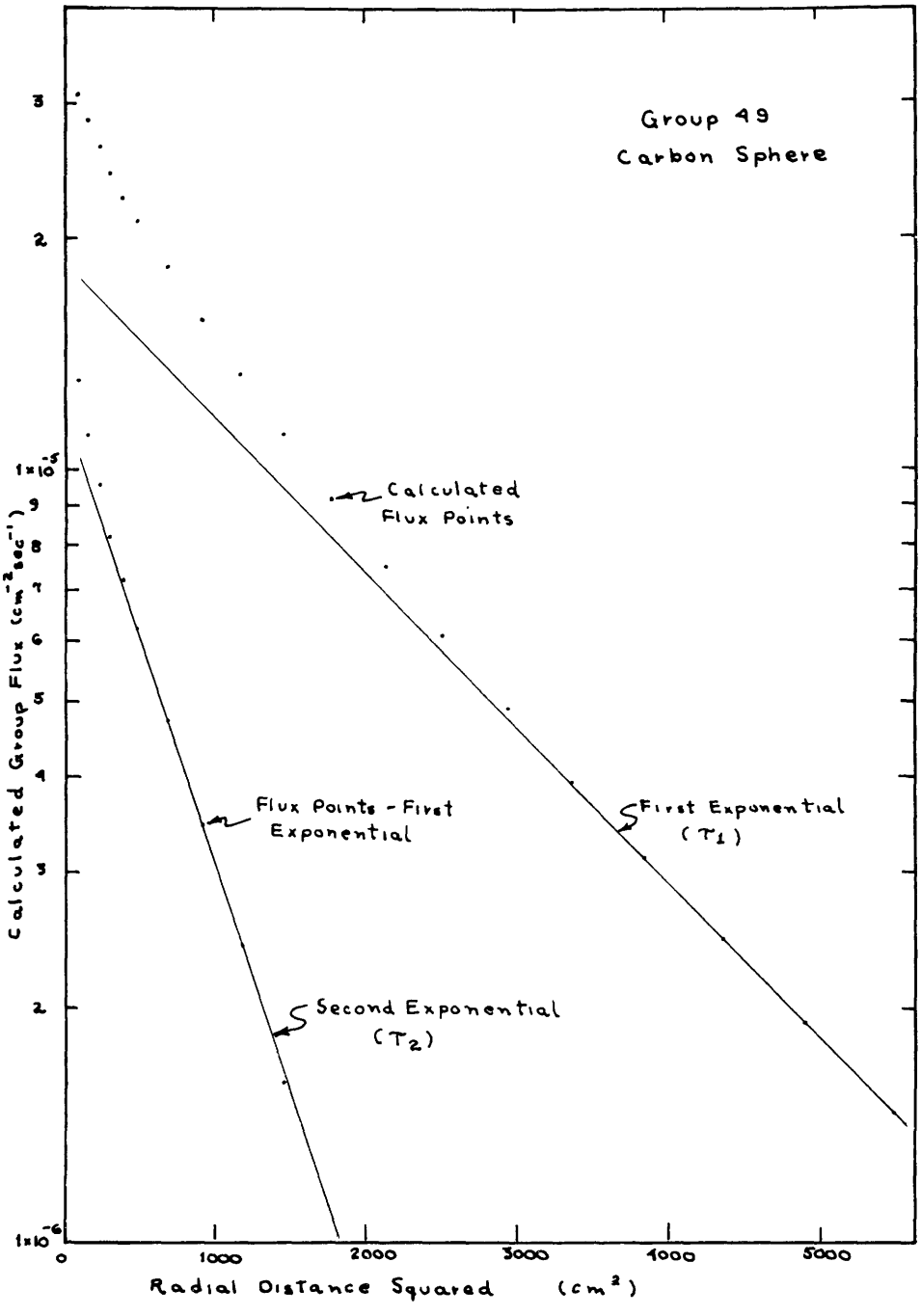

Fig. 12. Fermi age plot for group 49.

Table 4. Comparison of theoretical and experimental determinations of the age-to-thermal energy of D-T neutrons in graphite.

		Neutrons experiencing a single nonelastic scattering			Neutrons experiencing multiple nonelastic scattering		
Method of Determination	Flux Energy	Age-to-Group Energy	Correction to Thermal Energy	Age-to-Thermal Energy	Age-to-Group Energy	Correction to Thermal Energy	Age-to-Thermal Energy
Calculation using Group 48 flux distributions	31.5 ev	535 cm^2	106 cm^2	641 cm^2	172 cm^2	106 cm^2	278 cm^2
Calculation using Group 49 flux distributions	14.5 ev	539 cm^2	95 cm^2	634 cm^2	177 cm^2	95 cm^2	272 cm^2
Experiment [6] using thermal flux distributions	0.025 ev	–	–	600 cm^2	–	–	240 cm^2

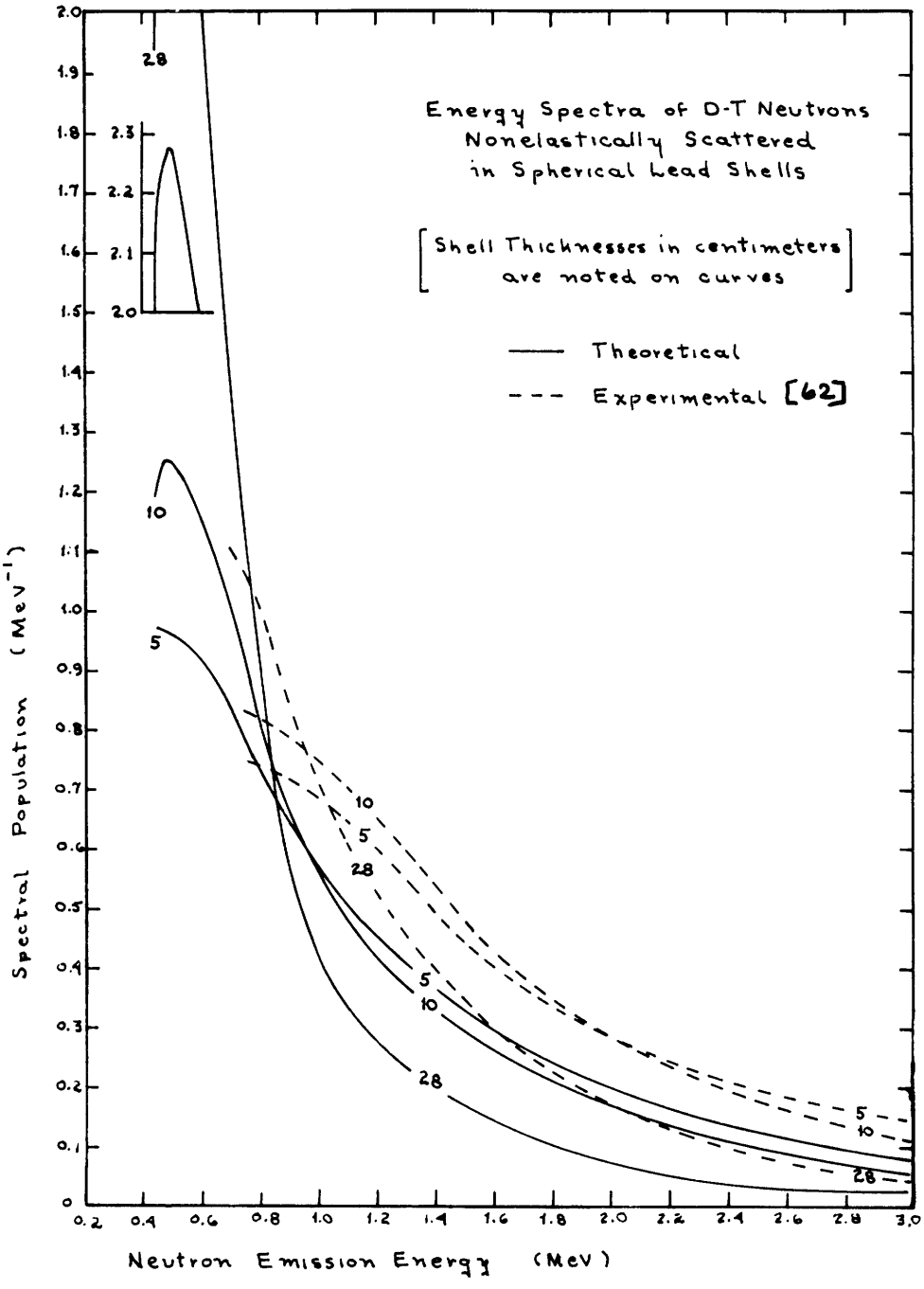

Fig. 13. Neutron emission-energy spectra.

The correlation made by Dlougy of the group of neutrons of "very small" age with neutrons slowed down by purely elastic scattering appears to be incorrect, since elastically scattered neutrons should have greater ages than neutrons slowed down in part by nonelastic collisions. Goldstein et al.[65] obtained a calculated age of ~1620 cm^2 for such neutrons. The existence of this group in the theoretical results presented here cannot be demonstrated, because of the masking effects of the other groups and boundary influences. The third group of neutrons reported by Dlougy is more likely to be a source effect, which was also observed in the theoretical calculations. (The author is indebted to Professor I. Kaplan for bringing the Goldstein calculation to his attention.)

d. Neutron Emission Spectra from Lead Shells

The energy distributions of neutrons emerging from spherical lead shells 5, 10, and 28 cm thick, as determined by experiment and calculation, are plotted in Fig. 13. In each case the distribution has been normalized to unit area under the corresponding curve for purposes of comparison. It is evident that the spectra obtained by computation show the same systematic shift toward lower mean energies with increasing shell thickness, as is observed in the experimental results. The agreement between computed and measured spectra for a given shell thickness, however, is not good. The measured distributions show consistently a larger fraction of higher energy neutrons than do the calculated distributions.

7.4 ANALYSIS OF THE COMPARISONS OF THEORY AND EXPERIMENT

a. Shapes of Detector Response Curves at Shallow Penetrations

The most pronounced disagreement between theory and experiment is that observed in comparing predicted and measured threshold detector responses at shallow penetrations in lead and boron carbide. It appears that the difference between the theoretical and experimental determinations of response for detectors whose primary sensitivity is to neutrons at rather high energies is directly associated with the inability of the calculational procedure thus far developed to reproduce the true anisotropy, and particularly the backscattering, of high energy elastic collisions. The assumption was made in developing the neutron transport equations that neutrons above 5 Mev, when scattered elastically, scatter straight ahead in angle, while those below 5 Mev experience isotropic elastic scatterings. The primary mechanisms by which source neutrons reach the energy region above 5 Mev is elastic scattering, since nonelastic collisions tend to degrade the scattered neutrons to lower energies. It is expected, and indeed has been observed, that detectors such as iron and aluminum, which are sensitive primarily to neutrons in the energy region between 5 Mev and 14 Mev, yield calculated response curves approximating pure exponential attenuation in shape. Calculations for thorium, uranium 238 and phosphorus, responding at least in part to neutrons that have experienced either elastic or nonelastic collisions, yield response curves in which the

contribution of backscattered neutrons is evident, although less strong than measurements indicate. Finally, the calculated results for low-energy detectors responding to neutrons that have experienced several isotropic elastic and inelastic scatterings show a pronounced backscattering effect which is in agreement with experiment. From the foregoing discussion, it is reasonable to conclude that the calculated flux distributions at energies above 5 Mev and relatively close spatially to the primary source are indeed in error, owing to the failure of the models employed, to treat properly anisotropic elastic scattering.

Two points should be made in connection with this discussion. First, as a result of the normalization introduced in the detector-response plots, no indication is given of the absolute error in the calculated neutron-induced reaction rate distributions introduced by ignoring backscattering. Because of the strong influence of nonelastic scattering in practical systems of interest in this study, the total neutron population in the energy regime in which the neglect of backscattering is most serious is smaller by an order of magnitude, or more, than that in the higher and lower energy regions. Hence, the actual error introduced in the calculation of critical reaction rates such as tritium production and neutron absorption is correspondingly less than it would be, were the neutrons uniformly distributed in energy as the normalization appears to imply. The error in energy deposition is further diminished by the fact that the dominant neutron-induced energy depositing reaction in the energy region under scrutiny is inelastic scattering with subsequent de-excitation of the target nuclei by gamma-ray emission. Since the gamma rays themselves travel some distance in the attenuator before absorption, the effect of the higher flux levels near the first surface, as revealed by the experiments, is distributed over a wider spatial region.

A second, and perhaps equally salient, point is that the spherical configuration in which the comparison is made between theory and experiment places greater emphasis on the effect of backscattering than does the large-radius cylindrical attenuator, cylindrical-source configuration of more direct interest in the blanket problem. The reason for this may be developed in an intuitive manner.

The weighting of the detector responses as a function of position by the square of the radial distance has the effect in a spherical configuration of cancelling the purely geometric attenuation represented by the $(r)^{-2}$ factors in the spherical transport equation. In the absence of this purely geometric effect, the attenuation experienced by a neutron is that of collision only and is a function of the neutron flight distance from the source to the point of measurement. A spherical shell emitting backscattered neutrons has positive curvature in all directions with respect to an interior point of measurement. Hence, the flight distance from emitter to detector in a spherical system is smaller, collision-induced attenuation is less likely, and the contribution of the backscattered neutrons to flux and detector response is greater than in more nearly flat configurations such as the cylinder or, in the extreme, the slab. Conversely, in comparison with the slab case, for example, forward-scattered neutrons in a sphere have a lesser weighting at points

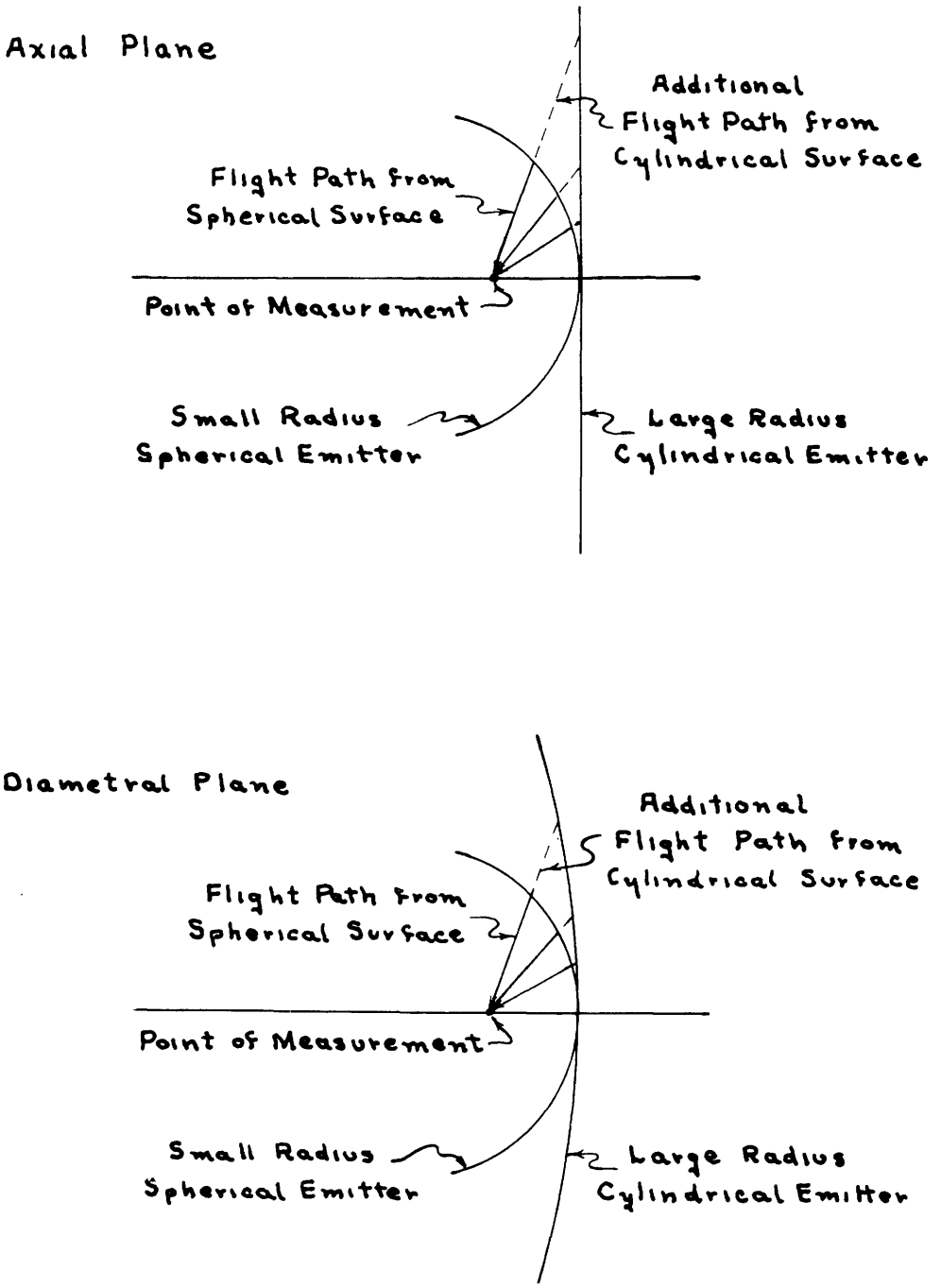

Fig. 14. Comparison of flight paths from surfaces of large and small curvature.

exterior to the emitting spherical surface, owing to the apparent negative curvature of the surface with respect to the point of measurement. A schematic comparison of flight-path lengths for backscattered neutrons is shown in Fig. 14.

It is also evident that the degree to which the backscattering effect is amplified by the configuration varies directly, although not linearly, with the effective curvature of the emitting surface as seen by the detector. Hence, the perturbation observed in the measured responses of the intermediate energy activation detectors near the origin in the spherical systems is seen to be appreciably more pronounced than would be the same effect, were it measured at corresponding depths of penetration in cylindrical systems having large inner radii. Some additional theoretical evidence in support of this contention will be cited in Section VIII. An approximate graphical calculation indicates that the contribution of backscattered neutrons within a mean-free path of the first surface is approximately 50% greater in the experimental spherical systems than in practical cylindrical configurations.

In view of these two points – the relatively low neutron populations in the energy regions in which elastic scattering anisotropy is most pronounced, and the lesser emphasis placed on backscattered neutrons in practical configurations – it is believed that the error introduced in the calculation of neutron-induced reaction rate distributions is appreciably less than would appear on the basis of the observed discrepancies between the measured and calculated detector responses in spherical assemblies of lead and boron carbide.

b. Asymptotic Slopes of Detector Response Curves

The next point of interest in comparing theoretical and experimental detector responses concerns the asymptotic slopes of the respective response curves for the several detectors used. In lead, theory and experiment are in good agreement. From this, it may be construed that, at least at the higher energies, both the cross sections and the scattering models used to develop the lead scattering matrices are reliable. In boron carbide the agreement is not as good. It is suspected that the cross sections assigned for nonelastic collisions at high energies in boron are the primary source of difficulty. Relatively few measured values, particularly of the inelastic cross sections in both boron 10 and boron 11, have been published. The measurements cover only limited energy regions and are, at least in part, contradictory. The cross sections introduced into the scattering matrices for energies above a few Mev are then largely judicious extrapolations and interpolations among fragments of data and as such are of rather limited reliability.

Additional uncertainties in evaluating the actual degree of discrepancy between theory and experiment in the asymptotic response curves arise from the fact that the original paper[48] reporting the detector-response measurements gave few experimental details. It has consequently been necessary to make assumptions concerning critical dimensions such as the inner radius of the attenuator, and to accept values given as exact. Since

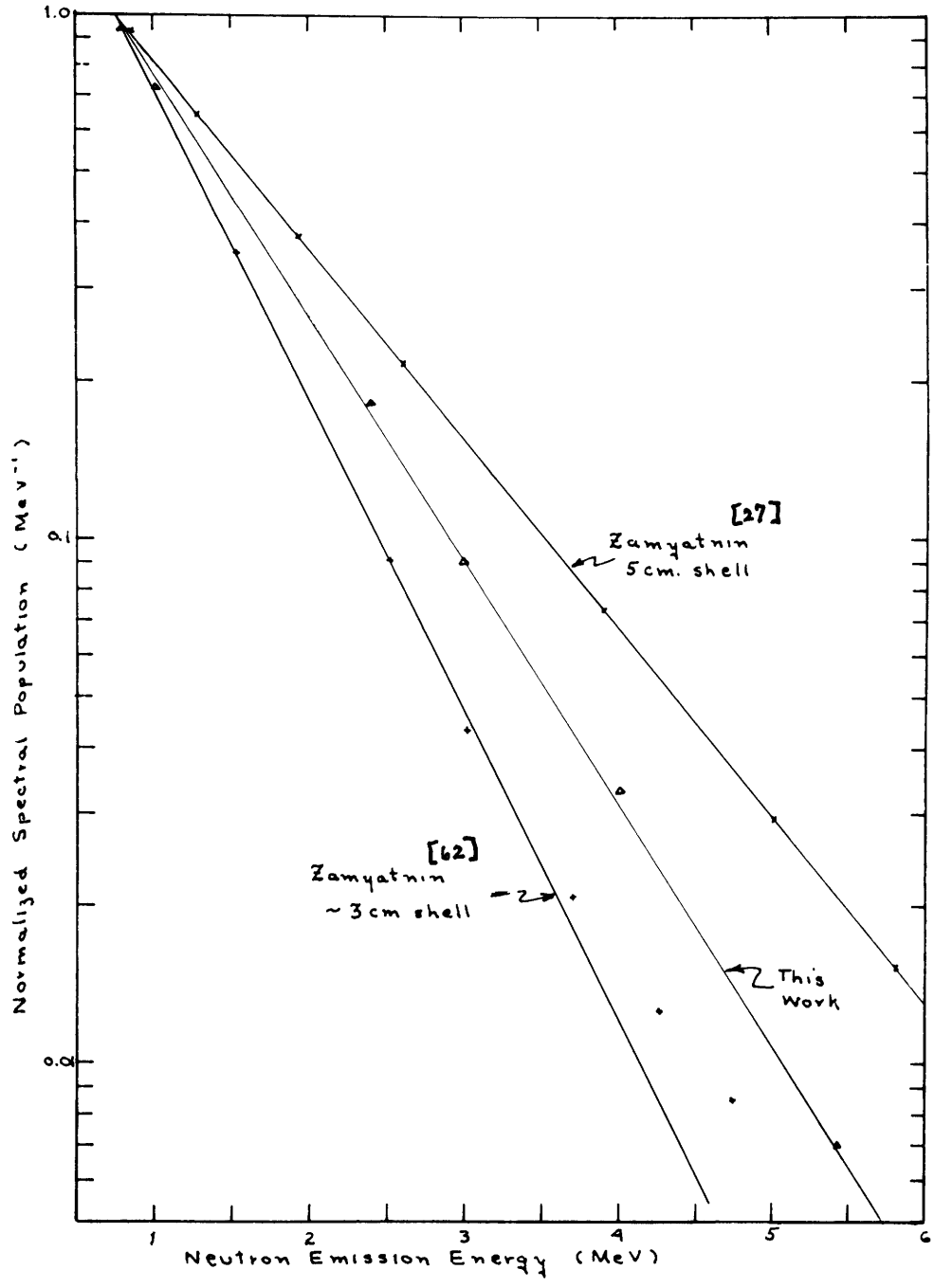

Fig. 15. Comparison of calculated and measured neutron emission-energy spectra from thin lead shells.

boron is of interest in fusion reactor blankets only as a slow neutron attenuator in the coil-shielding region, it was not considered profitable to attempt to develop boron scattering matrices consistent with the published measurements.

c. Fermi Age Determinations

The rather good agreement obtained between theory and experiment in the determination of neutron ages in graphite indicates that the carbon matrices are suitable in terms of both cross sections and scattering mechanisms. It seems likely that the methods utilized for treating low-energy elastic scattering and transport of neutrons are valid, at least for the heavier moderators.

d. Emergent Energy Spectra

In comparing the calculated and measured spectra of neutrons emitted from lead shells of various thicknesses, it was observed that although the systematic variation of neutron mean energy with shell thickness observed experimentally was reproduced theoretically, the measured and calculated spectra for each thickness show rather serious disagreement. In Fig. 15 the exponential portions of the previously compared spectra of neutrons emerging from a 5-cm lead shell are plotted in semi-logarithmic coordinates, together with the corresponding portion of the energy spectrum of neutrons emerging from a lead shell, approximately 3 cm thick, measured somewhat earlier by Zamyatnin,[27] again with a D-T neutron primary source. At shell thicknesses of approximately 5 cm or less, the contribution of multiply scattered neutrons to the spectra is small; the two experimental results, both of which are due to Zamyatnin, should be comparable. Of the two, the measurement in 1957 is in better agreement with similar measurements of effective neutron spectrum temperatures in lead made by O'Neill[64] and by Graves and Rosen.[26]

The experimental error estimates given by Zamyatnin for his earlier spectrum measurement are such that the individual contributions of first and second neutrons from the dominant (n, 2n) reaction cannot be distinguished. Hence, the data plotted for the experimental spectra represent a combination of the two separate spectra. In the energy region considered in Fig. 15, the calculated spectrum represents primarily the somewhat more energetic first neutrons, a fact that may account, at least in part, for the difference between the more reliable measurement, in 1957, and the calculated results.

7.5 INFERRED VALIDITY OF THE COMPUTATIONAL METHODS

In view of the preceding remarks concerning the agreement and disagreement observed in comparing theoretical and experimental results in several cases, it is thought that the theoretical methods employed are capable of yielding reasonably reliable predictions of neutron-induced reaction rate distributions, especially in the small-curvature configurations that are of greatest interest in this study.

VIII. RESULTS

8.1 INTRODUCTION

Neutron flux distributions in space and energy and spatial distributions of neutron-induced nuclear reactions have been calculated for a number of different blanket systems of the general configuration discussed in Section II. The calculations were made on an IBM 7090 digital computer, with the Fortran II codes described in Appendix B.

The procedure has been adopted of establishing whenever possible a standard configuration, the form of which will be noted below, and examining the effects of systematically changing individual characteristics of the configuration. The several variations treated fall into three groups. The first is made up of systems, in some cases more hypothetical than practical, designed to test the methods of calculation. The second consists of a series of variations on the basic configurations, so chosen that the effects of modifying individual components of potentially acceptable blanket designs may be assessed in terms of neutron economy and tritium regeneration. The third extends the regime of interest to include the coil-shielding region surrounding the primary attenuator. Analysis of appropriate systems allows at least a preliminary evaluation of the usefulness of two different arrangements of shielding materials proposed as protection for the magnetic coils. Each system considered here is identified by a characteristic number consisting of a single digit followed by three digits. The first digit identifies the set of computer routines, either three-region or five-region, used in making the calculations. The remaining digits form a sequence number. Systems in the 500 series contain fissile nuclides and are treated by using the fission iteration option described in Appendix B; those in the 100 series exclude fission.

We shall devote considerable space to presenting and analyzing the results of the computations. The general procedure consists of considering in sequence each of the three groups of systems, comparing the results obtained for related configurations and interjecting remarks, when appropriate, concerning the significance of the results obtained. Tabulations of nuclide densities and of the dimensions and constituents of the several systems, identified by their characteristic numbers, will be included.

It should be noted that many of the systems investigated from the point of view of neutron economy and tritium regeneration are also the subjects of analysis in terms of nuclear heating in the collateral study conducted by Homeyer.[1] Thus the present conclusions may be only partial answers to the general question of over-all blanket feasibility. More nearly satisfactory answers may be formulated only by considering the results of this work and the parallel investigations of Homeyer, Spangler,[2] and Lontai.[5]

Before proceeding, one point of clarification is in order. The term "surface" will be seen to appear in several of the tabulations that follow. This item accounts for those neutron captures that occur at the interface between the first wall and the coolant channel by virtue of the resonance surface effect, which is due in turn to absorption

resonances in several of the proposed first-wall materials.

8.2 BASIC CONFIGURATION

The standard blanket configuration used here consists of a first wall of molybdenum cooled by fused salt flowing in a coolant channel and backed by a primary attenuator composed of a graphite matrix through which fused-salt coolant flows. The fused salt considered as standard is composed of 66 mole per cent lithium fluoride and 34 mole per cent beryllium fluoride. Graphite is assumed to constitute 21% by volume of the standard primary attenuator; the rest is the lithium beryllium fluoride fused salt. Thicknesses of the respective regions are 2, 6.25, and 56 cm. Figure 16 shows schematically the standard configuration. Preliminary calculations have shown that a blanket so formed

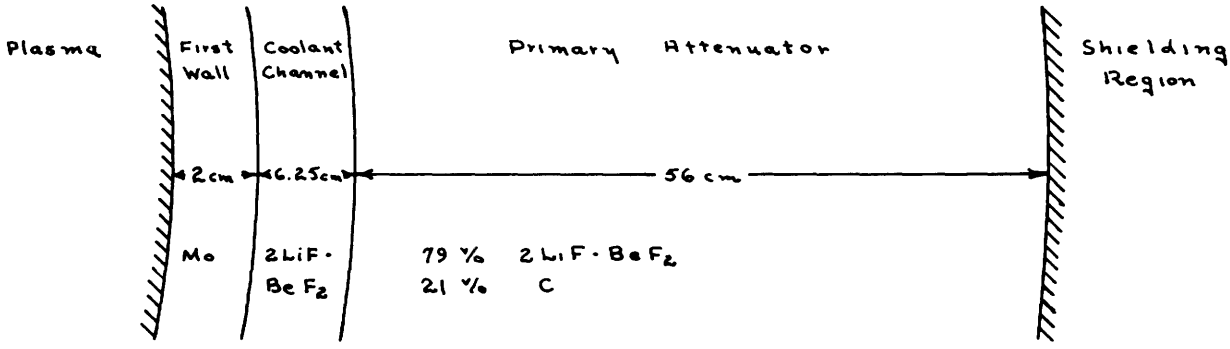

Fig. 16. Standard configuration.

should be satisfactory from the standpoint of neutron economy and nuclear heating. It is admitted that the quantities chosen for both the depth of the coolant channel and the fractions of fused salt and graphite in the primary attenuator, while reasonable, are more the results of a need for consistency in the calculations than of exhaustive optimization studies, and should be so regarded. Note, however, that since the primary attenuator is expected to be made up mainly of a fused salt either identical to, or closely resembling, that serving as first-wall coolant, the thickness chosen for the first-wall coolant channel has little effect on neutron economy. It is expected that heat transfer considerations will dominate the determination of the final width of the channel. The effect of varying the graphite fraction in the primary attenuator is dealt with briefly in section 8.4.

8.3 COMPUTATIONAL TESTS

Under the general heading of test computations, runs were made to investigate the effects on the calculated results of: (a) system curvature; (b) method of calculation (neutron transport model); (c) outer boundary conditions; and (d) neutron anisotropic

Table 5. System curvature effects.

Run Number	3-123	3-124	3-125
Source	Line	Point	Slab
Attenuator	Cylinder	Sphere	Slab
Be (n, 2n)	0.0935	0.0911	0.0912
F (n, 2n)	0.0256	0.0259	0.0249
Li^6 (n, 2n)	0.0027	0.0026	0.0026
Mo (n, 2n)	0.1811	0.1351	0.2038
Multiplication	0.3030	0.2547	0.3225
Be (n, α)	0.0093	0.0090	0.0091
C (n, α)	0.0137	0.0150	0.0131
F (n, abs)	0.1175	0.1147	0.1147
Li^6 (n, abs)	0.7758*	0.6189	0.7657
Mo (n, p)	0.0036	0.0027	0.0040
Mo (n, γ)	0.0916	0.0596	0.0897
Surface	0.0050*	0.0041	0.0062
Absorption	1.0165	0.8239	1.0026
Be (n, t)	0.0015	0.0015	0.0015
Li^6 (n, t)	0.7758*	0.6189	0.7657
Li^7 (n, tn)	0.1001	0.0973	0.0979
Tritium	0.8774*	0.7177	0.8650
Leakage > 0.4 Mev	0.1345	0.2212	0.1331
Leakage < 0.4 Mev	0.1445	0.2111	0.1903
Total Leakage	0.2790	0.4323	0.3234
Error	-0.0055	+0.0015	+0.0035

*Estimated values – Calculated surface absorption is incorrect.

downscattering models. The results of these studies will be noted in order.

a. System Curvature Effects

System curvature effects were studied by making identical calculations for a specific system in cylindrical, spherical and slab configurations. The dimensions of the first wall, coolant channel, and primary attenuator were 1.5, 6.0, and 28.0 cm, respectively; the materials were those of the standard configuration. The angular distribution of source neutrons in the slab case corresponds to that of an infinitely long cylindrical source whose radius is two-thirds that of the first wall. The line and point sources were assumed to be isotropic.

The results of the calculations are listed in Table 5. The values of the multiplication show that the calculated results for the slab are in rather good agreement with those for the cylinder in the high-energy region where the integral transport formulation is used. The line source sees a somewhat thinner first wall than does the directionally distributed slab source. A simple hand calculation shows that a distributed cylindrical source, equivalent to that assumed for the slab, would yield approximately 1.08 times the line-source multiplication in the first wall, and somewhat smaller increases in multiplication and high-energy losses at deeper penetrations into the blanket. Hence the slab configuration is considered slightly conservative in multiplication. At lower energies where the S_n method is used, the cylinder shows less leakage and more absorption than the slab, in contradiction both to physical intuition and to the results obtained for the sphere. It is suspected that the contradiction arises more from the use of an overly coarse mesh spacing in cylindrical S_n calculations than from effects arising from system curvature. On the basis of interpolation between the slab and the sphere, it is apparent that more of the neutrons should escape at low energies than the calculations show, and fewer should be absorbed. On taking the recognized uncertainties in the cylindrical S_n calculation into account, the over-all agreement between the cylinder and the equivalent slab is good. The effect of curvature in the cylinder appears to be rather small and the use of slab configurations in lieu of cylinders, well justified.

A point of some interest may be made in terms of the backscattering effect discussed in Section VII. It was suggested that the effect of backscattering is accentuated in systems of strong curvature. At the same time, we observed that for sufficiently low neutron energies the transport calculation reproduced experimental measurements rather well. Figure 17 shows the results of plotting the calculated distributions of the predominantly thermal $Li^6(n,t)$ reaction in the sphere, cylinder, and slab, with the same normalization method as was used in comparing calculated and measured detector activation distributions in Section VII. The initial rise in the normalized curves does not occur in the slab and is barely detectable in the cylinder, while it is clearly evident in the sphere, substantiating the earlier hypothesis that the error caused by neglect of anisotropic backscattering at high energies is appreciably less serious in practical blanket configurations than in the large-curvature spheres in which comparison

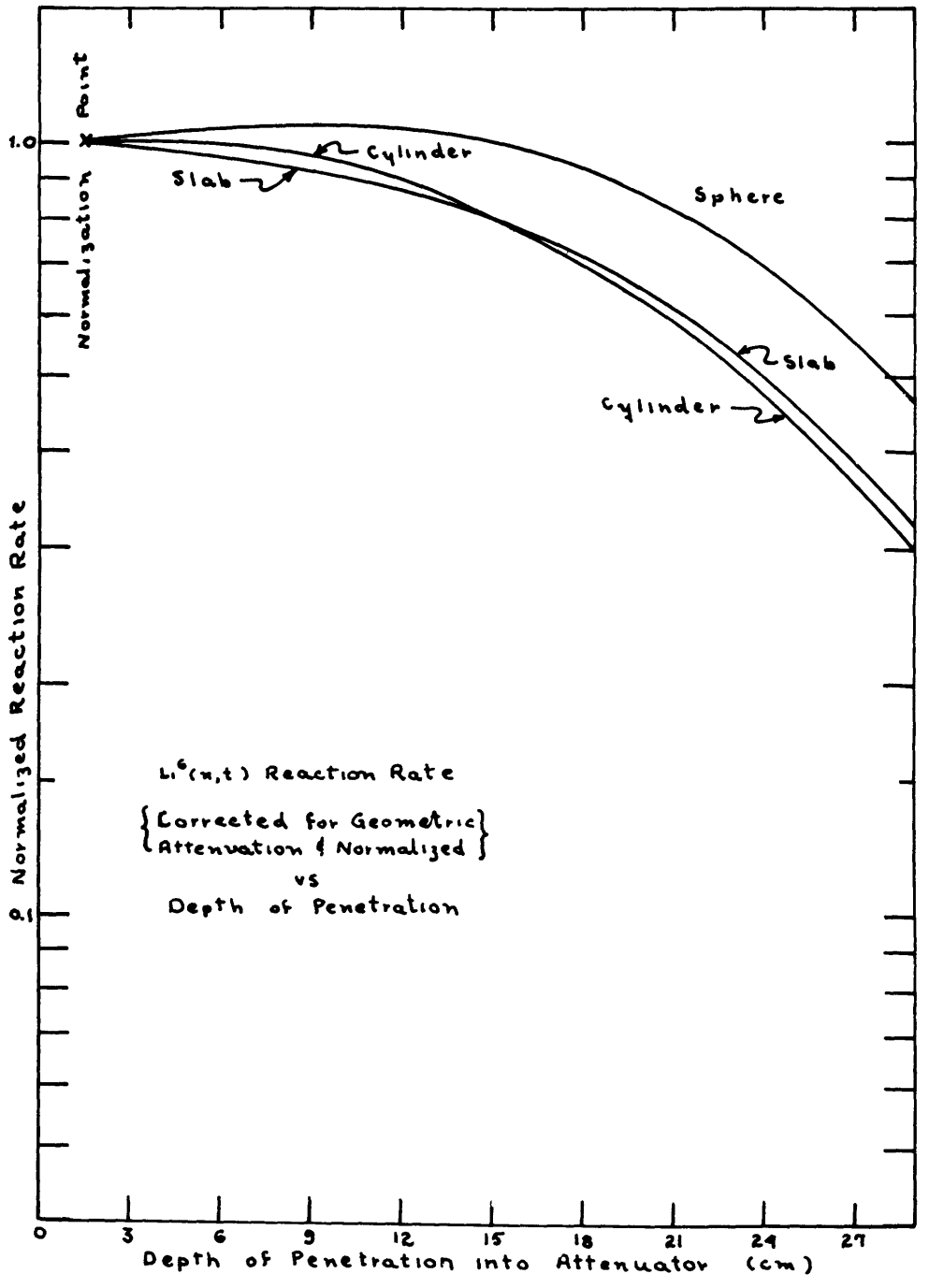

Fig. 17. Comparison of backscattering effects in configurations with various degrees of curvature.

Table 6. Effects caused by the method of calculation of neutron transport.

Run Number	3-122	3-126
Method > 5 Mev	Int. Trans	Int. Trans
Method < 5 Mev	S_n	Int. Trans
Be (n, 2n)	0.0926	0.0926
F (n, 2n)	0.0236	0.0236
Li^6 (n, 2n)	0.0026	0.0026
Mo (n, 2n)	0.2578	0.2578
Multiplication	0.3767	0.3767
Be (n, α)	0.0094	0.0094
C (n, α)	0.0137	0.0137
F (n, abs)	0.1160	0.1160
Li^6 (n, abs)	0.0138	0.0140
Mo (n, p)	0.0051	0.0051
Mo (n, γ)	0.0107	0.0102
Absorption	0.1687	0.1684
Be (n, t)	0.0014	0.0014
Li^6 (n, t)	0.0138	0.0140
Li^7 (n, tn)	0.0997	0.0997
Tritium	0.1149	0.1151
Downscattering		
Subregion A	0.2658	0.2588
Subregion B	0.3972	0.3959
Subregion C	0.5285	0.5513
Total	1.1915	1.2060
Leakage > 0.4 Mev	0.0205	0.0221
Error	+0.0040	+0.0198

between theory and experiment was made.

b. Neutron Transport Model Effect

The next point to be investigated was the effect of the neutron transport models used in the calculation. Two runs were made in the standard configuration to discover the difference between using integral transport theory and differential transport theory at energies below 5 Mev. In both cases the calculations extended only to 0.4 Mev. Table 6 lists the reaction rates predicted in these two cases.

Since the integral-transport calculations ignore ingroup scattering, as discussed in

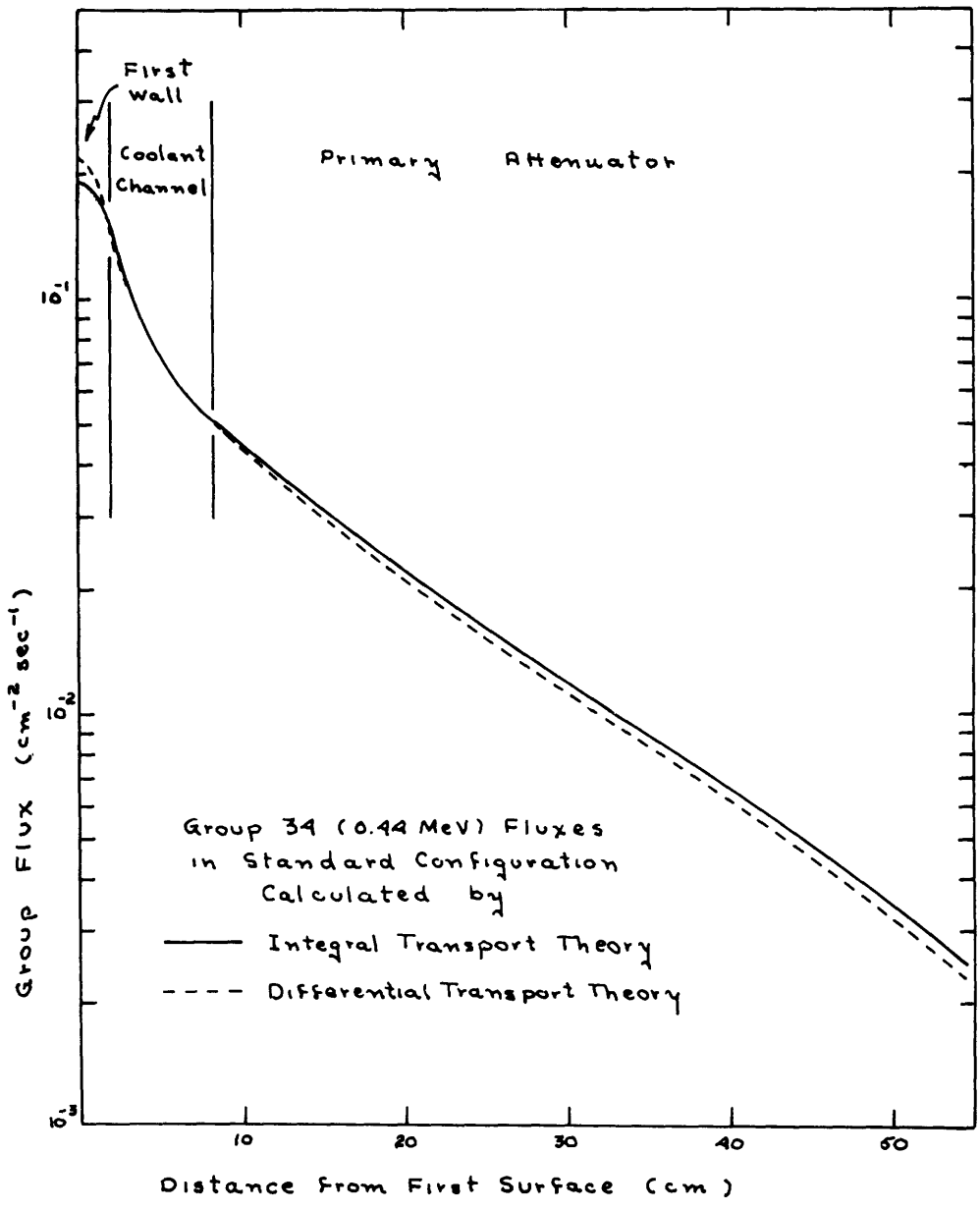

Fig. 18. Comparison of group flux distributions.

section 4.5, it is expected that S_n theory would predict higher fluxes and higher absorption rates in the first wall and lower fluxes and reaction rates in the fused-salt regions than would integral-transport theory. This was, indeed, observed, although the effect is surprisingly small in terms of tritium production. Somewhat more pronounced is the effect on downscattering and on neutron conservation. In the last case the calculational error, defined as absorption plus leakage less source and multiplication, is the basis of comparison. The effect of ignoring ingroup scattering is illustrated more graphically in Fig. 18 in which the flux distributions in the vicinity of 440 kev, as predicted by integral and differential transport calculations, respectively, are compared. On the basis of these calculations it is evident that the method of calculation has relatively little effect on the results obtained. However, since the treatment of ingroup scattering by differential transport methods is more satisfactory in theory than the approximation introduced into the integral transport formulation, at least at energies below about 5 Mev, the differential model is used in all calculations to be reported subsequently.

c. Outer Boundary Condition Effects

Test runs were also made to evaluate the effect on the calculated results of the assumption that the outer boundary of all configurations is a perfect absorber. Reaction rates were computed for two systems differing only in the depth of the primary attenuator. The systems were of the standard configuration except that the first walls were one centimeter thick. Table 7 shows the results of the calculations. The reaction rates listed for run 3-111, involving the deeper attenuator, include only the first 36 centimeters of the primary attenuator so that the tabulations are directly comparable.

It is evident that the assumption of a perfectly absorbing boundary overestimates leakage and underestimates low energy absorption in the region of calculation. At a depth of 36 cm into the primary attenuator, the fused salt-graphite matrix has an effective albedo, averaged over all energies, of approximately 0.35.

Similar conclusions may be drawn from a comparison of predicted reaction rates obtained in the standard configuration with a perfectly absorbing outer boundary and with reflectors of lead with twenty volume per cent borated water and of lithium hydride adjacent to the primary attenuator. Details of the two reflected systems will be discussed in connection with coil shielding. It is sufficient here to note that the albedos of lead with borated water and of lithium hydride, facing a 56-cm primary attenuator, are 0.32 and 0.22, respectively. Nearly all of the reflected neutrons are eventually captured by Lithium-6 to yield increases in the tritium breeding ratios of 0.02 for an absorbing lead reflector, and 0.01 for lithium hydride. Hence, the assumption of a perfectly absorbing outer boundary leads, in general, to slightly conservative estimates of the tritium production and shielding capabilities of blanket assemblies.

Table 7. Effects caused by assumed outer boundary condition.

Run Number	3-109	3-111
Primary Attenuator Thickness	36 cm	57 cm*
Be (n, 2n)	0.1020	0.1026
F (n, 2n)	0.0230	0.0229
Li^6 (n, 2n)	0.0028	0.0028
Mo (n, 2n)	0.1436	0.1436
Multiplication	0.2714	0.2719
Be (n, α)	0.0101	0.0101
C (n, α)	0.0129	0.0129
F (n, abs)	0.1278	0.1278
Li^6 (n, abs)	0.8773	0.9475
Mo (n, p)	0.0028	0.0028
Mo (n, γ)	0.0564	0.0566
Surface	0.0065	0.0066
Absorption	1.0938	1.1643
Be (n, t)	0.0014	0.0014
Li^6 (n, t)	0.8773	0.9475
Li^7 (n, tn)	0.1109	0.1110
Tritium	0.9896	1.0599
Leakage	0.1965	0.1266

*Reaction rates listed are for first 36 cm of primary attenuator only.

d. Anisotropic Downscattering Effects

In compiling the scattering matrices used in a few of the earlier calculations reported here, the assumption was made that neutrons emerge from anisotropic elastic scatterings with energy distributions characteristic of isotropic elastic collisions. As additional data were incorporated into the calculations and the scattering models refined, more nearly correct account was taken of the effects of anisotropic collisions on neutron emergent energy distributions. Comparison calculations were made by using the earlier and the more recent versions of the scattering matrices in the standard configuration and in a solid lithium system. The resulting calculated regional reaction rates are listed in Table 8.

Table 8. Effects caused by elastic downscattering model.

Run Number	3-113	3-119	3-112	3-120
Configuration	Standard	Standard	Lithium	Lithium
Downscattering Model	Isotropic	Anisotropic	Isotropic	Anisotropic
Be (n, 2n)	0.0899	0.0929		
F (n, 2n)	0.0196	0.0236		
Li^6 (n, 2n)	0.0024	0.0026	0.0142	0.0178
Mo (n, 2n)	0.2578	0.2578		
Multiplication	0.3697	0.3770	0.0142	0.0178
Be (n, α)	0.0091	0.0094		
C (n, α)	0.0116	0.0136		
F (n, abs)	0.1124	0.1163		
Li^6 (n, abs)	1.0692	1.0548	0.6009	0.5569
Mo (n, p)	0.0051	0.0051		
Mo (n, γ)	0.1300	0.1288		
Surface	0.0068	0.0067		
Absorption	1.3441	1.3347	0.6009	0.5569
Be (n, t)	0.0012	0.0014		
Li^6 (n, t)	1.0692	1.0548	0.6009	0.5569
Li^7 (n, tn)	0.0976	0.0995	0.6361	0.7511
Tritium	1.1679	1.1557	1.2369	1.3079
Leakage (> 0.4 Mev)	0.0127	0.0188	0.1771	0.2466
Leakage (< 0.4 Mev)	0.0293	0.0305	0.2304	0.2161
Total Leakage	0.0420	0.0493	0.4074	0.4627
Error	+0.0164	+0.0070	-0.0059	+0.0016

In the standard configuration the smaller energy losses and increased in-group scattering associated with anisotropic collisions lead to a larger number of high-energy reactions and to increased high-energy leakage, with correspondingly decreased low-energy fluxes and reaction rates. The over-all effect on tritium production is rather small, in the neighborhood of 1-2%, since the relatively high probability that source neutrons are scattered nonelastically, especially in the first wall, decreases the importance of anisotropic elastic collisions at greater penetrations into the blanket.

In the solid lithium system nonelastic scattering is less likely, and anisotropic elastic events are of greater significance in establishing energy distributions. In this system the calculations show a definite increase in the high-energy $Li^7(n,tn)$ reaction rate, and a somewhat smaller decrease in the $Li^6(n,t)$ rate.

The calculation of neutron energy distributions resulting from anisotropic elastic collisions necessarily involves a number of numerical quadratures which, in the present procedure, still lead to an overestimation of the average neutron energy loss, compared with the results of more detailed calculations. In view of these results, we feel that additional refinement of the numerical operations is not justified.

8.4 SYSTEM COMPONENT STUDIES

The second group of systems considered was that in which the effects of varying individual components of the basic blanket configuration were investigated. Of primary interest are the effects resulting from first-wall material, first-wall thickness, fused-salt constituents, Lithium isotopic content, back-up beryllium, and graphite fraction in primary attenuator.

a. First-Wall Material

Investigations into material requirements made by Rose and Clark[6] and Homeyer[1] have indicated that the first wall must almost certainly be made of a refractory or nearly refractory metal. Potentially useful materials are molybdenum, niobium, tantalum, and tungsten. If energy densities prove to be sufficiently low, nickel, and possibly thorium, may also find application. Of the true refractory metals, tungsten and tantalum, with effective resonance integrals of 330 barns and 1100 barns; respectively, may be eliminated on the basis of neutron capture alone. The lack of measured values for certain critical cross sections, notably that of the (n, 2n) reaction, has prevented quantitative evaluation of niobium as a first-wall material. Hence the only refractory metal investigated in detail was molybdenum. Sufficient data are available for both nickel and thorium to permit realistic comparison of these materials with molybdenum. Exploratory calculations have also been made for first walls of beryllium, lead, and uranium 238, although physical limitations prevent their use as first-wall materials in foreseeable systems.

Systems with first walls of molybdenum, nickel, thorium, and uranium 238 (and,

for comparison, with no first wall) combined with coolant channels and primary attenuators of the standard configuration were investigated first. The resulting reaction rates are listed in Table 9. Systems composed of no first wall and of beryllium and lead first walls with 3.75-cm coolant channels and 36-cm primary attenuators were also considered. Table 10 lists the corresponding reaction rates.

It is evident that among the refractory first-wall materials molybdenum and thorium actually enhance the tritium breeding ratio. Nickel, as a result of low (n, 2n) and high (n, p) cross section gives a net loss in tritium generation, compared with the hypothetical no first-wall case. On the other hand, impractical materials such as beryllium, lead, and uranium have good nuclear properties and lead to pronounced improvements in the calculated tritium breeding potential. It might be noted that the beryllium thickness considered here is well short of optimum; thicknesses of approximately 10 cm are expected to yield results comparable to the more nearly optimum lead and uranium systems.

b. First-Wall Thickness

Since molybdenum alone appears to be a practical first-wall material, a series of runs was made to investigate the effects of molybdenum thickness on tritium breeding ratio. The results of comparison runs for no first wall and for first walls of 1, 2, and

Table 9. Effects of varying first-wall materials (I).
with { Coolant channel = 6.25 cm; Primary attenuator = 56.0 cm }

Run Number	3-114	3-122	3-115	3-503*	3-504*
First-Wall Material	none	Molybdenum	Nickel	Thorium	Uranium
Thickness	none	2 cm	1 cm	2 cm	1.5 cm
First-Wall Multiplication	0.	0.2578	0.0243	0.3721	0.7205
Other Multiplications	0.1571	0.1189	0.1283	0.1231	0.1288
Multiplication	0.1571	0.3767	0.1526	0.4952	0.8493
First-Wall Loss	0.	0.1408	0.0780	0.2614	0.3523
Other Loss	1.1192	1.1880	1.0435	1.1749	1.4482
Absorption	1.1192	1.3288	1.1215	1.4363	1.8005
Li^6 (n, t)	0.9337	1.0489	0.8915	1.0311	1.3110
Li^7 (n, tn)	0.1364	0.0997	0.1114	0.1026	0.1056
Tritium	1.0717	1.1499	1.0042	1.1351	1.4166
Leakage (> 0.4 Mev)	0.0163	0.0205	0.0141	0.0209	0.0211
Leakage (< 0.4 Mev)	0.0359	0.0334	0.0311	0.0349	0.0378
Total Leakage	0.0522	0.0539	0.0452	0.0558	0.0589

*Calculations made by L. N. Lontai.

Table 10. Effects of varying first-wall materials (II).
with [Coolant channel width = 3. 75 cm; Primary attenuator depth = 36. 0 cm]

Run Number	3-105	3-103	3-104
First-Wall Material	none	Beryllium	Lead
Thickness	none	3 cm	8 cm
First-Wall Multiplication	0.	0. 3432	0. 6121
Other Multiplications	0. 1483	0. 1135	0. 0568
Multiplication	0. 1483	0. 4567	0. 6689
First-Wall Loss	0.	0. 0332	0. 0291
Other Loss	0. 9176	1. 2368	1. 4668
Absorption	0. 9176	1. 2700	1. 4959
Li^6 (n, t)	0. 7389	1. 0939	1. 3980
Li^7 (n, tn)	0. 1286	0. 1062	0. 0480
Tritium	0. 8691	1. 2069	1. 4465
Leakage (> 0. 4 Mev)	0. 1001	0. 0771	0. 0449
Leakage (< 0. 4 Mev)	0. 1482	0. 1368	0. 1455
Total Leakage	0. 2483	0. 2139	0. 1904

3 cm thickness, with all else standard, are shown in Table 11. The net multiplication available in molybdenum first walls is the difference between (n, 2n) multiplication and (n, p) and (n, γ) losses. The gain in multiplication associated with successive increments of thickness of molybdenum decreases with increasing thickness. The predominant loss mechanism, the (n, γ) reaction, increases more rapidly than linearly with thickness; also, as the attenuation of source neutrons in the first wall increases with increasing thickness, the contributions from the various high-energy reactions in the coolant channel and primary attenuator are correspondingly decreased. Since the balance of high-energy reactions in the fused salt yields net tritium production, an increase in first-wall thickness effects a loss in high-energy neutron economy in the interior regions.

For over-all neutron economy, a 2-cm molybdenum first wall appears to be most suitable. However, since the tritium breeding ratio is relatively insensitive to molybdenum thickness in the vicinity of two centimeters, determination of the optimum thickness will probably depend in large part on nuclear heating and heat transfer considerations to be summarized by Homeyer.[1]

c. Fused-Salt Constituents

A series of systems was investigated to determine the relative merits of several different fused-salt mixes in terms of neutron economy and tritium breeding potential. All systems treated were of the standard configuration, the variables being the nuclide

Table 11. Effects of varying first-wall thickness in the standard configuration.

Run Number	3-114	3-111	3-113	3-110
First-Wall Material	none	Molybdenum	Molybdenum	Molybdenum
Thickness	none	1 cm	2 cm	3 cm
First-Wall Multiplication	0.	0.1436	0.2578	0.3510
Other Multiplications	0.1571	0.1319	0.1119	0.0959
Multiplication	0.1571	0.2755	0.3697	0.4469
First-Wall Loss	0.	0.0660	0.1409	0.2251
Other Loss	1.1192	1.1750	1.1964	1.1885
Absorption	1.1192	1.2410	1.3373	1.4136
Li^6 (n,t)	0.9337	1.0251	1.0692	1.0786
Li^7 (n,tn)	0.1364	0.1163	0.0997	0.0834
Tritium	1.0717	1.1414	1.1679	1.1620
Leakage (> 0.4 Mev)	0.0163	0.0144	0.0127	0.0112
Leakage (< 0.4 Mev)	0.0359	0.0325	0.0293	0.0294
Total Leakage	0.0522	0.0469	0.0420	0.0406

densities in the fused-salt regions. The calculated reaction rates are compiled in Table 12.

The 66/34 salt, selected as the standard for this study, because of its desirable physical and thermal properties as compared with other lithium fluoride-beryllium fluoride systems, appears also to be the most suitable in terms of its nuclear properties. This combination of nuclide densities yields almost exact equivalence of multiplication by (n, 2n) reactions in beryllium and fluorine and high-energy loss by (n, α) and (n, p) reactions in the various nuclides. Under these circumstances, the entire tritium yield of the Li^7(n,tn) reaction represents a net gain. If the lithium fluoride content is increased appreciably, the reduced beryllium multiplication is insufficient to compensate for high-energy losses, particularly in fluorine. When the beryllium fluoride fraction is increased, increased neutron multiplication is obtained only at the cost of a greater decrease in the Li^7(n,tn) tritium yield.

Lithium nitrite, with no significant multiplying capability and large neutron losses caused by (n, charged-particle) reactions in nitrogen and oxygen, appears to be unacceptable in terms of neutron economy. Lithium nitrate, although not investigated in detail, may be expected to be even less acceptable, because of the presence of additional oxygen in the salt. Introduction of uranium 238 into the fused salt leads to a pronounced increase in multiplication, but resonance capture losses in the uranium and increased resonance capture in the molybdenum first wall lead to a net loss in neutron economy and tritium production.

Table 12. Effects of varying fused-salt constituents in the standard configuration.

Run Number	3-122	3-128	3-129	3-130	3-507*
First-Wall Coolant	FS)$_1$	FS)$_2$	FS)$_2$	FS)$_3$	FS)$_4$
Primary Attenuator	FS)$_1$	FS)$_1$	FS)$_2$	FS)$_3$	FS)$_1$
Be (n, 2n)	0.0926	0.1056	0.1256		0.0738
N (n, 2n)				0.0009	
F (n, 2n)	0.0236	0.0241	0.0245		0.0217
Li^6 (n, 2n)	0.0026	0.0023	0.0018	0.0022	0.0021
Mo (n, 2n)	0.2578	0.2578	0.2578	0.2586	0.3067
U (n, mult)					0.0920
Multiplication	0.3767	0.3897	0.4096	0.2617	0.4963
Be (n, α)	0.0094	0.0106	0.0127		0.0077
C (n, α)	0.0137	0.0138	0.0140	0.0163	0.0121
N (n, abs)				0.1208	
O (n, abs)				0.1884	
F (n, abs)	0.1160	0.1174	0.1198		0.1032
Li^6 (n, abs)	1.0489	1.0468	1.0510	0.7131	0.9903
Mo (n, p)	0.0051	0.0051	0.0051	0.0055	0.0061
Mo (n, γ)	0.1291	0.1388	0.1446	0.1009	0.1769
U (n, γ)					0.1111
Surface	0.0067	0.0088	0.0101	0.0047	0.0106
Absorption	1.3288	1.3414	1.3573	1.1497	1.4074
Be (n, t)	0.0014	0.0017	0.0019		0.0011
Li^6 (n, t)	1.0489	1.0468	1.0510	0.7131	0.9903
Li^7 (n, tn)	0.0997	0.0881	0.0697	0.0966	0.0800
N (n, t)				0.0069	
Tritium	1.1499	1.1366	1.1226	0.8166	1.0714
Leakage (> 0.4 Mev)	0.0205	0.0206	0.0219	0.0505	0.0294
Leakage (< 0.4 Mev)	0.0334	0.0337	0.0378	0.0588	0.0498
Total Leakage	0.0539	0.0543	0.0597	0.1092	0.0792

FS)$_1$; $66LiF \cdot 34BeF_2$
FS)$_2$; $50LiF \cdot 50BeF_2$
FS)$_3$; $100LiNO_2$
FS)$_4$; $60LiF \cdot 30BeF_2 \cdot 10UF_4$

{in units of mole per cent}

*Calculations made by L. N. Lontai.

The results reported here, while agreeing qualitatively with those obtained by Myers, Wells, and Canfield[66] as to the relative merits of the fluoride and nitrite salts, disagree seriously with the predictions of Myers and his co-workers of the absolute value of the respective salts as tritium breeders. The discrepancy is attributed in part to differences in basic configuration, since Myers et al. do not treat refractory metal first walls, and in part to the use of different methods of calculation. The earlier results were obtained by using modified fission reactor diffusion theory methods with wide energy groups in the higher energy region. The present work is based on a combination of integral and differential transport theories devised for this specific problem, and allows a more detailed description of the energy distribution of the neutron flux in the high energy region.

d. Lithium Isotopic Content

The effect of varying the lithium-6 to lithium-7 isotopic ratio in the standard 66/34 lithium fluoride-beryllium fluoride fused salt was investigated by comparing calculated reaction rates in the standard configuration for several isotopic ratios. The reaction rates are listed in Table 13. It is evident that increasing the lithium-6 content of the blanket leads to a modest increase in tritium production, largely at the expense of resonance absorption in the molybdenum first wall. The results obtained with a 0.50 lithium-6 isotopic fraction throughout the system, compared with those obtained for the lower enrichments, indicate that additional enrichment will probably not lead to any appreciable further gain in tritium production, since capture in molybdenum is nearing an irreducible minimum and reductions in leakage will be offset by decreases in the tritium yield because of the $Li^7(n,tn)$ reaction.

In addition to improving the tritium production potential of the fused salts, enrichment in the lithium-6 isotope has the desirable features of reducing radiation damage and nuclear heating in the first wall by reducing first-wall resonance capture and of improving the coil-shielding capabilities by reducing leakage. In other configurations in which resonance capture is more significant in the over-all neutron economy, enrichment of the fused salt in lithium-6 leads to an appreciably greater improvement in neutron economy than has been observed here.

Comparison of the $Li^6(n,t)$ and $Li^7(n,tn)$ reaction rates shows that lithium make-up in natural enrichment systems must be enriched to 90% in lithium. In high-enrichment systems the required isotopic fraction of lithium-6 in make-up is ~0.95. Hence, the cost of enriching make-up lithium is roughly independent of the isotopic ratio maintained within the system.

e. Back-up Beryllium

Calculations were made to investigate the effects of introducing additional beryllium, either as the metal or the oxide, into the standard configuration between the coolant channel and the primary attenuator. First walls of both molybdenum and nickel were

Table 13. Effects of varying Lithium 6 isotopic fraction in the standard configuration.

Run Number	3-122	3-131	3-132
Li^6 Isotopic Fraction			
First-Wall Coolant	natural	0.20	0.50
Primary Attenuator	natural	natural	0.50
Be (n, 2n)	0.0926	0.0925	0.0922
F (n, 2n)	0.0236	0.0235	0.0231
Li^6 (n, 2n)	0.0026	0.0045	0.0174
Mo (n, 2n)	0.2578	0.2578	0.2579
Multiplication	0.3767	0.3784	0.3905
Be (n, α)	0.0094	0.0094	0.0093
C (n, α)	0.0137	0.0136	0.0133
F (n, abs)	0.1160	0.1159	0.1154
Li^6 (n, abs)	1.0489	1.0849	1.1614
Mo (n, p)	0.0051	0.0051	0.0051
Mo (n, γ)	0.1291	0.0993	0.0604
Surface	0.0067	0.0025	0.0002
Absorption	1.3288	1.3308	1.3652
Be (n, t)	0.0014	0.0014	0.0013
Li^6 (n, t)	1.0489	1.0849	1.1614
Li^7 (n, tn)	0.0997	0.0944	0.0535
Tritium	1.1499	1.1806	1.2163
Leakage (> 0.4 Mev)	0.0205	0.0204	0.0188
Leakage (< 0.4 Mev)	0.0334	0.0329	0.0083
Total Leakage	0.0539	0.0533	0.0271

considered. The calculated reaction rates are shown in Table 14.

The gain in multiplication and in the tritium-breeding ratio when beryllium metal is introduced into the system is quite pronounced. Indeed, it appears that 2-3 cm of beryllium metal in the primary attenuator, coupled with a 2-cm molybdenum first wall will provide a comfortable margin in the tritium generation potential. Approximately 5 cm of beryllium metal appears sufficient to offset the negative worth of nickel as a first-wall material, and yields an acceptable tritium breeding ratio.

If the beryllium is introduced in the form of the oxide, its value is severely reduced, owing to competitive absorption and downscattering of high-energy neutrons by oxygen. The beryllium content in 9 cm of oxide is very nearly that of 5 cm of metal, so that the

Table 14. Effects of introducing additional Beryllium into primary attenuator.

Run Number	3-122	5-133	5-135	5-134
First Wall				
Material	Molybdenum	Molybdenum	Molybdenum	Nickel
Thickness	2 cm	2 cm	2 cm	1 cm
Beryllium Region				
Material	none	Beryllium	BeO	Beryllium
Thickness	none	5 cm	9 cm	10 cm
Be (n, 2n)	0.0926	0.2955	0.2383	0.5217
F (n, 2n)	0.0236	0.0185	0.0152	0.0182
Li^6 (n, 2n)	0.0026	0.0022	0.0016	0.0021
Ni (n, 2n)				0.0243
Mo (n, 2n)	0.2578	0.2578	0.2578	
Multiplication	0.3767	0.5740	0.5129	0.5662
Be (n, α)	0.0094	0.0302	0.0263	0.0546
C (n, α)	0.0137	0.0097	0.0045	0.0072
O (n, abs)			0.0934	
F (n, abs)	0.1160	0.1016	0.0762	0.1012
Li^6 (n, abs)	1.0489	1.2539	1.1340	1.2783
Ni (n, charged part)				0.0068
Ni (n, γ)				0.0245
Mo (n, p)	0.0051	0.0051	0.0051	
Mo (n, γ)	0.1291	0.1422	0.1446	
Surface	0.0067	0.0098	0.0098	0.
Absorption	1.3288	1.5526	1.4942	1.5328
Be (n, t)	0.0014	0.0040	0.0029	0.0059
Li^6 (n, t)	1.0489	1.2539	1.1340	1.2783
Li^7 (n, tn)	0.0997	0.0878	0.0646	0.0867
Tritium	1.1499	1.3457	1.2015	1.3709
Leakage (> 0.4 Mev)	0.0205	0.0057		0.0042
Leakage (< 0.4 Mev)	0.0334	0.0102		0.0083
Total Leakage	0.0539	0.0159		0.0125

results of runs 5-133 and 5-135 are directly comparable; the deleterious effect of oxygen is evident. It should be noted that a realistic evaluation of the relative merits of the metal and the oxide will depend on additional factors, particularly cost, since the oxide is much less expensive than the metal for given beryllium content.

f. Graphite Fraction in Primary Attenuator

Preliminary age theory calculations indicated that at energies below ~1 Mev neutron slowing-down densities and absorption rates are only weakly dependent on the graphite volume fraction in graphite-lithium fluoride-beryllium fluoride systems. The weak dependence arises from the close similarity in neutron elastic slowing-down characteristics between graphite and the fused salt. Examination of the relevant cross sections indicates that this equivalence should not hold at higher energies. In particular, while the elastic scattering cross sections of the various fused-salt constituents tend to remain more or less constant with increasing neutron energy, the corresponding cross section in graphite decreases rather rapidly for energies above 1 Mev. To substantiate the predicted negative worth of graphite, a pair of comparison runs with primary attenuator graphite fractions of 0.21 and 0.71 were made in configurations consisting of no first wall followed by a 3-cm coolant channel and the prescribed primary attenuator.

The systems selected for this comparison are not directly relevant to the more practical configurations treated in the rest of the comparison runs. Also, the anisotropic-scattering model used in these early calculations was the pseudo-isotropic model mentioned above. Hence, the results obtained are, at best, qualitative. Nonetheless, they indicate the effect of changing the graphite fraction. The results show that an increase in the graphite fraction yields a corresponding increase in leakage at energies above ~1 Mev, and to a more negative contribution to the neutron economy, owing to additional (n, α) losses in graphite. Of the two effects the increase in leakage is the more pronounced, which indicates that graphite acts primarily as a dilutant for the fused salt, at least as seen by high-energy neutrons, and yields an increase in the blanket thickness for a given tritium-breeding ratio as the graphite fraction is increased.

8.5 COIL-SHIELDING CALCULATIONS

a. Systems Investigated

Calculations were made with the five-region codes to obtain a preliminary evaluation of the coil-shielding capabilities of blanket designs. It has been observed that neutron leakage from the primary attenuator region in configurations thus far investigated tends to include a sizable fraction at energies above the fission spectrum. The need to shield against these fast neutrons, together with the equally important and equally severe gamma-shielding requirement and the basic minimum volume requirement, suggested the use of attenuator materials not normally encountered in fission reactor shield design. In particular, lithium hydride for fast-neutron moderation and absorption and lead for

nonelastic neutron slowing down and gamma attenuation appeared to offer distinct advantages over more conventional materials.

The systems investigated consisted of the standard configuration of first wall, coolant channel and primary attenuator, backed by two additional shielding regions making up the secondary attenuator. The shielding regions of interest were:

(i) A region, 30 cm thick, containing eighty volume per cent lead and twenty volume per cent water borated to approximately 0.1 molar concentration with boric acid.

(ii) A region, 20 cm thick, containing lithium hydride with the natural isotopic content of lithium-6.

The thicknesses of the regions were selected to give neutron current attenuations of approximately one order of magnitude in each region.

Optimized configurations for shielding against neutrons and gamma rays, respectively, tend to be mutually exclusive, in that the nuclear reactions of primary importance in neutron attenuation are, for the most part, sources of gamma radiation. Accordingly, comparison runs were made with the lead-water region preceding and following the lithium hydride. The former arrangement was expected to be the more effective against neutrons, the latter, against gamma rays. Flux distributions were also calculated for a composite shield identical to the latter case, but with a final gamma attenuator consisting of 6 cm of lead, and for a system identical to the former case noted above with an additional 10-cm region of molybdenum to approximate the coil support structure. Since these last two composite cases differed only slightly from the first two, distributions of the neutron-induced reaction rates were not calculated in either case. The results of the more relevant nuclear heating calculations for these two composite cases are reported by Homeyer.[1] The results of the reaction rate computations in the two more simple cases are listed in Table 15.

b. Effectiveness of Coil Shields

Of particular interest are the ultimate fates of neutrons transported from the primary to the secondary attenuator. As has been observed earlier, the lead-water region is the more effective reflector, returning ~0.32 of the incident neutrons to the primary attenuator, compared with an albedo of 0.22 for lithium hydride. In either case the $Li^6(n,t)$ reaction in the primary attenuator profitably accounts for nearly all reflected neutrons. Lithium hydride appears to be the more effective final attenuator against neutrons degraded in energy. The arrangement of lead with borated water, followed by lithium hydride, appears to be preferable for both reflection and absorption and yields a total attenuation in neutron current of at least two hundred. The inverted system is less effective by a factor of two.

The second composite run, incorporating an allowance for coil support structure, indicates that the support structure will have an albedo of ~0.4 facing a lead-water region. Against lithium hydride the support structure may be expected to have a slightly higher albedo. Including the effects of neutron reflection from the coil support, the

Table 15. Comparison of coil-shield configurations behind the standard configuration.

Run Number	5-136		5-137	
Coil-Shield Regions				
Type	Type A	Type B	Type B	Type A
Thickness	30 cm	20 cm	20 cm	30 cm
Li^6 (n, 2n)		0.000003	0.000057	
Pb (n, 2n)	0.002821			0.000352
Multiplication	0.002821	0.000003	0.000057	0.000352
H (n, γ)	0.000336	0.000011	0.000186	0.000017
Li^6 (n, abs)		0.002314	0.039779	
Li^7 (n, γ)		0.000001	0.000012	
B (n, α)	0.032999			0.001631
O (n, abs)	0.000244			0.000034
Pb (n, γ)	0.000663			0.000035
Absorption	0.034242	0.002326	0.039977	0.001717
Neutron Current into Coil-Shield Region	0.0539		0.0539	
Neutrons Reflected into Primary Attenuator	0.0171		0.0117	
Albedo of Coil Shield	0.32		0.22	
Total Absorption in Shield Region	0.0366		0.0417	
Leakage (> 0.4 Mev)	0.0002		0.0003	
Leakage (< 0.4 Mev)	0.0000		0.0002	
Total Leakage Through Coil Shield	0.0002		0.0005	
Type A Shield: 80% Lead + 20% Borated Water Type B Shield: Lithium Hydride				

over-all attenuations of the two shield configurations are approximately 300 and 150, respectively, in secondary attenuators 50 cm thick.

Although the effectiveness of the proposed shielding configurations against neutrons is demonstrated at least theoretically, as in other cases the ultimate feasibility and utility of the secondary attenuator depends very strongly on nuclear heating and gamma attenuation considerations.

8.6 SUMMARY

It is profitable to summarize some of the conclusions and implications of the theoretical results presented above (see Tables 16 and 17). To the extent that the results of comparative calculations are meaningful, the major assumptions introduced in developing transport and scattering models are seen to be reasonable and conservative. Furthermore, it appears that in most cases additional refinement of the models is not justified without improvement of the available experimental data.

The number of configurations that yielded acceptable theoretical tritium breeding ratios is indicative of the degree of flexibility available to the designer. The isolated systems treated thus far demonstrate that some degree of latitude for satisfying nuclear-heating limitations may be obtained by suitably combining first-wall, beryllium back-up, and lithium-enrichment effects. Also, the variations already considered do not by any means exhaust the possibilities. A more extensive survey incorporating materials not considered in the present work and exploiting combinations of mutually advantageous nuclides may be expected to yield an appreciably larger number of systems, acceptable from the point of view of tritium breeding, from which to develop more generally optimized configurations.

The few systems considered in connection with coil shielding indicate that at least a reasonable degree of protection can be afforded the magnetic coils by physically practical shielding configurations of acceptable dimensions. Again, the investigation of two related systems, while yielding results that are representative of what is to be expected of coil shields, barely touches the range of potentially useful shield configurations. In the case of shielding in particular, evaluation of over-all capabilities depends more on nuclear heating studies than on calculations of neutron-induced reaction rates as such.

Table 16 (Part I). Summary of investigated blanket configurations.

Run Number	Subregion A		Subregion B		Subregion C		Subregion D		Subregion E	
	depth	material	depth	material	depth	material	depth	material	depth	material
3-110*†	3 cm	Mo	5 cm	FS)$_1$	30 cm	0.25 C 0.75 FS)$_1$				
3-111*†	1 cm	Mo	5 cm	FS)$_1$	48 cm	0.25 C 0.75 FS)$_1$				
3-112†	5 cm	Li	20 cm	Li	45 cm	Li				
3-113*†	2 cm	Mo	5 cm	FS)$_1$	48 cm	0.25 C 0.75 FS)$_1$				
3-114*†	2 cm	FS)$_1$	3 cm	FS)$_1$	48 cm	FS)$_1$				
3-115*†	1 cm	Ni	5 cm	FS)$_1$	48 cm	0.25 C 0.75 FS)$_1$				
3-119*	2 cm	Mo	5 cm	FS)$_1$	48 cm	0.25 C 0.75 FS)$_1$				
3-120	5 cm	Li	20 cm	Li	45 cm	Li				
3-121	5 cm	FS)$_1$	25 cm	FS)$_1$	60 cm	FS)$_1$				
3-122	2 cm	Mo	6.25 cm	FS)$_1$	56 cm	0.21 C 0.79 FS)$_1$				
3-123 cylinder	1.5 cm	Mo	6 cm	FS)$_1$	28 cm	0.21 C 0.79 FS)$_1$				
3-124 sphere	1.5 cm	Mo	6 cm	FS)$_1$	28 cm	0.21 C 0.79 FS)$_1$				

Table 16 (Part II). Summary of investigated blanket configurations.

Run Number	Subregion A		Subregion B		Subregion C		Subregion D		Subregion E	
	depth	material	depth	material	depth	material	depth	material	depth	material
3-125	1.5 cm	Mo	6 cm	$FS)_1$	28 cm	0.21 C 0.79 $FS)_1$				
3-126 Int. Trans.	2 cm	Mo	6 1/4 cm	$FS)_1$	56 cm	0.21 C 0.79 $FS)_1$				
3-127	2 cm	Mo	6 1/4 cm	$FS)_1$	56 cm	0.21 C 0.79 $FS)_1$				
3-128	2 cm	Mo	6 1/4 cm	$FS)_2$	56 cm	0.21C 0.79 $FS)_1$				
3-129	2 cm	Mo	6 1/4 cm	$FS)_2$	56 cm	0.21 C 0.79 $FS)_2$				
3-130	2 cm	Mo	6 1/4 cm	$FS)_3$	56 cm	0.21 C 0.79 $FS)_3$				
3-131	2 cm	Mo	6 1/4 cm	$FS)_1$,20% Li^6	56 cm	0.21 C 0.79 $FS)_1$				
3-132	2 cm	Mo	6 1/4 cm	$FS)_1$,50% Li^6	56 cm	0.21 C. 0.79 $FS)_1$,50% Li^6				
5-133	2 cm	Mo	6 1/4 cm	$FS)_1$	5 cm	Be	35 cm	0.21 C 0.79 $FS)_1$	35 cm	0.21 C 0.79 $FS)_1$
5-134	1 cm	Ni	6 1/4 cm	$FS)_1$	10 cm	Be	35 cm	0.21 C 0.79 $FS)_1$	35 cm	0.21 C 0.79 $FS)_1$
5-135	2 cm	Mo	6 1/4 cm	$FS)_1$	9 cm	BeO	35 cm	0.21 C 0.79 $FS)_1$	35 cm	0.21 C 0.79 $FS)_1$
5-136	2 cm	Mo	6 1/4 cm	$FS)_1$	56 cm	0.21 C 0.79 $FS)_1$	30 cm	0.80 Pb 0.20 H_2O w/B	20 cm	LiH

Table 16 (Part III). Summary of investigated blanket configurations.

Run Number	Subregion A		Subregion B		Subregion C		Subregion D		Subregion E	
	depth	material	depth	material	depth	material	depth	material	depth	material
5-137	2 cm	Mo	6 1/4 cm	FS)$_1$	56 cm	0.21 C 0.79 FS)$_1$	20 cm	LiH	30 cm	0.80 Pb 0.20 H_2O w/B
5-138	2 cm	Mo	63 cm	0.187 C 0.813 FS)$_1$	20 cm	LiH	30 cm	0.80 Pb 0.20 H_2O w/B	10 cm	Mo
5-139	2 cm	Mo	63 cm	0.187 C 0.813 FS)$_1$	30 cm	0.80 Pb 0.20 H_2O w/B	20 cm	LiH	6 cm	Pb
3-503‡	2 cm	Th	6 1/4 cm	FS)$_1$	56 cm	0.21 C 0.79 FS)$_1$				
3-504‡	1 1/2 cm	U^{238}	6 1/4 cm	FS)$_1$	56 cm	0.21 C 0.79 FS)$_1$				
3-505‡	2 cm	Mo	6 1/4 cm	FS)$_4$	56 cm	0.21 C 0.79 FS)$_1$				

*Fused-salt nuclide densities too high by 25%.

†Pseudo isotropic high-energy scattering matrices.

‡Systems investigated by L. N. Lontai.

Table 17 (Part I). Nuclide densities of investigated materials.

Material/Nuclide	Nuclide Density
Molybdenum	$0.0635 = 10^{24}/cm^3$
Nickel	0.0914
Lead	0.0330
Carbon	0.0804
Beryllium	0.1230
Lithium	
Lithium 6	0.00344
Lithium 7	0.04296
Beryllium Oxide	
Beryllium	0.07249
Oxygen	0.07249
Borated Water	
Hydrogen	0.06666
Boron	0.00300
Oxygen	0.03333
Lithium Hydride	
Hydrogen	0.06200
Lithium 6	0.00460
Lithium 7	0.05740
Fused Salt)$_1$. 66 LiF, . 31 BeF_2 (Natural Li)	
Lithium 6	0.00175
Lithium 7	0.02185
Beryllium	0.01215
Fluorine	0.04790

Table 17 (Part II). Nuclide densities of investigated materials.

Material/Nuclide	Nuclide Density
Fused Salt)$_1$. 66 LiF, . 34 BeF_2 (20% Li^6)	
Lithium 6	0. 00472 × 10^{24}/cm^3
Lithium 7	0. 01888
Beryllium	0. 01215
Fluorine	0. 04790
Fused Salt)$_1$. 66 LiF, . 34 BeF_2 (50% Li^6)	
Lithium 6	0. 01180
Lithium 7	0. 01180
Beryllium	0. 01215
Fluorine	0. 04790
Fused Salt)$_2$. 50 LiF, . 50 BeF_2 (Natural Li)	
Lithium 6	0. 00121
Lithium 7	0. 01511
Beryllium	0. 01632
Fluorine	0. 04896
Fused Salt)$_3$ $LiNO_2$ (Natural Li)	
Lithium 6	0. 00124
Lithium 7	0. 01546
Nitrogen	0. 01670
Oxygen	0. 03340
Fused Salt)$_4$. 60 LiF, . 30 BeF_2, . 10 UF_4	
Lithium 6	
Lithium 7	
Beryllium	
Fluorine	
Uranium 238	

IX. GENERAL CONCLUSIONS

From the results and conclusions reached in this study some general points of basic importance can be made.

It is evident that tritium breeding with sufficient margin to allow for all anticipated losses can be achieved in physically practical blanket configurations by using present available materials and techniques. Thus, the basic question of the feasibility of D-T fusion reactors from the point of view of tritium regeneration appears to be favorably resolved.

Furthermore, by exploiting various combinations of mutually suitable materials, it is possible to obtain some degree of flexibility in meeting the other requirements and limitations imposed on a fusion reactor blanket assembly. In particular, there appears to be enough latitude in the conceptual design developed here to permit at least some degree of optimization of such critical aspects of the blanket as nuclear heating and magnetic-coil shielding.

In support of these points, it should be noted that the models developed for treating neutron transport and scattering lead to results that are in fairly good agreement with experimental measurements in several different systems. The disagreement between theory and experiment in certain areas of application is attributed in large part, and with some justification, to the fact that the theoretical methods were of necessity applied to systems for which they had not been intended and in which certain basic assumptions were of questionable validity. Nevertheless, the agreement obtained suggests that the predicted results for more suitable configurations should be realistic.

As a corollary to the preceding remarks, it is considered that the nuclear data now available, when supplemented by suitable models, are sufficient to allow reasonably reliable predictions to be made of neutron-induced reaction rate distributions in a variety of configurations pertaining to the blanket problem. The limitations imposed on the credibility of the results obtained thus far, because of a lack of nuclear data, are as severe as those imposed by the relative simplicity of the models utilized.

X. RECOMMENDATIONS

As we indicated initially, this work is a first look at the question of the feasibility of fusion power from the point of view of neutron economy and tritium breeding. A preliminary answer to the question of feasibility has been formulated, but much additional work must be done before final conclusions can be drawn. Some guide lines for future work are already evident; others are implicit in remarks made throughout this report. Areas in which more work should be undertaken may be summarized as follows.

1. Measurements should be made to extend the currently available knowledge of high-energy neutron cross sections and of the energy distributions of nonelastically scattered fast neutrons. Although the data now available are sufficient to permit a preliminary estimate to be made of over-all feasibility, an adequate basis does not exist for optimization studies. Particularly needed are: (a) measurements of nonelastic cross sections at energies below 14 Mev; (b) spectrum measurements both for (n, n') reactions in heavy nuclides below perhaps 5 Mev and for nearly all nonelastic reactions in light nuclides below 14 Mev.

2. The calculational procedures used here should be extended and improved to permit a more realistic treatment of anisotropic elastic scattering. Improved S_n methods with better convergence properties (especially in cylindrical configurations) could probably be more conveniently adapted to an approximate treatment of anisotropic scattering than could the more unwieldy integral procedures. The use of the analytical transport method at energies just below the source energy is probably still preferable to S_n procedures, which entail source boundary conditions.

3. Experimental measurements should be carried out to obtain a more realistic basis for testing the theoretical procedures. The efforts of Spangler[2] should prove of appreciable value in alleviating the current dearth of relevant experimental studies.

4. Additional theoretical studies bearing on neutron economy should be conducted to evaluate systems and configurations not yet treated. A number of still unexplored areas are evident. Niobium deserves more detailed consideration for the first wall as do composite assemblies of materials with good nuclear, but poor physical, properties sheathed with molybdenum for protection and strength. The prospective fused salts have not been fully evaluated. The ceramic carbide Be_2C may be a needed compromise between costly beryllium metal and the relatively inefficient oxide. The preliminary results already obtained by Lontai[5] and alluded to above show definite promise for fissile materials.

5. The results of this work and of the concurrent efforts of Homeyer[1] and Lontai[5] should be combined, and further studies should be made to investigate the blanket problem from such points of view as shielding, radiation damage, and costs (both capital and operating). Cost considerations, in particular, may well prove decisive in the question of ultimate feasibility of power generation by thermonuclear processes.

APPENDIX A

Derivation of the Neutron Inelastic Scattering Energy Operator

It is convenient, in discussions of neutron nonelastic scattering, to represent the emergent energy, E', of the neutron in terms of an operator, O, operating on the incident energy, E, of the neutron according to the relation

$$E' = O\,E \tag{A. 1}$$

The explicit form of the operator is desired.

Consider the impending collision sketched in Fig. A-1a. The quantity v_1 $(=\sqrt{2E/m_1})$ is the incident speed of the neutron in laboratory coordinates. The target mass, m_2, is at rest. Figure A-1b shows the same impending event as seen in the center-of-mass system. In this case the neutron speed v_1^c is given by

$$v_1^c = \frac{m_2}{m_1 + m_2} v_1 = \frac{A}{1 + A} v_1, \tag{A. 2a}$$

and the target speed, which is equivalent to the speed of the center of mass in laboratory coordinates, is

$$v_2^c = \frac{m_1}{m_1 + m_2} v_1 = \frac{1}{1 + A} v_1 = v_{CM}. \tag{A. 2b}$$

The quantity A is the mass number of the target particle. The energy of collision, E, is the sum of the kinetic energies of the neutron and target nucleus in the center of mass system. Thus

$$E^* = \frac{m_1}{2} \left(v_1^c\right)^2 + \frac{m_2}{2} \left(v_2^c\right)^2. \tag{A. 3a}$$

By substituting from Eqs. A. 2a and A. 2b, Eq. A. 3a takes the form

$$E^* = \left(\frac{A}{A+1}\right)^2 E + A\left(\frac{1}{A+1}\right)^2 E = \frac{A}{A + 1} E. \tag{A. 3b}$$

The energy, E^{**}, remaining in the center-of-mass system after excitation of a level of energy E_λ in the target nucleus is

$$E^{**} = E^* - E_\lambda = \frac{A}{A + 1} E - E_\lambda. \tag{A. 4}$$

The neutron and excited target nucleus subsequently separate by mutual recoil in center-of-mass coordinates as shown in Fig. A-1c. The quantity ν is the cosine of the angle between the initial and final directions of the neutron in the center-of-mass system, v_3^c and v_4^c are the speeds of the recoiling neutron and target, respectively. The recoil energy is apportioned between the neutron and the target so that

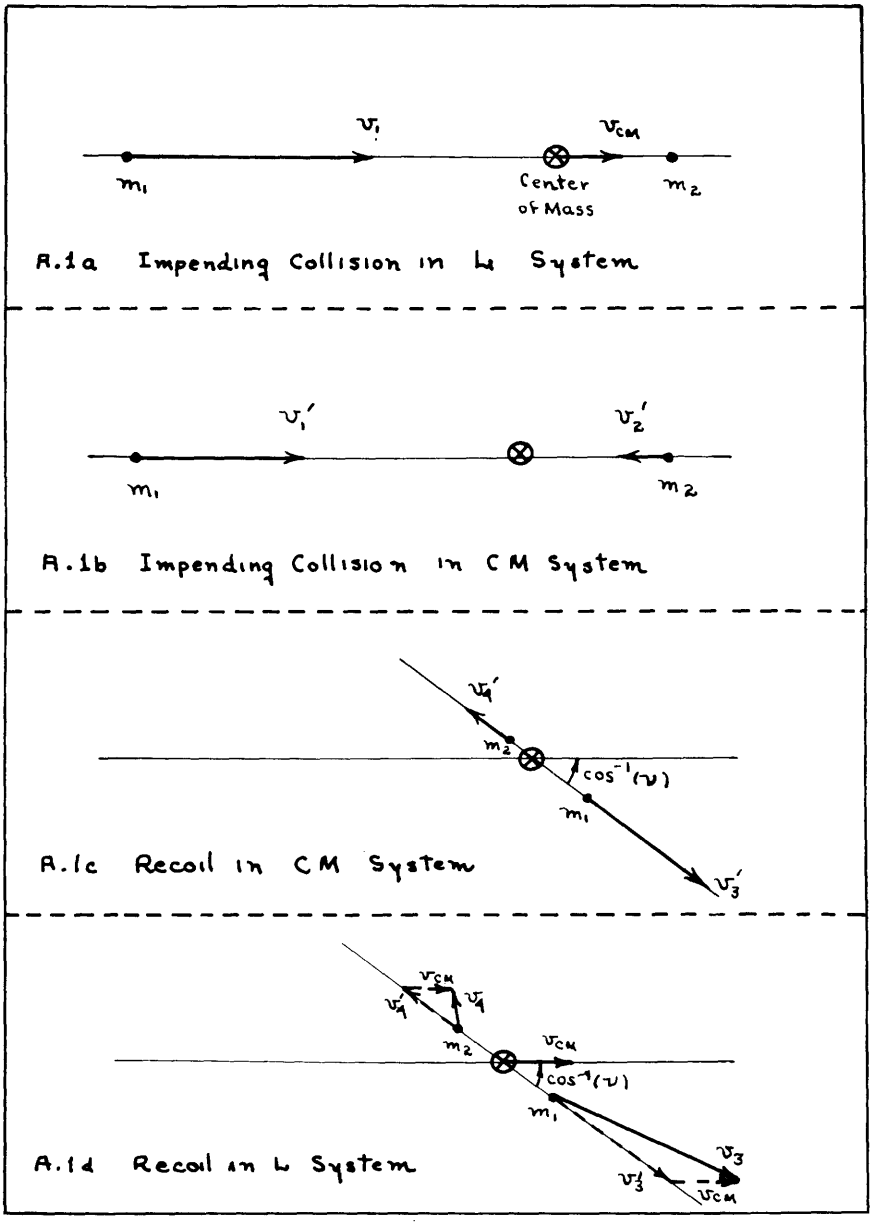

Fig. A-1. Schematic history of an inelastic scattering event.

$$E_3^c = \frac{A}{A+1} E^{**} \tag{A. 5a}$$

and

$$E_4^c = \frac{1}{A+1} E^{**}. \tag{A. 5b}$$

The corresponding speed, v_3^c, of the scattered neutron in center-of-mass coordinates is given by

$$v_3^c = \sqrt{\frac{2E_3^c}{m_1}} = \sqrt{\frac{2}{m_1}\left(\frac{A}{A+1}\right) E^{**}}. \tag{A. 6}$$

Transformation back to the laboratory system is effected as shown in Fig. A-1d. The final velocity, v_3, of the scattered neutron in the laboratory system is readily obtained through the law of cosines in the form

$$v_3^2 = \left(v_3^c\right)^2 + (v_{CM})^2 - 2v_3^c v_{CM}\nu.$$

Substituting from Eqs. A. 2b and A. 6, we obtain

$$v_3^2 = \frac{2}{m_1}\left(\frac{A}{A+1}\right) E^{**} + \frac{2}{m_1}\left(\frac{1}{A+1}\right)^2 E - 2\left(\frac{2}{m_1}\right)\frac{1}{A+1}\sqrt{\frac{A}{A+1} EE^{**}}\,\nu, \tag{A. 7a}$$

and, finally, incorporating Eq. A. 4, we obtain

$$v_3^2 = \frac{2E}{m_1}\left\{\frac{A}{A+1}\left[\frac{A}{A+1} - \frac{E_\lambda}{E}\right] + \frac{1}{(A+1)^2} - \frac{2}{A+1}\sqrt{\frac{A}{A+1}\left[\frac{A}{A+1} - \frac{E_\lambda}{E}\right]}\,\nu\right. \tag{A. 7b}$$

With some minor rearrangements of terms, the neutron emergent energy, $E'\left(= \frac{m_1\left(v_3^c\right)^2}{2}\right)$, takes the form

$$E' = \left\{\left(\frac{A}{A+1}\right)^2\left[1 + \frac{1}{A^2} - \frac{(A+1)}{A}\frac{E_\lambda}{E} - \frac{2}{A}\sqrt{1 - \frac{(A+1)}{A}\frac{E_\lambda}{E}}\,\nu\right]\right\} E. \tag{A. 8}$$

The expression within the braces is the desired multiplying operator

$$O = \left(\frac{A}{A+1}\right)^2\left[1 + \frac{1}{A^2} - \frac{(A+1)}{A}\frac{E_\lambda}{E} - \frac{2}{A}\sqrt{1 - \frac{(A+1)}{A}\frac{E_\lambda}{E}}\,\nu\right]$$

$$= O[E, E_\lambda, \nu, A]. \tag{A. 9}$$

If the inelastic collision is isotropic in the center-of-mass system, all values of ν in the range $-1 \leq \nu \leq +1$ are equally probable, and the average value of ν for a large number of collisions is zero. In this case, Eq. A. 9 reduces to

$$\overline{O} = \left(\frac{A}{A+1}\right)^2 \left[1 + \frac{1}{A^2} - \frac{(A+1)}{A}\,\frac{E_\lambda}{E}\right]$$

$$= \overline{O}[E, E_\lambda, A]. \qquad \text{(A. 10)}$$

The result of operating on incident energy, E, with the averaging operator, $\overline{O}$, is the average value of the emergent energy, $\overline{E}_3$. Symbolically,

$$\overline{E}_3 = \overline{O}[E, E_\lambda, A]\, E. \qquad \text{(A. 11)}$$

GLOSSARY

Symbol	Definition	Units
A	Atomic number	
E	Incident energy	Mev
E'	Emergent energy	Mev
$\overline{E}'$	Average emergent energy	Mev
E^*	Collision energy in center-of-mass system	Mev
E^{**}	Residual energy in center-of-mass system after excitation	Mev
E_λ	Energy of excited level	Mev
$E_{subscript}$	Particle energy	Mev
O	Operator	
m	Particle mass	amu
v	Particle speed	
ν	Cosine of scattering angle	

Subscript	Reference
1	Neutron before collision
2	Target before collision
3	Neutron after collision
4	Target after collision

Superscript	Reference
c	Defined in center-of-mass system

APPENDIX B

Digital Computer Codes

B. 1 INTRODUCTION

Two sets of digital computer codes have been developed to expedite carrying out the neutron transport and scattering calculations involved in predicting neutron-induced reaction rate distributions in blanket assemblies. While the preparation of machine codes was not of itself an explicit goal of this study, a brief description of the routines developed for, and used in, making the calculations is considered desirable. Accordingly, we shall discuss in rather general terms the characteristics and capabilities of the codes. Complete listings of all relevant routines are not included here (see Preface). Details of the inputs to the codes form the substance of Appendix C.

B. 2 GENERAL CHARACTERISTICS OF THE CODES

a. Coding Language and Machine Requirements

With the exception of a few modified FAP library routines, all routines developed in this study were written in FORTRAN-11 language and are intended for IBM 709 and IBM 7090 digital computers. Specifically, the codes are designed for the IBM 7090 facility of the Computation Center, M. I. T., and are compatible with the FORTRAN MONITOR system that was in use at the Computation Center in September, 1962.

b. Maximum Mesh Sizes

The codes are available in two versions, a three-region set that incorporates a fission iteration option (described below), and an extended five-region set with no fission iteration capability. In the three-region set a total of 31 spatial positions, including the inner and outer boundaries, and 8 directional cosine values make up the maximum geometric mesh available for slab and spherical configurations. For cylindrical systems the geometric mesh is limited to 15 spatial positions and 4 values of each of the 2 directional cosines. The five-region set incorporates two additional regions to permit either more detailed analysis of the interior sections, the wall, the coolant channel and the primary attenuator, or extension of the region of calculation to include the coil shield. A total of 62 spatial positions and 4 directional cosine values make up the maximum geometric mesh for slabs and spherical shells. The mesh for cylindrical shells is limited to 31 spatial positions and 4 values of each of the 2 directional cosines.

c. Major Subdivisions

Both the three-region and the five-region sets are made up of three distinct portions:

(i) A high-energy program that computes neutron flux distributions in space and energy in the first 34 groups corresponding to the energy regime from 14. 2 Mev to 0.42 Mev;

(ii) A low-energy program that calculates flux distributions in space and energy in the last 16 groups that span the energy range from 0.42 Mev to thermal energy; and

(iii) A reaction rate program that uses flux decks generated by the first two programs to calculate neutron-induced reaction rate distributions in space.

Each program is further subdivided into a main routine and a number of subroutines. In several cases specific subroutines may take any one of several forms, the choice depending on the particular nature of the blanket configuration that is being investigated.

The higher and lower energy programs are of immediate interest to this study. These will be discussed in the sequel. The reaction rate program is a simple service code, incorporating no special or unique devices, and need not be further considered here.

d. Program Coupling

The higher energy and lower energy programs are designed to be run separately. Coupling of the programs is obtained by means of an intermediary punched card deck generated as output by the higher energy program and supplied as input to the lower energy program. An option to allow direct coupling of the programs as links of a CHAIN job is provided in the five-region version of the programs. Note that the configuration descriptions supplied to the higher and lower energy programs for a given case must be identical in all respects, including mesh spacing, if meaningful results are to be obtained.

B.3 HIGHER ENERGY PROGRAM

a. Special Characteristics

Treatment of source degeneration. The high-energy program is based on a multipass concept whereby certain subroutines are activated either two or three times with successive minor internal changes to carry out scattering and transport calculations. The first case in which multipass operations are involved is that concerned with cylindrical or spherical sources. It was noted in Section V that the various directional quadrature methods generate poor approximations to the true integrals of vector flux as the angle subtended by the distributed source, as seen from the flux point, decreases. A logical choice is incorporated in the main routines of the higher energy program to determine at what spatial point the source is better treated as degenerate (that is, as a line or point source), to interrupt the calculations and revise the values of the geometric constants, and to reactivate the appropriate subroutines with modified logic patterns and continue flux distribution calculations.

Treatment of mixed anisotropic and isotropic scattering. The second instance of multipass operations is that concerned with the transition from pure straight-ahead scattering to either pure isotropic or mixed scattering. At high energies few neutrons have experienced an isotropic scattering. Hence, the directional distribution of the flux is initially dominated by a strongly anisotropic component because of neutrons that

have been scattered only elastically. At lower energies the isotropic component becomes stronger and, below 5 Mev, constitutes the entire distribution. Since the numerical methods used here tend to obscure the weaker component of the directional distributions, calculations in the first 10 energy groups are carried out first for neutrons that have not been scattered isotropically and are then repeated in a second pass for the neutrons which have experienced at least one isotropic collision.

The two multipass cases are not completely separable. Under appropriate circumstances a total of 3 passes calculating in succession the straight-ahead distributed source component, the straight-ahead degenerate source component and the isotropic source-independent component are required.

Fission iteration scheme. One special characteristic of the three-region high-energy code is the fission iteration option. When this option is activated fission reactions initiated by first-generation (fusion) neutrons are treated as absorptions in the first iteration, and as sources in the second iteration. Fission reactions caused by second-generation neutrons born of first-generation fission reactions are absorptions in the second iteration and sources for the third, and so on. In each iteration neutron fluxes at all points in the space-energy mesh are calculated. When the prescribed number of iterations has been made, the contributions of the several iterations are summed at each mesh point and, if required, an estimate of the contributions of additional iterations is calculated.

b. Code Logic

The over-all logic flow in the higher energy programs is controlled by the higher energy (MAIN) routine. Calculations proceed as follows:

1. The description of the configuration and the designated nuclide decks are read in and necessary constants are established by the INPUT subroutine;

2. Fluxes in the first four energy groups are calculated under the control of routine MAINA; subroutine ANALYT is utilized to calculate source factors and penetration terms, and subroutine XXX to generate collision factors. If source degeneration occurs, subroutine CONSRV provides necessary normalization;

3. Fluxes in groups 5 through 10 are calculated by the MAINB routine which incorporates the integral transport subroutines LINFLX for slab configurations and RADFLX for nonplanar systems. RADFLX calls the subroutine RADINT to evaluate the transport integrals. Sources in the several groups are calculated by SASRC for straight-ahead scattering and ISOSRC for isotropic scatterings. For degeneration of the primary source, CONSRV is again actuated for normalization;

4. Fluxes in the next 24 groups are calculated under the control of routine MAINC. This routine selects the desired transport routine, LINFLX or RADFLX (and RADINT) for the integral transport model, SNSNSN for the differential transport model or DIFFSN for the diffusion model, and uses ISOSRC for the source calculations. Since the diffusion model was not used in production calculations, an IBM 7090 version of the DIFFSN subroutine has not been prepared;

5. If fission iterations are indicated, control is returned to MAINB, and the required number of iterations, activating successively MAINB and MAINC and their respective subroutines, is made; and

6. When all flux calculations have been completed, the source distributions in groups 35 through 38 are calculated by subroutine LWSRC. Control of punched card output (via tape) of flux and source decks is in the (MAIN) routine; control of printed output is in routines OUTPUT and OUTTWO.

c. Auxiliary Routines

In addition to the routines listed above and the standard library routines available in the MONITOR system, two FAP-coded subroutines are required. These are the MI-FLIP routine for generating punched identification cards in the output decks and a modified version of the library routine SQRT, so revised that occurrence of a negative argument in the square root function leads to a zero value of the function rather than to an error step.

d. Typical Running Times

Loading of program binary decks and data decks for a higher energy run and the subsequent computations and preparation on tape of punched and printed output for a typical nonfissile slab configuration in three subregions requires 1.0 to 1.2 minutes of IBM 7090 time. Since the five-region high-energy program is more efficient than its predecessor, the three-region code, calculations in a five-region slab configuration with the maximum geometric mesh require approximately the same amount of machine time as does the three-region version. As might be expected, input and output operations consume a large fraction of the total running time. If fission iterations are called for in a three-region slab, each iteration will require 0.3 to 0.4 minutes, including breakpoint output.

The spherical shell configurations require appreciably more running time than do slabs, particularly if the integral-transport model is used for all high-energy calculations. Test runs made using the integral transport subroutines in a three-region spherical shell required approximately 5 minutes. Corresponding runs made using the S_n routine in the last 24 groups required approximately 2 minutes.

Cylindrical configurations are even more time-consuming. A run made for a cylinder in 3 regions with the limited geometric mesh and using S_n procedures required 3.4 minutes.

B.4 LOWER ENERGY PROGRAMS

a. Special Characteristics

Code simplifications. Several convenient simplications in coding are permitted in the lower energy region.

1. The elimination of multipass operations;
2. The elimination of integral transport calculations, and

3. The elimination of fission iterations.

In practical blankets few, if any, neutrons reach the energy region below 0.42 Mev without experiencing at least one isotropic scattering. Hence, neither of the two special cases requiring multipass operations in the higher energy code occur here. Also, isotropic scattering effectively decouples the flux distribution from the primary source distribution so that the particular advantages of the integral transport model are no longer evident in the lower energy region. Elimination of the fission iteration option is based on the premise that the only fissile nuclides of interest in blanket design are those which are not suitable for conventional fission reactor applications, because of high fission threshold energies. Thus, fissions in the lower energy region do not occur.

Treatment of resonance capture. The method developed in Section VI for estimating resonance absorption rates recognizes both volume and surface contributions to the over-all absorption rate. The volume capture probabilities can be expressed as effective macroscopic cross sections and require no special consideration. It was shown, however, that surface effects can be best represented as weighting factors applied to interface source strengths. The neutron transport subroutines used in the lower energy programs require additional logic steps to identify the points in the space-direction mesh at which weighting factors are to be applied and to suitably modify the calculated source strengths at those points.

Treatment of last group cross sections. It was also pointed out in Section VI that the lowest energy group, extending from 10 ev to thermal energy, is very broad in terms of lethargy, and properly averaged capture cross sections must be used if reasonable approximations to group absorption rates are to be obtained. The lower energy programs read in 0.025 ev cross-section data in lieu of group 50 values, determine whether thermalization is likely in each subregion, and, when necessary, calculate group cross sections according to the scheme outlined in section 6.3.

b. Code Logic

The over-all logic pattern of the lower energy programs is established by the lower (MAIN) routine. The calculations proceed as follows:

1. The physical description of the configuration, the lower energy nuclide decks, and the source deck generated by the higher energy code are read into core storage by the LWINPT subroutine. Generation of properly weighted cross sections for the last group is accomplished by subroutine CSAVG;

2. Fluxes in each of the 16 lower energy groups are calculated by calling first the LWSRCE subroutine and then either the SNSNSN or the DIFFSN subroutine. Again, the IBM 7090 version of the diffusion routine (DIFFSN) has not been prepared, since S_n calculations have proved entirely adequate. In either case the neutron transport routine is modified to allow for resonance surface effects; and

3. When flux calculations are finished punched output of lower energy flux decks and surface absorption and leakage losses is prepared on tape under control of the (MAIN)

routine and printed output is written on tape by the LWOTPT subroutine.

c. Auxiliary Routines

In addition to the routines mentioned above and the standard library routines available to the MONITOR system, the lower energy routines require only the FAP-coded routine MI-FLIP.

d. Typical Running Times

In simple three-region slab and spherical-shell configurations the lower energy program requires slightly less than 1 minute of machine time for an entire calculation, including loading time and input and output. In cylindrical configurations typical running times are 2-3 minutes. When the five-region routines are used with full meshes the times required are increased to approximately 1 minute for slabs and spheres and 3 minutes for cylinders.

Provision is made with the five-region set of routines for chaining the higher and lower programs in a single run. It is expected that a chained run will require somewhat less time for completion than would separate submissions of the higher and lower energy programs. Thus far, no attempt has been made to activate the chain option.

APPENDIX C

Computer Code Input Decks

C. 1 INTRODUCTION

Inputs to all of the programs must follow a rigidly prescribed form if the codes are to function properly. The purpose of this appendix is to describe in detail the format of the input decks associated with the higher and lower energy programs in both the three-region and the five-region versions. The first half of this appendix is devoted to identifying the various constants and parameters supplied to the programs and indicating the significance of the several values allowed for control parameters. The detailed formats of the higher and lower energy nuclide decks are also considered. In the second half of this appendix the structure of the input deck for each of the programs is set down in FORTRAN symbolic form.

C. 2 INPUT QUANTITIES

a. Program Logic Inputs

Certain of the variables and constants supplied to the programs are used as control parameters to establish the logical path to be followed in the course of calculation or as descriptive constants for output purposes. Such quantities are to be distinguished from the parameters that are supplied to specify the physical and nuclear characteristics of the blanket configuration that is being considered. The control parameters are identified as follows:

a) METHOD – The calculational method to be used below 5 Mev. Permitted values are:

1 – diffusion model, no fission extrapolation,

2 – diffusion model with fission extrapolation,

3 – integral transport model, no fission extrapolation,

4 – integral transport model with fission extrapolation,

5 – differential transport model, no fission extrapolation,

6 – differential transport model with fission extrapolation.

b) JJ – The order of the directional quadrature. Permitted values are 4 and 8 (unless restricted by program capabilities).

c) NCLDS – The number of different nuclides to be considered in the blanket. The maximum number is 10.

d) MAXF – The total number of fission iterations desired.

e) IFIS – The value 1 bypasses breakpoint output of flux distributions after each fission iteration. The value 2 yields breakpoint output.

f) LINK – The value 1 couples the higher and lower energy programs as a chain job for a given configuration. The value 0 separates the programs into two independent submissions.

g) CONVRG – The convergence criterion for differential transport and diffusion iterations (0.005 has proved adequate).

h) XQ(i) – A one dimensional array of twelve floating point variables provided as reserve input. The quantity XQ(1) is the thermalization criterion in the lower energy programs (30.0 is suitable for practical materials). No other elements are used.

i) LY(i) – A one-dimensional array of 12 fixed-point variables provided as reserve input. No elements are used as input although several are used internally. The values read must be 0.

j) IQQA, IQQB, IQQC – The value 0 indicates that no resonance absorbing nuclides are present in subregions A, B, and C, respectively. The value 1 indicates that resonance-absorbing nuclides are present.

k) KKF – The subregion in which a fissile nuclide is present. The values 1, 2, and 3 indicate subregions A, B, and C, respectively. When no fissile nuclides are present, the value should be 0.

l) ITER – Not used. The value must be 0.

A few additional quantities are provided for output purposes. These are:

m) E(i) – A one-dimensional array of 38 elements in the higher energy program, 16 in the lower, listing the upper energy bounds of the energy groups.

b. Physical and Nuclear Inputs

In addition to the logical and output parameters, the programs require as input a description of the physical and nuclear characteristics of the blanket assembly that is being considered. In all that follows, distances are expressed in centimeters, cross sections in barns, and atomic densities in units of 10^{24} atoms per cubic centimeter. Note that in this convention the product of microscopic cross section and atomic density is macroscopic cross section in reciprocal centimeters. The variables have the forms:

a) MODE – The geometric form of the configuration to be considered. Permitted values are:

1 – slab blanket with straight-ahead plane source,

2 – slab blanket with slab source,

3 – cylindrical blanket with line isotropic source,

4 – cylindrical blanket with cylindrical isotropic source,

5 – spherical blanket with point isotropic source,

6 – spherical blanket with spherical isotropic source.

b) RP – The radius of the cylindrical or spherical source.

c) RW – The radius of the first surface of the wall.

d) A, B, C, U, V – The thicknesses of subregions A, B, C, D, and E, respectively.

e) SPCA, SPCB, SPCC, SPCU, SPCV – The mesh spacings in subregions A, B, C, D, and E, respectively.

f) AAN, BBN, CCN, UUN, VVN – The atomic densities of a given nuclide in subregions A, B, C, D, and E, respectively.

g) FFN – The atomic density of the fissile nuclide in the subregion specified by KKF.

h) ESFX(i) – A one-dimensional array of 34 elements listing the product of fission cross section by neutron yield per fission in the first 34 energy groups.

i) FSPCT(i) – A one-dimensional array of 38 elements listing the probabilities that a fission-born neutron appears in each of the first 38 energy groups. (The sum of the elements must be unity.)

j) S(i) – A one-dimensional array with a maximum of 8 elements giving the angular distribution of primary source neutrons for each of the Legendre-Gauss directional cosines, beginning with the most nearly straight-ahead.

An array and a single variable, together with identifying FLIP cards, are generated as punched-card output by the higher energy program for use as input to the corresponding lower energy program. These are:

k) TSD(i, j) – The distribution in space, i, and energy, j, of neutron sources in the 35^{th} through the 38^{th} groups arising from neutron-induced reactions in the first 34 higher energy groups.

l) TTLLKG – The neutron loss caused by leakage through the outer boundary in the first 34 higher energy groups.

c. Nuclide Decks

General Form

In addition to the input quantities already considered, it is necessary to supply to the programs tabulations of neutron scattering and absorption probabilities in each energy group for each of the nuclides in a blanket assembly. The word "nuclide" is used here to indicate a material of unique nuclear properties. In most cases elements, consisting of one or more isotopes, are considered to be "nuclides." Occasionally, isotopes are treated as individual nuclides. The tabulation for a single nuclide takes the form of a deck of cards supplied as input to the appropriate programs. Each deck incorporates all data necessary for describing the probability of occurrence of the several neutron-induced reactions of interest and the results of the reaction for neutrons in all energy groups colliding with nuclei of the nuclide that is being considered. The precise forms of the higher and lower energy decks are specified below, together with symbolic listings of the decks. Listings of the decks themselves are incorporated in Appendix D.

Higher Energy Nuclide Deck

The deck associated with the higher energy program consists of 163 cards. The deck is arranged in sections giving in sequence the title card, the elastic scattering matrix, the directional correlation array, the nonelastic scattering matrix, a special scattering matrix used in generating the source array for coupling to the lower energy routines, and the total cross-section array. The nonelastic matrix is in reality a triangular array, since upscattering is forbidden. In the interest of conservation of machine storage registers, all identically zero elements of the matrix have been discarded and the array

has been folded into a more compact form. Table C. 1 is a symbolic listing of a higher energy nuclide deck. The symbols at the far right are sequence numbers appearing in columns 73-80. Entries set off by asterisks are inserted only for heuristic purposes and must not appear in the actual nuclide decks. The title entry has the format 2A6; all numerical entries are in the form F12. 8.

Lower Energy Nuclide Deck

The lower energy deck, used with the lower energy program, contains a total of 17 cards if the corresponding nuclide does not exhibit significant resonance capture, or 21 cards if resonance effects must be treated explicitly. The deck consists of a title card, a mixture of one- and two-dimensional arrays covering volume based effects, and, when required, a one-dimensional source weight array. Each of the volume-oriented cards corresponds to a single energy group and contains in successive entries the cross sections for ingroup scattering and for scattering to the next three lower energy groups, the mean scattering cosine and the total cross section for that group. On the card corresponding to the lowest energy group the fourth entry is the logarithmic energy decrement of the nuclide. Each card also contains an identifying sequence number in columns 73-80. Table C. 2 is a symbolic listing of a lower energy nuclide deck including surface absorption entries. Entries set off by asterisks are introduced for clarification only and do not appear in actual decks. The title entry has the format 2A6; all numerical entries are in the form F12. 8.

C. 3 STRUCTURE OF THE INPUT DECKS

a. Higher Energy, Three-Region Program

Card	Format	Entries
1	9I6, F12. 5	NRUN, MODE, METHOD, JJ, NCLDS MAXF, KKF, IFIS, ITER, CONVRG
2	8F8. 4	RP, RW, SPCA, A, SPCB, B, SPCC, C
3-6	10F7. 3	E(i)
7, 8	6F12. 8	XQ(i)
9	12I6	LY(i)
	(The following subdeck is supplied for each nuclide.)	
N0	3F8. 6	AAN, BBN, CCN
N1-N163	(as required)	Higher Energy Nuclide Deck
	(The following subdeck is supplied only if MAXF is nonzero.)	
F0	F8. 6	FFN
F1-F6	6F12. 8	ESFX(i)
F7-13	6F12. 8	FSPCT
	(The following card is supplied only if MODE = 2.)	
Source	8F8. 4	S(i)

```
*6-  ,12-137-3-LANGFORD-IMPINK    478RC 05400C         02          34002FORTSYST

 * * * * * * * * * * * * * * * * * TITLE CARD * * * * * * * * * * * * * * * * *
XXIUM                                                                      XX001
 * * * * * * * * * * * * * * * * ELASTIC SCATTERING MATRIX * * * * * * * * * * *
 ( 1, 1)     ( 2, 2)     ( 3, 3)     ( 4, 4)     ( 5, 5)     ( 6, 6)     XX002
 ( 7, 7)     ( 8, 8)     ( 9, 9)     (10,10)     (11,11)     (12,12)     XX003
 (13,13)     (14,14)     (15,15)     (16,16)     (17,17)     (18,18)     XX004
 (19,19)     (20,20)     (21,21)     (22,22)     (23,23)     (24,24)     XX005
 (25,25)     (26,26)     (27,27)     (28,28)     (29,29)     (30,30)     XX006
 (31,31)     (32,32)     (33,33)     (34,34)                             XX007
 ( 1, 2)     ( 2, 3)     ( 3, 4)     ( 4, 5)     ( 5, 6)     ( 6, 7)     XX008
 ( 7, 8)     ( 8, 9)     ( 9,10)     (10,11)     (11,12)     (12,13)     XX009
 (13,14)     (14,15)     (15,16)     (16,17)     (17,18)     (18,19)     XX010
 (19,20)     (20,21)     (21,22)     (22,23)     (23,24)     (24,25)     XX011
 (25,26)     (26,27)     (27,28)     (28,29)     (29,30)     (30,31)     XX012
 (31,32)     (32,33)     (33,34)     (34,35)                             XX013
 ( 1, 3)     ( 2, 4)     ( 3, 5)     ( 4, 6)     ( 5, 7)     ( 6, 8)     XX014
 ( 7, 9)     ( 8,10)     ( 9,11)     (10,12)     (11,13)     (12,14)     XX015
 (13,15)     (14,16)     (15,17)     (16,18)     (17,19)     (18,20)     XX016
 (19,21)     (20,22)     (21,23)     (22,24)     (23,25)     (24,26)     XX017
 (25,27)     (26,28)     (27,29)     (28,30)     (29,31)     (30,32)     XX018
 (31,33)     (32,34)    (33-4,35)                                        XX019
 ( 1, 4)     ( 2, 5)     ( 3, 6)     ( 4, 7)     ( 5, 8)     ( 6, 9)     XX020
 ( 7,10)     ( 8,11)     ( 9,12)     (10,13)     (11,14)     (12,15)     XX021
 (13,16)     (14,17)     (15,18)     (16,19)     (17,20)     (18,21)     XX022
 (19,22)     (20,23)     (21,24)     (22,25)     (23,26)     (24,27)     XX023
 (25,28)     (26,29)     (27,30)     (28,31)     (29,32)     (30,33)     XX024
 (31,34)  (32-3-4,35)                                                    XX025
 ( 1, 5)     ( 2, 6)     ( 3, 7)     ( 4, 8)     ( 5, 9)     ( 6,10)     XX026
 ( 7,11)     ( 8,12)     ( 9,13)     (10,14)     (11,15)     (12,16)     XX027
 (13,17)     (14,18)     (15,19)     (16,20)     (17,21)     (18,22)     XX028
 (19,23)     (20,24)     (21,25)     (22,26)     (23,27)     (24,28)     XX029
 (25,29)     (26,30)     (27,31)     (28,32)     (29,33)     (30,34)     XX030
(31-2-3-4,35)                                                            XX031
 ( 1, 6)     ( 2, 7)     ( 3, 8)     ( 4, 9)     ( 5,10)     ( 6,11)     XX032
 ( 7,12)     ( 8,13)     ( 9,14)     (10,15)     (11,16)     (12,17)     XX033
 (13,18)     (14,19)     (15,20)     (16,21)     (17,22)     (18,23)     XX034
```

```
(19,24)     (20,25)     (21,26)     (22,27)     (23,28)     (24,29)     XX035
(25,30)     (26,31)     (27,32)     (28,33)     (29,34) (30-1-2-3-4,35) XX036
                                                                        XX037
* * * * * * * * * * * * * * MEAN SCATTERING COSINE * * * * * * * * * * * * *
 ( 1)        ( 2)        ( 3)        ( 4)        ( 5)        ( 6)        XX038
 ( 7)        ( 8)        ( 9)        (10)        (11)        (12)        XX039
 (13)        (14)        (15)        (16)        (17)        (18)        XX040
 (19)        (20)        (21)        (22)        (23)        (24)        XX041
 (25)        (26)        (27)        (28)        (29)        (30)        XX042
 (31)        (32)        (33)        (34)                                XX043
* * * * * * * * * * * * NONELASTIC SCATTERING MATRIX * * * * * * * * * * * *
( 1,20)     ( 2,20)     ( 3,20)     ( 4,20)     ( 5,20)                 XX044
( 6,20)     ( 7,20)     ( 8,20)     ( 9,20)     (10,20)                 XX045
(11,20)     (12,20)     (13,20)     (14,20)     (15,20)                 XX046
(16,20)     ( 1,19)     ( 2,19)     ( 3,19)     ( 4,19)                 XX047
( 5,19)     ( 6,19)     ( 7,19)     ( 8,19)     ( 9,19)                 XX048
(10,19)     (11,19)     (12,19)     (13,19)     (14,19)     (15,19)     XX049
( 1,21)     ( 2,21)     ( 3,21)     ( 4,21)     ( 5,21)                 XX050
( 6,21)     ( 7,21)     ( 8,21)     ( 9,21)     (10,21)                 XX051
(11,21)     (12,21)     (13,21)     (14,21)     (15,21)                 XX052
(16,21)     (17,21)     ( 1,18)     ( 2,18)     ( 3,18)                 XX053
( 4,18)     ( 5,18)     ( 6,18)     ( 7,18)     ( 8,18)                 XX054
( 9,18)     (10,18)     (11,18)     (12,18)     (13,18)     (14,18)     XX055
( 1,22)     ( 2,22)     ( 3,22)     ( 4,22)     ( 5,22)                 XX056
( 6,22)     ( 7,22)     ( 8,22)     ( 9,22)     (10,22)                 XX057
(11,22)     (12,22)     (13,22)     (14,22)     (15,22)                 XX058
(16,22)     (17,22)     (18,22)     ( 1,17)     ( 2,17)                 XX059
( 3,17)     ( 4,17)     ( 5,17)     ( 6,17)     ( 7,17)                 XX060
( 8,17)     ( 9,17)     (10,17)     (11,17)     (12,17)     (13,17)     XX061
( 1,23)     ( 2,23)     ( 3,23)     ( 4,23)     ( 5,23)                 XX062
( 6,23)     ( 7,23)     ( 8,23)     ( 9,23)     (10,23)                 XX063
(11,23)     (12,23)     (13,23)     (14,23)     (15,23)                 XX064
(16,23)     (17,23)     (18,23)     (19,23)     ( 1,16)                 XX065
( 2,16)     ( 3,16)     ( 4,16)     ( 5,16)     ( 6,16)                 XX066
( 7,16)     ( 8,16)     ( 9,16)     (10,16)     (11,16)     (12,16)     XX067
( 1,24)     ( 2,24)     ( 3,24)     ( 4,24)     ( 5,24)                 XX068
```

(6,24)	(7,24)	(8,24)	(9,24)	(10,24)		XX069
(11,24)	(12,24)	(13,24)	(14,24)	(15,24)		XX070
(16,24)	(17,24)	(18,24)	(19,24)	(20,24)		XX071
(1,15)	(2,15)	(3,15)	(4,15)	(5,15)		XX072
(6,15)	(7,15)	(8,15)	(9,15)	(10,15)	(11,15)	XX073
(1,25)	(2,25)	(3,25)	(4,25)	(5,25)		XX074
(6,25)	(7,25)	(8,25)	(9,25)	(10,25)		XX075
(11,25)	(12,25)	(13,25)	(14,25)	(15,25)		XX076
(16,25)	(17,25)	(18,25)	(19,25)	(20,25)		XX077
(21,25)	(1,14)	(2,14)	(3,14)	(4,14)		XX078
(5,14)	(6,14)	(7,14)	(8,14)	(9,14)	(10,14)	XX079
(1,26)	(2,26)	(3,26)	(4,26)	(5,26)		XX080
(6,26)	(7,26)	(8,26)	(9,26)	(10,26)		XX081
(11,26)	(12,26)	(13,26)	(14,26)	(15,26)		XX082
(16,26)	(17,26)	(18,26)	(19,26)	(20,26)		XX083
(21,26)	(22,26)	(1,13)	(2,13)	(3,13)		XX084
(4,13)	(5,13)	(6,13)	(7,13)	(8,13)	(9,13)	XX085
(1,27)	(2,27)	(3,27)	(4,27)	(5,27)		XX086
(6,27)	(7,27)	(8,27)	(9,27)	(10,27)		XX087
(11,27)	(12,27)	(13,27)	(14,27)	(15,27)		XX088
(16,27)	(17,27)	(18,27)	(19,27)	(20,27)		XX089
(21,27)	(22,27)	(23,27)	(1,12)	(2,12)		XX090
(3,12)	(4,12)	(5,12)	(6,12)	(7,12)	(8,12)	XX091
(1,28)	(2,28)	(3,28)	(4,28)	(5,28)		XX092
(6,28)	(7,28)	(8,28)	(9,28)	(10,28)		XX093
(11,28)	(12,28)	(13,28)	(14,28)	(15,28)		XX094
(16,28)	(17,28)	(18,28)	(19,28)	(20,28)		XX095
(21,28)	(22,28)	(23,28)	(24,28)	(1,11)		XX096
(2,11)	(3,11)	(4,11)	(5,11)	(6,11)	(7,11)	XX097
(1,29)	(2,29)	(3,29)	(4,29)	(5,29)		XX098
(6,29)	(7,29)	(8,29)	(9,29)	(10,29)		XX099
(11,29)	(12,29)	(13,29)	(14,29)	(15,29)		XX100
(16,29)	(17,29)	(18,29)	(19,29)	(20,29)		XX101
(21,29)	(22,29)	(23,29)	(24,29)	(25,29)		XX102
(1,10)	(2,10)	(3,10)	(4,10)	(5,10)	(6,10)	XX103
(1,30)	(2,30)	(3,30)	(4,30)	(5,30)		XX104

(6,30)	(7,30)	(8,30)	(9,30)	(10,30)		XX105
(11,30)	(12,30)	(13,30)	(14,30)	(15,30)		XX106
(16,30)	(17,30)	(18,30)	(19,30)	(20,30)		XX107
(21,30)	(22,30)	(23,30)	(24,30)	(25,30)		XX108
(26,30)	(1, 9)	(2, 9)	(3, 9)	(4, 9)	(5, 9)	XX109
(1,31)	(2,31)	(3,31)	(4,31)	(5,31)		XX110
(6,31)	(7,31)	(8,31)	(9,31)	(10,31)		XX111
(11,31)	(12,31)	(13,31)	(14,31)	(15,31)		XX112
(16,31)	(17,31)	(18,31)	(19,31)	(20,31)		XX113
(21,31)	(22,31)	(23,31)	(24,31)	(25,31)		XX114
(26,31)	(27,31)	(1, 8)	(2, 8)	(3, 8)	(4, 9)	XX115
(1,32)	(2,32)	(3,32)	(4,32)	(5,32)		XX116
(6,32)	(7,32)	(8,32)	(9,32)	(10,32)		XX117
(11,32)	(12,32)	(13,32)	(14,32)	(15,32)		XX118
(16,32)	(17,32)	(18,32)	(19,32)	(20,32)		XX119
(21,32)	(22,32)	(23,32)	(24,32)	(25,32)		XX120
(26,32)	(27,32)	(28,32)	(1, 7)	(2, 7)	(3, 7)	XX121
(1,33)	(2,33)	(3,33)	(4,33)	(5,33)		XX122
(6,33)	(7,33)	(8,33)	(9,33)	(10,33)		XX123
(11,33)	(12,33)	(13,33)	(14,33)	(15,33)		XX124
(16,33)	(17,33)	(18,33)	(19,33)	(20,33)		XX125
(21,33)	(22,33)	(23,33)	(24,33)	(25,33)		XX126
(26,33)	(27,33)	(28,33)	(29,33)	(1, 6)	(2, 6)	XX127
(1,34)	(2,34)	(3,34)	(4,34)	(5,34)		XX128
(6,34)	(7,34)	(8,34)	(9,34)	(10,34)		XX129
(11,34)	(12,34)	(13,34)	(14,34)	(15,34)		XX130
(16,34)	(17,34)	(18,34)	(19,34)	(20,34)		XX131
(21,34)	(22,34)	(23,34)	(24,34)	(25,34)		XX132
(26,34)	(27,34)	(28,34)	(29,34)	(30,34)	(1, 5)	XX133
* * * * * * * * * * *	NONELASTIC COUPLING DECK MATRIX				* * * * * * * * *	
(1,35)	(2,35)	(3,35)	(4,35)	(5,35)	(6,35)	XX134
(7,35)	(8,35)	(9,35)	(10,35)	(11,35)	(12,35)	XX135
(13,35)	(14,35)	(15,35)	(16,35)	(17,35)	(18,35)	XX136
(19,35)	(20,35)	(21,35)	(22,35)	(23,35)	(24,35)	XX137
(25,35)	(26,35)	(27,35)	(28,35)	(29,35)	(30,35)	XX138
(31,35)	(32,35)	(33,35)	(34,35)			XX139

(1,36)	(2,36)	(3,36)	(4,36)	(5,36)	(6,36)	XX140
(7,36)	(8,36)	(9,36)	(10,36)	(11,36)	(12,36)	XX141
(13,36)	(14,36)	(15,36)	(16,36)	(17,36)	(18,36)	XX142
(19,36)	(20,36)	(21,36)	(22,36)	(23,36)	(24,36)	XX143
(25,36)	(26,36)	(27,36)	(28,36)	(29,36)	(30,36)	XX144
(31,36)	(32,36)	(33,36)	(34,36)			XX145
(1,37)	(2,37)	(3,37)	(4,37)	(5,37)	(6,37)	XX146
(7,37)	(8,37)	(9,37)	(10,37)	(11,37)	(12,37)	XX147
(13,37)	(14,37)	(15,37)	(16,37)	(17,37)	(18,37)	XX148
(19,37)	(20,37)	(21,37)	(22,37)	(23,37)	(24,37)	XX149
(25,37)	(26,37)	(27,37)	(28,37)	(29,37)	(30,37)	XX150
(31,37)	(32,37)	(33,37)	(34,37)			XX151
(1,38)	(2,38)	(3,38)	(4,38)	(5,38)	(6,38)	XX152
(7,38)	(8,38)	(9,38)	(10,38)	(11,38)	(12,38)	XX153
(13,38)	(14,38)	(15,38)	(16,38)	(17,38)	(18,38)	XX154
(19,38)	(20,38)	(21,38)	(22,38)	(23,38)	(24,38)	XX155
(25,38)	(26,38)	(27,38)	(28,38)	(29,38)	(30,38)	XX156
(31,38)	(32,38)	(33,38)	(34,38)			XX157
* * * * * * * * * * * * * * TOTAL CROSS SECTIONS * * * * * * * * * * * * * *						
(1)	(2)	(3)	(4)	(5)	(6)	XX158
(7)	(8)	(9)	(10)	(11)	(12)	XX159
(13)	(14)	(15)	(16)	(17)	(18)	XX160
(19)	(20)	(21)	(22)	(23)	(24)	XX161
(25)	(26)	(27)	(28)	(29)	(30)	XX162
(31)	(32)	(33)	(34)			XX163

TABLE C.1 SYMBOLIC LISTING OF THE HIGHER ENERGY NUCLIDE DECK

```
* * * * * * * * * * * * * * * * * TITLE CARD * * * * * * * * * * * * * * * * *
XXIUM                                                                    XX164
* * * * * * * * * * * * * VOLUME BASED PROPERTIES * * * * * * * * * * * * * *
(35,35)     (35,36)     (35,37)     (35,38)     (35)        (35)        XX165
(36,36)     (36,37)     (36,38)     (36,39)     (36)        (36)        XX166
(37,37)     (37,38)     (37,39)     (37,40)     (37)        (37)        XX167
(38,38)     (38,39)     (38,40)     (38,41)     (38)        (38)        XX168
(39,39)     (39,40)     (39,41)     (39,42)     (39)        (39)        XX169
(40,40)     (40,41)     (40,42)     (40,43)     (40)        (40)        XX170
(41,41)     (41,42)     (41,43)     (41,44)     (41)        (41)        XX171
(42,42)     (42,43)     (42,44)     (42,45)     (42)        (42)        XX172
(43,43)     (43,44)     (43,45)     (43,46)     (43)        (43)        XX173
(44,44)     (44,45)     (44,46)     (44,47)     (44)        (44)        XX174
(45,45)     (45,46)     (45,47)     (45,48)     (45)        (45)        XX175
(46,46)     (46,47)     (46,48)     (46,49)     (46)        (46)        XX176
(47,47)     (47,48)     (47,49)     (47,50)     (47)        (47)        XX177
(48,48)     (48,49)     (48,50)                 (48)        (48)        XX178
(49,49)     (49,50)                             (49)        (49)        XX179
(50,50)                                 ZETA    (50)        (50)        XX180
* * * * * * * * * * * SURFACE BASED PROPERTIES * * * * * * * * * * * * * * *
   (35)        (36)        (37)        (38)                             XX SR 1
   (39)        (40)        (41)        (42)                             XX SR 2
   (43)        (44)        (45)        (46)                             XX SR 3
   (47)        (48)        (49)        (50)                             XX SR 4
```

TABLE C.2 SYMBOLIC LISTING OF THE LOWER ENERGY NUCLIDE DECK

b. Higher Energy, Five-Region Program

Card	Format	Entries
1	A6, 4I6,	NRUN, MODE, METHOD, NCLDS, LINK
	F12.5	CONVRG
2A, 2B	8F8.4	RP, RW, SPCA, A, SPCB, B, SPCC, C SPCU, U, SPCV, V
3-6	10F7.3	E(i)
7, 8	6F12.8	XQ(i)
9	12I6	LY(i)
	(The following subdeck is supplied for each nuclide.)	
N0	5F8.6	AAN, BBN, CCN, UUN, VVN
N1-N163	(as required)	Higher Energy Nuclide Deck
	(The following card is supplied only if MODE = 2.)	
Source	4F8.4	S(i)

c. Lower Energy, Three-Region Program

Card	Format	Entries
1	9I6, F12.5	NRUN, MODE, METHOD, JJ, NCLDS, MAXF, KKF, IFIS, ITER, CONVRG
2	8F8.4	RP, RW, SPCA, A, SPCB, B, SPCC, C
3-6	4F12.6	E(i)
7, 8	6F12.8	XQ(i)
9	12I6	LY(i)
	(The following subdeck is supplied for each nuclide.)	
N0	3F8.6, 3I6	AAN, BBN, CCN, IQQA, IQQB, IQQC
N164-N180	(as required)	Lower Energy Nuclide Deck (Volume Cards)
(The following additional cards are included if IQQA, IQQB, or IQQC is nonzero.)		
SR1-SR4	4F12.6	Lower Energy Nuclide Deck (Surface Cards)
	(The following card is supplied only if MODE = 2.)	
Source	8F8.4	S(i)
	(The following 25 cards are generated by the Higher Energy Program.)	
	6E12.4	TSD(i, j)
	F12.8	TTLLKG

d. Lower Energy, Five-Region Program

Card	Format	Entries
1	A6, 3I6,	NRUN, MODE, METHOD, NCLDS, CONVRG
	F18.5	

Card	Format	Entries
2A, 2B	8F8.4	RP, RW, SPCA, A, SPCB, B, SPCC, C SPCU, U, SPCV, V
3-6	4F12.6	E(i)
7, 8	6F12.8	XQ(i)
9	12I6	LY(i)
	(The following subdeck is supplied for each nuclide.)	
NO	5F8.6, 3I6	AAN, BBN, CCN, UUN, VVN, IQQA, IQQB, IQQC
N164-N180	(as required)	Lower Energy Nuclide Deck (Volume Cards)
(The following additional cards are included if IQQA, IQQB or IQQC is nonzero.)		
SR1-SR4	4F12.6	Lower Energy Nuclide Deck (Surface Cards)
	(The following card is supplied only if MODE = 2.)	
Source	4F8.4	S(i)
	(The following 45 cards are generated by the Higher Energy Program.)	
	6E12.4	TSD(i, j)
	F12.8	TTLLKG

APPENDIX D

Neutron Cross Sections and Scattering Matrices

D. 1 INTRODUCTION

One of the expressed goals of this study is to compile nuclear reaction data for nuclides of potential value in fusion reactor blanket assemblies. Of particular interest are the cross sections for neutron-induced reactions at neutron incident energies in the range from thermal energy to ~14 Mev, and the energy distributions of neutrons emitted during neutron-induced reactions.

A literature survey has yielded enough published information to permit the development of a set of 50 group cross sections and corresponding elastic and nonelastic scattering matrices for 14 nuclides of immediate interest in the blanket problem. The search for, and preparation of, data for two of these nuclides, thorium 232 and uranium 238, were carried out by L. N. Lontai in connection with the study of applications of fissile materials in fusion reactor blankets. Lontai's results are summarized in the report dealing with that aspect of the over-all problem.[5] The remaining 12 nuclides are more directly within the scope of the present study and are dealt with here.

It is our purpose here to indicate the sources from which data are drawn, weigh the apparent reliability of the data, outline how gaps in published data were filled, and present in tabular form the group cross sections and nuclide decks used in making the calculations reported in Sections VII and VIII. The rest of this appendix is divided into 12 independent sections, each dealing with a single element or nuclide. Subsections are devoted to discussions of cross sections in the high-energy (0. 42 Mev to 14. 2 Mev) and low-energy (thermal to 0. 42 Mev) regions with tables of group cross sections and to remarks concerning energy distributions of nonelastically scattered neutrons, together with listings of the nuclide decks.

The notation used in referring to the various nuclear reactions of interest here is that recommended by the U. S. Atomic Energy Commission's Nuclear Cross Section Advisory Group, and set forth by Shev and Moore,[67] among others. Extensive use has been made of the cross section compilations of Hughes and Schwartz,[52] Howerton,[68] and Buckingham, Parker, and Pendlebury,[18] and particularly of the bibliography of cross section information prepared by Prince.[69]

D. 2 HYDROGEN

a. High-Energy Cross Sections

Total Cross Section: Plotted for all energies of interest by Hughes and Schwartz[52] and is used as given.

Nonelastic Cross Section: Hydrogen has no appreciable nonelastic cross section at energies above 400 kev.

Elastic Cross Section: Identical to the total cross section.

b. Low-Energy Cross Sections

Total Cross Section: Taken from Hughes and Schwartz.[52]

Nonelastic Cross Section: The only nonelastic reaction evinced by hydrogen is a pure (v^{-1}) capture cross section. The magnitude is given by Hughes and Schwartz at 0.025 ev and is extrapolated to all other energies.

Elastic Cross Section: Taken as the difference between the total cross section and the nonelastic cross section.

Radiative Capture Cross Section: The magnitude of $\sigma_{n,\gamma}$ is given at 0.025 ev by Hughes and Schwartz.[52] Values at other energies are obtained by extrapolation.

c. Neutron Nonelastic Spectra

No neutrons are emitted as a result of nonelastic collisions with hydrogen.

	σ_{nT}	$\sigma_{n,n}$	$\sigma_{n,x}$	$\sigma_{n,\gamma}$
01	0.6800	0.6800	0.0000	0.0000
02	0.7500	0.7500	0.0000	0.0000
03	0.8250	0.8250	0.0000	0.0000
04	0.9100	0.9100	0.0000	0.0000
05	0.9950	0.9950	0.0000	0.0000
06	1.0900	1.0900	0.0000	0.0000
07	1.1800	1.1800	0.0000	0.0000
08	1.2900	1.2900	0.0000	0.0000
09	1.4000	1.4000	0.0000	0.0000
10	1.5200	1.5200	0.0000	0.0000
11	1.6400	1.6400	0.0000	0.0000
12	1.7600	1.7600	0.0000	0.0000
13	1.8900	1.8900	0.0000	0.0000
14	2.0100	2.0100	0.0000	0.0000
15	2.1500	2.1500	0.0000	0.0000
16	2.3100	2.3100	0.0000	0.0000
17	2.4500	2.4500	0.0000	0.0000
18	2.6200	2.6200	0.0000	0.0000
19	2.8000	2.8000	0.0000	0.0000
20	2.9500	2.9500	0.0000	0.0000
21	3.1300	3.1300	0.0000	0.0000
22	3.3300	3.3300	0.0000	0.0000
23	3.5200	3.5200	0.0000	0.0000
24	3.7300	3.7300	0.0000	0.0000
25	3.9700	3.9700	0.0000	0.0000
26	4.2200	4.2200	0.0000	0.0000
27	4.4500	4.4500	0.0000	0.0000
28	4.7000	4.7000	0.0000	0.0000
29	5.0000	5.0000	0.0000	0.0000
30	5.3000	5.3000	0.0000	0.0000
31	5.6000	5.6000	0.0000	0.0000
32	5.9200	5.9200	0.0000	0.0000
33	6.2000	6.2000	0.0000	0.0000
34	6.5500	6.5500	0.0000	0.0000
35	7.2000	7.2000	0.0000	0.0000
36	8.4500	8.4500	0.0000	0.0000
37	10.4500	10.4499	0.0001	0.0001
38	13.0000	12.9998	0.0002	0.0002
39	15.7000	15.6997	0.0003	0.0003
40	18.0000	17.9996	0.0004	0.0004
41	20.0000	19.9994	0.0006	0.0006
42	20.0000	19.9991	0.0009	0.0009
43	20.0000	19.9986	0.0014	0.0014
44	20.1000	20.0980	0.0020	0.0020
45	20.2000	20.1970	0.0030	0.0030
46	20.3000	20.2957	0.0043	0.0043
47	20.4000	20.3941	0.0059	0.0059
48	20.5000	20.4907	0.0093	0.0093
49	20.6000	20.5863	0.0137	0.0137
50	35.5000	35.1680	0.3320	0.3320

TABLE D.1 FIFTY GROUP NEUTRON CROSS SECTIONS FOR HYDROGEN

HYDROGEN		SEPTEMBER 17,1962				H 001
0.03410368	0.03857557	0.04226453	0.04665424	0.05148743	0.05574004	H 002
0.06016263	0.06657842	0.07138515	0.07800138	0.08548463	0.09051520	H 003
0.09651653	0.10314656	0.10966835	0.11933230	0.12712482	0.13500437	H 004
0.14105281	0.15138426	0.16080274	0.17024100	0.18151656	0.19066951	H 005
0.20495517	0.21593464	0.22933058	0.24147355	0.25590955	0.27039164	H 006
0.29016747	0.30379486	0.31625290	0.30482000			H 007
0.06473348	0.07102504	0.07820180	0.08703791	0.09403069	0.10277551	H 008
0.11260933	0.12158227	0.13286148	0.14640991	0.15578299	0.16615725	H 009
0.17934834	0.18957022	0.20535805	0.22143933	0.23322040	0.24406207	H 010
0.26589470	0.28016944	0.29583078	0.31747748	0.33258853	0.35600974	H 011
0.37545181	0.40206454	0.42255262	0.44471236	0.47171354	0.50772073	H 012
0.53098322	0.55833616	0.53488608	0.			H 013
0.05802038	0.06398124	0.07102732	0.07736702	0.08441392	0.09366882	H 014
0.10009719	0.11018392	0.12140790	0.12983513	0.13921032	0.15033275	H 015
0.16046957	0.17284343	0.18548469	0.19771368	0.20523395	0.22409334	H 016
0.23956850	0.25092099	0.26860709	0.28315558	0.30235319	0.31744204	H 017
0.34036286	0.36061456	0.37884030	0.39910083	0.43128096	0.45218872	H 018
0.47509027	0.45980626	0.	0.			H 019
0.05226629	0.05811140	0.06313539	0.06945449	0.07693420	0.08326118	H 020
0.09071308	0.10068531	0.10766362	0.11602287	0.12595220	0.13450825	H 021
0.14631049	0.15611665	0.16561133	0.17398804	0.18844207	0.20190588	H 022
0.21455861	0.22783010	0.23956847	0.25741415	0.26959828	0.28777457	H 023
0.30527389	0.32330962	0.33998488	0.36489220	0.38410956	0.40458993	H 024
0.39125080	0.	0.	0.			H 025
0.04747122	0.05165457	0.05667837	0.06330030	0.06838597	0.07545543	H 026
0.08289298	0.08928698	0.09621003	0.10497307	0.11269407	0.12263987	H 027
0.13215141	0.13938987	0.14573797	0.15975265	0.16978444	0.18082780	H 028
0.19481395	0.20319982	0.21778951	0.22952764	0.24440219	0.25810707	H 029
0.27369384	0.29014966	0.31084333	0.32498208	0.34367700	0.33319171	H 030
0.	0.	0.	0.			H 031
0.04219663	0.04637172	0.05165623	0.05626693	0.06197477	0.06895065	H 032
0.07350888	0.07978836	0.08704717	0.09392328	0.10275048	0.11077150	H 033
0.11799233	0.12266308	0.13381395	0.14393556	0.15205970	0.16418721	H 034
0.17375298	0.18472710	0.19419566	0.20807646	0.21920607	0.23140635	H 035
0.24562268	0.26527970	0.27684481	0.29077345	0.28302812	0.	H 036
0.	0.	0.	0.			H 037

TABLE D.2 Hydrogen Nuclide Decks

1.00000000	1.00000000	1.00000000	1.00000000	1.00000000	1.00000000	H 038
1.00000000	1.00000000	1.00000000	1.00000000	0.	0.	H 039
0.	0.	0.	0.	0.	0.	H 040
0.	0.	0.	0.	0.	0.	H 041
0.	0.	0.	0.	0.	0.	H 042
0.	0.	0.	0.			H 043
0.00968605	0.01185707	0.01449244	0.01775925	0.02158432		H 044
0.02627931	0.03159317	0.03837439	0.04627244	0.05580147		H 045
0.06695353	0.07991372	0.09533779	0.11262701	0.		H 046
0.	0.01054916	0.01291364	0.01578385	0.01934175		H 047
0.02350767	0.02862103	0.03440841	0.04179390	0.05039573		H 048
0.06077389	0.07291969	0.08703475	0.10383325	0.	0.	H 049
0.00872703	0.01068310	0.01305754	0.01600090	0.01944725		H 050
0.02367739	0.02846514	0.03457496	0.04169101	0.05027658		H 051
0.06032447	0.07200147	0.08589841	0.10147582	0.12056504		H 052
0.	0.	0.01198768	0.01467459	0.01793619		H 053
0.02197926	0.02671326	0.03252389	0.03910046	0.04749307		H 054
0.05726787	0.06906123	0.08286329	0.09890313	0.	0.	H 055
0.00781596	0.00956783	0.01169439	0.01433048	0.01741704		H 056
0.02120557	0.02549350	0.03096548	0.03733866	0.04502793		H 057
0.05402686	0.06448483	0.07693100	0.09088220	0.10797859		H 058
0.12890932	0.	0.	0.01342620	0.01643554		H 059
0.02008853	0.02461678	0.02991886	0.03642676	0.04379252		H 060
0.05319224	0.06414002	0.07734858	0.09280688	0.	0.	H 061
0.00709671	0.00868735	0.01061822	0.01301172	0.01581425		H 062
0.01925414	0.02314747	0.02811590	0.03390259	0.04088425		H 063
0.04905506	0.05855065	0.06985146	0.08251880	0.09804191		H 064
0.11704650	0.13806648	0.	0.	0.01486472		H 065
0.01819649	0.02224088	0.02725429	0.03312445	0.04032963		H 066
0.04848457	0.05889141	0.07101217	0.08563593	0.	0.	H 067
0.00632949	0.00774819	0.00947031	0.01160505	0.01410460		H 068
0.01717261	0.02064504	0.02507634	0.03023744	0.03646433		H 069
0.04375181	0.05222085	0.06229994	0.07359785	0.08744278		H 070
0.10439283	0.12314036	0.14643724	0.	0.		H 071
0.01630324	0.01995745	0.02439322	0.02989180	0.03633004		H 072
0.04423250	0.05317663	0.06459057	0.07788432	0.	0.	H 073
0.00575408	0.00704380	0.00860937	0.01055004	0.01282236		H 074

0.01561146	0.01876822	0.02279667	0.02748857	0.03314938		H 075
0.03977437	0.04747349	0.05663631	0.06690713	0.07949343		H 076
0.09490256	0.11194578	0.13312475	0.15795724	0.		H 077
0.	0.01822127	0.02230538	0.02726101	0.03340849		H 078
0.04060416	0.04943632	0.05943271	0.07218947	0.	0.	H 079
0.00513072	0.00628072	0.00767668	0.00940713	0.01143327		H 080
0.01392023	0.01673499	0.02032703	0.02451065	0.02955820		H 081
0.03546549	0.04233053	0.05050071	0.05965886	0.07088165		H 082
0.08462146	0.09981833	0.11870291	0.14084522	0.16471501		H 083
0.	0.	0.02013930	0.02465332	0.03013280		H 084
0.03692517	0.04487828	0.05464014	0.06568878	0.	0.	H 085
0.00465122	0.00569374	0.00695924	0.00852796	0.01036474		H 086
0.01261927	0.01517098	0.01842731	0.02221993	0.02679576		H 087
0.03215095	0.03837441	0.04578102	0.05408527	0.06425720		H 088
0.07671291	0.09048951	0.10760918	0.12768212	0.14932108		H 089
0.17604654	0.	0.	0.02253684	0.02758824		H 090
0.03372004	0.04132102	0.05022094	0.06114493	0.	0.	H 091
0.00417171	0.00510675	0.00624179	0.00764878	0.00929622		H 092
0.01131831	0.01360696	0.01652759	0.01992922	0.02403331		H 093
0.02883642	0.03441828	0.04106133	0.04850767	0.05763274		H 094
0.06880436	0.08116069	0.09651545	0.11451901	0.13392714		H 095
0.15789740	0.18662526	0.	0.	0.02541388		H 096
0.03111014	0.03802472	0.04659605	0.05663212	0.	0.	H 097
0.00374015	0.00457847	0.00559609	0.00685753	0.00833453		H 098
0.01014745	0.01219934	0.01481783	0.01786757	0.02154710		H 099
0.02585334	0.03085777	0.03681360	0.04348963	0.05167073		H 100
0.06168667	0.07276476	0.08653110	0.10267222	0.12007262		H 101
0.14156319	0.16731922	0.19652959	0.	0.		H 102
0.02781142	0.03404506	0.04161196	0.05099190	0.	0.	H 103
0.00335655	0.00410888	0.00502213	0.00615419	0.00747971		H 104
0.00910669	0.01094813	0.01329806	0.01603501	0.01933714		H 105
0.02320172	0.02769287	0.03303785	0.03902916	0.04637117		H 106
0.05535983	0.06530171	0.07765611	0.09214173	0.10775748		H 107
0.12704389	0.15015826	0.17637271	0.20767237	0.		H 108
0.	0.03068846	0.03756697	0.04591665	0.	0.	H 109
0.00306884	0.00375669	0.00459166	0.00562669	0.00683859		H 110
0.00832611	0.01000971	0.01215822	0.01466057	0.01767968		H 111

0.02121300	0.02531920	0.03020603	0.03568380	0.04239650		H 112
0.05061470	0.05970442	0.07099988	0.08424587	0.09852113		H 113
0.11615442	0.13728756	0.16125505	0.18987188	0.22456931		H 114
0.	0.	0.03452452	0.04226283	0.	0.	H 115
0.00273319	0.00334580	0.00408944	0.00501127	0.00609062		H 116
0.00741544	0.00891490	0.01082841	0.01305708	0.01574596		H 117
0.01889282	0.02254990	0.02690224	0.03178088	0.03775938		H 118
0.04507872	0.05317424	0.06323425	0.07502969	0.08774537		H 119
0.10345002	0.12227172	0.14361776	0.16910463	0.20000702		H 120
0.23626471	0.	0.	0.03788108	0.	0.	H 121
0.00244548	0.00299361	0.00365898	0.00448377	0.00544950		H 122
0.00663487	0.00797649	0.00968859	0.01168254	0.01408849		H 123
0.01690411	0.02017623	0.02407043	0.02843553	0.03378471		H 124
0.04033359	0.04757696	0.05657802	0.06713183	0.07850902		H 125
0.09256054	0.10940102	0.12850011	0.15130415	0.17895366		H 126
0.21139474	0.24770326	0.	0.	0.	0.	H 127
0.00201393	0.00246533	0.00301328	0.00369252	0.00448783		H 128
0.00546401	0.00656887	0.00797883	0.00962100	0.01160228		H 129
0.01392103	0.01661572	0.01982271	0.02341750	0.02782270		H 130
0.03321590	0.03918102	0.04659367	0.05528504	0.06465448		H 131
0.07622633	0.09009495	0.10582362	0.12460341	0.14737360		H 132
0.17408979	0.20399092	0.23946049	0.	0.	0.	H 133
0.00479507	0.00586984	0.00717448	0.00879171	0.01068530	0.01300956	H 134
0.01564018	0.01899722	0.02290715	0.02762449	0.03314532	0.03956125	H 135
0.04719693	0.05575594	0.06624453	0.07908547	0.09328816	0.11093730	H 136
0.13163105	0.15393925	0.18149127	0.21451181	0.25196102	0.29667481	H 137
0.35088955	0.41449951	0.48569269	0.57014405	0.67387649	0.79331362	H 138
0.93154958	1.09477684	1.27353834	1.48694763			H 139
0.00479507	0.00586984	0.00717448	0.00879171	0.01068530	0.01300956	H 140
0.01564018	0.01899722	0.02290715	0.02762449	0.03314531	0.03956125	H 141
0.04719692	0.05575594	0.06624453	0.07908547	0.09328815	0.11093730	H 142
0.13163104	0.15393925	0.18149127	0.21451180	0.25196101	0.29667480	H 143
0.35088953	0.41449950	0.48569267	0.57014403	0.67387646	0.79331359	H 144
0.93154955	1.09477679	1.27353829	1.48694757			H 145
0.00479507	0.00586984	0.00717448	0.00879171	0.01068530	0.01300956	H 146
0.01564018	0.01899722	0.02290715	0.02762449	0.03314532	0.03956125	H 147
0.04719693	0.05575594	0.06624453	0.07908547	0.09328815	0.11093730	H 148

0.13163105	0.15393925	0.18149127	0.21451180	0.25196101	0.29667481	H 149
0.35088954	0.41449951	0.48569268	0.57014404	0.67387648	0.79331360	H 150
0.93154956	1.09477681	1.27353832	1.48694760			H 151
0.00575408	0.00704380	0.00860937	0.01055004	0.01282237	0.01561147	H 152
0.01876822	0.02279667	0.02748858	0.03314939	0.03977437	0.04747350	H 153
0.05663632	0.06690713	0.07949343	0.09490257	0.11194579	0.13312476	H 154
0.15795726	0.18472710	0.21778952	0.25741417	0.30235321	0.35600977	H 155
0.42106745	0.49739941	0.58283121	0.68417285	0.80865177	0.95197632	H 156
1.11785947	1.31373216	1.52824599	1.78433710			H 157
0.68000000	0.75000000	0.82500000	0.91000000	0.99500000	1.08999999	H 158
1.17999999	1.28999999	1.39999999	1.52000000	1.63999999	1.75999999	H 159
1.88999999	2.00999999	2.14999998	2.30999997	2.44999999	2.61999997	H 160
2.79999998	2.94999999	3.13000000	3.32999998	3.51999998	3.72999999	H 161
3.97000000	4.21999997	4.44999999	4.69999999	5.00000000	5.29999995	H 162
5.59999996	5.91999996	6.19999999	6.54999995			H 163

HYDROGEN						H 164
0.8510	1.9800	1.9800	2.3890	0.6667	7.2000	H 165
2.0750	3.1900	1.5950	1.5900	0.6667	8.4500	H 166
2.7100	3.3200	2.5800	1.8399	0.6667	10.4500	H 167
3.0600	5.6700	2.8400	1.4298	0.6667	13.0000	H 168
5.3800	6.8500	1.8300	1.6397	0.6667	15.7000	H 169
7.5900	5.5800	2.5800	2.2496	0.6667	18.0000	H 170
6.3700	7.3000	3.3860	2.9434	0.6667	20.0000	H 171
6.3700	7.3000	3.3860	2.9431	0.6667	20.0000	H 172
6.3700	7.3000	3.3860	2.9426	0.6667	20.0000	H 173
6.4100	7.3400	3.4050	2.9430	0.6667	20.1000	H 174
6.4500	7.3700	3.4200	2.9570	0.6667	20.2000	H 175
6.4700	7.4000	3.4400	2.9857	0.6667	20.3000	H 176
6.5100	7.4500	3.4600	2.7941	0.6667	20.4000	H 177
6.5400	7.4800	6.4707	0.0000	0.6667	20.5000	H 178
6.5600	14.0263	0.0000	0.0000	0.6667	20.6000	H 179
35.1680	0.0000	0.0000	1.0000	0.6667	35.5000	H 180

D. 3 LITHIUM-6

a. High-Energy Cross Sections

Total Cross Section: Plotted over the entire range of interest by Hughes and Schwartz.[52]

Nonelastic Cross Section: Gorbachev and Poretsky[70] give for the 14-Mev nonelastic cross section in Li^6 a value of 0.66 ± 0.056 b. Rosen and Stewart[71] give for the elastic cross section in Li^6 at 14 Mev a value of 840 ± 95 mb (attributed to Armstrong[72]), while the total cross section given by Hughes and Schwartz is 1.53 b, which, by subtraction, gives a value of 0.69 b for the nonelastic cross section. The directly measured value is preferred.

The possible nonelastic neutron-induced reactions in Li^6 at 14 Mev are:

(a) $Li^6(n, t)He^4$

(b) $Li^6(n, d)He^5 \rightarrow n + He^4$; $Li^6(n, d)He^{5*} \rightarrow n + He^4$

(c) $Li^6(n, p)He^6 \rightarrow n + n + He^4$; $Li^6(n, p)He^6 \overset{\beta}{\rightarrow} Li^6$

(d) $Li^6(n, 2np)He^4$

(e) $Li^6(n, n')Li^6$.

Separate measurements of the cross sections for the various nonelastic processes at 14 Mev yield

$\sigma_{n, t}$	26 mb	(5)
$\sigma_{n, dn}$	300 mb	(3)
$\sigma_{n, p}$	6.7 mb	(6)
$\sigma_{n, p2n}$	122 mb	(4)
Total	454 mb	

Compared with the Gorbachev and Poretsky value of σ_{nx} in Li^6 at 14 Mev, the listing above fails to account for approximately 200 mb in nonelastic events. Ajzenberg-Selove and Lauritsen[73] observe that certain levels in Li^6 decay only by gamma emission. The assumption is made that the 200 mb unaccounted for is the cross section for the various (n, n') processes.

Below 14 Mev the nonelastic cross section includes contributions from $\sigma_{n, t}$ at all energies, $\sigma_{n, dn}$ above 2 Mev, $\sigma_{n, n'}$ (3.58γ) and $\sigma_{n, 2np}$ above 3.7 Mev, and $\sigma_{n, n'}$ (>9.0γ) above ~9 Mev.

Elastic Cross Section: A value for $\sigma_{n, n}$ of 0.81 b, derived by subtracting measured values of $\sigma_{n, x}$ from $\sigma_{n, T}$, is in good agreement with the Armstrong value of 0.84 ± 0.095 b at 14 Mev. The calculated value is preferred for consistency. Below 14 Mev no measured values are available and the difference between total and nonelastic cross sections is used.

Radiative Capture Cross Section: Has not been observed at energies above 400 Mev.

The 0.025-ev value of $\sigma_{n,\gamma}$ is sufficiently small, 28 mb,[52] that the reaction may be safely disregarded in the higher energy region.

Proton Emission Cross Section: Battat and Ribe[74] give the value 6.7 mb for $\sigma_{n,p}$ at 14 Mev in Li^6. Frye[75] gives for the same cross section approximately 6 mb, in good agreement. The reaction is neglected.

Triton Emission Cross Section: The cross section for the reaction $Li^6(n,t)He^4$ has been plotted over the entire energy range of interest by Hughes and Schwartz,[52] and is used as plotted.

Inelastic Cross Section: Inelastic excitation of a level at 3.56 Mev in Li^6, followed by de-excitation by gamma-ray emission, has been observed.[73] De-excitation of levels above 9 Mev in Li^7 has also been observed,[73] and corresponding excitation with de-excitation by gamma-ray emission in Li^6 is assumed for levels above 9 Mev. The total inelastic cross section at all energies is taken to be the difference between the non-elastic cross section and the sum of the cross sections for the other nonelastic processes. Apportioning of the inelastic cross section between excitation of the 3.56-Mev level and the levels above 9 Mev is made on the premise that excitation of the high-energy levels competes with, and at sufficiently high energy overcomes, excitation of the lower isolated level.

Breakup Cross Sections: Both breakup cross sections of importance in Li^6 ($\sigma_{n,dn}$ and $\sigma_{n,2np}$) have been measured by Rosen and Stewart and are used as plotted.[71]

b. Low-Energy Cross Sections

Total Cross Section: Plotted over the entire energy range of interest by Hughes and Schwartz,[52] and is used as plotted.

Nonelastic Cross Section: The nonelastic cross section, identical to the (n, t) cross section, is plotted by Hughes and Schwartz at energies above 20 kev. Below 20 kev the only direct information available is $\sigma_{n,t}$ at 0.025 ev. In the region below 20 kev, σ_{nx} is obtained in the form $\sigma_{nT} - \sigma_{n,n}$, where the elastic cross section is assumed constant at 0.85 b, the average of $\sigma_{n,n}$ in the region from 10 kev to 120 kev.

Elastic Cross Section: In the energy region above 20 kev, σ_{nT} and σ_{nx} are available and the elastic cross section is taken to be the difference between these. Below 20 kev $\sigma_{n,n}$ is assumed constant at 0.85 b, the average value between 10 kev and 120 kev.

c. Neutron Nonelastic Spectra

The energy distribution of secondary neutrons, which is due to the (n, nd) reaction in Li^6, is given over all but the lowest incident energy range by Rosen and Stewart,[71] and is used as published. In the low incident energy range, the distribution is assumed independent of incident energy.

Because of the complexity of the four-body (n, 2np) reaction, the assumption is made that the neutrons appear with equal probability at all energies below the incident energy.

Scattering from the levels above 9 Mev is treated as though the high levels form a continuum; the neutrons appear with equal probability at all allowed energies.

Scattering from the 3.56-Mev level is treated by the isolated-level model.

	$\sigma_{n,T}$	$\sigma_{n,n}$	$\sigma_{n,X}$	$\sigma_{n,t}$	$\sigma_{n,2np}$
01	1.5300	0.8650	0.6650	0.0260	0.1260
02	1.5700	0.9050	0.6650	0.0290	0.1310
03	1.6200	0.9500	0.6650	0.0320	0.1410
04	1.6600	0.9950	0.6650	0.0370	0.1460
05	1.7200	1.0550	0.6650	0.0410	0.1410
06	1.7700	1.1050	0.6650	0.0460	0.1100
07	1.8300	1.1650	0.6650	0.0520	0.0700
08	1.9000	1.3250	0.6650	0.0590	0.0320
09	1.9500	1.3850	0.6650	0.0670	0.0150
10	2.0000	1.3600	0.6400	0.0750	0.0000
11	2.0400	1.4100	0.6290	0.0840	0.0000
12	2.0600	1.4600	0.6000	0.0950	0.0000
13	2.0500	1.5130	0.5370	0.1070	0.0000
14	2.0200	1.5490	0.4710	0.1210	0.0000
15	1.9300	1.5430	0.3870	0.1370	0.0000
16	1.8500	1.5850	0.2650	0.1550	0.0000
17	1.7000	1.4570	0.2430	0.1830	0.0000
18	1.5700	1.3450	0.2250	0.1950	0.0000
19	1.4500	1.2250	0.2250	0.2100	0.0000
20	1.3800	1.1610	0.2190	0.2190	0.0000
21	1.3500	1.1230	0.2270	0.2270	0.0000
22	1.3500	1.1100	0.2400	0.2400	0.0000
23	1.3600	1.1080	0.2520	0.2520	0.0000
24	1.3800	1.1150	0.2650	0.2650	0.0000
25	1.4100	1.1330	0.2770	0.2770	0.0000
26	1.4500	1.1600	0.2900	0.2900	0.0000
27	1.5100	1.2100	0.3000	0.3000	0.0000
28	1.5800	1.2650	0.3150	0.3150	0.0000
29	1.6500	1.3150	0.3350	0.3350	0.0000
30	1.7500	1.3850	0.3650	0.3650	0.0000
31	1.8700	1.4800	0.3900	0.3900	0.0000
32	2.0500	1.5750	0.4750	0.4750	0.0000
33	2.3000	1.7150	0.5850	0.5850	0.0000
34	2.5500	1.7600	0.7900	0.7900	0.0000
35	4.0000	2.6700	1.3300	1.3300	0.0000
36	7.7500	5.4000	2.3500	2.3500	0.0000
37	3.8000	2.4300	1.3700	1.3700	0.0000
38	1.6500	0.9200	0.7300	0.7300	0.0000
39	1.5500	0.7700	0.7800	0.7800	0.0000
40	2.1700	0.8500	1.3200	1.3200	0.0000
41	2.6400	0.8500	1.7900	1.7900	0.0000
42	3.5200	0.8500	2.6700	2.6700	0.0000
43	4.4880	0.8500	4.0300	4.0300	0.0000
44	6.8200	0.8500	5.9700	5.9700	0.0000
45	9.5600	0.8500	8.7100	8.7100	0.0000
46	13.3900	0.8500	12.5400	12.5400	0.0000
47	18.8000	0.8500	17.9500	17.9500	0.0000
48	26.6000	0.8500	25.7500	25.7500	0.0000
49	38.3000	0.8500	37.4500	37.4500	0.0000
50	945.8500	0.8500	945.0000	945.0000	0.0000

TABLE D.3 FIFTY GROUP NEUTRON CROSS SECTIONS FOR LITHIUM 6

	$\sigma_{n,n'(3.56)}$	$\sigma_{n,n'(>9)}$	$\sigma_{n,dn}$
01	0.0890	0.1240	0.3000
02	0.0910	0.0990	0.3150
03	0.1030	0.0540	0.3350
04	0.1030	0.0190	0.3600
05	0.0900	0.0000	0.3930
06	0.0670	0.0000	0.4420
07	0.0430	0.0000	0.5000
08	0.0290	0.0000	0.5450
09	0.0150	0.0000	0.5650
10	0.0000	0.0000	0.5650
11	0.0000	0.0000	0.5450
12	0.0000	0.0000	0.5050
13	0.0000	0.0000	0.4300
14	0.0000	0.0000	0.3500
15	0.0000	0.0000	0.2500
16	0.0000	0.0000	0.1100
17	0.0000	0.0000	0.0600
18	0.0000	0.0000	0.0300
19	0.0000	0.0000	0.0150
20	0.0000	0.0000	0.0000
21	0.0000	0.0000	0.0000
22	0.0000	0.0000	0.0000
23	0.0000	0.0000	0.0000
24	0.0000	0.0000	0.0000
25	0.0000	0.0000	0.0000
26	0.0000	0.0000	0.0000
27	0.0000	0.0000	0.0000
28	0.0000	0.0000	0.0000
29	0.0000	0.0000	0.0000
30	0.0000	0.0000	0.0000
31	0.0000	0.0000	0.0000
32	0.0000	0.0000	0.0000
33	0.0000	0.0000	0.0000
34	0.0000	0.0000	0.0000
35	0.0000	0.0000	0.0000
36	0.0000	0.0000	0.0000
37	0.0000	0.0000	0.0000
38	0.0000	0.0000	0.0000
39	0.0000	0.0000	0.0000
40	0.0000	0.0000	0.0000
41	0.0000	0.0000	0.0000
42	0.0000	0.0000	0.0000
43	0.0000	0.0000	0.0000
44	0.0000	0.0000	0.0000
45	0.0000	0.0000	0.0000
46	0.0000	0.0000	0.0000
47	0.0000	0.0000	0.0000
48	0.0000	0.0000	0.0000
49	0.0000	0.0000	0.0000
50	0.0000	0.0000	0.0000

TABLE D.3 (CONT.) FIFTY GROUP CROSS SECTIONS FOR LITHIUM 6

LITHIUM(6)		JUNE 21,1962				LI(6)001
.3000	0.3139	0.3312	0.3451	0.3238	0.3391	LI(6)002
0.3575	0.4066	0.4251	0.4174	0.4330	0.4481	LI(6)003
0.4643	0.3555	0.3541	0.3638	0.3344	0.3087	LI(6)004
0.2811	0.2664	0.2577	0.2547	0.1265	0.1273	LI(6)005
0.1294	0.1325	0.1382	0.1445	0.1502	0.1582	LI(6)006
0.1690	0.1799	0.1235	0.1267			LI(6)007
0.3673	0.3820	0.4000	0.4207	0.4132	0.4326	LI(6)008
0.4570	0.5192	0.5425	0.5328	0.5526	0.5706	LI(6)009
0.5912	0.4995	0.4965	0.5101	0.4689	0.4328	LI(6)010
0.3942	0.3736	0.3614	0.3572	0.2127	0.2141	LI(6)011
0.2175	0.2227	0.2323	0.2429	0.2525	0.2659	LI(6)012
0.2842	0.3024	0.2454	0.			LI(6)013
0.1292	0.1295	0.1108	0.1151	0.1390	0.1461	LI(6)014
0.1515	0.1700	0.1804	0.1763	0.1816	0.1856	LI(6)015
0.1910	0.2407	0.2368	0.2422	0.2226	0.2055	LI(6)016
0.1872	0.1774	0.1716	0.1696	0.1539	0.1549	LI(6)017
0.1574	0.1611	0.1681	0.1757	0.1827	0.1924	LI(6)018
0.2056	0.2188	0.	0.			LI(6)019
0.1208	0.0838	0.1193	0.0823	0.0905	0.0929	LI(6)020
0.0930	0.1050	0.1141	0.1104	0.1119	0.1113	LI(6)021
0.1129	0.1877	0.1850	0.1869	0.1709	0.1578	LI(6)022
0.1437	0.1362	0.1317	0.1302	0.1326	0.1335	LI(6)023
0.1356	0.1389	0.1448	0.1514	0.1574	0.1658	LI(6)024
0.1772	0.	0.	0.			LI(6)025
0.0175	0.0183	0.0193	0.0201	0.0400	0.0419	LI(6)026
0.0442	0.0502	0.0525	0.0515	0.0535	0.0553	LI(6)027
0.0573	0.1169	0.1165	0.1197	0.1100	0.1015	LI(6)028
0.0925	0.0877	0.0848	0.0838	0.0962	0.0968	LI(6)029
0.0983	0.1007	0.1050	0.1098	0.1141	0.1202	LI(6)030
0.	0.	0.	0.			LI(6)031
0.0185	0.0194	0.0204	0.0213	0.0293	0.0307	LI(6)032
0.0324	0.0368	0.0385	0.0378	0.0392	0.0406	LI(6)033
0.0423	0.0589	0.0586	0.0602	0.0554	0.0511	LI(6)034
0.0465	0.0441	0.0427	0.0422	0.1425	0.1434	LI(6)035
0.1457	0.1492	0.1556	0.2943	0.4581	0.4825	LI(6)036

TABLE D.4 Lithium 6 Nuclide Decks

0.6440	0.8739	1.3461	1.6333			LI(6)037
1.0	1.0	1.0	1.0	1.0	1.0	LI(6)038
1.0	1.0	1.0	1.0	0.0	0.0	LI(6)039
0.0	0.0	0.0	0.0	0.0	0.0	LI(6)040
0.0	0.0	0.0	0.0	0.0	0.0	LI(6)041
0.0	0.0	0.0	0.0	0.0	0.0	LI(6)042
0.0	0.0	0.0	0.0			LI(6)043
0.016	0.018	0.021	0.020	0.021		LI(6)044
0.025	0.027	0.031	0.035	0.034		LI(6)045
0.0300	0.0270	0.0560	0.0670	0.0090		LI(6)046
0.003	0.019	0.021	0.023	0.023		LI(6)047
0.023	0.027	0.031	0.034	0.038		LI(6)048
0.0330	0.0290	0.0819	0.0550	0.0110	0.0070	LI(6)049
0.015	0.016	0.018	0.017	0.018		LI(6)050
0.022	0.025	0.028	0.030	0.034		LI(6)051
0.0300	0.0310	0.0260	0.0648	0.0638		LI(6)052
0.004	0.001	0.020	0.022	0.025		LI(6)053
0.025	0.025	0.030	0.035	0.038		LI(6)054
0.0460	0.0310	0.0597	0.0526	0.0140	0.0090	LI(6)055
0.012	0.014	0.017	0.016	0.016		LI(6)056
0.019	0.022	0.024	0.027	0.033		LI(6)057
0.0290	0.0320	0.0280	0.0190	0.0597		LI(6)058
0.0601	0.0030	0.	0.0230	0.0250		LI(6)059
0.022	0.028	0.029	0.035	0.038		LI(6)060
0.0420	0.0490	0.0586	0.0615	0.0150	0.0120	LI(6)061
0.012	0.013	0.015	0.014	0.015		LI(6)062
0.018	0.020	0.021	0.024	0.032		LI(6)063
0.028	0.031	0.029	0.021	0.013		LI(6)064
0.0560	0.0538	0.0010	0.	0.0260		LI(6)065
0.028	0.025	0.031	0.034	0.038		LI(6)066
0.0430	0.0530	0.0762	0.0602	0.0240	0.0130	LI(6)067
0.009	0.012	0.013	0.014	0.013		LI(6)068
0.015	0.018	0.019	0.022	0.030		LI(6)069
0.026	0.029	0.028	0.022	0.015		LI(6)070
0.0080	0.0490	0.0480	0.	0.		LI(6)071
0.028	0.032	0.028	0.033	0.039		LI(6)072
0.0420	0.0470	0.0918	0.0757	0.0230	0.0200	LI(6)073

0.009	0.010	0.011	0.014	0.012		LI(6)074
0.014	0.016	0.017	0.019	0.026		LI(6)075
0.025	0.027	0.026	0.023	0.016		LI(6)076
0.0080	0.0050	0.0436	0.0419	0.		LI(6)077
0.0	0.031	0.036	0.031	0.036		LI(6)078
0.0440	0.0450	0.0862	0.0874	0.0400	0.0210	LI(6)079
0.009	0.009	0.010	0.013	0.010		LI(6)080
0.012	0.014	0.015	0.017	0.023		LI(6)081
0.023	0.026	0.024	0.024	0.017		LI(6)082
0.0080	0.0050	0.0030	0.0379	0.0397		LI(6)083
0.0	0.0	0.034	0.028	0.034		LI(6)084
0.0390	0.0480	0.0759	0.0992	0.0440	0.0310	LI(6)085
0.007	0.008	0.009	0.011	0.010		LI(6)086
0.011	0.012	0.013	0.015	0.021		LI(6)087
0.022	0.025	0.022	0.022	0.018		LI(6)088
0.0090	0.0060	0.0030	0.0010	0.0359		LI(6)089
0.0384	0.	0.	0.0380	0.0310		LI(6)090
0.0370	0.0420	0.0767	0.1038	0.0550	0.0350	LI(6)091
0.007	0.008	0.008	0.009	0.008		LI(6)092
0.009	0.011	0.011	0.013	0.018		LI(6)093
0.020	0.024	0.020	0.021	0.017		LI(6)094
0.008	0.006	0.004	0.002	0.0		LI(6)095
0.0347	0.0380	0.	0.	0.0390		LI(6)096
0.0350	0.0410	0.0622	0.0835	0.0930	0.0400	LI(6)097
0.006	0.007	0.007	0.008	0.008		LI(6)098
0.008	0.009	0.010	0.011	0.016		LI(6)099
0.018	0.022	0.018	0.019	0.015		LI(6)100
0.007	0.005	0.003	0.002	0.0		LI(6)101
0.	0.0343	0.1282	0.	0.		LI(6)102
0.0310	0.0370	0.0616	0.0662	0.1050	0.0480	LI(6)103
0.006	0.006	0.007	0.007	0.006		LI(6)104
0.007	0.008	0.008	0.009	0.014		LI(6)105
0.017	0.020	0.016	0.016	0.013		LI(6)106
0.007	0.004	0.003	0.003	0.0		LI(6)107
0.	0.	0.1154	0.1290	0.		LI(6)108
0.	0.0340	0.0576	0.0664	0.0660	0.0930	LI(6)109
0.004	0.005	0.005	0.007	0.006		LI(6)110

0.007	0.007	0.007	0.008	0.012		LI(6)111
0.016	0.018	0.014	0.014	0.012		LI(6)112
0.006	0.003	0.002	0.002	0.0		LI(6)113
0.	0.	0.	0.1160	0.1312		LI(6)114
0.	0.	0.0540	0.0645	0.0510	0.1150	LI(6)115
0.003	0.004	0.004	0.006	0.005		LI(6)116
0.005	0.007	0.006	0.007	0.010		LI(6)117
0.014	0.016	0.013	0.012	0.010		LI(6)118
0.005	0.002	0.002	0.001	0.0		LI(6)119
0.	0.	0.	0.	0.1179		LI(6)120
0.1341	0.	0.	0.0607	0.0510	0.1050	LI(6)121
0.003	0.004	0.004	0.005	0.004		LI(6)122
0.005	0.005	0.005	0.006	0.009		LI(6)123
0.012	0.013	0.011	0.011	0.009		LI(6)124
0.004	0.002	0.001	0.0	0.0		LI(6)125
0.0	0.0	0.0	0.0	0.0		LI(6)126
0.1208	0.1400	0.	0.	0.0480	0.0950	LI(6)127
0.002	0.002	0.004	0.005	0.004		LI(6)128
0.005	0.004	0.005	0.005	0.008		LI(6)129
0.010	0.010	0.010	0.009	0.007		LI(6)130
0.003	0.001	0.0	0.0	0.0		LI(6)131
0.0	0.0	0.0	0.0	0.0		LI(6)132
0.	0.1260	0.1464	0.	0.	0.0470	LI(6)133
0.007	0.008	0.008	0.009	0.008	0.009	LI(6)134
0.010	0.009	0.011	0.016	0.021	0.021	LI(6)135
0.019	0.017	0.013	0.005	0.003	0.002	LI(6)136
0.001	0.0	0.0	0.0	0.0	0.0	LI(6)137
0.0	0.0	0.0	0.0	0.0	0.0	LI(6)138
0.0	0.0	0.0	0.0			LI(6)139
0.007	0.008	0.007	0.009	0.008	0.009	LI(6)140
0.010	0.009	0.011	0.015	0.020	0.020	LI(6)141
0.018	0.016	0.013	0.005	0.003	0.001	LI(6)142
0.001	0.0	0.0	0.0	0.0	0.0	LI(6)143
0.0	0.0	0.0	0.0	0.0	0.0	LI(6)144
0.0	0.0	0.0	0.0			LI(6)145
0.007	0.007	0.007	0.009	0.008	0.009	LI(6)146
0.009	0.008	0.011	0.014	0.019	0.019	LI(6)147

0.017	0.015	0.012	0.004	0.002	0.001	LI(6)148
0.001	0.0	0.0	0.0	0.0	0.0	LI(6)149
0.0	0.0	0.0	0.0	0.0	0.0	LI(6)150
0.0	0.0	0.0	0.0			LI(6)151
0.003	0.003	0.003	0.005	0.004	0.004	LI(6)152
0.004	0.004	0.005	0.007	0.010	0.010	LI(6)153
0.008	0.007	0.006	0.002	0.001	0.0	LI(6)154
0.0	0.0	0.0	0.0	0.0	0.0	LI(6)155
0.0	0.0	0.0	0.0	0.0	0.0	LI(6)156
0.0	0.0	0.0	0.0			LI(6)157
1.530	1.570	1.620	1.660	1.720	1.770	LI(6)158
1.830	1.900	1.950	2.000	2.040	2.060	LI(6)159
2.050	2.020	1.930	1.850	1.700	1.570	LI(6)160
1.450	1.380	1.350	1.350	1.360	1.380	LI(6)161
1.410	1.450	1.510	1.580	1.650	1.750	LI(6)162
1.870	2.050	2.300	2.550			LI(6)163

LITHIUM(6)						LI(6)164
0.743	1.475	0.452	0.0	0.1109	4.000	LI(6)165
1.952	3.420	0.028	0.0	0.1109	7.750	LI(6)166
1.361	1.040	0.029	0.0	0.1109	3.800	LI(6)167
0.459	0.461	0.0	0.0	0.1109	1.650	LI(6)168
0.555	0.215	0.0	0.0	0.1109	1.550	LI(6)169
0.693	0.157	0.0	0.0	0.1109	2.170	LI(6)170
0.580	0.270	0.0	0.0	0.1109	2.640	LI(6)171
0.580	0.270	0.0	0.0	0.1109	3.520	LI(6)172
0.580	0.270	0.0	0.0	0.1109	4.880	LI(6)173
0.580	0.270	0.0	0.0	0.1109	6.820	LI(6)174
0.580	0.270	0.0	0.0	0.1109	9.560	LI(6)175
0.580	0.270	0.0	0.0	0.1109	13.390	LI(6)176
0.580	0.270	0.0	0.0	0.1109	18.800	LI(6)177
0.580	0.270	0.0	0.0	0.1109	26.600	LI(6)178
0.580	0.270	0.0	0.0	0.1109	38.300	LI(6)179
0.850	0.0	0.0	0.300	0.1109	945.850	LI(6)180

D.4 LITHIUM-7

a. High-Energy Cross Sections

Total Cross Section: Plotted over the energy region 0.01-10 Mev by Hughes and Schwartz.[52] The value given for σ_{nT} at 14 Mev by Hughes and Schwartz is that due to Cook and Bonner,[76] and is in close agreement with the value given by Coon et al.[77] The value given by Khatetskii[78] is in serious disagreement and is discarded. Between 10 Mev and 14 Mev σ_{nT} is interpolated. The total cross section of Li^6 is plotted over the entire energy range of interest by Hughes and Schwartz.[52] The total cross section of Li^7 is calculated from the natural lithium and Li^6 cross sections.

Nonelastic Cross Section: Gorbachev and Poretsky[70] give for the nonelastic cross section in Li^7 at 14 Mev a value 0.52 ± 0.06 b. Since the corresponding value for Li^6 is in good agreement with $\sigma_{nT} - \sigma_{n,n}$ given by Rosen and Stewart,[71] the assumption is made that the Li^7 result is reliable, although independent verification is lacking.

The possible nonelastic neutron-induced reactions in Li^7 at 14 Mev are:

(a) $Li^7(n, t)He^5 \rightarrow n + He^4$

$Li^7(n, nt)He^4$

(b) $Li^7(n, d)He^6 \rightarrow n + n + He^4$

$Li^7(n, d)He^6 \xrightarrow{\beta} Li^6$

(c) $Li^7(n, pn)He^6 \rightarrow n + n + He^4$

$Li^7(n, pn)He^6 \xrightarrow{\beta} Li^6$

(d) $Li^7(n, 2n)Li^6$

$Li^7(n, 2n)Li^6$

(e) $Li^7(n, 3np)He^4$

(f) $Li^7(n, 2nd)He^4$

(g) $Li^7(n, n')Li^7$.

Separate measurements of the cross sections for the various nonelastic processes at 14 Mev give

		Reference
$\sigma_{n,nt} + \sigma_{n,t}$	310 mb	Rosen and Stewart[71]
$\sigma_{n,n'}$	75 mb	Battat (quoted by Rosen and Stewart[71])
$\sigma_{n,d} + \sigma_{n,pn}$	10 mb	Battat and Ribe[74] and Frye[75]
$\sigma_{n,2n} + \sigma_{n,3np} + \sigma_{n,2nd}$	~ 0	Graves (quoted by Rosen and Stewart[71])
Total	~ 0.4 b	

Compared with the Gorbachev and Poretsky nonelastic cross section, approximately 120 mb are unaccounted for. Ajzenberg-Selove and Lauritsen[73] indicate that excited levels above ~9 Mev in Li^7 decay by gamma or neutron emission. The Graves results indicate, however, that decay by neutron emission is very unlikely, while examination of the Rosen and Stewart (n, nt) plot suggests that a competing nonelastic reaction becomes significant above ~9 Mev. The conclusions are that the competing process is an inelastic (n, n') reaction involving excitation of levels above 9 Mev, and that the (n, n') cross section of Battat is for excitation of the level at 0.478 Mev only. Attributing 75 mb to the 0.478-Mev level excitation function at 14 Mev is supported by the remark of Rosen and Stewart that Beyster's measurement[71] at 7 Mev is, in effect, a $\sigma_{n,x}$ measurement, and is approximately 100 mb higher than their (n, nt) measurement. The nonelastic reaction other than (n, nt) which is possible at 7 Mev is excitation of the 0.478-Mev level.

Below 14 Mev the nonelastic cross section includes contributions from $\sigma_{n,n'}$ (0.478γ) above ~0.5 Mev, $\sigma_{n,tn}$ above 3 Mev, and $\sigma_{n,n'}$ (>9γ) above ~9 Mev.

Elastic Cross Section: No direct measurements of $\sigma_{n,n}$ are known. At all energies above 0.4 Mev the elastic cross section is taken to be the difference between the total and the nonelastic cross sections.

Radiative Capture Cross Section: Has not been observed at energies above 400 kev. The 0.025-ev value of $\sigma_{n,\gamma}$ is sufficiently small, 33 mb,[52] that the reaction may be safely disregarded in the higher energy region.

Proton and Deuteron Emission Cross Sections: Battat and Ribe[74] and Frye[75] give for the sum of $\sigma_{n,pn}$ and $\sigma_{n,d}$ a total of ~10 mb. The reactions are neglected.

Inelastic Cross Section: Inelastic cross sections, apparently corresponding to the excitation function for the 0.478-Mev level in Li^7, are given by Battat at 14 Mev, and by Beyster (both quoted by Rosen and Stewart[71]) at 7 Mev. A single value at 14 Mev, associated with excitation of levels above 9 Mev, has been derived as the difference between the nonelastic cross section and those resulting from all other possible nonelastic reactions. The excitation function for the high-energy levels is extrapolated to zero at the threshold. The excitation function of the 0.478-Mev level is taken as the difference between σ_{nx} and the sum of the other nonelastic cross sections.

Breakup Cross Sections: The cross section for the (n, tn) reaction is given over the energy range of interest by Rosen and Stewart[71] and is used as plotted. Graves[71] indicates that the sum of the cross sections for the reactions (n, 2n), (n, 3np), and (n, 2nd) is negligible. These reactions are ignored.

b. Low-Energy Cross Sections

Total Cross Section: Plotted by Hughes and Schwartz[52] over the range 1-320 kev, and is used as plotted. Above 320 kev, σ_{nT} for Li^7 is calculated from the total cross sections of natural lithium and Li^6. Below 1 kev, σ_{nT} is assumed to be constant.

Nonelastic Cross Section: The nonelastic cross section for Li^7 is very small,

consisting only of $\sigma_{n,\gamma}$ (33 mb at 0.025 ev), and is neglected above thermal energy.

Elastic Cross Section: Taken equal to the total cross section, except at 0.025 ev where an allowance is made for the radiative capture cross section.

c. Neutron Nonelastic Spectra

The energy distribution of secondary neutrons which is due to the (n, nt) reaction in Li^7 is given for all but the lowest incident energies by Rosen and Stewart,[71] and is used as published. At energies below those plotted by Rosen and Stewart, the distribution is assumed to be the same as that given in the lowest energy plot.

Scattering from the levels above 9 Mev is treated as though the high levels form a continuum. The neutrons are assumed to emerge with equal probability at all allowed energies.

Scattering from the 0.478-Mev level is treated by the isolated-level model.

	σ_{nT}	$\sigma_{n,n}$	$\sigma_{n,x}$	$\sigma_{n,tn}$	$\sigma_{n,\gamma}$
01	1.4500	0.9310	0.5190	0.3140	0.0000
02	1.4700	0.9340	0.5360	0.3550	0.0000
03	1.5200	0.9710	0.5490	0.4110	0.0000
04	1.5900	1.0300	0.5600	0.4550	0.0000
05	1.6900	1.1200	0.5700	0.4820	0.0000
06	1.7900	1.2190	0.5710	0.4810	0.0000
07	1.9100	1.3530	0.5570	0.4650	0.0000
08	2.0100	1.4840	0.5260	0.4320	0.0000
09	2.1600	1.6850	0.4750	0.3790	0.0000
10	2.3200	1.9020	0.4180	0.3190	0.0000
11	2.5200	2.1780	0.3420	0.2400	0.0000
12	2.4600	2.1980	0.2620	0.1570	0.0000
13	2.3300	2.1360	0.1940	0.0870	0.0000
14	2.2300	2.0770	0.1530	0.0440	0.0000
15	2.1100	1.9810	0.1290	0.0170	0.0000
16	2.0100	1.8910	0.1190	0.0000	0.0000
17	1.9100	1.7850	0.1250	0.0000	0.0000
18	1.8200	1.6880	0.1320	0.0000	0.0000
19	1.8100	1.6640	0.1460	0.0000	0.0000
20	1.7800	1.6200	0.1600	0.0000	0.0000
21	1.7500	1.5720	0.1780	0.0000	0.0000
22	1.7300	1.5410	0.1896	0.0000	0.0000
23	1.7100	1.5100	0.2000	0.0000	0.0000
24	1.6400	1.4360	0.2040	0.0000	0.0000
25	1.5900	1.4060	0.1840	0.0000	0.0000
26	1.5300	1.3790	0.1510	0.0000	0.0000
27	1.4700	1.3690	0.1010	0.0000	0.0000
28	1.4200	1.3390	0.0810	0.0000	0.0000
29	1.3000	1.2410	0.0590	0.0000	0.0000
30	1.2300	1.1920	0.0380	0.0000	0.0000
31	1.1800	1.1660	0.0240	0.0000	0.0000
32	1.1300	1.1190	0.0110	0.0000	0.0000
33	1.1100	1.1100	0.0000	0.0000	0.0000
34	1.1200	1.1200	0.0000	0.0000	0.0000
35	1.7000	1.7000	0.0000	0.0000	0.0000
36	7.2600	7.2600	0.0000	0.0000	0.0000
37	1.7500	1.7500	0.0000	0.0000	0.0000
38	1.0300	1.0300	0.0000	0.0000	0.0000
39	1.0400	1.0400	0.0000	0.0000	0.0000
40	1.0500	1.0500	0.0000	0.0000	0.0000
41	1.0600	1.0600	0.0000	0.0000	0.0000
42	1.0700	1.0700	0.0000	0.0000	0.0000
43	1.0800	1.0800	0.0000	0.0000	0.0000
44	1.0900	1.0900	0.0000	0.0000	0.0000
45	1.1000	1.1000	0.0000	0.0000	0.0000
46	1.1000	1.1000	0.0000	0.0000	0.0000
47	1.1000	1.1000	0.0000	0.0000	0.0000
48	1.1000	1.1000	0.0000	0.0000	0.0000
49	1.1000	1.1000	0.0000	0.0000	0.0000
50	1.1330	1.1000	0.0330	0.0000	0.0330

TABLE D.5 FIFTY GROUP NEUTRON CROSS SECTIONS FOR LITHIUM 7

	$\sigma_{n,n'}$ (0.478)	$\sigma_{n,n'}$ (> 9.0)
01	0.0810	0.1240
02	0.0820	0.0990
03	0.0840	0.0540
04	0.0860	0.0190
05	0.0880	0.0000
06	0.0900	0.0000
07	0.0920	0.0000
08	0.0940	0.0000
09	0.0960	0.0000
10	0.0990	0.0000
11	0.1020	0.0000
12	0.1050	0.0000
13	0.1070	0.0000
14	0.1090	0.0000
15	0.1120	0.0000
16	0.1190	0.0000
17	0.1250	0.0000
18	0.1320	0.0000
19	0.1460	0.0000
20	0.1600	0.0000
21	0.1780	0.0000
22	0.1890	0.0000
23	0.2000	0.0000
24	0.2040	0.0000
25	0.1840	0.0000
26	0.1510	0.0000
27	0.1010	0.0000
28	0.0810	0.0000
29	0.0590	0.0000
30	0.0380	0.0000
31	0.0240	0.0000
32	0.0110	0.0000
33	0.0000	0.0000
34	0.0000	0.0000
35	0.0000	0.0000
36	0.0000	0.0000
37	0.0000	0.0000
38	0.0000	0.0000
39	0.0000	0.0000
40	0.0000	0.0000
41	0.0000	0.0000
42	0.0000	0.0000
43	0.0000	0.0000
44	0.0000	0.0000
45	0.0000	0.0000
46	0.0000	0.0000
47	0.0000	0.0000
48	0.0000	0.0000
49	0.0000	0.0000
50	0.0000	0.0000

TABLE D.5 (CONT.) FIFTY GROUP CROSS SECTIONS FOR LITHIUM 7

LITHIUM(7)		JUNE 21,1962				LI(7)001
0.4330	0.4061	0.4181	0.4374	0.4220	0.4502	LI(7)002
0.4902	0.5302	0.5897	0.6556	0.7412	0.7379	LI(7)003
0.7171	0.5035	0.4802	0.4584	0.4327	0.4092	LI(7)004
0.4034	0.3927	0.3811	0.3735	0.2025	0.1926	LI(7)005
0.1885	0.1849	0.1836	0.1796	0.1664	0.1598	LI(7)006
0.1564	0.1501	0.1060	0.1070			LI(7)007
0.4049	0.4352	0.4553	0.4859	0.4948	0.5418	LI(7)008
0.6030	0.6620	0.7532	0.8510	0.9726	0.9807	LI(7)009
0.9456	0.7482	0.7038	0.6604	0.6057	0.5520	LI(7)010
0.5441	0.5297	0.5140	0.5039	0.3413	0.3245	LI(7)011
0.3178	0.3117	0.3094	0.3026	0.2805	0.2694	LI(7)012
0.2635	0.2529	0.2069	0.			LI(7)013
0.0814	0.0816	0.0849	0.0900	0.1176	0.1280	LI(7)014
0.1421	0.1558	0.1769	0.1997	0.2287	0.2438	LI(7)015
0.2493	0.3420	0.3440	0.3520	0.3585	0.3454	LI(7)016
0.3269	0.2905	0.2436	0.2241	0.2495	0.2372	LI(7)017
0.2323	0.2278	0.2262	0.2212	0.2050	0.1969	LI(7)018
0.1926	0.1849	0.	0.			LI(7)019
0.0437	0.0448	0.0464	0.0470	0.0760	0.0846	LI(7)020
0.0894	0.0981	0.1114	0.1257	0.1440	0.1453	LI(7)021
0.1412	0.2660	0.2538	0.2422	0.2327	0.2482	LI(7)022
0.2742	0.3125	0.3304	0.2964	0.2569	0.2072	LI(7)023
0.2029	0.1990	0.1975	0.1932	0.1791	0.1720	LI(7)024
0.1683	0.	0.	0.			LI(7)025
0.0158	0.0159	0.0165	0.0175	0.0418	0.0455	LI(7)026
0.0505	0.0554	0.0629	0.0709	0.0812	0.0820	LI(7)027
0.0797	0.1747	0.1666	0.1590	0.1501	0.1420	LI(7)028
0.1399	0.1362	0.1322	0.1296	0.1418	0.1348	LI(7)029
0.1320	0.1295	0.1285	0.1257	0.1165	0.1119	LI(7)030
0.	0.	0.	0.			LI(7)031
0.0362	0.0364	0.0378	0.0402	0.0578	0.0629	LI(7)032
0.0698	0.0765	0.0869	0.0981	0.1123	0.1133	LI(7)033
0.1101	0.1516	0.1446	0.1380	0.1303	0.1232	LI(7)034
0.1215	0.1184	0.1147	0.1125	0.3570	0.3397	LI(7)035
0.3325	0.3261	0.3238	0.3167	0.2935	0.2820	LI(7)036

TABLE D.6 Lithium 7 Nuclide Decks

0.3852	0.5311	0.7971	1.0130			LI(7)037
1.0	1.0	1.0	1.0	1.0	1.0	LI(7)038
1.0	1.0	1.0	1.0	0.0	0.0	LI(7)039
0.0	0.0	0.0	0.0	0.0	0.0	LI(7)040
0.0	0.0	0.0	0.0	0.0	0.0	LI(7)041
0.0	0.0	0.0	0.0	0.0	0.0	LI(7)042
0.0	0.0	0.0	0.0			LI(7)043
0.012	0.014	0.017	0.015	0.020		LI(7)044
0.021	0.038	0.036	0.016	0.015		LI(7)045
0.003	0.001	0.0	0.0	0.0		LI(7)046
0.0	0.014	0.016	0.019	0.018		LI(7)047
0.026	0.025	0.040	0.035	0.011		LI(7)048
0.009	0.002	0.0	0.0	0.0	0.0	LI(7)049
0.011	0.013	0.013	0.012	0.016		LI(7)050
0.017	0.035	0.034	0.020	0.021		LI(7)051
0.005	0.002	0.0	0.0	0.0		LI(7)052
0.0	0.0	0.015	0.017	0.022		LI(7)053
0.023	0.032	0.032	0.041	0.032		LI(7)054
0.006	0.004	0.001	0.0	0.0	0.0	LI(7)055
0.009	0.010	0.012	0.010	0.012		LI(7)056
0.013	0.031	0.032	0.024	0.023		LI(7)057
0.008	0.003	0.001	0.0	0.0		LI(7)058
0.0	0.0	0.0	0.017	0.020		LI(7)059
0.020	0.028	0.038	0.039	0.039		LI(7)060
0.024	0.003	0.0	0.0	0.0	0.0	LI(7)061
0.008	0.009	0.011	0.008	0.009		LI(7)062
0.009	0.025	0.027	0.027	0.025		LI(7)063
0.012	0.005	0.002	0.0	0.0		LI(7)064
0.0	0.0	0.0	0.0	0.019		LI(7)065
0.023	0.023	0.033	0.042	0.045		LI(7)066
0.025	0.014	0.002	0.0	0.0	0.0	LI(7)067
0.006	0.008	0.009	0.009	0.007		LI(7)068
0.007	0.022	0.025	0.028	0.024		LI(7)069
0.016	0.010	0.003	0.001	0.0		LI(7)070
0.0	0.0	0.0	0.0	0.0		LI(7)071
0.021	0.027	0.027	0.037	0.045		LI(7)072
0.047	0.012	0.006	0.001	0.0	0.0	LI(7)073

0.006	0.006	0.008	0.008	0.006		LI(7)074
0.006	0.019	0.023	0.027	0.022		LI(7)075
0.018	0.011	0.006	0.002	0.0		LI(7)076
0.0	0.0	0.0	0.0	0.0		LI(7)077
0.034	0.024	0.031	0.029	0.040		LI(7)078
0.048	0.048	0.005	0.003	0.0	0.0	LI(7)079
0.006	0.006	0.006	0.007	0.005		LI(7)080
0.005	0.015	0.019	0.026	0.020		LI(7)081
0.017	0.012	0.008	0.002	0.0		LI(7)082
0.0	0.0	0.0	0.0	0.0		LI(7)083
0.0	0.090	0.026	0.023	0.032		LI(7)084
0.042	0.046	0.047	0.001	0.002	0.0	LI(7)085
0.004	0.005	0.005	0.006	0.004		LI(7)086
0.004	0.014	0.016	0.023	0.017		LI(7)087
0.016	0.013	0.009	0.004	0.001		LI(7)088
0.0	0.0	0.0	0.0	0.0		LI(7)089
0.0	0.0	0.131	0.029	0.025		LI(7)090
0.034	0.040	0.037	0.038	0.0	0.0	LI(7)091
0.004	0.005	0.005	0.005	0.004		LI(7)092
0.004	0.012	0.014	0.021	0.016		LI(7)093
0.014	0.012	0.010	0.005	0.001		LI(7)094
0.0	0.0	0.0	0.0	0.0		LI(7)095
0.0	0.0	0.030	0.100	0.030		LI(7)096
0.028	0.035	0.037	0.030	0.026	0.0	LI(7)097
0.004	0.004	0.004	0.004	0.003		LI(7)098
0.003	0.011	0.011	0.018	0.015		LI(7)099
0.013	0.011	0.008	0.006	0.002		LI(7)100
0.0	0.0	0.0	0.0	0.0		LI(7)101
0.0	0.0	0.0	0.104	0.015		LI(7)102
0.021	0.029	0.034	0.029	0.015	0.015	LI(7)103
0.004	0.003	0.004	0.004	0.003		LI(7)104
0.003	0.010	0.010	0.016	0.014		LI(7)105
0.012	0.009	0.006	0.005	0.004		LI(7)106
0.0	0.0	0.0	0.0	0.0		LI(7)107
0.0	0.0	0.0	0.0	0.108		LI(7)108
0.0	0.023	0.029	0.033	0.017	0.009	LI(7)109
0.003	0.003	0.003	0.004	0.003		LI(7)110

0.003	0.008	0.009	0.014	0.012		LI(7)111
0.011	0.008	0.005	0.004	0.003		LI(7)112
0.0	0.0	0.0	0.0	0.0		LI(7)113
0.0	0.0	0.0	0.0	0.061		LI(7)114
0.035	0.0	0.024	0.030	0.028	0.009	LI(7)115
0.002	0.002	0.002	0.003	0.002		LI(7)116
0.002	0.007	0.008	0.012	0.011		LI(7)117
0.010	0.007	0.004	0.003	0.002		LI(7)118
0.0	0.0	0.0	0.0	0.0		LI(7)119
0.0	0.0	0.0	0.0	0.0		LI(7)120
0.081	0.0	0.0	0.026	0.027	0.009	LI(7)121
0.002	0.002	0.002	0.003	0.002		LI(7)122
0.002	0.007	0.007	0.011	0.009		LI(7)123
0.009	0.006	0.003	0.002	0.001		LI(7)124
0.0	0.0	0.0	0.0	0.0		LI(7)125
0.0	0.0	0.0	0.0	0.0		LI(7)126
0.035	0.026	0.0	0.0	0.027	0.019	LI(7)127
0.002	0.002	0.002	0.003	0.002		LI(7)128
0.002	0.006	0.006	0.009	0.008		LI(7)129
0.009	0.006	0.003	0.002	0.0		LI(7)130
0.0	0.0	0.0	0.0	0.0		LI(7)131
0.0	0.0	0.0	0.0	0.0		LI(7)132
0.0	0.044	0.0	0.0	0.0	0.022	LI(7)133
0.004	0.005	0.004	0.005	0.004	0.005	LI(7)134
0.012	0.012	0.019	0.016	0.019	0.012	LI(7)135
0.006	0.003	0.001	0.0	0.0	0.0	LI(7)136
0.0	0.0	0.0	0.0	0.0	0.0	LI(7)137
0.0	0.0	0.031	0.065	0.0	0.0	LI(7)138
0.0	0.0	0.0	0.0			LI(7)139
0.004	0.004	0.004	0.005	0.004	0.004	LI(7)140
0.012	0.011	0.018	0.016	0.018	0.012	LI(7)141
0.006	0.002	0.001	0.0	0.0	0.0	LI(7)142
0.0	0.0	0.0	0.0	0.0	0.0	LI(7)143
0.0	0.0	0.0	0.016	0.059	0.003	LI(7)144
0.0	0.0	0.0	0.0			LI(7)145
0.004	0.003	0.003	0.005	0.004	0.003	LI(7)146
0.012	0.010	0.018	0.015	0.018	0.011	LI(7)147

0.005	0.002	0.001	0.0	0.0	0.0	LI(7)148
0.0	0.0	0.0	0.0	0.0	0.0	LI(7)149
0.0	0.0	0.0	0.0	0.0	0.035	LI(7)150
0.013	0.0	0.0	0.0			LI(7)151
0.002	0.002	0.002	0.003	0.002	0.002	LI(7)152
0.006	0.006	0.009	0.007	0.009	0.006	LI(7)153
0.002	0.001	0.0	0.0	0.0	0.0	LI(7)154
0.0	0.0	0.0	0.0	0.0	0.0	LI(7)155
0.0	0.0	0.0	0.0	0.0	0.0	LI(7)156
0.011	0.011	0.0	0.0			LI(7)157
1.450	1.470	1.520	1.590	1.690	1.790	LI(7)158
1.910	2.010	2.160	2.320	2.520	2.460	LI(7)159
2.330	2.230	2.110	2.010	1.910	1.820	LI(7)160
1.810	1.780	1.750	1.730	1.710	1.640	LI(7)161
1.590	1.530	1.470	1.420	1.300	1.230	LI(7)162
1.180	1.130	1.110	1.120			LI(7)163

LITHIUM(7)						LI(7)164
0.530	1.009	0.161	0.0	0.0929	1.700	LI(7)165
2.940	4.320	0.0	0.0	0.0929	7.260	LI(7)166
1.104	0.644	0.002	0.0	0.0929	1.750	LI(7)167
0.575	0.455	0.0	0.0	0.0929	1.030	LI(7)168
0.794	0.246	0.0	0.0	0.0929	1.040	LI(7)169
0.885	0.165	0.0	0.0	0.0929	1.050	LI(7)170
0.774	0.286	0.0	0.0	0.0929	1.060	LI(7)171
0.781	0.289	0.0	0.0	0.0929	1.070	LI(7)172
0.788	0.292	0.0	0.0	0.0929	1.080	LI(7)173
0.796	0.294	0.0	0.0	0.0929	1.090	LI(7)174
0.803	0.297	0.0	0.0	0.0929	1.100	LI(7)175
0.803	0.297	0.0	0.0	0.0929	1.100	LI(7)176
0.803	0.297	0.0	0.0	0.0929	1.100	LI(7)177
0.803	0.297	0.0	0.0	0.0929	1.100	LI(7)178
0.803	0.297	0.0	0.0	0.0929	1.100	LI(7)179
1.100	0.0	0.0	0.260	0.0929	1.133	LI(7)180

D.5 BERYLLIUM

a. High-Energy Cross Sections

Total Cross Section: The total cross sections in the energy range of interest given by Parker,[79] Hughes and Schwartz,[52] Fossan et al.,[80] and Levin and Cranberg[81] are in good agreement. The Parker values are used for consistency with the other cross sections.

Nonelastic Cross Section: Values for the nonelastic cross section in beryllium are given in the region 2.5-6.0 Mev by Marion, Levin and Cranberg,[82] and by Levin and Cranberg[81]; in the range 4.0-14.2 Mev by Ball, MacGregor and Booth[83,84]; at 14 Mev by Rosen and Stewart[85]; and over the entire range of interest by Parker.[79] The various published values are in good agreement. The Parker value is used.

Elastic Cross Section: The elastic scattering cross section is plotted in the region 2.6-6.0 Mev by Marion, Levin and Cranberg,[82] and by Parker[79] over the entire range of interest. The Parker results are in agreement with those of Marion and his co-workers, and are used for consistency with the other cross sections.

Radiative Capture Cross Section: The radiative capture cross section given by Hughes and Schwartz[52] at 0.025 ev is very small (~9 mb), and has not been measured at higher energies. The reaction is ignored.

Proton and Deuteron Emission Cross Sections: Neither proton nor deuteron emission resulting from neutron-induced reactions in beryllium has been observed. Since the sum of the measured individual nonelastic cross sections is sufficient to account for the observed total nonelastic cross section over a range of energies, emission of protons and deuterons is assumed to be negligible.

Triton Emission Cross Section: The values given by Parker[9] and Vasil'ov, Komaron and Popova[86] for $\sigma_{n,t}$ in the vicinity of 14 Mev differ by about an order of magnitude. The Parker values are used partly for consistency and partly because they are based on additional, more recent measurements.

Alpha Emission Cross Section (yielding Li^6 via beta decay): The (n,α) cross section is plotted in the range from threshold to 4.5 Mev by Stelson and Campbell[87]; and by Vasil'ov, Nomarov and Popova[86]; in the range 4-8 Mev by Bass, Bonner and Haenni[88]; and in the range from threshold to 15 Mev by Parker.[79] Values of isolated energies between 2.5 Mev and 6.0 Mev are also tabulated by Marion, Levin and Cranberg.[82] The agreement is good; the Parker plot is most nearly complete and is used.

(n, 2n) Cross Section: Values for the (n, 2n) cross section in beryllium are given by Catron et al.,[89] Parker,[79] and Hughes and Schwartz[52] over the energy range of interest. Additional values are plotted near the apparent threshold by Fischer.[90] Above ~3 Mev, all values are in good agreement. Below 3 Mev, two schools of thought exist, made up of Fischer, supported by Shev and Moore,[91] and Catron et al. on the one hand, and of Parker and Marion, Levin, and Cranberg[82] on the other. According to the Fischer school the threshold of the (n, 2n) process is directly associated with excitation of the

2.43 Mev level in Be^9 by inelastic scattering, the level subsequently decaying by neutron emission. Parker infers that the threshold is somewhat lower in energy and is associated with breakup reactions that yield two neutrons and two alphas. The Fischer results are substantiated by the more recent measurements and are preferred near the threshold. Otherwise Parker's values are used.

Inelastic Cross Section: Anderson et al.[92] observe that no gamma rays associated with Be^{9*} have been detected. Decay of excited levels proceeds by emission of a second neutron or a charged particle. The inelastic cross section is taken to be zero at all energies.

b. Low-Energy Cross Sections

Total Cross Section: The $\sigma_{n,t}$ plots of Parker[79] and Hughes and Schwartz[52] are in good agreement in the lower energy region. The Parker plot is used for consistency.

Nonelastic Cross Section: The only nonelastic reaction energetically permitted below 400 Mev is radiative capture. The (n, γ) cross section is so small even at thermal energy[52] that the reaction is ignored. The nonelastic cross section is assumed to be zero in the entire lower energy region.

Elastic Cross Section: In the absence of a nonelastic cross section the elastic cross section is identically the total cross section. The Parker[79] values are used.

Radiative Capture Cross Section: Radiative capture is ignored due to the very low (n, γ) cross section at thermal energy.

c. Neutron Nonelastic Spectra

If excitation of the apparent level at 1.75 Mev is ignored, all nonelastic, non-loss reactions in beryllium give rise eventually to two neutrons and two alpha particles, although the detailed processes are numerous. Among them are:

$$n + Be^9 \rightarrow n' + Be^{9*}(2.43\gamma) \rightarrow n' + n + Be^8 \rightarrow n' + n + 2He^4$$

$$n + Be^9 \rightarrow n' + Be^{9*}(2.43\gamma) \rightarrow n' + He^4 + He^5 \rightarrow n' + n + He^4 + He^4$$

$$n + Be^9 \rightarrow n' + Be^{9*}(2.43\gamma) \rightarrow \quad (?) \quad \rightarrow n' + n + 2He^4$$

$$n + Be^9 \rightarrow He^4 + He^{6*}(1.71\gamma) \rightarrow \quad (?) \quad \rightarrow He^4 + 2n + He^4$$

$$n + Be^9 \rightarrow He^4 + He^{6*}(>1.71\gamma) \rightarrow \quad (?) \quad \rightarrow He^4 + 2n + He^4$$

$$n + Be^9 \rightarrow 2He^4 + 2n \qquad \text{(via direct breakup)}.$$

Ajzenberg-Selove and Lauritsen[93] and Anderson et al.[92] observe that the cross section for excitation of Be^{9*}(2.43γ) by 14-Mev neutrons is ~170 mb, roughly one third of the total (n, 2n) cross section at 14 Mev. This process should yield one neutron at ~11.6 Mev. The spectrum of Rosen and Stewart[85] shows no response in that energy region, thereby indicating a serious contradiction between published results. It is conceivable, but unlikely, that processes involving excitation of higher levels in Be^{9*} and

a mixed cascade of gamma rays down to the 2.43-Mev level, with neutron de-excitation from there to ground state, do occur. The result is that the small amount of available information is of questionable value, while the variety of allowed processes is so great that theoretical prediction of the spectra is out of the question.

Parker[79] assigns probabilities in the form of delta functions in lieu of spectra. These probabilities of all allowed energies are used as published.

	$\sigma_{n,T}$	$\sigma_{n,n}$	$\sigma_{n,x}$	$\sigma_{n,2n}$	$\sigma_{n,t}$
01	1.5000	0.9750	0.5250	0.5000	0.0150
02	1.5400	0.9980	0.5420	0.5200	0.0070
03	1.5900	1.0300	0.5600	0.5400	0.0000
04	1.6000	1.0150	0.5850	0.5600	0.0000
05	1.6200	1.0200	0.5990	0.5700	0.0000
06	1.7300	1.1170	0.6130	0.5800	0.0000
07	1.8400	1.2150	0.0250	0.6000	0.0000
08	1.8100	1.1930	0.6170	0.6000	0.0000
09	1.8200	1.2040	0.6160	0.6000	0.0000
10	1.8200	1.1870	0.6330	0.6000	0.0000
11	1.8500	1.2090	0.6410	0.5900	0.0000
12	1.9000	1.2640	0.6360	0.5700	0.0000
13	2.0000	1.3550	0.6450	0.5600	0.0000
14	2.1100	1.4960	0.6140	0.5200	0.0000
15	2.5500	1.9600	0.5900	0.4900	0.0000
16	3.3000	2.9180	0.3820	0.2800	0.0000
17	2.9000	2.8080	0.0920	0.0000	0.0000
18	2.0800	2.0100	0.0700	0.0000	0.0000
19	1.7500	1.6940	0.0560	0.0000	0.0000
20	1.6500	1.6090	0.0410	0.0000	0.0000
21	1.8000	1.7700	0.0300	0.0000	0.0000
22	2.0000	1.9820	0.0180	0.0000	0.0000
23	2.4000	2.3900	0.0100	0.0000	0.0000
24	2.8500	2.8450	0.0050	0.0000	0.0000
25	3.2000	3.1980	0.0020	0.0000	0.0000
26	3.3500	3.3500	0.0000	0.0000	0.0000
27	3.4500	3.4500	0.0000	0.0000	0.0000
28	3.8000	3.8000	0.0000	0.0000	0.0000
29	3.6000	3.6000	0.0000	0.0000	0.0000
30	3.9000	3.9000	0.0000	0.0000	0.0000
31	5.5000	5.5000	0.0000	0.0000	0.0000
32	3.7500	3.7500	0.0000	0.0000	0.0000
33	3.6500	3.6500	0.0000	0.0000	0.0000
34	4.0000	4.0000	0.0000	0.0000	0.0000
35	3.8500	3.8500	0.0000	0.0000	0.0000
36	4.2500	4.2500	0.0000	0.0000	0.0000
37	4.9500	4.9500	0.0000	0.0000	0.0000
38	5.7000	5.7000	0.0000	0.0000	0.0000
39	5.8500	5.8500	0.0000	0.0000	0.0000
40	5.9000	5.9000	0.0000	0.0000	0.0000
41	5.9500	5.9500	0.0000	0.0000	0.0000
42	6.0000	6.0000	0.0000	0.0000	0.0000
43	6.0000	6.0000	0.0000	0.0000	0.0000
44	6.0000	6.0000	0.0000	0.0000	0.0000
45	6.0000	6.0000	0.0000	0.0000	0.0000
46	6.0000	6.0000	0.0000	0.0000	0.0000
47	6.0000	6.0000	0.0000	0.0000	0.0000
48	6.0000	6.0000	0.0000	0.0000	0.0000
49	6.0000	6.0000	0.0000	0.0000	0.0000
50	6.0000	6.0000	0.0000	0.0000	0.0000

TABLE D.7 FIFTY GROUP NEUTRON CROSS SECTIONS FOR BERYLLIUM

	$\sigma_{n,\alpha}$
01	0.0100
02	0.0150
03	0.0200
04	0.0250
05	0.0290
06	0.0330
07	0.0250
08	0.0170
09	0.0160
10	0.0330
11	0.0510
12	0.0660
13	0.0850
14	0.0940
15	0.1000
16	0.1020
17	0.0920
18	0.0700
19	0.0560
20	0.0410
21	0.0300
22	0.0180
23	0.0100
24	0.0050
25	0.0020
26	0.0000
27	0.0000
28	0.0000
29	0.0000
30	0.0000
31	0.0000
32	0.0000
33	0.0000
34	0.0000
35	0.0000
36	0.0000
37	0.0000
38	0.0000
39	0.0000
40	0.0000
41	0.0000
42	0.0000
43	0.0000
44	0.0000
45	0.0000
46	0.0000
47	0.0000
48	0.0000
49	0.0000
50	0.0000

TABLE D.7 (CONT.) FIFTY GROUP CROSS SECTIONS FOR BERYLLIUM

BERYLLIUM		JUNE 21.1962				BE001
0.4298	0.4399	0.4534	0.4468	0.4490	0.4503	BE002
0.4898	0.4809	0.4597	0.4264	0.4343	0.4232	BE003
0.4537	0.4855	0.6360	0.8804	0.9522	0.4225	BE004
0.3561	0.3035	0.3338	0.3738	0.4852	0.5775	BE005
0.6492	0.6801	0.5013	0.5521	0.5231	0.5667	BE006
0.7992	0.5348	0.5205	0.5704			BE007
0.4535	0.4642	0.4840	0.4769	0.4793	0.4923	BE008
0.5355	0.5258	0.5093	0.4977	0.5069	0.4992	BE009
0.5351	0.5692	0.7458	1.0087	1.0912	0.5471	BE010
0.4611	0.5067	0.5574	0.6241	0.7827	0.9317	BE011
1.0473	1.0971	0.8874	0.9774	0.9259	1.0031	BE012
1.4146	1.0241	0.9968	0.			BE013
0.0490	0.0502	0.0485	0.0478	0.0480	0.0706	BE014
0.0768	0.0754	0.0897	0.1097	0.1117	0.1230	BE015
0.1318	0.1485	0.1946	0.2997	0.2603	0.2565	BE016
0.2162	0.3574	0.3931	0.4402	0.5093	0.6063	BE017
0.6815	0.7139	0.7483	0.8242	0.7808	0.8459	BE018
1.1930	0.9214	0.	0.			BE019
0.0573	0.2532	0.0729	0.0737	0.0750	0.0846	BE020
0.0699	0.0663	0.0874	0.0895	0.0912	0.1225	BE021
0.1313	0.1676	0.2195	0.4204	0.2934	0.4050	BE022
0.3413	0.2830	0.3113	0.3486	0.3905	0.4649	BE023
0.5226	0.5474	0.7783	0.8573	0.8122	0.8798	BE024
1.2408	0.	0.	0.			BE025
0.0482	0.1856	0.3805	0.3939	0.2066	0.0601	BE026
0.0409	0.0402	0.0526	0.0574	0.0585	0.0858	BE027
0.0920	0.1140	0.1494	0.2790	0.1915	0.3260	BE028
0.2748	0.1437	0.1581	0.1770	0.2005	0.2387	BE029
0.2683	0.2811	0.4754	0.5236	0.4961	0.5374	BE030
0.	0.	0.	0.			BE031
0.1522	0.0002	0.0013	0.0013	0.1949	0.0041	BE032
0.0045	0.0044	0.0053	0.0063	0.0064	0.0104	BE033
0.0111	0.0112	0.0147	0.0298	0.0194	0.0529	BE034
0.0445	0.0147	0.0163	0.0183	0.0218	0.0259	BE035
0.0291	0.0305	0.0593	0.0654	0.0619	0.0671	BE036

TABLE D.8 Beryllium Nuclide Decks

0.8524	1.2697	2.1327	3.4296			BE037
1.0	1.0	1.0	1.0	1.0	1.0	BE038
1.0	1.0	1.0	1.0	0.0	0.0	BE039
0.0	0.0	0.0	0.0	0.0	0.0	BE040
0.0	0.0	0.0	0.0	0.0	0.0	BE041
0.0	0.0	0.0	0.0	0.0	0.0	BE042
0.0	0.0	0.0	0.0			BE043
0.0	0.0	0.0	0.0	0.1140		BE044
0.0	0.0	0.0240	0.0240	0.0		BE045
0.059	0.0	0.023	0.020	0.0		BE046
0.0220	0.1310	0.0	0.0	0.1120		BE047
0.0	0.0	0.0240	0.0240	0.0		BE048
0.0600	0.4010	0.0460	0.0220	0.0	0.0390	BE049
0.0	0.0	0.0	0.0	0.0		BE050
0.1160	0.0	0.0	0.0240	0.0480		BE051
0.0	0.2510	0.0	0.0210	0.0		BE052
0.0	0.0	0.0	0.0	0.1080		BE053
0.0	0.0	0.0	0.0240	0.0		BE054
0.0600	0.0	0.0470	0.0	0.0	0.0410	BE055
0.1105	0.0	0.0	0.0	0.0		BE056
0.0	0.1200	0.0	0.0	0.0		BE057
0.0470	0.1940	0.0560	0.0	0.0390		BE058
0.0	0.0	0.0	0.0	0.1041		BE059
0.0	0.0	0.0	0.0465	0.0		BE060
0.0600	0.0	0.4320	0.0	0.0	0.0450	BE061
0.0	0.0	0.0	0.0	0.0		BE062
0.0	0.0	0.1200	0.0	0.0		BE063
0.0	0.0230	0.0	0.0520	0.0		BE064
0.0220	0.0	0.0	0.0	0.0830		BE065
0.0	0.0	0.0	0.0456	0.0		BE066
0.0600	0.0	0.456	0.0240	0.0	0.0460	BE067
0.0	0.1458	0.0	0.0	0.0		BE068
0.0	0.0	0.0	0.1200	0.0		BE069
0.0	0.0230	0.3810	0.0	0.0490		BE070
0.0	0.0	0.0	0.0	0.0		BE071
0.0	0.0	0.0	0.0448	0.0		BE072
0.0580	0.0	0.0480	0.0	0.0	0.0470	BE073

0.0	0.0	0.1510	0.0	0.0		BE074
0.0	0.0	0.0	0.0	0.1200		BE075
0.0	0.0	0.0450	0.0210	0.0		BE076
0.0280	0.0	0.0	0.0	0.0		BE077
0.0	0.0	0.0208	0.0432	0.0		BE078
0.0570	0.0	0.0480	0.4080	0.0	0.0480	BE079
0.0845	0.0	0.0	0.1570	0.0		BE080
0.0	0.0	0.0	0.0	0.0		BE081
0.1180	0.0	0.0	0.0210	0.0390		BE082
0.0	0.0	0.0	0.0	0.0		BE083
0.0	0.0	0.1225	0.0208	0.0		BE084
0.0560	0.0	0.0465	0.0240	0.0	0.0480	BE085
0.0	0.0	0.0	0.0	0.1600		BE086
0.0	0.0	0.0	0.0	0.0		BE087
0.0	0.1140	0.0	0.3540	0.0		BE088
0.0220	0.0	0.0	0.0	0.0		BE089
0.0	0.0	0.0	0.0	0.0		BE090
0.0540	0.0	0.0456	0.0	0.4310	0.0480	BE091
0.0	0.2600	0.2700	0.2800	0.2850		BE092
0.4530	0.3000	0.3000	0.3000	0.3000		BE093
0.296	0.283	0.392	0.260	0.245		BE094
0.142	0.0	0.0	0.0	0.0		BE095
0.0	0.0	0.0	0.0	0.0845		BE096
0.0932	0.0432	0.0448	0.0	0.395	0.001	BE097
0.0	0.0	0.0	0.0	0.0		BE098
0.0	0.1680	0.0	0.0	0.0		BE099
0.0	0.0	0.0	0.1040	0.0		BE100
0.0	0.0	0.0	0.0	0.0		BE101
0.0	0.0	0.0	0.0	0.0		BE102
0.0	0.0	0.0	0.0	0.0	0.0	BE103
0.0	0.0	0.0	0.0	0.0		BE104
0.0	0.0	0.1680	0.0	0.0		BE105
0.0	0.0	0.0	0.0	0.0980		BE106
0.0	0.0	0.0	0.0	0.0		BE107
0.0	0.0	0.0	0.0	0.0		BE108
0.0	0.0	0.0	0.0	0.0	0.0	BE109
0.0	0.0	0.0	0.0	0.0		BE110

0.0	0.0	0.0	0.1680	0.0		BE111
0.0	0.0	0.0	0.0	0.3340		BE112
0.056	0.0	0.0	0.0	0.0		BE113
0.0	0.0	0.0	0.0	0.0		BE114
0.0	0.0	0.0	0.0	0.0	0.0	BE115
0.0	0.0	0.0	0.0	0.0		BE116
0.0	0.0	0.0	0.0	0.1680		BE117
0.0	0.0	0.0	0.0	0.0		BE118
0.0	0.0	0.0	0.0	0.0		BE119
0.0	0.0	0.0	0.0	0.0		BE120
0.0	0.0	0.0	0.0	0.0	0.0	BE121
0.1690	0.0	0.0	0.0	0.0		BE122
0.0	0.0	0.0	0.0	0.0		BE123
0.1650	0.0	0.0	0.0	0.0		BE124
0.0	0.0	0.0	0.0	0.0		BE125
0.0	0.0	0.0	0.0	0.0		BE126
0.0	0.0	0.0	0.0	0.0	0.0	BE127
0.0	0.0	0.0	0.0	0.0		BE128
0.0	0.0	0.0	0.0	0.0		BE129
0.0	0.160	0.0775	0.0	0.0		BE130
0.0	0.0	0.0	0.0	0.0		BE131
0.0	0.0	0.0	0.0	0.0		BE132
0.0	0.0	0.0	0.0	0.0	0.0	BE133
0.0	0.0	0.0	0.0	0.0	0.0	BE134
0.0	0.0	0.0	0.0	0.0	0.0	BE135
0.0785	0.1460	0.0690	0.0	0.0	0.0	BE136
0.0	0.0	0.0	0.0	0.0	0.0	BE137
0.0	0.0	0.0	0.0	0.0	0.0	BE138
0.0	0.0	0.0	0.0			BE139
0.0	0.0	0.0	0.0	0.0	0.0	BE140
0.0	0.0	0.0	0.0	0.0	0.0	BE141
0.0	0.0	0.0680	0.0770	0.0	0.0	BE142
0.0	0.0	0.0	0.0	0.0	0.0	BE143
0.0	0.0	0.0	0.0	0.0	0.0	BE144
0.0	0.0	0.0	0.0			BE145
0.0	0.0	0.0	0.0	0.0	0.0	BE146
0.0	0.0	0.0	0.0	0.0	0.0	BE147

0.0	0.0	0.0	0.1910	0.0	0.0	BE148
0.0	0.0	0.0	0.0	0.0	0.0	BE149
0.0	0.0	0.0	0.0	0.0	0.0	BE150
0.0	0.0	0.0	0.0			BE151
0.0	0.0	0.0	0.0	0.0	0.0	BE152
0.0	0.0	0.0	0.0	0.0	0.0	BE153
0.0	0.0	0.0	0.0	0.0	0.0	BE154
0.0	0.0	0.0	0.0	0.0	0.0	BE155
0.0	0.0	0.0	0.0	0.0	0.0	BE156
0.0	0.0	0.0	0.0			BE157
1.500	1.540	1.590	1.600	1.620	1.730	BE158
1.840	1.810	1.820	1.820	1.850	1.900	BE159
2.000	2.110	2.550	3.300	2.900	2.080	BE160
1.750	1.650	1.800	2.000	2.400	2.850	BE161
3.200	3.350	3.450	3.800	3.600	3.900	BE162
5.500	3.750	3.650	4.000			BE163

BERYLLIUM						BE164
1.450	2.320	0.080	0.0	0.07391	3.850	BE165
2.093	2.157	0.0	0.0	0.07391	4.250	BE166
3.530	1.420	0.0	0.0	0.07391	4.950	BE167
3.810	1.890	0.0	0.0	0.07391	5.700	BE168
4.803	1.047	0.0	0.0	0.07391	5.850	BE169
5.200	0.700	0.0	0.0	0.07391	5.900	BE170
4.720	1.230	0.0	0.0	0.07391	5.950	BE171
4.760	1.240	0.0	0.0	0.07391	6.000	BE172
4.760	1.240	0.0	0.0	0.07391	6.000	BE173
4.760	1.240	0.0	0.0	0.07391	6.000	BE174
4.760	1.240	0.0	0.0	0.07391	6.000	BE175
4.760	1.240	0.0	0.0	0.07391	6.000	BE176
4.760	1.240	0.0	0.0	0.07391	6.000	BE177
4.760	1.240	0.0	0.0	0.07391	6.000	BE178
4.760	1.240	0.0	0.0	0.07391	6.000	BE179
5.990	0.0	0.0	0.209	0.07391	6.000	BE180

D. 6 BORON

a. High-Energy Cross Sections

Total Cross Section: The values given by Fosson et al.[94] for the total cross section in the energy range of interest are in agreement with those of Hughes and Schwartz,[52] and of Buckingham, Parker and Pendlebury.[18] The Fosson values are used.

Nonelastic Cross Section: The nonelastic cross sections for natural boron were taken to be the sum of the several individual nonelastic cross sections. The value thus obtained at 14 Mev is in good agreement with the "inelastic" (almost certainly an error in translation) cross section measured by Gorbachev[78] at 14 Mev.

Elastic Cross Section: Taken to be the difference between the total and the nonelastic cross sections of all energies of interest.

Radiative Capture Cross Section: The radiative capture cross sections in B^{10} and B^{11} at 0.025 ev are given by Hughes and Schwartz[52] as 500 mb and less than 50 mb, respectively. Owing to the much larger (n, α) cross section in B^{10}, the (n, γ) cross section in boron is neglected.

Proton Emission Cross Section: Neutron-induced reactions in B^{10} and B^{11} yielding protons have not been observed. Thresholds are high for both isotopes. The reactions are neglected.

Deuteron Emission Cross Section: In B^{10} the (n, dn) reaction has a theoretical threshold, with Coulomb barrier effects neglected, of 4.36 Mev. The effective threshold is ~11 Mev. The cross section above 12 Mev is given by Frye and Gammel[95] and is extrapolated to threshold at 11 Mev. In B^{11} the threshold is at ~11 Mev also. The reaction has not been observed and is neglected.

Triton Emission Cross Section: The (n, t) cross section in B^{10} has been measured in the range 4-16 Mev by Wyman, Fryer and Thorpe[96] who compile their measurement with previously published results. There is apparently some discrepancy between these results and some unpublished results (noted by Shev and Moore[97]) which indicate that the values of Wyman et al. may be high. These values are used for lack of better ones. In B^{11} the threshold is high, ~11 Mev. Wyman et al. give the cross section at 14.2 Mev. The cross section at lower energies is extrapolated.

Alpha Emission Cross Section: For B^{10} $\sigma_{n,\alpha}$ is given in the range 0.02-4.8 Mev by Cook and Bonner[76] and Bischel and Bonner.[98] Above 4 Mev, the alpha emission cross section decreases rapidly, because of competition from other reactions. The plot is extrapolated to zero at ~6.5 Mev. For B^{11} the cross section is given in the range 12.6-20 Mev by Frye and Gammel.[95] Below 12.6 Mev, the plot is extrapolated to yield a nominal threshold of ~9.5 Mev.

(n, 2n) Cross Section: Thresholds for (n, 2n) processes in both B^{10} and B^{11} are high. The reaction has not been observed for either nuclide. The cross section is assumed to be zero at all energies of interest.

Inelastic Cross Section: The excitation function for emission of a 0.72 Mev gamma

ray from B^{10*} has been measured in the range 1.5-5.0 Mev by Day and Walt.[99] The resonances observed by Day are readily correlated (with the exception of the first very sharp peak) with levels listed by Ajzenberg-Selove and Lauritsen[73] who used the relation E (resonance $\approx$ E) level (11/10) + 0.8. If the first peak is deleted, the curve from 2.5 Mev to 5.0 Mev is in fair agreement with the plot given by Buckingham, Parker and Pendlebury.[18] By subtracting the sum of the cross sections of the other nonelastic processes from the measured $\sigma_{n,x}$ value given by MacGregor et al.[100] at 14 Mev an estimate of $\sigma_{n,n'}$ at 14 Mev is obtained. The plot is interpolated between 5 Mev and 14 Mev. The resultant plot, with allowance for resonances evident in the $\sigma_{n,t}$ plot, is at least in qualitative agreement with the curve of Buckingham et al. For B^{11} the excitation function for the lowest level, at 2.14 Mev, was measured and has been tabulated by Howerton.[101] The value at 14 Mev was estimated as in B^{10}. The curve is interpolated between the measured value at 3 Mev and the estimate at 14 Mev, with predicted resonances taken into account.

The plot obtained for natural boron by combining the inelastic cross sections for the two stable isotopes is in rather pronounced disagreement with that given by Buckingham et al.[18] In particular, they show that the threshold for (n, n') reactions in boron correponds to excitation of a level at 0.45 Mev. No such level in either B^{10} or B^{11} is known. A level in Li^{7} at 0.43 Mev, excited by the process $B^{10}(n, \alpha)Li^{7*}$, is known and is believed to be the source of response in the vicinity of 0.45 Mev.

b. Low-Energy Cross Sections

Total Cross Section: The total cross section in the lower energy region is plotted by Hughes and Schwartz[52] and by Buckingham, Parker and Pendlebury[18] with good agreement. The Hughes and Schwartz plot is used.

Nonelastic Cross Section: The nonelastic cross section below 400 kev is identical to the B^{10} (n, x) cross section. The plots of Hughes and Schwartz[52] and of Buckingham, Parker and Pendlebury[18] are in good agreement.

Elastic Cross Section: Taken to be the difference between the total and nonelastic cross sections.

Radiative Capture Cross Section: The (n, γ) cross sections in B^{10} and B^{11} are very small compared with the $B^{10}(n, \alpha)$ cross section and are ignored.

Alpha Emission Cross Section: The cross sections for the reaction in $B^{10}(n, \alpha)$ are plotted by Hughes and Schwartz[52] and by Buckingham, Parker and Pendlebury[18] with good agreement. The Hughes and Schwartz plot is used for consistency.

c. Neutron Nonelastic Spectra

For incident neutron energies above 9 Mev the statistical model is assumed to be valid. For energies between 6 Mev and 9 Mev the empirical model is used. Neutrons in the range 5-6 Mev are assumed to excite the 4.46-Mev level in B^{11}; the emergent spectrum is calculated by using the isolated-level model. Neutrons in the region 2.5-5.0 Mev

are assumed to scatter from the 2.14-Mev level in B^{11}, and the 2.15-Mev level in B^{10}; the emission energy spectrum follows the isolated-level model. Below 2.5 Mev nonelastic scattering does not occur.

	$\sigma_{n,T}$	$\sigma_{n,n}$	$\sigma_{n,X}$	$\sigma_{n,t}$	$\sigma_{n,\alpha}$
01	1.3510	0.7166	0.6344	0.0290	0.0260
02	1.3880	0.7769	0.6111	0.0300	0.0310
03	1.4000	0.8212	0.5788	0.0290	0.0320
04	1.4150	0.8655	0.5495	0.0270	0.0230
05	1.4250	0.8985	0.5265	0.0260	0.0000
06	1.4300	1.0040	0.4260	0.0280	0.0000
07	1.5800	1.1671	0.4129	0.0350	0.0000
08	1.5200	1.1883	0.3317	0.0430	0.0000
09	1.6200	1.3444	0.2756	0.0460	0.0010
10	1.5300	1.2734	0.2566	0.0460	0.0040
11	1.5600	1.3903	0.1697	0.0410	0.0100
12	1.5300	1.4005	0.1295	0.0330	0.0160
13	1.4100	1.3208	0.0892	0.0200	0.0210
14	1.5500	1.4919	0.0581	0.0010	0.0240
15	1.5300	1.4800	0.0500	0.0000	0.0260
16	1.7000	1.6421	0.0579	0.0000	0.0370
17	1.9200	1.8636	0.0564	0.0000	0.0390
18	1.9500	1.8940	0.0560	0.0000	0.0400
19	1.7100	1.6580	0.0520	0.0000	0.0520
20	1.8400	1.7650	0.0750	0.0000	0.0750
21	2.2000	2.1210	0.0790	0.0000	0.0790
22	2.1000	2.0420	0.0580	0.0000	0.0580
23	2.2500	2.2070	0.0430	0.0000	0.0430
24	2.9000	2.8630	0.0370	0.0000	0.0370
25	2.2500	2.2130	0.0370	0.0000	0.0370
26	1.7700	1.7310	0.0390	0.0000	0.0390
27	1.7500	1.7070	0.0430	0.0000	0.0430
28	1.9500	1.9010	0.0490	0.0000	0.0490
29	2.2000	2.1420	0.0580	0.0000	0.0580
30	2.4000	2.3300	0.0700	0.0000	0.0700
31	2.7000	2.6200	0.0800	0.0000	0.0800
32	3.0500	2.9470	0.1030	0.0000	0.1030
33	3.4000	3.2780	0.1220	0.0000	0.1220
34	4.8000	4.6750	0.1250	0.0000	0.1250
35	4.1000	3.9700	0.1300	0.0000	0.1300
36	3.6000	3.4500	0.1500	0.0000	0.1500
37	3.8000	3.5600	0.2400	0.0000	0.2400
38	4.2000	3.6500	0.5500	0.0000	0.5500
39	4.6000	3.7500	0.8500	0.0000	0.8500
40	5.1000	3.8000	1.3000	0.0000	1.3000
41	5.7000	4.0000	1.7000	0.0000	1.7000
42	6.0000	4.0000	2.0000	0.0000	2.0000
43	6.3000	4.0000	2.3000	0.0000	2.3000
44	6.8400	4.0000	2.8400	0.0000	2.8400
45	8.1800	4.0000	4.1800	0.0000	4.1800
46	10.1400	4.0000	6.1400	0.0000	6.1400
47	13.6100	4.0000	9.6100	0.0000	9.6100
48	19.6100	4.0000	15.6100	0.0000	15.6100
49	30.6000	4.0000	20.6000	0.0000	20.6000
50	759.0000	4.0000	755.0000	0.0000	755.0000

TABLE D.9 FIFTY GROUP NEUTRON CROSS SECTIONS FOR BORON

	$\sigma_{n,dn}$	$\sigma_{n,n'}$
01	0.0200	0.5794
02	0.0170	0.5501
03	0.0120	0.5178
04	0.0070	0.4995
05	0.0030	0.5005
06	0.0000	0.3980
07	0.0000	0.3779
08	0.0000	0.2887
09	0.0000	0.2286
10	0.0000	0.2066
11	0.0000	0.1187
12	0.0000	0.0805
13	0.0000	0.0482
14	0.0000	0.0331
15	0.0000	0.0240
16	0.0000	0.0209
17	0.0000	0.0174
18	0.0000	0.0160
19	0.0000	0.0000
20	0.0000	0.0000
21	0.0000	0.0000
22	0.0000	0.0000
23	0.0000	0.0000
24	0.0000	0.0000
25	0.0000	0.0000
26	0.0000	0.0000
27	0.0000	0.0000
28	0.0000	0.0000
29	0.0000	0.0000
30	0.0000	0.0000
31	0.0000	0.0000
32	0.0000	0.0000
33	0.0000	0.0000
34	0.0000	0.0000
35	0.0000	0.0000
36	0.0000	0.0000
37	0.0000	0.0000
38	0.0000	0.0000
39	0.0000	0.0000
40	0.0000	0.0000
41	0.0000	0.0000
42	0.0000	0.0000
43	0.0000	0.0000
44	0.0000	0.0000
45	0.0000	0.0000
46	0.0000	0.0000
47	0.0000	0.0000
48	0.0000	0.0000
49	0.0000	0.0000
50	0.0000	0.0000

TABLE D.9 (CONT.) FIFTY GROUP CROSS SECTIONS FOR BORON

BORON		JULY 24,1962				
						B 001
0.2986	0.3237	0.3422	0.3607	0.3744	0.4184	B 002
0.4863	0.4952	0.5602	0.4303	0.4698	0.4732	B 003
0.4463	0.5041	0.5001	0.5549	0.6297	0.6400	B 004
0.5602	0.3509	0.4217	0.4059	0.4388	0.5692	B 005
0.4399	0.3441	0.3394	0.3779	0.4809	0.5231	B 006
0.5882	0.6616	0.7359	1.0495			B 007
0.3250	0.3523	0.3724	0.3925	0.4075	0.4553	B 008
0.5293	0.5389	0.6097	0.5090	0.5557	0.5598	B 009
0.5279	0.5963	0.5916	0.6563	0.7449	0.7570	B 010
0.6627	0.5590	0.6717	0.6467	0.6989	0.9067	B 011
0.7008	0.5482	0.5406	0.6020	0.7923	0.8619	B 012
0.9691	1.0901	1.2125	0.			B 013
0.0519	0.0562	0.0594	0.0627	0.0650	0.0727	B 014
0.0845	0.0860	0.0973	0.1728	0.1887	0.1900	B 015
0.1792	0.2024	0.2008	0.2228	0.2529	0.2570	B 016
0.2250	0.4427	0.5319	0.5121	0.5535	0.7180	B 017
0.5550	0.4341	0.4281	0.4768	0.5396	0.5869	B 018
0.6600	0.7423	0.	0.			B 019
0.0333	0.0362	0.0382	0.0402	0.0418	0.0467	B 020
0.0543	0.0552	0.0625	0.1277	0.1394	0.1405	B 021
0.1325	0.1497	0.1484	0.1648	0.1869	0.1900	B 022
0.1663	0.3235	0.3888	0.3744	0.4046	0.5248	B 023
0.4058	0.3173	0.3129	0.3484	0.2787	0.3031	B 024
0.3409	0.	0.	0.			B 025
0.0078	0.0085	0.0090	0.0094	0.0098	0.0109	B 026
0.0127	0.0130	0.0147	0.0336	0.0367	0.0370	B 027
0.0349	0.0394	0.0391	0.0433	0.0492	0.0500	B 028
0.0438	0.0889	0.1069	0.1029	0.1112	0.1443	B 029
0.1115	0.0873	0.0860	0.0959	0.0505	0.0550	B 030
0.	0.	0.	0.			B 031
0.	0.	0.	0.	0.	0.	B 032
0.	0.	0.	0.	0.	0.	B 033
0.	0.	0.	0.	0.	0.	B 034
0.	0.	0.	0.	0.	0.	B 035
0.	0.	0.	0.	0.	0.	B 036

TABLE D.10 Boron Nuclide Decks

0.0618	0.4530	1.3296	3.6255			B 037
1.0	1.0	1.0	1.0	1.0	1.0	B 038
1.0	1.0	1.0	1.0	0.0	0.0	B 039
0.0	0.0	0.0	0.0	0.0	0.0	B 040
0.0	0.0	0.0	0.0	0.0	0.0	B 041
0.0	0.0	0.0	0.0	0.0	0.0	B 042
0.0	0.0	0.0	0.0			B 043
0.0308	0.0284	0.0259	0.0236	0.0223		B 044
0.0	0.0	0.0	0.0	0.0		B 045
0.0	0.0245	0.0072	0.0	0.0		B 046
0.0	0.0288	0.0260	0.0232	0.0208		B 047
0.01940	0.0	0.0	0.0	0.0		B 048
0.0	0.0	0.0384	0.0	0.0	0.0	B 049
0.0324	0.0301	0.0277	0.0259	0.0248		B 050
0.0	0.0	0.0	0.0	0.0		B 051
0.0	0.0	0.0207	0.0	0.0		B 052
0.0	0.0	0.0257	0.0228	0.0201		B 053
0.01780	0.01622	0.0	0.0	0.0		B 054
0.0	0.0	0.0321	0.0176	0.0	0.0	B 055
0.0330	0.0312	0.0290	0.0274	0.0267		B 056
0.00112	0.00106	0.00081	0.00064	0.0		B 057
0.0	0.0	0.0187	0.0	0.0		B 058
0.0	0.0	0.0	0.0226	0.01968		B 059
0.01683	0.01450	0.01357	0.0	0.0		B 060
0.0	0.0	0.0	0.0637	0.0	0.0	B 061
0.0328	0.0312	0.0297	0.0282	0.0279		B 062
0.00856	0.00814	0.00621	0.00492	0.0		B 063
0.0	0.0	0.0016	0.0118	0.0		B 064
0.0	0.0	0.0	0.0	0.01869		B 065
0.01587	0.01290	0.01139	0.00991	0.0		B 066
0.0	0.0	0.0	0.0	0.0229	0.0	B 067
0.0322	0.0311	0.0297	0.0286	0.0286		B 068
0.0238	0.0226	0.01728	0.01369	0.0		B 069
0.0	0.0	0.0	0.0115	0.0		B 070
0.0	0.0	0.0	0.0	0.0		B 071
0.01507	0.01246	0.01024	0.00844	0.00716		B 072
0.0	0.0	0.0	0.0	0.0	0.0	B 073

0.0309	0.0300	0.0290	0.0282	0.0284		B 074
0.0449	0.0426	0.0326	0.0258	0.0		B 075
0.0	0.0	0.0	0.0098	0.00056		B 076
0.0	0.0	0.0	0.0	0.0		B 077
0.0	0.01142	0.00926	0.00747	0.00593		B 078
0.00486	0.0	0.0	0.0	0.0	0.0	B 079
0.0291	0.0285	0.0278	0.0273	0.0278		B 080
0.0603	0.0572	0.0437	0.0346	0.0		B 081
0.0	0.0	0.0	0.0	0.00759		B 082
0.0	0.0	0.0	0.0	0.0		B 083
0.0	0.0	0.00797	0.00646	0.00505		B 084
0.00388	0.00307	0.0	0.0	0.0	0.0	B 085
0.0269	0.0266	0.0257	0.0258	0.0266		B 086
0.0648	0.0616	0.0470	0.0372	0.0222		B 087
0.0	0.0	0.0	0.0	0.00680		B 088
0.0	0.0	0.0	0.0	0.0		B 089
0.0	0.0	0.0	0.00565	0.00428		B 090
0.00325	0.00242	0.001867	0.0	0.0	0.0	B 091
0.0242	0.0240	0.0230	0.0238	0.0246		B 092
0.0579	0.0550	0.0420	0.0332	0.0310		B 093
0.0	0.0	0.0	0.0	0.00600		B 094
0.0	0.0	0.0	0.0	0.0		B 095
0.0	0.0	0.0	0.0	0.00359		B 096
0.00261	0.001950	0.001390	0.001000	0.0	0.0	B 097
0.0218	0.0219	0.02107	0.0219	0.0228		B 098
0.0450	0.0427	0.0326	0.0258	0.0279		B 099
0.0	0.0	0.0	0.0	0.00302		B 100
0.00204	0.0	0.0	0.0	0.0		B 101
0.0	0.0	0.0	0.0	0.0		B 102
0.002145	0.001479	0.001046	0.000715	0.000503	0.0	B 103
0.01968	0.01969	0.019160	0.02000	0.0210		B 104
0.0325	0.0308	0.0236	0.01870	0.0252		B 105
0.0	0.0	0.0	0.0	0.0		B 106
0.00474	0.0	0.0	0.0	0.0		B 107
0.0	0.0	0.0	0.0	0.0		B 108
0.0	0.000926	0.000785	0.000530	0.000342	0.000222	B 109
0.01752	0.01770	0.01771	0.01810	0.01909		B 110

0.0223	0.0212	0.01618	0.01281	0.0228		B 111
0.0	0.0	0.0	0.0	0.0		B 112
0.00430	0.0	0.0	0.0	0.0		B 113
0.0	0.0	0.0	0.0	0.0		B 114
0.0	0.0	0.000591	0.000379	0.000234	0.000145	B 115
0.01543	0.01572	0.01584	0.01568	0.01721		B 116
0.0143	0.0136	0.01039	0.00824	0.0206		B 117
0.0	0.0	0.0	0.0	0.0		B 118
0.00388	0.0	0.0	0.0	0.0		B 119
0.0	0.0	0.0	0.0	0.0		B 120
0.0	0.0	0.0	0.000269	0.000160	0.000090	B 121
0.01340	0.01368	0.01378	0.01418	0.01509		B 122
0.00904	0.00859	0.00656	0.00520	0.0185		B 123
0.0	0.0	0.0	0.0	0.0		B 124
0.00348	0.0	0.0	0.0	0.0		B 125
0.0	0.0	0.0	0.0	0.0		B 126
0.0	0.0	0.0	0.0	0.000122	0.000108	B 127
0.01155	0.01182	0.01213	0.01215	0.01327		B 128
0.00525	0.00498	0.00380	0.00302	0.0166		B 129
0.0	0.0	0.0	0.0	0.0		B 130
0.00245	0.0	0.0	0.0	0.0		B 131
0.0	0.0	0.0	0.0	0.0		B 132
0.0	0.0	0.0	0.0	0.0	0.000052	B 133
0.0240	0.0240	0.0244	0.0254	0.0274	0.0	B 134
0.0	0.0	0.0	0.0218	0.0	0.0	B 135
0.0	0.0	0.0	0.0	0.00647	0.0	B 136
0.0	0.0	0.0	0.0	0.0	0.0	B 137
0.0	0.0	0.0	0.0	0.0	0.0	B 138
0.0	0.0	0.0	0.0			B 139
0.01938	0.0202	0.02065	0.0216	0.0235	0.0	B 140
0.0	0.0	0.0	0.0	0.0	0.0	B 141
0.0	0.0	0.0	0.0	0.00647	0.0	B 142
0.0	0.0	0.0	0.0	0.0	0.0	B 143
0.0	0.0	0.0	0.0	0.0	0.0	B 144
0.0	0.0	0.0	0.0			B 145
0.01392	0.0147	0.01512	0.0159	0.0175	0.00572	B 146
0.00544	0.00415	0.00329	0.0	0.0	0.0	B 147

0.0	0.0	0.0	0.0	0.00446	0.0	B 148
0.0	0.0	0.0	0.0	0.0	0.0	B 149
0.0	0.0	0.0	0.0	0.0	0.0	B 150
0.0	0.0	0.0	0.0			B 151
0.00685	0.0073	0.00750	0.0080	0.0082	0.00256	B 152
0.00243	0.00186	0.00147	0.0	0.0	0.0	B 153
0.0	0.0	0.0	0.0	0.0	0.016	B 154
0.0	0.0	0.0	0.0	0.0	0.0	B 155
0.0	0.0	0.0	0.0	0.0	0.0	B 156
0.0	0.0	0.0	0.0			B 157
1.3510	1.3880	1.4000	1.4150	1.4250	1.4300	B 158
1.58	1.52	1.62	1.53	1.56	1.53	B 159
1.41	1.55	1.53	1.70	1.92	1.95	B 160
1.71	1.84	2.20	2.10	2.25	2.90	B 161
2.25	1.77	1.75	1.95	2.20	2.40	B 162
2.70	3.05	3.40	4.80			B 163

```
BORON                                                                   B 164
 1.740      2.230      0.0        0.0        0.06162      4.100        B 165
 1.958      1.492      0.0        0.0        0.06162      3.600        B 166
 2.718      0.842      0.0        0.0        0.06162      3.800        B 167
 2.638      1.012      0.0        0.0        0.06162      4.200        B 168
 3.190      0.560      0.0        0.0        0.06162      4.600        B 169
 3.423      0.377      0.0        0.0        0.06162      5.100        B 170
 3.330      0.670      0.0        0.0        0.06162      5.700        B 171
 3.330      0.670      0.0        0.0        0.06162      6.000        B 172
 3.330      0.670      0.0        0.0        0.06162      6.300        B 173
 3.330      0.670      0.0        0.0        0.06162      6.840        B 174
 3.330      0.670      0.0        0.0        0.06162      8.180        B 175
 3.330      0.670      0.0        0.0        0.06162     10.540        B 176
 3.330      0.670      0.0        0.0        0.06162     13.610        B 177
 3.330      0.670      0.0        0.0        0.06162     19.610        B 178
 3.330      0.670      0.0        0.0        0.06162     30.600        B 179
 4.000      0.0        0.0        0.171      0.06162    759.00         B 180
```

D. 7 CARBON

a. High-Energy Cross Sections

Total Cross Section: The total cross section over the entire energy range of interest is plotted by Hughes and Schwartz[52] and by Fosson et al.[94] The agreement is good. The Hughes and Schwartz values are used.

Nonelastic Cross Section: Values for the nonelastic cross section in carbon over the energy range of interest are given by Ball et al.,[102] MacGregor et al.,[103] and MacGregor and Booth,[104] and Hughes and Schwartz.[52] The agreement is reasonable. Below 6 Mev the nonelastic cross section is identically the inelastic cross section plotted by Hughes and Schwartz[52] in the region from threshold to 9.2 Mev.

Elastic Cross Section: At all energies the elastic cross section is taken to be the difference between the total and the nonelastic cross section. Below ~4.8 Mev no nonelastic processes are significant, and the elastic cross section is identical to the total cross section.

Radiative Capture Cross Section: The (n, γ) cross section at 0.025 ev given by Hughes and Schwartz[52] is 3.4 mb. The reaction is ignored at all energies.

Proton, Deuteron and Triton Emission Cross Sections: The thresholds for the (n, p), (n, d) and (n, t) reactions are high. The (n, p) cross section has a value[105] of ~2 mb at 14 Mev, and is neglected at all energies. The (n,d) and (n,t) thresholds are above 14 Mev.

Alpha Emission Cross Section: The (n, α) cross section at 14 Mev was estimated from data given by Graves and Davis.[106] The values of the cross section in the range from threshold (~8 Mev) to 14 Mev are estimated on the basis of systematics. The cross sections thus obtained are approximately an order of magnitude higher than those estimated by Buckingham, Parker and Pendlebury.[18]

(n, 2n) Cross Section: The (n, 2n) reaction in carbon of energies below 14 Mev is energetically impossible.

Inelastic Cross Section: There appears to be some uncertainty in the values to be assigned to the (n, n') reaction above ~9 Mev. If one concedes (a) that the (n, n') reactions that excite levels in carbon at 9.61 Mev and above lead to breakup of C^{12*} into three He^4 particles via the Be^8 ground state, (b) that the 7.65-Mev level in C^{12*} is negligible, and (c) that the 4.43-Mev level decays only by gamma-ray emission the Graves and Rosen[26] spectrum for 14-Mev neutrons indicates that the ratio $\sigma_{n,n'3\alpha}/\sigma_{n,n'\gamma}$ has a value of approximately 4. The ratio of the measured values of $\sigma_{n,n'3\alpha}$ and $4\pi\sigma_{n,n'\alpha}(90°)$, however, is approximately 1. Anderson et al.[92] show that the (n, n' + 4.43 Mev γ) reaction at 14 Mev is predominantly forward so that $\sigma_{n,n'+4.43\gamma} \gg 4\pi\sigma_{n,n'+4.43\gamma}(90°)$ which is in complete disagreement with the MacGregor et al.[104, 105] total cross sections.

Estimated values based on systematics were used for $\sigma_{n,n'+4.43\gamma}$ between 10 Mev and 14 Mev, and for $\sigma_{n,n'3\alpha}$ below 13 Mev.

b. Low-Energy Cross Sections

Total Cross Section: Taken from Hughes and Schwartz.[52]

Nonelastic Cross Section: No nonelastic reactions are significant in the lower energy region except at thermal energies where the (n, γ) cross section of Hughes and Schwartz[52] is used.

Elastic Cross Section: Identical to the total cross section except at thermal energy where a small correction for the (n, γ) reaction is made.

Radiative Capture Cross Section: Radiative capture is ignored at all energies except thermal where the Hughes and Schwartz[52] value is used.

c. Neutron Nonelastic Spectra

Neutron scattering from the 4.43-Mev and 9.61-Mev levels in carbon is treated by the isolated-level method. The neutron spectra arising from (n, n'3α) reactions is treated by the statistical model.

	σ_{nT}	$\sigma_{n,n}$	$\sigma_{n,x}$	$\sigma_{n,\gamma}$	$\sigma_{n,\alpha}$
01	1.3100	0.7500	0.5600	0.0000	0.0800
02	1.4000	0.8520	0.5480	0.0000	0.1080
03	1.4500	0.9240	0.5260	0.0000	0.1300
04	1.2800	0.7870	0.4930	0.0000	0.1400
05	1.3100	0.8200	0.4900	0.0000	0.1250
06	1.4200	1.0000	0.4200	0.0000	0.0680
07	1.6800	1.3500	0.3300	0.0000	0.0000
08	0.7700	0.5000	0.2700	0.0000	0.0000
09	1.3000	1.0000	0.3000	0.0000	0.0000
10	1.1000	1.0000	0.1000	0.0000	0.0000
11	1.2800	1.2500	0.0300	0.0000	0.0000
12	1.6500	1.6500	0.0000	0.0000	0.0000
13	1.9500	1.9500	0.0000	0.0000	0.0000
14	2.4000	2.4000	0.0000	0.0000	0.0000
15	1.8000	1.8000	0.0000	0.0000	0.0000
16	2.0000	2.0000	0.0000	0.0000	0.0000
17	1.6000	1.6000	0.0000	0.0000	0.0000
18	1.5500	1.5500	0.0000	0.0000	0.0000
19	1.6500	1.6500	0.0000	0.0000	0.0000
20	1.7700	1.7700	0.0000	0.0000	0.0000
21	1.9000	1.9000	0.0000	0.0000	0.0000
22	2.0600	2.0600	0.0000	0.0000	0.0000
23	2.1700	2.1700	0.0000	0.0000	0.0000
24	2.3000	2.3000	0.0000	0.0000	0.0000
25	2.4200	2.4200	0.0000	0.0000	0.0000
26	2.5800	2.5800	0.0000	0.0000	0.0000
27	2.7500	2.7500	0.0000	0.0000	0.0000
28	2.8200	2.8200	0.0000	0.0000	0.0000
29	2.9500	2.9500	0.0000	0.0000	0.0000
30	3.0700	3.0700	0.0000	0.0000	0.0000
31	3.1900	3.1900	0.0000	0.0000	0.0000
32	3.3100	3.3100	0.0000	0.0000	0.0000
33	3.4200	3.4200	0.0000	0.0000	0.0000
34	3.5500	3.5500	0.0000	0.0000	0.0000
35	3.7000	3.7000	0.0000	0.0000	0.0000
36	4.0500	4.0500	0.0000	0.0000	0.0000
37	4.3500	4.3500	0.0000	0.0000	0.0000
38	4.5000	4.5000	0.0000	0.0000	0.0000
39	4.6000	4.6000	0.0000	0.0000	0.0000
40	4.7000	4.7000	0.0000	0.0000	0.0000
41	4.7000	4.7000	0.0000	0.0000	0.0000
42	4.7000	4.7000	0.0000	0.0000	0.0000
43	4.7000	4.7000	0.0000	0.0000	0.0000
44	4.7000	4.7000	0.0000	0.0000	0.0000
45	4.7000	4.7000	0.0000	0.0000	0.0000
46	4.7000	4.7000	0.0000	0.0000	0.0000
47	4.7000	4.7000	0.0000	0.0000	0.0000
48	4.7000	4.7000	0.0000	0.0000	0.0000
49	4.7000	4.7000	0.0000	0.0000	0.0000
50	4.7000	4.6970	0.0030	0.0030	0.0000

TABLE D.11 FIFTY GROUP NEUTRON CROSS SECTIONS FOR CARBON

	$\sigma_{n,n'}$ (1.43)	$\sigma_{n,n'}$ (9.61)	$\sigma_{n,n'3\alpha}$
01	0.2450	0.0630	0.1720
02	0.2450	0.0450	0.1500
03	0.2450	0.0230	0.1280
04	0.2450	0.0000	0.1080
05	0.3050	0.0000	0.0600
06	0.3520	0.0000	0.0000
07	0.3300	0.0000	0.0000
08	0.2700	0.0000	0.0000
09	0.3000	0.0000	0.0000
10	0.1000	0.0000	0.0000
11	0.0300	0.0000	0.0000
12	0.0000	0.0000	0.0000
13	0.0000	0.0000	0.0000
14	0.0000	0.0000	0.0000
15	0.0000	0.0000	0.0000
16	0.0000	0.0000	0.0000
17	0.0000	0.0000	0.0000
18	0.0000	0.0000	0.0000
19	0.0000	0.0000	0.0000
20	0.0000	0.0000	0.0000
21	0.0000	0.0000	0.0000
22	0.0000	0.0000	0.0000
23	0.0000	0.0000	0.0000
24	0.0000	0.0000	0.0000
25	0.0000	0.0000	0.0000
26	0.0000	0.0000	0.0000
27	0.0000	0.0000	0.0000
28	0.0000	0.0000	0.0000
29	0.0000	0.0000	0.0000
30	0.0000	0.0000	0.0000
31	0.0000	0.0000	0.0000
32	0.0000	0.0000	0.0000
33	0.0000	0.0000	0.0000
34	0.0000	0.0000	0.0000
35	0.0000	0.0000	0.0000
36	0.0000	0.0000	0.0000
37	0.0000	0.0000	0.0000
38	0.0000	0.0000	0.0000
39	0.0000	0.0000	0.0000
40	0.0000	0.0000	0.0000
41	0.0000	0.0000	0.0000
42	0.0000	0.0000	0.0000
43	0.0000	0.0000	0.0000
44	0.0000	0.0000	0.0000
45	0.0000	0.0000	0.0000
46	0.0000	0.0000	0.0000
47	0.0000	0.0000	0.0000
48	0.0000	0.0000	0.0000
49	0.0000	0.0000	0.0000
50	0.0000	0.0000	0.0000

TABLE D.11 (CONT.) FIFTY GROUP CROSS SECTIONS FOR CARBON

CARBON		JUNE 21,1962				C 001
0.3098	0.3520	0.3817	0.3251	0.2289	0.2791	C 002
0.3768	0.1396	0.2791	0.2791	0.2591	0.3420	C 003
0.4042	0.4975	0.3510	0.3900	0.3120	0.3934	C 004
0.4188	0.4492	0.4822	0.5228	0.3823	0.4053	C 005
0.4264	0.4546	0.4846	0.4969	0.5198	0.5409	C 006
0.5621	0.5832	0.6026	0.6255			C 007
0.3461	0.3931	0.4263	0.3631	0.3389	0.4133	C 008
0.5580	0.2066	0.4133	0.4133	0.3441	0.4542	C 009
0.5368	0.6607	0.4982	0.5536	0.4429	0.5451	C 010
0.5803	0.6225	0.6682	0.7245	0.7265	0.7700	C 011
0.8102	0.8638	0.9207	0.9441	0.9877	1.0278	C 012
1.0681	1.1082	1.1450	0.			C 013
0.0610	0.0693	0.0751	0.0640	0.1753	0.2138	C 014
0.2886	0.1069	0.2138	0.2138	0.2984	0.3939	C 015
0.4655	0.5729	0.4637	0.5152	0.4122	0.3390	C 016
0.3609	0.3871	0.4155	0.4505	0.6538	0.6930	C 017
0.7291	0.7774	0.8286	0.8497	0.8888	0.9250	C 018
0.9611	0.9973	0.	0.			C 019
0.1431	0.0674	0.0357	0.0304	0.0711	0.0867	C 020
0.1170	0.0434	0.0867	0.0867	0.2809	0.3707	C 021
0.4382	0.5393	0.4018	0.4464	0.3571	0.2299	C 022
0.2447	0.2625	0.2818	0.3055	0.3585	0.3800	C 023
0.3998	0.4262	0.4543	0.4659	0.4873	0.5072	C 024
0.5270	0.	0.	0.			C 025
0.1355	0.1695	0.1092	0.0111	0.0058	0.0071	C 026
0.0096	0.0035	0.0071	0.0071	0.0675	0.0892	C 027
0.1053	0.1296	0.0853	0.0948	0.0758	0.0426	C 028
0.0453	0.0487	0.0523	0.0567	0.0489	0.0517	C 029
0.0545	0.0580	0.0618	0.0634	0.0664	0.0691	C 030
0.	0.	0.	0.			C 031
0.	0.0490	0.1413	0.1913	0.0488	0.	C 032
0.	0.	0.	0.	0.	0.	C 033
0.	0.	0.	0.	0.	0.	C 034
0.	0.	0.	0.	0.	0.	C 035
0.	0.	0.	0.	0.	0.	C 036

TABLE D.12 Carbon Nuclide Decks

0.0717	0.6213	1.6724	2.9245			C 037
1.0	1.0	1.0	1.0	1.0	1.0	C 038
1.0	1.0	1.0	1.0	0.0	0.0	C 039
0.0	0.0	0.0	0.0	0.0	0.0	C 040
0.0	0.0	0.0	0.0	0.0	0.0	C 041
0.0	0.0	0.0	0.0	0.0	0.0	C 042
0.0	0.0	0.0	0.0			C 043
0.00978	0.00848	0.01095	0.00590	0.00322		C 044
0.	0.	0.0076	0.0856	0.		C 045
0.0	0.0	0.0	0.0	0.0		C 046
0.0	0.00957	0.00818	0.01104	0.00555		C 047
0.00298	0.0	0.0	0.0845	0.0		C 048
0.0	0.0	0.0	0.0	0.0	0.0	C 049
0.00965	0.00844	0.01051	0.00600	0.00330		C 050
0.	0.	0.	0.0855	0.		C 051
0.0	0.0	0.0	0.0	0.0		C 052
0.0	0.0	0.00911	0.00769	0.01103		C 053
0.00505	0.00267	0.	0.	0.0929		C 054
0.0	0.0	0.0	0.0	0.0	0.0	C 055
0.00957	0.00846	0.01040	0.00617	0.00346		C 056
0.0	0.0	0.0	0.0763	0.0		C 057
0.0	0.0	0.0	0.0	0.0		C 058
0.0	0.0	0.0	0.00850	0.01442		C 059
0.00570	0.00450	0.002332	0.0	0.0249		C 060
0.0850	0.	0.	0.	0.	0.	C 061
0.00915	0.00816	0.00988	0.00608	0.00343		C 062
0.0	0.0	0.0	0.0526	0.00606		C 063
0.0	0.0	0.0	0.0	0.0		C 064
0.0	0.0	0.0	0.0	0.00765		C 065
0.0165	0.00494	0.00382	0.00194	0.0		C 066
0.1270	0.0	0.0	0.0	0.0	0.0	C 067
0.00865	0.00780	0.00769	0.00590	0.00337		C 068
0.0	0.0	0.0	0.0	0.02300		C 069
0.0	0.0	0.0	0.0	0.0		C 070
0.0	0.0	0.0	0.0	0.0		C 071
0.00660	0.0167	0.00410	0.003105	0.001541		C 072
0.	0.1407	0.	0.	0.	0.	C 073

0.00805	0.00732	0.00645	0.00563	0.00324		C 074
0.0	0.0	0.0	0.0	0.02075		C 075
0.0	0.0	0.0	0.0	0.0		C 076
0.0	0.0	0.0	0.0	0.0		C 077
0.0	0.00551	0.0171	0.00328	0.002422		C 078
0.001177	0.1152	0.0374	0.0	0.0	0.0	C 079
0.00739	0.00674	0.00600	0.00526	0.00306		C 080
0.0	0.0	0.0	0.0	0.01868		C 081
0.0	0.0	0.0	0.0	0.0		C 082
0.0	0.0	0.0	0.0	0.0		C 083
0.0	0.0	0.0200	0.003362	0.002482		C 084
0.001793	0.000846	0.1696	0.	0.	0.	C 085
0.00666	0.00612	0.00547	0.00484	0.00282		C 086
0.0	0.0	0.0	0.0	0.01672		C 087
0.0	0.0	0.0	0.0	0.0		C 088
0.0	0.0	0.0	0.0	0.0		C 089
0.0	0.0	0.0	0.0235	0.002495		C 090
0.001795	0.001258	0.0937	0.0672	0.0	0.0	C 091
0.00585	0.00540	0.00486	0.00433	0.00254		C 092
0.0	0.0	0.0	0.0	0.01479		C 093
0.0	0.0	0.0	0.0	0.0		C 094
0.0	0.0	0.0	0.0	0.0		C 095
0.0	0.0	0.0	0.0	0.0250		C 096
0.001759	0.001223	0.0480	0.1631	0.0	0.0	C 097
0.00518	0.00480	0.00435	0.00389	0.00230		C 098
0.0	0.0	0.0	0.0	0.0		C 099
0.00441	0.0	0.0	0.0	0.0		C 100
0.0	0.0	0.0	0.0	0.0		C 101
0.0	0.0	0.0	0.0	0.0		C 102
0.00596	0.001148	0.000772	0.0005055	0.0002155	0.0	C 103
0.00457	0.00425	0.00386	0.00347	0.002067		C 104
0.0	0.0	0.0	0.0	0.0		C 105
0.00398	0.0	0.0	0.0	0.0		C 106
0.0	0.0	0.0	0.0	0.0		C 107
0.0	0.0	0.0	0.0	0.0		C 108
0.0	0.001042	0.000705	0.000458	0.000288	0.0001174	C 109
0.00401	0.00374	0.00342	0.00308	0.001841		C 110

0.0	0.0	0.0	0.0	0.0		C 111
0.00363	0.	0.	0.	0.		C 112
0.0	0.0	0.0	0.0	0.0		C 113
0.0	0.0	0.0	0.0	0.0		C 114
0.0	0.0	0.0006150	0.000399	0.0002482	0.0001492	C 115
0.00348	0.00327	0.002998	0.00271	0.001626		C 116
0.0	0.0	0.0	0.0	0.0		C 117
0.00327	0.0	0.0	0.0	0.0		C 118
0.0	0.0	0.0	0.0	0.0		C 119
0.0	0.0	0.0	0.0	0.0		C 120
0.0	0.0	0.0	0.0003355	0.000208	0.0001239	C 121
0.002978	0.00280	0.002578	0.00234	0.001409		C 122
0.0	0.0	0.0	0.0	0.0		C 123
0.00292	0.0	0.0	0.0	0.0		C 124
0.0	0.0	0.0	0.0	0.0		C 125
0.0	0.0	0.0	0.0	0.0		C 126
0.0	0.0	0.0	0.0	0.0001660	0.0000985	C 127
0.002533	0.002393	0.002210	0.002015	0.001212		C 128
0.0	0.0	0.0	0.0	0.0		C 129
0.00262	0.0	0.0	0.0	0.0		C 130
0.0	0.0	0.0	0.0	0.0		C 131
0.0	0.0	0.0	0.0	0.0		C 132
0.0	0.0	0.0	0.0	0.0	0.0000746	C 133
0.00503	0.00477	0.00442	0.00405	0.00246	0.0	C 134
0.0	0.0	0.0	0.0	0.00573	0.0	C 135
0.0	0.0	0.0	0.0	0.0	0.0	C 136
0.0	0.0	0.0	0.0	0.0	0.0	C 137
0.0	0.0	0.0	0.0	0.0	0.0	C 138
0.0	0.0	0.0	0.0			C 139
0.00410	0.00391	0.00364	0.00335	0.00205	0.0	C 140
0.0	0.0	0.0	0.0	0.00344	0.0	C 141
0.0	0.0	0.0	0.0	0.0	0.0	C 142
0.0	0.0	0.0	0.0	0.0	0.0	C 143
0.0	0.0	0.0	0.0	0.0	0.0	C 144
0.0	0.0	0.0	0.0			C 145
0.00287	0.00276	0.002585	0.00240	0.001475	0.0	C 146
0.0	0.0	0.0	0.0	0.0	0.0	C 147

0.0	0.0	0.0	0.0	0.0	0.0	C 148
0.0	0.0	0.0	0.0	0.0	0.0	C 149
0.0	0.0	0.0	0.0	0.0	0.0	C 150
0.0	0.0	0.0	0.0			C 151
0.001371	0.001325	0.001251	0.001169	0.000725	0.0	C 152
0.0	0.0	0.0	0.0	0.0	0.0	C 153
0.0	0.0	0.0	0.0	0.0	0.0	C 154
0.0	0.0	0.0	0.0	0.0	0.0	C 155
0.0	0.0	0.0	0.0	0.0	0.0	C 156
0.0	0.0	0.0	0.0			C 157
1.31	1.40	1.45	1.28	1.31	1.42	C 158
1.68	0.77	1.30	1.10	1.28	1.65	C 159
1.95	2.40	1.80	2.00	1.60	1.55	C 160
1.65	1.77	1.90	2.06	2.17	2.30	C 161
2.42	2.58	2.75	2.82	2.95	3.07	C 162
3.19	3.31	3.42	3.55			C 163

CARBON						C 164
1.770	1.930	0.0	0.0	0.05551	3.700	C 165
2.510	1.540	0.0	0.0	0.05551	4.050	C 166
3.440	0.910	0.0	0.0	0.05551	4.350	C 167
3.415	1.085	0.0	0.0	0.05551	4.500	C 168
4.000	0.600	0.0	0.0	0.05551	4.600	C 169
4.300	0.400	0.0	0.0	0.05551	4.700	C 170
4.000	0.700	0.0	0.0	0.05551	4.700	C 171
4.000	0.700	0.0	0.0	0.05551	4.700	C 172
4.000	0.700	0.0	0.0	0.05551	4.700	C 173
4.000	0.700	0.0	0.0	0.05551	4.700	C 174
4.000	0.700	0.0	0.0	0.05551	4.700	C 175
4.000	0.700	0.0	0.0	0.05551	4.700	C 176
4.000	0.700	0.0	0.0	0.05551	4.700	C 177
4.000	0.700	0.0	0.0	0.05551	4.700	C 178
4.000	0.700	0.0	0.0	0.05551	4.700	C 179
4.697	0.0	0.0	0.158	0.05551	4.700	C 180

D. 8 NITROGEN

a. High-Energy Cross Sections

Total Cross Section: The total cross section for nitrogen is plotted by Buckingham, Parker, and Pendlebury,[18] and by Hughes and Schwartz[52] over the entire energy range of interest with good agreement. For consistency, the Buckingham et al. curve is used.

Nonelastic Cross Section: The $\sigma_{n,x}$ curve of Buckingham, Parker, and Pendlebury[18] is equal to the sum of the several individual nonelastic cross sections given in the same reference and is used for consistency.

Elastic Cross Section: The elastic cross section is taken to be the difference between the total and the nonelastic cross sections at all energies.

Radiative Capture Cross Section: The radiative capture cross section is sufficiently small (0. 082 b at 0. 025 ev) that its contribution in the higher energy region may be neglected.

Proton Emission Cross Section: The (n, p) cross section is plotted over the energy range of interest by Buckingham et al.,[18] and by Hughes and Schwartz[52] with good agreement. The Buckingham et al. curve is used for consistency.

Deuteron and Triton Emission Cross Sections: The (n, d) and (n, t) cross sections plotted by Buckingham et al.[18] are used.

Alpha Emission Cross Section: The (n, α) cross section is plotted over the energy range of interest by Buckingham et al.,[18] and by Hughes and Schwartz[52] with good agreement. The former curve is used for consistency.

(n, 2n) and (n, 2α) Cross Sections: The (n, 2n) and (n, 2α) cross sections of Buckingham et al.[18] are used.

Inelastic Cross Section: The (n, n') cross section plotted by Buckingham et al.[18] is used.

b. Low-Energy Cross Sections

Total Cross Section: Plotted by Buckingham, Parker, and Pendlebury,[18] and by Hughes and Schwartz.[52] In the lower energy region the later curve is used.

Nonelastic Cross Section: Is the sum of the (n, p) and (n, γ) cross sections in the lower energy region.

Elastic Cross Section: The (n, n) cross section is taken to be the difference between the total and the nonelastic cross sections at all energies.

Radiative Capture Cross Section: A value of 82 mb is given by Hughes and Schwartz[52] for the (n, γ) cross section at 0. 025 ev. The cross section is assumed v^{-1} and is extrapolated to ~300 ev. Above that energy the reaction is ignored.

Proton Emission Cross Section: The (n, p) cross section is plotted by Buckingham, Parker, and Pendlebury[18] over the entire energy region. Values for the cross section at 0. 025 ev and above 200 kev are given by Hughes and Schwartz[52] in good agreement with the Buckingham et al. plot. The latter is used.

c. Neutron Nonelastic Spectra

The nonelastic scattering correlations given by Buckingham, Parker, and Pendlebury[18] are used as published.

	σ_{nT}	$\sigma_{n,n}$	$\sigma_{n,X}$	$\sigma_{n,n'}$	$\sigma_{n,2n}$
01	1.6000	0.8273	0.7727	0.5600	0.0060
02	1.4900	0.6780	0.8120	0.5900	0.0010
03	1.4000	0.5705	0.8295	0.6000	0.0000
04	1.3100	0.4745	0.8355	0.6000	0.0000
05	1.2800	0.4480	0.8320	0.5900	0.0000
06	1.3500	0.5425	0.8075	0.5600	0.0000
07	1.4000	0.6185	0.7815	0.5350	0.0000
08	1.3300	0.5785	0.7515	0.5050	0.0000
09	1.4300	0.7325	0.6975	0.4550	0.0000
10	1.6000	0.9605	0.6395	0.4000	0.0000
11	1.4500	0.8720	0.5780	0.3400	0.0000
12	1.5000	0.9860	0.5140	0.2800	0.0000
13	1.7200	1.2670	0.4530	0.2150	0.0000
14	1.7000	1.3340	0.3660	0.1350	0.0000
15	1.7000	1.4080	0.2920	0.0700	0.0000
16	1.6000	1.3810	0.2190	0.0080	0.0000
17	1.4800	1.3010	0.1790	0.0040	0.0000
18	1.5500	1.4500	0.1000	0.0000	0.0000
19	1.6000	1.5390	0.0610	0.0000	0.0000
20	1.6800	1.6170	0.0630	0.0000	0.0000
21	2.2000	2.1100	0.0900	0.0000	0.0000
22	2.5000	2.4560	0.0350	0.0000	0.0000
23	2.4000	2.2800	0.1200	0.0000	0.0000
24	2.0000	1.9510	0.0490	0.0000	0.0000
25	2.0000	1.9910	0.0090	0.0000	0.0000
26	1.7000	1.6905	0.0095	0.0000	0.0000
27	1.2000	1.1910	0.0090	0.0000	0.0000
28	1.7000	1.6890	0.0110	0.0000	0.0000
29	2.1000	1.8500	0.0250	0.0000	0.0000
30	2.3000	2.2000	0.1000	0.0000	0.0000
31	1.7000	1.6300	0.0700	0.0000	0.0000
32	2.2000	2.1500	0.0500	0.0000	0.0000
33	2.4000	2.3400	0.0600	0.0000	0.0000
34	4.0000	3.9800	0.0200	0.0000	0.0000
35	3.1000	3.0800	0.0200	0.0000	0.0000
36	3.4000	3.3985	0.0015	0.0000	0.0000
37	4.0000	3.9985	0.0015	0.0000	0.0000
38	4.3700	4.3685	0.0015	0.0000	0.0000
39	4.8000	4.7983	0.0017	0.0000	0.0000
40	5.6000	5.5976	0.0024	0.0000	0.0000
41	6.1500	6.1465	0.0035	0.0000	0.0000
42	6.9000	6.8948	0.0052	0.0000	0.0000
43	7.7000	7.6924	0.0076	0.0000	0.0000
44	8.5500	8.5391	0.0109	0.0000	0.0000
45	9.1500	9.1304	0.0196	0.0000	0.0000
46	9.5000	9.4753	0.0247	0.0000	0.0000
47	9.7500	9.7138	0.0362	0.0000	0.0000
48	9.9500	9.8968	0.0532	0.0000	0.0000
49	10.0000	9.9218	0.0780	0.0000	0.0000
50	12.7000	10.8680	1.8320	0.0000	0.0000

TABLE D.13 FIFTY GROUP NEUTRON CROSS SECTIONS FOR NITROGEN

	$\sigma_{n,p}$	$\sigma_{n,d}$	$\sigma_{n,t}$	$\sigma_{n,\alpha}$	$\sigma_{n,2\alpha}$
01	0.0410	0.0310	0.0277	0.0950	0.0120
02	0.0430	0.0275	0.0275	0.1130	0.0100
03	0.0460	0.0250	0.0260	0.1260	0.0065
04	0.0480	0.0225	0.0245	0.1380	0.0025
05	0.0500	0.0205	0.0235	0.1480	0.0000
06	0.0520	0.0190	0.0215	0.1550	0.0000
07	0.0520	0.0135	0.0200	0.1610	0.0000
08	0.0540	0.0100	0.0175	0.1650	0.0000
09	0.0560	0.0020	0.0145	0.1700	0.0000
10	0.0570	0.0000	0.0115	0.1710	0.0000
11	0.0570	0.0000	0.0070	0.1740	0.0000
12	0.0560	0.0000	0.0000	0.1780	0.0000
13	0.0560	0.0000	0.0000	0.1800	0.0000
14	0.0540	0.0000	0.0000	0.1770	0.0000
15	0.0500	0.0000	0.0000	0.1720	0.0000
16	0.0440	0.0000	0.0000	0.1670	0.0000
17	0.0350	0.0000	0.0000	0.1400	0.0000
18	0.0260	0.0000	0.0000	0.0740	0.0000
19	0.0160	0.0000	0.0000	0.0450	0.0000
20	0.0080	0.0000	0.0000	0.0550	0.0000
21	0.0100	0.0000	0.0000	0.0800	0.0000
22	0.0200	0.0000	0.0000	0.0150	0.0000
23	0.1000	0.0000	0.0000	0.0200	0.0000
24	0.0400	0.0000	0.0000	0.0090	0.0000
25	0.0050	0.0000	0.0000	0.0040	0.0000
26	0.0075	0.0000	0.0000	0.0020	0.0000
27	0.0080	0.0000	0.0000	0.0010	0.0000
28	0.0110	0.0000	0.0000	0.0000	0.0000
29	0.0250	0.0000	0.0000	0.0000	0.0000
30	0.1000	0.0000	0.0000	0.0000	0.0000
31	0.0700	0.0000	0.0000	0.0000	0.0000
32	0.0500	0.0000	0.0000	0.0000	0.0000
33	0.0600	0.0000	0.0000	0.0000	0.0000
34	0.0200	0.0000	0.0000	0.0000	0.0000
35	0.0200	0.0000	0.0000	0.0000	0.0000
36	0.0015	0.0000	0.0000	0.0000	0.0000
37	0.0015	0.0000	0.0000	0.0000	0.0000
38	0.0015	0.0000	0.0000	0.0000	0.0000
39	0.0017	0.0000	0.0000	0.0000	0.0000
40	0.0024	0.0000	0.0000	0.0000	0.0000
41	0.0035	0.0000	0.0000	0.0000	0.0000
42	0.0052	0.0000	0.0000	0.0000	0.0000
43	0.0076	0.0000	0.0000	0.0000	0.0000
44	0.0109	$\sigma_{n,\gamma}$	0.0000	0.0000	0.0000
45	0.0196	0.0000	0.0000	0.0000	0.0000
46	0.0237	0.0010	0.0000	0.0000	0.0000
47	0.0347	0.0015	0.0000	0.0000	0.0000
48	0.0510	0.0022	0.0000	0.0000	0.0000
49	0.0750	0.0032	0.0000	0.0000	0.0000
50	1.7500	0.0820	0.0000	0.0000	0.0000

TABLE D.13 %CONT.% FIFTY GROUP CROSS SECTIONS FOR NITROGEN

NITROGEN			SEPTEMBER 18,1962			N 001
0.7032	0.5763	0.4849	0.4033	0.3808	0.2200	N 002
0.2509	0.2346	0.2971	0.3896	0.3537	0.3999	N 003
0.5139	0.3474	0.3666	0.3596	0.3388	0.3506	N 004
0.3721	0.3910	0.5102	0.5960	0.5513	0.4718	N 005
0.4814	0.4088	0.2503	0.3550	0.3889	0.4624	N 006
0.3426	0.4519	0.4919	0.8366			N 007
0.0827	0.0678	0.0571	0.0474	0.0448	0.2608	N 008
0.2973	0.2781	0.3521	0.4617	0.4192	0.4740	N 009
0.6090	0.4986	0.5263	0.5162	0.4863	0.6225	N 010
0.6607	0.6942	0.9058	1.0582	0.9788	0.8376	N 011
0.8547	0.7257	0.4537	0.6433	0.7047	0.8380	N 012
0.6209	0.8189	0.8913	0.0000			N 013
0.0414	0.0339	0.0285	0.0238	0.0224	0.0512	N 014
0.0584	0.0546	0.0691	0.0907	0.0823	0.0931	N 015
0.1196	0.3196	0.3373	0.3309	0.3117	0.3744	N 016
0.3974	0.4175	0.5448	0.6365	0.5887	0.5037	N 017
0.5141	0.4365	0.4083	0.5790	0.6342	0.7542	N 018
0.5588	0.7370	0.0000	0.0000			N 019
0.0000	0.0000	0.0000	0.0000	0.0000	0.0105	N 020
0.0119	0.0112	0.0142	0.0185	0.0168	0.0190	N 021
0.0245	0.1684	0.1778	0.1743	0.1642	0.1025	N 022
0.1088	0.1143	0.1492	0.1743	0.1612	0.1379	N 023
0.1408	0.1195	0.0787	0.1117	0.1222	0.1454	N 024
0.1077	0.0000	0.0000	0.0000			N 025
0.0000	0.0000	0.0000	0.0000	0.0000	0.0000	N 026
0.0000	0.0000	0.0000	0.0000	0.0000	0.0000	N 027
0.0000	0.0000	0.0000	0.0000	0.0000	0.0000	N 028
0.0000	0.0000	0.0000	0.0000	0.0000	0.0000	N 029
0.0000	0.0000	0.0000	0.0000	0.0000	0.0000	N 030
0.0000	0.0000	0.0000	0.0000			N 031
0.0000	0.0000	0.0000	0.0000	0.0000	0.0000	N 032
0.0000	0.0000	0.0000	0.0000	0.0000	0.0000	N 033
0.0000	0.0000	0.0000	0.0000	0.0000	0.0000	N 034
0.0000	0.0000	0.0000	0.0000	0.0000	0.0000	N 035
0.0000	0.0000	0.0000	0.0000	0.0000	0.0000	N 036

TABLE D.14 Nitrogen Nuclide Decks

0.0000	0.1422	0.9568	3.1434			N 037
1.0000	1.0000	1.0000	1.0000	1.0000	1.0000	N 038
1.0000	1.0000	1.0000	1.0000	0.0000	0.0000	N 039
0.0000	0.0000	0.0000	0.0000	0.0000	0.0000	N 040
0.0000	0.0000	0.0000	0.0000	0.0000	0.0000	N 041
0.0000	0.0000	0.0000	0.0000	0.0000	0.0000	N 042
0.0000	0.0000	0.0000	0.0000			N 043
0.0016	0.0000	0.0000	0.0000	0.0000		N 044
0.0000	0.0000	0.0000	0.0000	0.0000		N 045
0.0000	0.0601	0.0000	0.0000	0.0000		N 046
0.0000	0.0016	0.0000	0.0000	0.0000		N 047
0.0000	0.0000	0.0000	0.0000	0.0000		N 048
0.0069	0.0113	0.0551	0.0000	0.0000	0.0000	N 049
0.0014	0.0000	0.0000	0.0000	0.0000		N 050
0.0000	0.0000	0.0000	0.0000	0.0000		N 051
0.0000	0.0248	0.0532	0.0000	0.0000		N 052
0.0000	0.0000	0.0121	0.0106	0.0067		N 053
0.0027	0.0000	0.0000	0.0000	0.0000		N 054
0.0000	0.0578	0.0802	0.0000	0.0000	0.0000	N 055
0.0014	0.0000	0.0000	0.0000	0.0000		N 056
0.0000	0.0000	0.0000	0.0000	0.0000		N 057
0.0000	0.0000	0.0835	0.0000	0.0000		N 058
0.0000	0.0000	0.0000	0.0153	0.0175		N 059
0.0198	0.0220	0.0227	0.0446	0.0384		N 060
0.0304	0.0214	0.0784	0.0785	0.0000	0.0000	N 061
0.0012	0.0002	0.0000	0.0000	0.0000		N 062
0.0244	0.0146	0.0082	0.0000	0.0000		N 063
0.0000	0.0000	0.0783	0.0000	0.0000		N 064
0.0000	0.0000	0.0000	0.0000	0.0170		N 065
0.0194	0.0220	0.0244	0.0264	0.0659		N 066
0.0698	0.0723	0.1420	0.0757	0.0000	0.0000	N 067
0.0010	0.0002	0.0000	0.0000	0.0000		N 068
0.0280	0.0297	0.0308	0.0302	0.0222		N 069
0.0000	0.0000	0.0000	0.0451	0.0000		N 070
0.0000	0.0000	0.0000	0.0000	0.0000		N 071
0.0186	0.0213	0.0241	0.0268	0.0290		N 072
0.0723	0.0698	0.0653	0.1372	0.0482	0.0000	N 073

0.0010	0.0002	0.0000	0.0000	0.0000		N 074
0.0255	0.0270	0.0280	0.0285	0.0276		N 075
0.0000	0.0000	0.0000	0.0426	0.0000		N 076
0.0000	0.0000	0.0000	0.0000	0.0000		N 077
0.0000	0.0170	0.0157	0.0131	0.0098		N 078
0.0064	0.0042	0.0000	0.0869	0.0024	0.0000	N 079
0.0008	0.0002	0.0000	0.0000	0.0000		N 080
0.0228	0.0241	0.0250	0.0255	0.0246		N 081
0.0029	0.0000	0.0000	0.0380	0.0000		N 082
0.0000	0.0000	0.0000	0.0000	0.0000		N 083
0.0000	0.0000	0.0000	0.0000	0.0000		N 084
0.0000	0.1033	0.0000	0.0182	0.0821	0.0000	N 085
0.0008	0.0002	0.0000	0.0000	0.0000		N 086
0.0206	0.0218	0.0226	0.0230	0.0222		N 087
0.0311	0.0000	0.0000	0.0093	0.0146		N 088
0.0000	0.0000	0.0000	0.0000	0.0000		N 089
0.0000	0.0000	0.0000	0.0000	0.0000		N 090
0.0000	0.0000	0.1200	0.0000	0.1164	0.0000	N 091
0.0006	0.0002	0.0000	0.0000	0.0000		N 092
0.0185	0.0196	0.0203	0.0206	0.0200		N 093
0.0279	0.0000	0.0000	0.0000	0.0179		N 094
0.0000	0.0000	0.0000	0.0000	0.0000		N 095
0.0000	0.0000	0.0000	0.0000	0.0000		N 096
0.0000	0.0000	0.0980	0.0295	0.0591	0.0544	N 097
0.0006	0.0002	0.0000	0.0000	0.0000		N 098
0.0166	0.0176	0.0182	0.0185	0.0164		N 099
0.0250	0.0000	0.0000	0.0000	0.0161		N 100
0.0000	0.0000	0.0000	0.0000	0.0000		N 101
0.0000	0.0000	0.0000	0.0000	0.0000		N 102
0.0871	0.0890	0.0860	0.2182	0.0752	0.1269	N 103
0.0000	0.0002	0.0000	0.0000	0.0000		N 104
0.0149	0.0158	0.0149	0.0057	0.0000		N 105
0.0224	0.0000	0.0000	0.0000	0.0144		N 106
0.0000	0.0000	0.0000	0.0000	0.0000		N 107
0.0000	0.0000	0.0000	0.0000	0.0000		N 108
0.0000	0.1042	0.1197	0.2519	0.1733	0.1775	N 109
0.0000	0.0002	0.0000	0.0000	0.0000		N 110

0.0136	0.0078	0.0000	0.0000	0.0000		N 111
0.0205	0.0000	0.0000	0.0000	0.0070		N 112
0.0006	0.0000	0.0000	0.0000	0.0000		N 113
0.0000	0.0000	0.0000	0.0000	0.0000		N 114
0.0000	0.0000	0.0487	0.0542	0.1764	0.0248	N 115
0.0000	0.0002	0.0000	0.0000	0.0000		N 116
0.0021	0.0000	0.0000	0.0000	0.0000		N 117
0.0183	0.0000	0.0000	0.0000	0.0000		N 118
0.0015	0.0000	0.0000	0.0000	0.0000		N 119
0.0000	0.0000	0.0000	0.0000	0.0000		N 120
0.0000	0.0000	0.0000	0.0000	0.1480	0.0000	N 121
0.0000	0.0000	0.0000	0.0000	0.0000		N 122
0.0000	0.0000	0.0000	0.0000	0.0000		N 123
0.0164	0.0000	0.0000	0.0000	0.0000		N 124
0.0013	0.0000	0.0000	0.0000	0.0000		N 125
0.0000	0.0000	0.0000	0.0000	0.0000		N 126
0.0000	0.0000	0.0000	0.0000	0.0590	0.0946	N 127
0.0000	0.0000	0.0000	0.0000	0.0000		N 128
0.0000	0.0000	0.0000	0.0000	0.0000		N 129
0.0055	0.0149	0.0000	0.0000	0.0000		N 130
0.0011	0.0000	0.0000	0.0000	0.0000		N 131
0.0000	0.0000	0.0000	0.0000	0.0000		N 132
0.0000	0.0000	0.0000	0.0000	0.0000	0.1810	N 133
0.0000	0.0000	0.0000	0.0000	0.0000	0.0000	N 134
0.0000	0.0000	0.0000	0.0000	0.0000	0.0298	N 135
0.0000	0.0000	0.0000	0.0026	0.0010	0.0000	N 136
0.0000	0.0000	0.0000	0.0000	0.0000	0.0000	N 137
0.0000	0.0000	0.0000	0.0000	0.0000	0.0000	N 138
0.0000	0.0000	0.0000	0.0000			N 139
0.0000	0.0000	0.0000	0.0000	0.0000	0.0000	N 140
0.0000	0.0000	0.0000	0.0000	0.0000	0.0298	N 141
0.0000	0.0000	0.0000	0.0009	0.0014	0.0000	N 142
0.0000	0.0000	0.0000	0.0000	0.0000	0.0000	N 143
0.0000	0.0000	0.0000	0.0000	0.0000	0.0000	N 144
0.0000	0.0000	0.0000	0.0000			N 145
0.0000	0.0000	0.0000	0.0000	0.0000	0.0000	N 146
0.0000	0.0000	0.0000	0.0000	0.0000	0.0298	N 147

0.0000	0.0000	0.0000	0.0000	0.0014	0.0000	N 148
0.0000	0.0000	0.0000	0.0000	0.0000	0.0000	N 149
0.0000	0.0000	0.0000	0.0000	0.0000	0.0000	N 150
0.0000	0.0000	0.0000	0.0000			N 151
0.0000	0.0000	0.0000	0.0000	0.0000	0.0000	N 152
0.0000	0.0000	0.0000	0.0000	0.0000	0.0357	N 153
0.0000	0.0000	0.0000	0.0000	0.0002	0.0000	N 154
0.0000	0.0000	0.0000	0.0000	0.0000	0.0000	N 155
0.0000	0.0000	0.0000	0.0000	0.0000	0.0000	N 156
0.0000	0.0000	0.0000	0.0000			N 157
1.6000	1.4900	1.4000	1.3100	1.2800	1.3500	N 158
1.4000	1.3300	1.4300	1.6000	1.4700	1.5000	N 159
1.7200	1.7000	1.7000	1.6000	1.4800	1.5500	N 160
1.6000	1.6800	2.2000	2.5000	2.4000	2.0000	N 161
2.0000	1.7000	1.2000	1.7000	2.1000	2.3000	N 162
1.7000	2.2000	2.4000	4.0000			N 163

NITROGEN SEPTEMBER 18,1962 N 164

1.6786	1.4014	0.0000	0.0000	0.0476	3.1000	N 165
2.2780	1.1205	0.0000	0.0000	0.0476	3.4000	N 166
3.2800	0.7185	0.0000	0.0000	0.0476	4.0000	N 167
3.4523	0.9162	0.0000	0.0000	0.0476	4.3700	N 168
4.2624	0.5359	0.0000	0.0000	0.0476	4.8000	N 169
5.1800	0.4176	0.0000	0.0000	0.0476	5.6000	N 170
5.3505	0.7960	0.0000	0.0000	0.0476	6.1500	N 171
6.0030	0.8918	0.0000	0.0000	0.0476	6.9000	N 172
6.6990	0.9934	0.0000	0.0000	0.0476	7.7000	N 173
7.4385	1.1006	0.0000	0.0000	0.0476	8.5500	N 174
7.9605	1.1699	0.0000	0.0000	0.0476	9.1500	N 175
8.2650	1.2103	0.0000	0.0000	0.0476	9.5000	N 176
8.4825	1.2313	0.0000	0.0000	0.0476	9.7500	N 177
8.6565	1.2403	0.0000	0.0000	0.0476	9.9500	N 178
8.7000	1.2218	0.0000	0.0000	0.0476	10.0000	N 179
10.8680	0.0000	0.0000	0.1364	0.0476	12.7000	N 180

D.9 OXYGEN

a. High-Energy Cross Sections

Total Cross Section: Plotted over the energy range of interest by Hughes and Schwartz,[52] and by Buckingham, Parker, and Pendlebury.[18] The curves are in good agreement. The latter values are used for consistency.

Nonelastic Cross Section: The $\sigma_{n,x}$ curve of Buckingham, Parker, and Pendlebury[18] is equal to the sum of the several individual nonelastic cross sections given by them and is used for consistency.

Elastic Cross Section: Taken to be the difference between the total and the nonelastic cross sections at all energies.

Radiative Capture Cross Section: Hughes and Schwartz[52] give for the (n, γ) cross section at 0.025 ev a value of less than 0.2 mb. The reaction is ignored.

Proton and Deuteron Emission Cross Sections: The cross sections for the (n, p) and (n, d) reactions are plotted by Buckingham et al.[18] Values of $\sigma_{n,p}$ are also given by Hughes and Schwartz[52] at energies above ~12 Mev in agreement with the Buckingham et al. curve. The Buckingham et al. plots are used.

Triton Emission and (n, 2n) Cross Sections: No values are given by either Buckingham, Parker, and Pendlebury[18] or Hughes and Schwartz[52] for the (n, t) and (n, 2n) cross section. The thresholds are high and the reactions are ignored.

Alpha Emission Cross Section: Plotted over the energy range of interest by Buckingham, Parker, and Pendlebury,[18] and in the range from threshold to ~5.2 Mev by Hughes and Schwartz.[52] In the energy range common to both curves, the agreement is good. The Buckingham et al. plot is used.

Inelastic Cross Section: The (n, n') cross section is plotted by Buckingham, Parker, and Pendlebury[18] and is used as published.

b. Low-Energy Cross Sections

Total Cross Section: Plotted in the low-energy region by Hughes and Schwartz,[52] and by Buckingham, Parker, and Pendlebury[18] with good agreement. The Hughes and Schwartz curve is used.

Nonelastic Cross Section: There are no nonelastic reactions of any significance in the lower energy region.

Elastic Cross Section: The elastic cross section is identical to the total cross section in the lower energy region.

c. Neutron Nonelastic Spectra

The nonelastic neutron emergent energy distributions given by Buckingham, Parker, and Pendlebury[18] are used as published.

	$\sigma_{n,T}$	$\sigma_{n,n}$	$\sigma_{n,X}$	$\sigma_{n,n'}$	$\sigma_{n,p}$
01	1.5900	0.7010	0.8890	0.4700	0.0820
02	1.5200	0.5590	0.9610	0.5800	0.0720
03	1.4200	0.4650	0.9550	0.6500	0.0180
04	1.2800	0.4300	0.8500	0.5900	0.0000
05	1.1500	0.4500	0.7000	0.4600	0.0000
06	1.2500	0.7300	0.5200	0.3000	0.0000
07	1.4500	1.1280	0.3220	0.1200	0.0000
08	1.4500	1.1950	0.2550	0.0700	0.0000
09	1.3500	1.2100	0.1400	0.0000	0.0000
10	1.3000	1.1950	0.1050	0.0000	0.0000
11	1.3000	1.2000	0.1000	0.0000	0.0000
12	1.7000	1.6500	0.0500	0.0000	0.0000
13	2.1000	2.0500	0.0500	0.0000	0.0000
14	3.3000	3.2950	0.0050	0.0000	0.0000
15	2.8000	2.8000	0.0000	0.0000	0.0000
16	1.2200	1.2200	0.0000	0.0000	0.0000
17	1.2200	1.2200	0.0000	0.0000	0.0000
18	0.8000	0.8000	0.0000	0.0000	0.0000
19	1.3000	1.3000	0.0000	0.0000	0.0000
20	2.2000	2.2000	0.0000	0.0000	0.0000
21	1.9000	1.9000	0.0000	0.0000	0.0000
22	2.1000	2.1000	0.0000	0.0000	0.0000
23	2.5000	2.5000	0.0000	0.0000	0.0000
24	4.0000	4.0000	0.0000	0.0000	0.0000
25	4.5000	4.5000	0.0000	0.0000	0.0000
26	6.0000	6.0000	0.0000	0.0000	0.0000
27	5.0000	5.0000	0.0000	0.0000	0.0000
28	3.1000	3.1000	0.0000	0.0000	0.0000
29	2.9500	2.9500	0.0000	0.0000	0.0000
30	2.9000	2.9000	0.0000	0.0000	0.0000
31	3.2000	3.2000	0.0000	0.0000	0.0000
32	3.7000	3.7000	0.0000	0.0000	0.0000
33	5.8000	5.8000	0.0000	0.0000	0.0000
34	11.5000	11.5000	0.0000	0.0000	0.0000
35	11.5000	11.5000	0.0000	0.0000	0.0000
36	3.5000	3.5000	0.0000	0.0000	0.0000
37	3.5000	3.5000	0.0000	0.0000	0.0000
38	3.5000	3.5000	0.0000	0.0000	0.0000
39	3.5000	3.5000	0.0000	0.0000	0.0000
40	3.5000	3.5000	0.0000	0.0000	0.0000
41	3.6000	3.6000	0.0000	0.0000	0.0000
42	3.7000	3.7000	0.0000	0.0000	0.0000
43	3.8000	3.8000	0.0000	0.0000	0.0000
44	3.8000	3.8000	0.0000	0.0000	0.0000
45	3.8000	3.8000	0.0000	0.0000	0.0000
46	3.8000	3.8000	0.0000	0.0000	0.0000
47	3.8000	3.8000	0.0000	0.0000	0.0000
48	3.8000	3.8000	0.0000	0.0000	0.0000
49	3.8000	3.8000	0.0000	0.0000	0.0000
50	4.2000	4.2000	0.0000	0.0000	0.0000

TABLE D.15 FIFTY GROUP NEUTRON CROSS SECTIONS FOR OXYGEN

	$\sigma_{n,d}$	$\sigma_{n,\alpha}$
01	0.0170	0.3200
02	0.0090	0.3000
03	0.0040	0.2830
04	0.0000	0.2600
05	0.0000	0.2400
06	0.0000	0.2200
07	0.0000	0.2020
08	0.0000	0.1850
09	0.0000	0.1400
10	0.0000	0.1050
11	0.0000	0.1000
12	0.0000	0.0500
13	0.0000	0.0500
14	0.0000	0.0050
15	0.0000	0.0000
16	0.0000	0.0000
17	0.0000	0.0000
18	0.0000	0.0000
19	0.0000	0.0000
20	0.0000	0.0000
21	0.0000	0.0000
22	0.0000	0.0000
23	0.0000	0.0000
24	0.0000	0.0000
25	0.0000	0.0000
26	0.0000	0.0000
27	0.0000	0.0000
28	0.0000	0.0000
29	0.0000	0.0000
30	0.0000	0.0000
31	0.0000	0.0000
32	0.0000	0.0000
33	0.0000	0.0000
34	0.0000	0.0000
35	0.0000	0.0000
36	0.0000	0.0000
37	0.0000	0.0000
38	0.0000	0.0000
39	0.0000	0.0000
40	0.0000	0.0000
41	0.0000	0.0000
42	0.0000	0.0000
43	0.0000	0.0000
44	0.0000	0.0000
45	0.0000	0.0000
46	0.0000	0.0000
47	0.0000	0.0000
48	0.0000	0.0000
49	0.0000	0.0000
50	0.0000	0.0000

TABLE D.15 (CONT.) FIFTY GROUP CROSS SECTIONS FOR OXYGEN

OXYGEN		SEPTEMBER 16,1962				O 001
0.2856	0.2278	0.1895	0.1752	0.1834	0.2975	O 002
0.4597	0.4965	0.5027	0.4965	0.4986	0.6856	O 003
0.8518	1.3691	1.1634	0.4917	0.4917	0.3224	O 004
0.5239	0.8866	0.7657	0.8463	0.7632	1.2212	O 005
1.3738	1.8318	1.5265	0.9464	0.9006	0.8854	O 006
0.9770	1.1296	1.7707	3.5110			O 007
0.3388	0.2702	0.2247	0.2078	0.2175	0.3528	O 008
0.5452	0.5848	0.5922	0.5848	0.5873	0.8075	O 009
1.0033	1.6126	1.3703	0.5911	0.5911	0.3876	O 010
0.6299	1.0659	0.9205	1.0175	1.1365	1.8184	O 011
2.0457	2.7276	2.2730	1.4093	1.3411	1.3183	O 012
1.4547	1.6820	2.6367	0.0000			O 013
0.0648	0.0517	0.0430	0.0398	0.0416	0.0675	O 014
0.1043	0.1010	0.1022	0.1010	0.1014	0.1394	O 015
0.1732	0.2784	0.2366	0.1183	0.1183	0.0776	O 016
0.1261	0.2134	0.1843	0.2037	0.4867	0.7788	O 017
0.8762	1.1682	0.9735	0.6036	0.5744	0.5646	O 018
0.6230	0.7204	0.0000	0.0000			O 019
0.0118	0.0093	0.0078	0.0072	0.0075	0.0122	O 020
0.0188	0.0127	0.0129	0.0127	0.0127	0.0175	O 021
0.0217	0.0349	0.0297	0.0189	0.0189	0.0124	O 022
0.0201	0.0341	0.0295	0.0325	0.1136	0.1816	O 023
0.2043	0.2724	0.2270	0.1407	0.1339	0.1317	O 024
0.1459	0.0000	0.0000	0.0000			O 025
0.0000	0.0000	0.0000	0.0000	0.0000	0.0000	O 026
0.0000	0.0000	0.0000	0.0000	0.0000	0.0000	O 027
0.0000	0.0000	0.0000	0.0000	0.0000	0.0000	O 028
0.0000	0.0000	0.0000	0.0000	0.0000	0.0000	O 029
0.0000	0.0000	0.0000	0.0000	0.0000	0.0000	O 030
0.0000	0.0000	0.0000	0.0000			O 031
0.0000	0.0000	0.0000	0.0000	0.0000	0.0000	O 032
0.0000	0.0000	0.0000	0.0000	0.0000	0.0000	O 033
0.0000	0.0000	0.0000	0.0000	0.0000	0.0000	O 034
0.0000	0.0000	0.0000	0.0000	0.0000	0.0000	O 035
0.0000	0.0000	0.0000	0.0000	0.0000	0.0000	O 036

TABLE D.16 Oxygen Nuclide Decks

0.0000	0.1680	1.3926	7.9890			0 037
1.0000	1.0000	1.0000	1.0000	1.0000	1.0000	0 038
1.0000	1.0000	1.0000	1.0000	0.0000	0.0000	0 039
0.0000	0.0000	0.0000	0.0000	0.0000	0.0000	0 040
0.0000	0.0000	0.0000	0.0000	0.0000	0.0000	0 041
0.0000	0.0000	0.0000	0.0000	0.0000	0.0000	0 042
0.0000	0.0000	0.0000	0.0000			0 043
0.0326	0.0435	0.0542	0.0546	0.0000		0 044
0.0614	0.0033	0.0000	0.0000	0.0000		0 045
0.0000	0.0000	0.0000	0.0000	0.0000		0 046
0.0000	0.0354	0.0473	0.0591	0.0595		0 047
0.0000	0.0750	0.0000	0.0000	0.0000		0 048
0.0000	0.0000	0.0000	0.0000	0.0000	0.0000	0 049
0.0293	0.0391	0.0489	0.0493	0.0000		0 050
0.0000	0.0276	0.0000	0.0000	0.0000		0 051
0.0000	0.0000	0.0000	0.0000	0.0000		0 052
0.0000	0.0000	0.0403	0.0537	0.0671		0 053
0.0677	0.0000	0.0852	0.0000	0.0000		0 054
0.0000	0.0000	0.0000	0.0000	0.0000	0.0000	0 055
0.0262	0.0350	0.0438	0.0441	0.0000		0 056
0.0000	0.0248	0.0000	0.0000	0.0000		0 057
0.0000	0.0000	0.0000	0.0000	0.0000		0 058
0.0000	0.0000	0.0000	0.0386	0.0408		0 059
0.0322	0.0162	0.0232	0.0784	0.0000		0 060
0.0000	0.0000	0.0000	0.0000	0.0000	0.0000	0 061
0.0238	0.0306	0.0197	0.0036	0.0000		0 062
0.0000	0.0225	0.0000	0.0000	0.0000		0 063
0.0000	0.0000	0.0000	0.0000	0.0000		0 064
0.0000	0.0000	0.0000	0.0000	0.0000		0 065
0.0000	0.0000	0.0000	0.1441	0.0000		0 066
0.0000	0.0000	0.0000	0.0000	0.0000	0.0000	0 067
0.0088	0.0000	0.0000	0.0000	0.0000		0 068
0.0000	0.0200	0.0000	0.0000	0.0000		0 069
0.0000	0.0000	0.0000	0.0000	0.0000		0 070
0.0000	0.0000	0.0000	0.0000	0.0000		0 071
0.0000	0.0000	0.0000	0.0000	0.1580		0 072
0.0000	0.0000	0.0000	0.0000	0.0000	0.0000	0 073

0.0000	0.0000	0.0000	0.0000	0.0000		0 074
0.0000	0.0182	0.0000	0.0000	0.0000		0 075
0.0000	0.0000	0.0000	0.0000	0.0000		0 076
0.0000	0.0000	0.0000	0.0000	0.0000		0 077
0.0000	0.0000	0.0000	0.0000	0.0243		0 078
0.1347	0.0000	0.0000	0.0000	0.0000	0.0000	0 079
0.0000	0.0000	0.0000	0.0000	0.0000		0 080
0.0000	0.0036	0.0082	0.0000	0.0000		0 081
0.0000	0.0000	0.0000	0.0000	0.0000		0 082
0.0000	0.0000	0.0000	0.0000	0.0000		0 083
0.0000	0.0000	0.0000	0.0000	0.0000		0 084
0.1138	0.0000	0.0000	0.0000	0.0000	0.0000	0 085
0.0000	0.0000	0.0000	0.0000	0.0000		0 086
0.0000	0.0000	0.0094	0.0000	0.0000		0 087
0.0000	0.0000	0.0000	0.0000	0.0000		0 088
0.0000	0.0000	0.0000	0.0000	0.0000		0 089
0.0000	0.0000	0.0000	0.0000	0.0000		0 090
0.0000	0.1271	0.0000	0.0000	0.0000	0.0000	0 091
0.0000	0.0000	0.0000	0.0000	0.0000		0 092
0.0000	0.0000	0.0085	0.0000	0.0000		0 093
0.0000	0.0000	0.0000	0.0000	0.0000		0 094
0.0000	0.0000	0.0000	0.0000	0.0000		0 095
0.0000	0.0000	0.0000	0.0000	0.0000		0 096
0.0000	0.1127	0.0298	0.0000	0.0000	0.0000	0 097
0.0000	0.0000	0.0000	0.0000	0.0000		0 098
0.0000	0.0000	0.0076	0.0000	0.0000		0 099
0.0000	0.0000	0.0000	0.0000	0.0000		0 100
0.0000	0.0000	0.0000	0.0000	0.0000		0 101
0.0000	0.0000	0.0000	0.0000	0.0000		0 102
0.0000	0.0000	0.1559	0.0000	0.0000	0.0000	0 103
0.0000	0.0000	0.0000	0.0000	0.0000		0 104
0.0000	0.0000	0.0068	0.0000	0.0000		0 105
0.0000	0.0000	0.0000	0.0000	0.0000		0 106
0.0000	0.0000	0.0000	0.0000	0.0000		0 107
0.0000	0.0000	0.0000	0.0000	0.0000		0 108
0.0000	0.0000	0.0945	0.0564	0.0000	0.0000	0 109
0.0000	0.0000	0.0000	0.0000	0.0000		0 110

0.0000	0.0000	0.0062	0.0000	0.0000		0 111
0.0000	0.0000	0.0000	0.0000	0.0000		0 112
0.0000	0.0000	0.0000	0.0000	0.0000		0 113
0.0000	0.0000	0.0000	0.0000	0.0000		0 114
0.0000	0.0000	0.0000	0.1537	0.0000	0.0000	0 115
0.0000	0.0000	0.0000	0.0000	0.0000		0 116
0.0000	0.0000	0.0055	0.0000	0.0000		0 117
0.0000	0.0000	0.0000	0.0000	0.0000		0 118
0.0000	0.0000	0.0000	0.0000	0.0000		0 119
0.0000	0.0000	0.0000	0.0000	0.0000		0 120
0.0000	0.0000	0.0000	0.0932	0.0418	0.0000	0 121
0.0000	0.0000	0.0000	0.0000	0.0000		0 122
0.0000	0.0000	0.0050	0.0000	0.0000		0 123
0.0000	0.0000	0.0000	0.0000	0.0000		0 124
0.0000	0.0000	0.0000	0.0000	0.0000		0 125
0.0000	0.0000	0.0000	0.0000	0.0000		0 126
0.0000	0.0000	0.0000	0.0000	0.1418	0.0000	0 127
0.0000	0.0000	0.0000	0.0000	0.0000		0 128
0.0000	0.0000	0.0041	0.0000	0.0000		0 129
0.0000	0.0000	0.0000	0.0000	0.0000		0 130
0.0000	0.0000	0.0000	0.0000	0.0000		0 131
0.0000	0.0000	0.0000	0.0000	0.0000		0 132
0.0000	0.0000	0.0000	0.0000	0.0000	0.0000	0 133
0.0000	0.0000	0.0000	0.0000	0.0000	0.0000	0 134
0.0000	0.0000	0.0000	0.0000	0.0000	0.0000	0 135
0.0000	0.0000	0.0000	0.0000	0.0000	0.0000	0 136
0.0000	0.0000	0.0000	0.0000	0.0000	0.0000	0 137
0.0000	0.0000	0.0000	0.0000	0.0000	0.0000	0 138
0.0000	0.0000	0.0000	0.0087			0 139
0.0000	0.0000	0.0000	0.0000	0.0000	0.0000	0 140
0.0000	0.0000	0.0000	0.0000	0.0000	0.0000	0 141
0.0000	0.0000	0.0000	0.0000	0.0000	0.0000	0 142
0.0000	0.0000	0.0000	0.0000	0.0000	0.0000	0 143
0.0000	0.0000	0.0000	0.0000	0.0000	0.0000	0 144
0.0000	0.0000	0.0000	0.0000			0 145
0.0000	0.0000	0.0000	0.0000	0.0000	0.0000	0 146
0.0000	0.0000	0.0000	0.0000	0.0000	0.0000	0 147

0.0000	0.0000	0.0000	0.0000	0.0000	0.0000	0 148
0.0000	0.0000	0.0000	0.0000	0.0000	0.0000	0 149
0.0000	0.0000	0.0000	0.0000	0.0000	0.0000	0 150
0.0000	0.0000	0.0000	0.0000			0 151
0.0000	0.0000	0.0000	0.0000	0.0000	0.0000	0 152
0.0000	0.0000	0.0000	0.0000	0.0000	0.0000	0 153
0.0000	0.0000	0.0000	0.0000	0.0000	0.0000	0 154
0.0000	0.0000	0.0000	0.0000	0.0000	0.0000	0 155
0.0000	0.0000	0.0000	0.0000	0.0000	0.0000	0 156
0.0000	0.0000	0.0000	0.0000			0 157
1.5900	1.5200	1.4200	1.2800	1.1500	1.2500	0 158
1.4500	1.4500	1.3500	1.3000	1.3000	1.7000	0 159
2.1000	3.3000	2.8000	1.2200	1.2200	0.8000	0 160
1.3000	2.2000	1.9000	2.1000	2.5000	4.0000	0 161
4.5000	6.0000	5.0000	3.1000	2.9500	2.9000	0 162
3.2000	3.7000	5.8000	11.5000			0 163

OXYGEN SEPTEMBER 16,1962

6.7022	4.7978	0.0000	0.0000	0.0417	11.5000	0 164
2.4962	1.0038	0.0000	0.0000	0.0417	3.5000	0 165
2.9523	0.5477	0.0000	0.0000	0.0417	3.5000	0 166
2.8613	0.6387	0.0000	0.0000	0.0417	3.5000	0 167
3.1577	0.3423	0.0000	0.0000	0.0417	3.5000	0 168
3.2718	0.2282	0.0000	0.0000	0.0417	3.5000	0 169
3.1950	0.4050	0.0000	0.0000	0.0417	3.6000	0 170
3.2838	0.4162	0.0000	0.0000	0.0417	3.7000	0 171
3.3725	0.4275	0.0000	0.0000	0.0417	3.8000	0 172
3.3725	0.4275	0.0000	0.0000	0.0417	3.8000	0 173
3.3725	0.4275	0.0000	0.0000	0.0417	3.8000	0 174
3.3725	0.4275	0.0000	0.0000	0.0417	3.8000	0 175
3.3725	0.4275	0.0000	0.0000	0.0417	3.8000	0 176
3.3725	0.4275	0.0000	0.0000	0.0417	3.8000	0 177
3.3725	0.4275	0.0000	0.0000	0.0417	3.8000	0 178
3.3725	0.4275	0.0000	0.0000	0.0417	3.8000	0 179
4.1998	0.0000	0.0000	0.1200	0.0417	4.2000	0 180

D. 10 FLUORINE

a. High-Energy Cross Sections

Total Cross Section: Plotted by Buckingham, Parker, and Pendlebury,[18] and by Hughes and Schwartz[52] with good agreement. The Hughes and Schwartz curve is used.

Nonelastic Cross Section: The only direct measurement of the nonelastic cross section is the measurement at 14 Mev of MacGregor, Ball, and Booth.[120] A second value can be inferred by summing the level excitation functions at 2. 45 Mev. The resultant values are in agreement with the nonelastic cross section plotted by Buckingham, Parker, and Pendlebury. At other energies, values of the nonelastic cross section obtained by summing the cross sections of the individual nonelastic reactions, obtained in part by direct measurement, and in part by extrapolation, are in consistently good agreement with the Buckingham et al. estimates. The Buckingham et al. curve is used, except in a few limited energy regions where the sum of the individual cross sections is preferred for consistency.

Elastic Cross Section: The elastic cross section at all energies is taken to be the difference between the total and the nonelastic cross sections.

Radiative-Capture Cross Section: Plotted by Hughes and Schwartz[52] in the energy region between 10 kev and 2 Mev and is tabulated at 0. 025 ev. The value of the cross section at the measured energies is 10 mb or less, except for a weak resonance worth approximately 20 mb at 25 kev. Unmeasured values are inferred, and the cross section is lumped into the absorption cross section.

Proton Emission Cross Section: The (n, p) cross section from threshold to ~8 Mev is given by Marion and Brugger.[107] Above 8 Mev the cross section appears to drop rapidly, because of competition from other nonelastic processes. The cross section is combined with those of the other absorption processes into a single cross section.

Deuteron and Triton Emission Cross Sections: The de-excitation schemes listed for F^{20} by Ajzenberg-Selove and Lauritsen[73] indicate that above the respective thresholds both (n, d) and (n, t) reactions should be significant. Neither cross section has been measured. An estimate of the (n, d) cross section can be obtained by assuming an apparent Coulomb barrier of 1. 3 Mev (based on the theoretical and observed (n, p) thresholds) and associating the drop in the (n, p) cross section above ~7 Mev with a rise in the competing (n, d) reaction. The threshold of the (n, t) reaction is ~9 Mev, in the energy region in which no nonelastic cross sections have been measured, and cannot be inferred. Both cross sections are lumped into the absorption cross section.

Alpha Emission Cross Section: The (n, α) cross section has been measured by Marion and Brugger[107] in the energy region from threshold to approximately 8 Mev. Above ~6 Mev the (n, α) cross section appears to be dropping, because of competition from the (n, p) reaction and, at higher energies, of the (n, d) and (n, t) reactions also. The alpha emission cross section is included in the absorption cross section.

Absorption Cross Section: Buckingham, Parker, and Pendlebury[18] plot an absorption

cross section in the energy region of interest. At energies of which either measured or rationally inferred values of the cross sections of the several neutron absorbing reactions are available the agreement between the sum of the individual reactions and the Buckingham et al. plot is good. Because of the uncertainties in the separate cross sections, especially above ~8 Mev, the Buckingham et al. estimate of a general absorption cross section is preferred to estimates of individual cross sections.

(n, 2n) Cross Section: The (n, 2n) cross section in the vicinity of 14 Mev has been measured by Ashby and his co-workers,[108] Paul and Clarke,[109] Rayburn,[110] and Prud'homme et al.[28] The agreement among the various measured values is good. The cross section used is based on an average among the measurements, extrapolated to threshold.

Inelastic Cross Section: In the energy region 0.1-1.0 Mev the excitation functions for the 0.111 Mev and 0.197 Mev levels in F^{19} have been measured absolutely by Freeman.[111] From 1.1 Mev to 2.2 Mev Freeman gives relative yield plots for 0.111 Mev and 0.197 Mev gamma rays in arbitrary units. Extrapolation of the lower energy absolute plots allows renormalization of the higher energy relative plots to an absolute basis. The renormalized plots are in agreement with the measurements of Day[112] at 2.56 Mev.

On the basis of the Freeman curves, it appears that the level excitation curves for the levels at 1.35, 1.46, and 1.56 Mev are all fitted fairly well by a Gaussian function. If the assumption is made that de-excitation from the 1.46-Mev and 1.56-Mev levels via cascade and directly to ground state are equally probable, the excitation cross sections at 2.45 Mev for these levels are in at least qualitative agreement with the values measured by Cranberg and Levin.[113]

Above ~3 Mev no direct information concerning the inelastic cross section is available. The cross section is taken to be the difference between the nonelastic cross section and the sum of the absorption and (n, 2n) cross sections.

b. Low-Energy Cross Sections

Total Cross Section: Plotted by Hughes and Schwartz,[52] and by Buckingham, Parker, and Pendlebury.[18] The former plot is used.

Nonelastic Cross Section: The nonelastic cross section in the lower energy region is identically the (n, n') cross section. Contributions attributable to the (n, γ) reaction are negligible.

Elastic Cross Section: Taken to be the difference between the total and the nonelastic cross sections. The resonances in the total cross section at 27, 49, 99, 280, 340, and 420 kev are identified as purely elastic by Ajzenberg-Selove and Lauritsen.[73]

Absorption Cross Section: No neutron absorption processes are significant in the lower energy region.

Inelastic Cross Section: The (n, n') cross section in the lower energy region is

composed of the excitation functions for the 0.111-Mev and 0.197-Mev levels, plotted by Freeman.[111]

c. Neutron Nonelastic Spectra

For neutron incident energies below 4.4 Mev, individual levels excited in inelastic reactions can be readily identified. Excitation functions either are known or can be approximated. Scattering reactions are treated by the isolated-level model. Sets of levels closely grouped at 4 Mev and at 1.45 Mev are treated as single levels.

Above 4.4 Mev the nonelastic spectra are calculated on the basis of the statistical model.

	σ_{nT}	$\sigma_{n,n}$	$\sigma_{n,X}$	$\sigma_{n,2n}$	$\sigma_{n,abs}$
01	1.7200	0.8908	0.8292	0.0620	0.1790
02	1.6900	0.8322	0.8578	0.0370	0.1820
03	1.6500	0.7698	0.8802	0.0060	0.1860
04	1.6100	0.7205	0.8895	0.0000	0.1900
05	1.5900	0.6916	0.8984	0.0000	0.1920
06	1.6400	0.7260	0.9140	0.0000	0.1970
07	1.8500	0.9218	0.9282	0.0000	0.2000
08	1.8200	0.8987	0.9213	0.0000	0.2150
09	1.8000	0.7820	1.0180	0.0000	0.2700
10	1.9500	0.7791	1.1709	0.0000	0.2400
11	1.8700	0.9150	0.9550	0.0000	0.1550
12	2.3500	1.4500	0.9000	0.0000	0.1200
13	1.9700	1.5490	0.4210	0.0000	0.0710
14	2.0000	1.1470	0.8530	0.0000	0.0430
15	2.1000	1.5790	0.5210	0.0000	0.0210
16	2.2000	1.8000	0.4000	0.0000	0.0000
17	2.7000	2.0500	0.6500	0.0000	0.0000
18	2.7000	1.7200	0.9800	0.0000	0.0000
19	2.7500	1.8500	0.9000	0.0000	0.0000
20	2.9500	2.1000	0.8500	0.0000	0.0000
21	2.9000	1.3250	1.5750	0.0000	0.0000
22	3.0500	2.1000	0.9500	0.0000	0.0000
23	2.9000	1.8000	1.1000	0.0000	0.0000
24	3.4000	2.0000	1.4000	0.0000	0.0000
25	3.2000	2.0900	1.1100	0.0000	0.0000
26	3.3000	1.8300	1.4700	0.0000	0.0000
27	3.7000	2.1200	1.5800	0.0000	0.0000
28	4.1000	2.6200	1.4800	0.0000	0.0000
29	3.7000	2.4100	1.2900	0.0000	0.0000
30	3.6500	2.5000	1.1500	0.0000	0.0000
31	4.6000	3.4700	1.1300	0.0000	0.0000
32	4.9000	3.4500	1.4500	0.0000	0.0000
33	4.3000	1.7700	2.5300	0.0000	0.0000
34	6.2000	3.2500	2.9500	0.0000	0.0000
35	7.6000	4.9000	2.7000	0.0000	0.0000
36	7.0000	2.9000	4.1000	0.0000	0.0000
37	4.5000	2.9000	1.6000	0.0000	0.0000
38	15.0000	14.6000	0.4000	0.0000	0.0000
39	8.5000	8.5000	0.0000	0.0000	0.0000
40	5.7000	5.7000	0.0000	0.0000	0.0000
41	3.8000	3.8000	0.0000	0.0000	0.0000
42	3.7000	3.7000	0.0000	0.0000	0.0000
43	3.6000	3.6000	0.0000	0.0000	0.0000
44	3.6000	3.6000	0.0000	0.0000	0.0000
45	3.5000	3.5000	0.0000	0.0000	0.0000
46	3.5000	3.5000	0.0000	0.0000	0.0000
47	3.5000	3.5000	0.0000	0.0000	0.0000
48	3.4000	3.4000	0.0000	0.0000	0.0000
49	3.4000	3.4000	0.0000	0.0000	0.0000
50	3.4000	3.4000	0.0000	0.0000	0.0000

TABLE D.17 FIFTY GROUP NEUTRON CROSS SECTIONS FOR FLUORINE

	$\sigma_{n,n'}$ (>4.4)	$\sigma_{n,n'}$ (0.196)	$\sigma_{n,n'}$ (1.45)	$\sigma_{n,n'}$ (2.78)	$\sigma_{n,n'}$ (4.0)
01	0.7130	0.0000	0.0000	0.0000	0.0000
02	0.7140	0.0000	0.0000	0.0000	0.0000
03	0.7020	0.0000	0.0000	0.0000	0.0000
04	0.7020	0.0000	0.0000	0.0000	0.0000
05	0.7100	0.0000	0.0000	0.0000	0.0000
06	0.7220	0.0000	0.0000	0.0000	0.0000
07	0.7350	0.0000	0.0000	0.0000	0.0000
08	0.7150	0.0000	0.0000	0.0000	0.0000
09	0.7600	0.0000	0.0000	0.0000	0.0000
10	0.9500	0.0000	0.0000	0.0000	0.0000
11	0.0000	0.0500	0.0000	0.0000	0.7500
12	0.0000	0.1000	0.0000	0.0000	0.6800
13	0.0000	0.1500	0.0000	0.2000	0.0000
14	0.0000	0.2000	0.0000	0.6100	0.0000
15	0.0000	0.2500	0.0000	0.2500	0.0000
16	0.0000	0.3000	0.1000	0.0000	0.0000
17	0.0000	0.3500	0.3000	0.0000	0.0000
18	$\sigma_{n,n'}$(0.111)	0.4000	0.5800	0.0000	0.0000
19	0.0000	0.5500	0.3500	0.0000	0.0000
20	0.1000	0.5500	0.2000	0.0000	0.0000
21	0.6000	0.9000	0.0750	0.0000	0.0000
22	0.3000	0.6500	0.0000	0.0000	0.0000
23	0.4000	0.7000	0.0000	0.0000	0.0000
24	0.6000	0.8000	0.0000	0.0000	0.0000
25	0.4500	0.6600	0.0000	0.0000	0.0000
26	0.8000	0.6700	0.0000	0.0000	0.0000
27	0.9800	0.6000	0.0000	0.0000	0.0000
28	0.6500	0.8300	0.0000	0.0000	0.0000
29	0.4800	0.8100	0.0000	0.0000	0.0000
30	0.4300	0.7200	0.0000	0.0000	0.0000
31	0.4500	0.6800	0.0000	0.0000	0.0000
32	0.6000	0.8500	0.0000	0.0000	0.0000
33	1.2000	1.3300	0.0000	0.0000	0.0000
34	1.0000	1.9500	0.0000	0.0000	0.0000
35	1.2000	1.5000	0.0000	0.0000	0.0000
36	3.5000	0.6000	0.0000	0.0000	0.0000
37	1.6000	0.0000	0.0000	0.0000	0.0000
38	0.4000	0.0000	0.0000	0.0000	0.0000
39	0.0000	0.0000	0.0000	0.0000	0.0000
40	0.0000	0.0000	0.0000	0.0000	0.0000
41	0.0000	0.0000	0.0000	0.0000	0.0000
42	0.0000	0.0000	0.0000	0.0000	0.0000
43	0.0000	0.0000	0.0000	0.0000	0.0000
44	0.0000	0.0000	0.0000	0.0000	0.0000
45	0.0000	0.0000	0.0000	0.0000	0.0000
46	0.0000	0.0000	0.0000	0.0000	0.0000
47	0.0000	0.0000	0.0000	0.0000	0.0000
48	0.0000	0.0000	0.0000	0.0000	0.0000
49	0.0000	0.0000	0.0000	0.0000	0.0000
50	0.0000	0.0000	0.0000	0.0000	0.0000

TABLE D.17 (CONT.) FIFTY GROUP CROSS SECTIONS FOR FLUORINE

FLUORINE		JUNE 21,1962				F 001
0.3852	0.3598	0.3329	0.3115	0.2990	0.3139	F 002
0.3986	0.3812	0.3317	0.3305	0.4190	0.6701	F 003
0.7357	0.5841	0.7726	0.6725	0.7419	0.6681	F 004
0.6816	0.7740	0.6840	0.8130	0.7174	0.7768	F 005
0.7446	0.6257	0.7248	0.8958	0.8240	0.8547	F 006
1.1864	1.1796	0.6052	1.1112			F 007
0.4454	0.4161	0.3849	0.3603	0.3458	0.3630	F 008
0.4609	0.4494	0.3910	0.3896	0.4766	0.7700	F 009
0.8459	0.6760	0.9367	1.0929	1.2770	1.1800	F 010
1.4259	1.6005	1.7585	1.7070	1.5880	1.8380	F 011
1.6150	1.6610	1.7800	1.7120	1.4290	1.3843	F 012
1.8140	1.7250	0.8850	0.			F 013
0.0602	0.0563	0.0520	0.0487	0.0468	0.0491	F 014
0.0623	0.0681	0.0593	0.0590	0.0694	0.1099	F 015
0.1174	0.0869	0.1197	0.3346	0.3811	0.2719	F 016
0.2925	0.3755	0.3825	0.5300	0.5946	0.7852	F 017
0.8404	0.9333	0.9652	1.0262	0.7840	0.6860	F 018
0.9276	0.9874	0.	0.			F 019
0.	0.	0.	0.	0.	0.	F 020
0.	0.	0.	0.	0.	0.	F 021
0.	0.	0.	0.	0.	0.	F 022
0.	0.	0.	0.	0.	0.	F 023
0.	0.0800	0.2300	0.4660	0.6000	0.4660	F 024
0.1940	0.	0.	0.			F 025
0.	0.	0.	0.	0.	0.	F 026
0.	0.	0.	0.	0.	0.	F 027
0.	0.	0.	0.	0.	0.	F 028
0.	0.	0.	0.	0.	0.	F 029
0.	0.	0.	0.	0.	0.	F 030
0.	0.	0.	0.			F 031
0.	0.	0.	0.	0.	0.	F 032
0.	0.	0.	0.	0.	0.	F 033
0.	0.	0.	0.	0.	0.	F 034
0.	0.	0.	0.	0.	0.	F 035
0.	0.	0.	0.	0.	0.	F 036

TABLE D.18 Fluorine Nuclide Decks

0.	0.	0.2798	2.1388			F 037
1.0	1.0	1.0	1.0	1.0	1.0	F 038
1.0	1.0	1.0	1.0	0.0	0.0	F 039
0.0	0.0	0.0	0.0	0.0	0.0	F 040
0.0	0.0	0.0	0.0	0.0	0.0	F 041
0.0	0.0	0.0	0.0	0.0	0.0	F 042
0.0	0.0	0.0	0.0			F 043
0.04016	0.04058	0.04004	0.03997	0.04012		F 044
0.04025	0.04016	0.03804	0.03910	0.04691		F 045
0.0	0.0	0.0	0.0	0.0		F 046
0.0	0.04059	0.04057	0.03958	0.03904		F 047
0.03870	0.03831	0.03769	0.03519	0.03561		F 048
0.04203	0.0	0.0	0.0	0.0	0.0	F 049
0.03856	0.03929	0.03911	0.03940	0.03994		F 050
0.04047	0.04082	0.03911	0.04069	0.04944		F 051
0.0	0.0	0.0	0.0	0.0		F 052
0.0	0.0	0.04015	0.03965	0.03820		F 053
0.03718	0.03633	0.03543	0.03431	0.03151		F 054
0.03133	0.03631	0.0	0.0	0.0	0.0	F 055
0.03707	0.03814	0.03838	0.03910	0.04010		F 056
0.04114	0.04204	0.04084	0.04310	0.05318		F 057
0.0	0.0	0.0	0.0	0.0		F 058
0.0082	0.0	0.0	0.03906	0.03807		F 059
0.03617	0.03469	0.03338	0.03203	0.03050		F 060
0.02751	0.02684	0.03050	0.0	0.0	0.0	F 061
0.03456	0.03584	0.03636	0.03737	0.03868		F 062
0.04007	0.04137	0.04062	0.04336	0.05414		F 063
0.	0.	0.0290	0.	0.		F 064
0.0818	0.0	0.0	0.0	0.03668		F 065
0.03523	0.03296	0.03111	0.02942	0.02773		F 066
0.02590	0.02291	0.02188	0.02431	0.0	0.0	F 067
0.03205	0.03347	0.03420	0.03543	0.03697		F 068
0.03864	0.04026	0.03990	0.04303	0.05431		F 069
0.02920	0.	0.0630	0.	0.		F 070
0.0100	0.1437	0.0	0.0	0.0		F 071
0.03334	0.03150	0.02896	0.02683	0.02488		F 072
0.02298	0.02100	0.01816	0.01693	0.01834	0.0	F 073

0.02925	0.03075	0.03164	0.03300	0.03470		F 074
0.03654	0.03839	0.03839	0.04177	0.05323		F 075
0.1719	0.0	0.0569	0.0	0.0		F 076
0.	0.1207	0.	0.	0.		F 077
0.0	0.02951	0.02738	0.02469	0.02242		F 078
0.02036	0.01838	0.01641	0.01384	0.01257	0.01325	F 079
0.02633	0.02783	0.02881	0.03024	0.03201		F 080
0.03395	0.03593	0.03621	0.03973	0.05107		F 081
0.1548	0.	0.0511	0.0923	0.		F 082
0.	0.0356	0.1820	0.	0.		F 083
0.0	0.0	0.02502	0.02275	0.02009		F 084
0.01784	0.01581	0.01393	0.01211	0.009939	0.008769	F 085
0.02335	0.02481	0.02582	0.02726	0.02903		F 086
0.03098	0.03302	0.03350	0.03703	0.04798		F 087
0.1386	0.0	0.0	0.1550	0.0		F 088
0.0	0.0	0.2255	0.0	0.0		F 089
0.0	0.0	0.0	0.02040	0.01815		F 090
0.01565	0.01356	0.01171	0.01004	0.008481	0.006751	F 091
0.02022	0.02158	0.02257	0.02394	0.02564		F 092
0.02753	0.02951	0.03013	0.03353	0.04375		F 093
0.1224	0.0	0.0	0.1369	0.0		F 094
0.	0.	0.1725	0.0229	0.		F 095
0.0	0.0	0.0	0.0	0.01599		F 096
0.01387	0.01165	0.009812	0.008228	0.006837	0.005589	F 097
0.01769	0.01896	0.01992	0.02123	0.02285		F 098
0.02465	0.02657	0.02729	0.03055	0.04012		F 099
0.1102	0.0	0.0	0.1232	0.0		F 100
0.0	0.0	0.0	0.1202	0.0		F 101
0.0	0.0	0.0	0.0	0.0		F 102
0.01177	0.009927	0.008097	0.006614	0.005368	0.004311	F 103
0.01540	0.01657	0.01747	0.01870	0.02021		F 104
0.02191	0.02373	0.02450	0.02758	0.03641		F 105
0.0229	0.0734	0.	0.1026	0.0040		F 106
0.0	0.0	0.0	0.1085	0.0		F 107
0.0	0.0	0.0	0.0	0.0		F 108
0.0	0.008254	0.006752	0.005332	0.004210	0.003295	F 109
0.01337	0.01443	0.01527	0.01641	0.01780		F 110

0.01938	0.02108	0.02186	0.02473	0.03283		F 111
0.0	0.0919	0.0	0.0	0.0460		F 112
0.0	0.0	0.0	0.0984	0.0		F 113
0.0	0.0	0.0	0.0	0.0		F 114
0.0	0.0	0.005408	0.004275	0.003256	0.002474	F 115
0.01151	0.01246	0.01323	0.01427	0.01554		F 116
0.01697	0.01854	0.01930	0.02193	0.02925		F 117
0.0	0.0830	0.0	0.0	0.0416		F 118
0.	0.	0.	0.	0.0548		F 119
0.0	0.0	0.0	0.0	0.0		F 120
0.0	0.0	0.0	0.003318	0.002525	0.001848	F 121
0.009749	0.01059	0.01127	0.01219	0.01331		F 122
0.01460	0.01600	0.01672	0.01907	0.02554		F 123
0.0	0.0735	0.0	0.0	0.0373		F 124
0.0	0.0	0.0	0.0	0.0505		F 125
0.0	0.0	0.0	0.0	0.0		F 126
0.0	0.0	0.0	0.0630	0.001878	0.001371	F 127
0.008246	0.008974	0.009579	0.01039	0.01138		F 128
0.01251	0.01375	0.01442	0.01651	0.02218		F 129
0.0	0.0666	0.0	0.0	0.0334		F 130
0.0	0.0	0.0	0.0	0.0452		F 131
0.0	0.0	0.0	0.0	0.0		F 132
0.0	0.0	0.0	0.0	0.2590	0.000975	F 133
0.01619	0.01769	0.01895	0.02063	0.02269	0.02506	F 134
0.02768	0.02916	0.03354	0.04531	0.0	0.1458	F 135
0.0	0.0	0.0731	0.0	0.0	0.0	F 136
0.0	0.0495	0.0190	0.0	0.0	0.0	F 137
0.0	0.0	0.0	0.0	0.0	0.0	F 138
0.4960	1.0080	1.2000	0.7440			F 139
0.01297	0.01424	0.01533	0.01678	0.01857	0.02064	F 140
0.02295	0.02434	0.02821	0.03840	0.0	0.1458	F 141
0.0	0.0	0.0146	0.0	0.0	0.0	F 142
0.0	0.0	0.0412	0.0	0.0	0.0	F 143
0.0	0.0	0.0	0.0	0.0	0.0	F 144
0.0	0.0	1.3300	2.2060			F 145
0.008963	0.009888	0.01071	0.01178	0.01312	0.01467	F 146
0.01642	0.01753	0.02047	0.02808	0.0	0.0	F 147

0.0	0.0	0.0	0.0	0.0	0.0	F 148
0.0	0.0	0.0148	0.0	0.0	0.0	F 149
0.0	0.0	0.0	0.0	0.0	0.0	F 150
0.0	0.0	0.0	0.0			F 151
0.004205	0.004665	0.005081	0.005627	0.006305	0.007098	F 152
0.008002	0.008611	0.01013	0.01402	0.0	0.0	F 153
0.0	0.0	0.0	0.0	0.0	0.0	F 154
0.0	0.0	0.0	0.0	0.0	0.0	F 155
0.0	0.0	0.0	0.0	0.0	0.0	F 156
0.0	0.0	0.0	0.0			F 157
1.72	1.69	1.65	1.61	1.59	1.64	F 158
1.85	1.82	1.80	1.95	1.87	2.35	F 159
1.97	2.00	2.10	2.20	2.70	2.70	F 160
2.75	2.95	2.90	3.05	2.90	3.40	F 161
3.20	3.30	3.70	4.10	3.70	3.65	F 162
4.60	4.90	4.30	6.20			F 163

FLUORINE F 164

4.330	3.270	0.0	0.0	0.03509	7.600	F 165
5.400	1.300	0.240	0.060	0.03509	7.000	F 166
3.185	1.010	0.305	0.0	0.03509	4.500	F 167
12.420	2.180	0.0	0.400	0.03509	15.000	F 168
7.830	0.670	0.0	0.0	0.03509	8.500	F 169
5.400	0.300	0.0	0.0	0.03509	5.700	F 170
3.450	0.350	0.0	0.0	0.03509	3.800	F 171
3.360	0.340	0.0	0.0	0.03509	3.700	F 172
3.270	0.330	0.0	0.0	0.03509	3.600	F 173
3.270	0.330	0.0	0.0	0.03509	3.600	F 174
3.180	0.320	0.0	0.0	0.03509	3.500	F 175
3.180	0.320	0.0	0.0	0.03509	3.500	F 176
3.180	0.320	0.0	0.0	0.03509	3.500	F 177
3.090	0.310	0.0	0.0	0.03509	3.400	F 178
3.090	0.310	0.0	0.0	0.03509	3.400	F 179
3.390	0.0	0.0	0.102	0.03509	3.400	F 180

D. 11 NICKEL

a. High-Energy Cross Sections

Total Cross Section: The total cross section over the entire energy range of interest is given by Hughes and Schwartz[52] and is used as given.

Nonelastic Cross Section: Plotted by Hughes and Schwartz[52] in the range 2.3-14 Mev. The value at 14 Mev is in good agreement with MacGregor, Ball, and Booth,[83] and Bonner and Slattery.[114] The Hughes and Schwartz value at 3.7 Mev is somewhat smaller than that given by Machwe, Kent, and Snowdon,[115] but agrees well with Strizhak and Beyster, Walt and Salmi[117] at 2.5 Mev and fairly well with Pasechnik[118] at 3.3 Mev. Below 2.3 Mev, $\sigma_{n,x}$ is taken to be the sum of $\sigma_{n,\gamma}$, $\sigma_{n,n'}$, and $\sigma_{n,p}$.

Elastic Cross Section: Taken to be the difference between σ_{nT} and σ_{nx} over the energy range of interest. The value so obtained is higher than the Machwe et al.[115] value at 3.7 Mev (their value of σ_{nx} appears to be large in comparison with other measurements) and appreciably higher than the Walt and Barshall value (Walt and Barshall use for σ_{nT} a value rather smaller than that given by Hughes and Schwartz).

Radiative Capture Cross Section: Taken from the Diven and Terrell plots[119] in the region 0.2-1 Mev, and is extrapolated to zero at 1.5 Mev.

Proton Emission Cross Section:

(i) Nickel 58 at 14 Mev

At 14 Mev, Colli et al.[33] obtain for $\sigma_{n,p}$ a value of 310 mb. Allen[32] obtains for the same cross section 440 ± 27 mb. In an earlier study, Allen[31] obtained σ_{np}(14 Mev) = 310 mb for compound nucleus interactions. Glover and Weigold[121] obtain $\sigma_{n,p}$(14.1) = 435 mb. The magnitude of $\sigma_{n,p\gamma}$(14 Mev) in Ni^{58} is taken to be 440 mb, of which 310 mb represents compound nucleus interactions and the remaining 130 mb direct interactions.

The cross section $\sigma_{n,pn}$ is given by Allen[31] to be 220 mb at 14 Mev. Glover and Weigold[121] find $\sigma_{n,pn} + \sigma_{n,np}$ to be 540 mb. Colli et al.[33] find $\sigma_{n,np}$(14 Mev) to be 220 mb, while Allen finds the same cross section to be 343 mb. Taking the sum of the Allen values for $\sigma_{n,pn}$ and $\sigma_{n,np}$, one obtains a total of 563 mb, compared with the Glover and Weigold combined result for $\sigma_{n,pn} + \sigma_{n,np}$ of 540 mb at 14 Mev. The agreement appears to be quite good.

At 14.2 Mev, Glover and Weigold give $\sigma_{n,p}$ the value 355 mb, while Preiss and Fink[122] give 277 mb. Glover and Purser[123] find $\sigma_{n,p} + \sigma_{n,pn}$ to be 490 mb, of which 430 are attributable to compound nucleus interactions. Kumabe and Fink[124] give for $\sigma_{n,p} + \sigma_{n,pn}$ at 14.8 Mev a total of 440 mb. Subtracting the Glover results, one finds $\sigma_{n,pn}$(14.8 Mev) to be 135 mb, while the Fink results yield 163 mb. Glover and Weigold also give for $\sigma_{n,pn} + \sigma_{n,np}$ at 14.8 Mev the value 570 mb. Subtracting the value $\sigma_{n,pn}$ = 135 mb obtained above, there obtains $\sigma_{n,np}$ = 435 mb.

(ii) Nickel 60 at 14 Mev

At 14 Mev, $\sigma_{n,p}$ is found to be 197 mb by Colli et al.[33]; 124 mb by Allen[32]; 240 mb by Allen[31]; and 9 mb by Preiss and Fink.[122] At 13.5 Mev, it is found to be 155 mb by March and Morton.[125] If the Preiss and Fink result and the earlier Allen value are discarded, $\sigma_{n,p}$ may be taken to be 160 mb at 14 Mev.

In his earlier paper Allen gives $\sigma_{n,pn}$ to be 60 mb at 14 Mev. In view of the fact that Allen uses proton spectrum measurements to determine cross sections, it appears likely that at least part of the 240 mb $\sigma_{n,p}$ noted above should be attributed to $\sigma_{n,pn}$ to give a value closer to 100-150 mb.

For $\sigma_{n,np}$, Allen gives 51 mb and Colli, 64 mb at 14 Mev, while March and Morton give 68 mb at 13.5 Mev; the mean value is taken to be 60 mb. (Note that (n, pn) and (n, np) have the same threshold and that (n, pn) should be favored by virtue of direct interaction with anomalously low Coulomb barriers over (n, np) which proceeds primarily by compound nucleus formation.)

(iii) Nickel 58 and 60 at 2.5 Mev

At 2.5 Mev, Van Loef[126] finds $\sigma_{n,p}$ in Ni^{58} to be approximately 180 mb, while Gonzalez, Rapaport, and Van Loef[127] find the same cross section to be 145 mb. Since the Q value for $\sigma_{n,p}$ in Ni^{60} is -2.03 Mev, the contribution of (n, p) reactions in Ni^{60} to $\sigma_{n,x}$ at 2.5 Mev is negligible, and $\sigma_{n,p}$ for elemental nickel may be taken to be approximately 110 mb.

(iv) Other Energies

In the regions where no measurements exist, estimates of the cross sections were obtained as follows. The (n, p) cross section is assumed to consist of a direct interaction and a compound nucleus component. Since the Q value for (n, p) in Ni^{58} is slightly positive, the threshold for the direct component is placed at 0.5 Mev, and agreement is forced with the measurements at 2.5 and 3.2 Mev. The compound component has a threshold at $-Q_{n,p}$ plus a 7 Mev Coulomb barrier.

The reactions $\sigma_{n,pn}$ and $\sigma_{n,np}$ are assigned a threshold at $-Q_{n,pn}$ plus a 3-Mev direct interaction Coulomb barrier, and are assumed to rise roughly linearly to the assigned values at 14 Mev.

Deuteron Emission Cross Section: Glover and Weigold[121] report for $\sigma_{n,d}$ in Ni^{58} at 14.8 Mev a value of 25 mb. Since the Q value for (n, d) in Ni^{60} is not far removed from that in Ni^{58}, the assumption is made that $\sigma_{n,d}$ in Ni^{60} is also 25 mb. It is further assumed that the threshold for (n, d) reactions (including the Coulomb barrier) is in the vicinity of 111 Mev and that the cross section rises linearly from threshold to the value at 14.8 Mev.

Alpha Emission Cross Section: No published values for $\sigma_{n,\alpha}$ in nickel have been found. The plot given by Buckingham, Parker, and Pendlebury[18] is in qualitative

agreement with estimates based on Q value plus Coulomb barrier and is used as published.

Inelastic and (n, 2n) Cross Sections: The value of $\sigma_{n, 2n}$ for Ni^{58} is plotted in Hughes and Schwartz[52] and is verified by Bayhurst and Prestwood[131] and Glover and Weigold.[121] The corresponding cross section for Ni^{60} is given by Colli et al.[33] at 14 Mev. The sum of the Colli value for Ni^{60} and the Hughes and Schwartz value for Ni^{58} at 14 Mev are in good agreement with the value of $\sigma_{n, 2n}$ in elemental nickel given by Beneveniste.[132]

Day[112] obtains for $\sigma_{n, n'}$ at 2.56 Mev a value of 585 mb. Cranberg and Levin[113] find $\sigma_{n, n'}$ at 2.45 Mev to be approximately 690 mb. Keihn and Goodman[128] find 1.37 b for $\sigma_{n, n'}$ at 2.55 Mev; however, it appears evident that a correction for (n, p) reactions was overlooked when Keihn and Goodman normalized their experimental results so that their relative results are useful but the absolute values are not. At 3.2 Mev, Scherrer Allison, and Faust[129] find for $\sigma_{n, n'}$ a value of 1.39 b, as compared with the Paschnik measurement of $\sigma_{n, x}$ at 3.3 Mev, thereby yielding 1.35 b ± 0.25.

At all other energies $\sigma_{n, n'}$ is taken to be the difference between $\sigma_{n, x}$ and the sum of all other allowed reactions.

b. Low-Energy Cross Sections

Total Cross Section: The σ_{nT} curve of Hughes and Schwartz[52] is used as given with suitable smoothing over resonances.

Nonelastic Cross Section: In the lower energy region the nonelastic cross section is identically the radiative capture cross section. The majority of the resonances in nickel are known to be scattering resonances, and the infinite dilution resonance integral is given by Tattersall[133] as less than 1.1 b. In the absence of resonance parameters the $\sigma_{n, \gamma}$ cross section is taken to be (v^{-1}) from thermal to 3 kev where the first resonance appears. Above 3 kev, $\sigma_{n, \gamma}$ is extrapolated to agree with the Diven and Terrell[119] data at 200 kev. No resonance surface absorption is considered.

Elastic Cross Section: Taken to be the difference between the total cross section and the nonelastic cross section. Resonance scattering is not considered.

c. Neutron Nonelastic Spectra

The assumption is made that nickel can be treated by the statistical model at incident neutron energies above 3.5 Mev. The statistical-model calculations are split into two parts, one to obtain (n, n'), (n, np) and (n, pn) spectra, the other to obtain (n, 2n) and some (n, n') spectra. The cross sections assigned for the latter case were chosen to approximate the Colli et al. (n, 2n) cross sections at 14 Mev; the corresponding cross sections assigned in the former case represent the difference between the total neutron emission cross sections and those already assigned.

The neutron spectra from (n, np) reactions were assumed to be identical to those from (n, n') reactions. The cross sections for the two reactions were combined and the

spectra calculated by the single-particle statistical model. The (n, pn) spectra were calculated also as single-particle spectra by using as excitation energies

$$U = E + Q_{n,\,pn} - \text{Coulomb barrier}$$
$$= E - 7.9 - 3.0.$$

The spectra so calculated are expected to be somewhat cooler than the true spectra, since direct interactions that are known to be important in nickel tend to yield neutrons of energies greater than those predicted by compound nucleus theories.

At energies below 2.2 Mev the Keihn and Goodman[128] excitation functions, renormalized to agree with other measurements, are applicable and are used.

In the intermediate range, between 2.2 Mev and 3.5 Mev, the empirical method is used. Since the lowest level of any consequence in nickel occurs at 1.33 Mev, only the levels above ~2.7 Mev satisfy the asymptotic criterion; those below are treated by means of the truncated version.

	σ_{nT}	$\sigma_{n,n}$	$\sigma_{n,X}$	$\sigma_{n,2n}$	$\sigma_{n,n'}$
01	2.7000	1.2998	1.4002	0.1843	0.4098
02	2.8600	1.4395	1.4205	0.0709	0.7855
03	2.9800	1.5399	1.4401	0.0000	1.0610
04	3.1500	1.6903	1.4597	0.0000	1.1217
05	3.3000	1.8203	1.4797	0.0000	1.2047
06	3.4300	1.9301	1.4999	0.0000	1.2649
07	3.5700	2.0495	1.5205	0.0000	1.3305
08	3.6200	2.0797	1.5403	0.0000	1.3903
09	3.6900	2.1379	1.5521	0.0000	1.4071
10	3.6500	2.1099	1.5401	0.0000	1.3991
11	3.5900	2.0598	1.5302	0.0000	1.3932
12	3.5000	1.9904	1.5096	0.0000	1.3766
13	3.4500	2.0003	1.4497	0.0000	1.3217
14	3.3900	2.1000	1.2900	0.0000	1.1670
15	3.3500	2.1300	1.2200	0.0000	1.1020
16	3.3000	2.2200	1.0800	0.0000	0.9660
17	3.2700	2.3200	0.9500	0.0000	0.8400
18	3.2400	2.4200	0.8200	0.0000	0.7140
19	3.2000	2.5670	0.6330	0.0000	0.5300
20	3.2100	2.7100	0.5000	0.0000	0.4000
21	3.2200	2.8350	0.3850	0.0000	0.2900
22	3.2400	2.9980	0.2420	0.0000	0.1500
23	3.2600	3.0810	0.1790	0.0000	0.0900
24	3.2800	3.1940	0.0860	0.0000	0.0000
25	3.3000	3.2170	0.0830	0.0000	0.0000
26	3.3300	3.2520	0.0780	0.0000	0.0000
27	3.3700	3.3000	0.0700	0.0000	0.0000
28	3.4100	3.3500	0.0600	0.0000	0.0000
29	3.4600	3.4100	0.0500	0.0000	0.0000
30	3.5100	3.4700	0.0400	0.0000	0.0000
31	3.6000	3.5700	0.0300	0.0000	0.0000
32	3.7100	3.6900	0.0200	0.0000	0.0000
33	3.8500	3.8350	0.0150	0.0000	0.0000
34	4.1500	4.1400	0.0100	0.0000	0.0000
35	4.5000	4.4900	0.0100	0.0000	0.0000
36	4.9000	4.8900	0.0100	0.0000	0.0000
37	5.5000	5.4900	0.0100	0.0000	0.0000
38	7.2000	7.1890	0.0110	0.0000	0.0000
39	8.4000	8.3880	0.0120	0.0000	0.0000
40	11.0000	10.9870	0.0130	0.0000	0.0000
41	13.3000	13.2860	0.0140	0.0000	0.0000
42	14.3000	14.2840	0.0160	0.0000	0.0000
43	15.0000	14.9810	0.0190	0.0000	0.0000
44	15.5000	15.4730	0.0270	0.0000	0.0000
45	17.0000	16.9600	0.0400	0.0000	0.0000
46	17.1000	17.0410	0.0590	0.0000	0.0000
47	17.2000	17.1130	0.0870	0.0000	0.0000
48	17.4000	17.2730	0.1270	0.0000	0.0000
49	17.5000	17.3130	0.1870	0.0000	0.0000
50	22.2000	17.5000	4.7000	0.0000	0.0000

TABLE D.19 FIFTY GROUP NEUTRON CROSS SECTIONS FOR NICKEL

	$\sigma_{n,p}$	$\sigma_{n,np}$	$\sigma_{n,pn}$	$\sigma_{n,d}+\sigma_{n,\alpha}$	$\sigma_{n,\gamma}$
01	0.3620	0.2620	0.1321	0.0500	0.0000
02	0.3550	0.1100	0.0651	0.0340	0.0000
03	0.3500	0.0020	0.0101	0.0170	0.0000
04	0.3300	0.0000	0.0000	0.0080	0.0000
05	0.2750	0.0000	0.0000	0.0000	0.0000
06	0.2350	0.0000	0.0000	0.0000	0.0000
07	0.1900	0.0000	0.0000	0.0000	0.0000
08	0.1500	0.0000	0.0000	0.0000	0.0000
09	0.1450	0.0000	0.0000	0.0000	0.0000
10	0.1410	0.0000	0.0000	0.0000	0.0000
11	0.1370	0.0000	0.0000	0.0000	0.0000
12	0.1330	0.0000	0.0000	0.0000	0.0000
13	0.1280	0.0000	0.0000	0.0000	0.0000
14	0.1230	0.0000	0.0000	0.0000	0.0000
15	0.1180	0.0000	0.0000	0.0000	0.0000
16	0.1140	0.0000	0.0000	0.0000	0.0000
17	0.1100	0.0000	0.0000	0.0000	0.0000
18	0.1060	0.0000	0.0000	0.0000	0.0000
19	0.1030	0.0000	0.0000	0.0000	0.0000
20	0.1000	0.0000	0.0000	0.0000	0.0000
21	0.0950	0.0000	0.0000	0.0000	0.0000
22	0.0900	0.0000	0.0000	0.0000	0.0020
23	0.0850	0.0000	0.0000	0.0000	0.0040
24	0.0800	0.0000	0.0000	0.0000	0.0060
25	0.0750	0.0000	0.0000	0.0000	0.0080
26	0.0680	0.0000	0.0000	0.0000	0.0100
27	0.0600	0.0000	0.0000	0.0000	0.0100
28	0.0500	0.0000	0.0000	0.0000	0.0100
29	0.0400	0.0000	0.0000	0.0000	0.0100
30	0.0300	0.0000	0.0000	0.0000	0.0100
31	0.0200	0.0000	0.0000	0.0000	0.0100
32	0.0100	0.0000	0.0000	0.0000	0.0100
33	0.0050	0.0000	0.0000	0.0000	0.0100
34	0.0000	0.0000	0.0000	0.0000	0.0100
35	0.0000	0.0000	0.0000	0.0000	0.0100
36	0.0000	0.0000	0.0000	0.0000	0.0100
37	0.0000	0.0000	0.0000	0.0000	0.0100
38	0.0000	0.0000	0.0000	0.0000	0.0110
39	0.0000	0.0000	0.0000	0.0000	0.0120
40	0.0000	0.0000	0.0000	0.0000	0.0130
41	0.0000	0.0000	0.0000	0.0000	0.0140
42	0.0000	0.0000	0.0000	0.0000	0.0160
43	0.0000	0.0000	0.0000	0.0000	0.0190
44	0.0000	0.0000	0.0000	0.0000	0.0270
45	0.0000	0.0000	0.0000	0.0000	0.0400
46	0.0000	0.0000	0.0000	0.0000	0.0590
47	0.0000	0.0000	0.0000	0.0000	0.0870
48	0.0000	0.0000	0.0000	0.0000	0.1270
49	0.0000	0.0000	0.0000	0.0000	0.1870
50	0.0000	0.0000	0.0000	0.0000	4.7000

TABLE D.19 (CONT.) FIFTY GROUP CROSS SECTIONS FOR NICKEL

NICKFL						NI001
1.2998	1.4395	1.5399	1.6903	1.8203	1.9301	NI002
2.0495	2.0797	2.1379	2.1099	1.4208	1.3734	NI003
1.3803	1.4490	1.4700	1.5310	1.6000	1.6700	NI004
1.7720	1.8700	1.9560	2.0690	2.1260	2.2040	NI005
2.2200	2.2430	2.2770	2.3110	2.3510	2.3920	NI006
2.4610	2.5460	2.6450	2.8590			NI007
0.	0.	0.	0.	0.	0.	NI008
0.	0.	0.	0.	0.6390	0.6170	NI009
0.6200	0.6510	0.6600	0.6890	0.7200	0.7500	NI010
0.7950	0.8400	0.8790	0.9290	0.9550	0.9900	NI011
0.9970	1.0090	1.0230	1.0390	1.0590	1.0780	NI012
1.1090	1.1440	1.1900	0.			NI013
0.	0.	0.	0.	0.	0.	NI014
0.	0.	0.	0.	0.	0.	NI015
0.	0.	0.	0.	0.	0.	NI016
0.	0.	0.	0.	0.	0.	NI017
0.	0.	0.	0.	0.	0.	NI018
0.	0.	0.	0.			NI019
0.	0.	0.	0.	0.	0.	NI020
0.	0.	0.	0.	0.	0.	NI021
0.	0.	0.	0.	0.	0.	NI022
0.	0.	0.	0.	0.	0.	NI023
0.	0.	0.	0.	0.	0.	NI024
0.	0.	0.	0.			NI025
0.	0.	0.	0.	0.	0.	NI026
0.	0.	0.	0.	0.	0.	NI027
0.	0.	0.	0.	0.	0.	NI028
0.	0.	0.	0.	0.	0.	NI029
0.	0.	0.	0.	0.	0.	NI030
0.	0.	0.	0.			NI031
0.	0.	0.	0.	0.	0.	NI032
0.	0.	0.	0.	0.	0.	NI033
0.	0.	0.	0.	0.	0.	NI034
0.	0.	0.	0.	0.	0.	NI035
0.	0.	0.	0.	0.	0.	NI036

TABLE D.20 Nickel Nuclide Decks

0.	0.	0.	1.2810			NI037
1.0	1.0	1.0	1.0	1.0	1.0	NI038
1.0	1.0	1.0	1.0	0.88	0.81	NI039
0.76	0.69	0.63	0.60	0.58	0.55	NI040
0.52	0.49	0.47	0.45	0.43	0.41	NI041
0.39	0.37	0.35	0.32	0.30	0.27	NI042
0.25	0.23	0.21	0.19			NI043
0.05740	0.05505	0.06061	0.06428	0.06906		NI044
0.07216	0.07515	0.07732	0.07660	0.07412		NI045
0.07135	0.06769	0.06202	0.05191	0.		NI046
0.	0.05489	0.05303	0.05960	0.06252		NI047
0.06639	0.06851	0.07042	0.07147	0.06979		NI048
0.06651	0.06299	0.05873	0.05286	0.04342	0.	NI049
0.05795	0.05517	0.05931	0.06352	0.06898		NI050
0.07290	0.07682	0.08003	0.08035	0.07883		NI051
0.07701	0.07421	0.06912	0.05885	0.		NI052
0.	0.	0.05369	0.05223	0.05977		NI053
0.06193	0.06489	0.06605	0.06692	0.06688		NI054
0.06426	0.06020	0.05599	0.05122	0.04519	0.03635	NI055
0.05718	0.05406	0.05662	0.06116	0.06707		NI056
0.07160	0.07626	0.08035	0.08163	0.08109		NI057
0.08028	0.07845	0.07414	0.06412	0.		NI058
0.	0.	0.	0.05054	0.04946		NI059
0.05745	0.05870	0.06061	0.06073	0.06054		NI060
0.05946	0.05610	0.05156	0.04699	0.04207	0.03629	NI061
0.05636	0.05294	0.05390	0.05866	0.06489		NI062
0.06991	0.07517	0.08001	0.08216	0.08255		NI063
0.08271	0.08185	0.07838	0.06873	0.01931		NI064
0.01714	0.	0.	0.	0.04589		NI065
0.04513	0.05302	0.05334	0.05417	0.05335		NI066
0.05221	0.05031	0.04651	0.04185	0.03728	0.03259	NI067
0.05380	0.05025	0.04966	0.05439	0.06063		NI068
0.06587	0.07144	0.07674	0.07956	0.08075		NI069
0.08178	0.08186	0.07933	0.07044	0.03765		NI070
0.03300	0.02715	0.	0.	0.		NI071
0.04028	0.03972	0.04703	0.04651	0.04638		NI072
0.04481	0.04299	0.04055	0.03666	0.03222	0.02799	NI073

0.05169	0.04805	0.04602	0.05067	0.05688		NI074
0.06225	0.06804	0.07369	0.07707	0.07893		NI075
0.08072	0.08163	0.07996	0.07180	0.08340		NI076
0.07310	0.06490	0.	0.	0.		NI077
0.	0.03503	0.03454	0.04106	0.03985		NI078
0.03895	0.03684	0.03456	0.03185	0.02809	0.02405	NI079
0.04814	0.04456	0.04133	0.04569	0.05163		NI080
0.05688	0.06261	0.06831	0.07200	0.07435		NI081
0.07670	0.07829	0.07743	0.07023	0.13110		NI082
0.11495	0.10200	0.07797	0.	0.		NI083
0.	0.	0.02917	0.02867	0.03410		NI084
0.03240	0.03097	0.02861	0.02619	0.02351	0.02017	NI085
0.04510	0.04160	0.03735	0.04141	0.04705		NI086
0.05215	0.05777	0.06345	0.06735	0.07006		NI087
0.07285	0.07497	0.07479	0.06847	0.16020		NI088
0.14030	0.12470	0.12280	0.03270	0.		NI089
0.	0.	0.	0.02370	0.02316		NI090
0.02744	0.02547	0.02374	0.02137	0.01903	0.01660	NI091
0.04138	0.03808	0.03308	0.03674	0.04196		NI092
0.04676	0.05209	0.05756	0.06148	0.06438		NI093
0.06742	0.06991	0.07029	0.06488	0.15930		NI094
0.13970	0.12390	0.12200	0.20590	0.		NI095
0.	0.	0.	0.	0.01857		NI096
0.01796	0.02111	0.01908	0.01730	0.01512	0.01306	NI097
0.03762	0.03454	0.02904	0.03228	0.03703		NI098
0.04147	0.04643	0.05158	0.05541	0.05838		NI099
0.06152	0.06422	0.06503	0.06046	0.14000		NI100
0.12270	0.10890	0.10710	0.18460	0.		NI101
0.	0.	0.	0.	0.		NI102
0.01348	0.01285	0.01494	0.01311	0.01152	0.00974	NI103
0.03396	0.03111	0.02533	0.02815	0.03243		NI104
0.03648	0.04103	0.04580	0.04945	0.05237		NI105
0.05551	0.05829	0.05940	0.05559	0.11120		NI106
0.09750	0.08650	0.08520	0.10680	0.02680		NI107
0.	0.	0.	0.	0.		NI108
0.	0.00943	0.00882	0.01009	0.00857	0.00728	NI109
0.03100	0.02836	0.02236	0.02481	0.02869		NI110

0.03240	0.03659	0.04103	0.04451	0.04736		NI111
0.05046	0.05328	0.05460	0.05141	0.08270		NI112
0.07250	0.06435	0.06330	0.	0.03170		NI113
0.	0.	0.	0.	0.		NI114
0.	0.	0.00634	0.00580	0.00649	0.00532	NI115
0.02738	0.02501	0.01910	0.02115	0.02455		NI116
0.02782	0.03154	0.03550	0.03867	0.04133		NI117
0.04424	0.04694	0.04835	0.04577	0.05850		NI118
0.05120	0.04550	0.04480	0.	0.08020		NI119
0.	0.	0.	0.	0.		NI120
0.	0.	0.	0.00390	0.00347	0.00378	NI121
0.02416	0.02203	0.01631	0.01802	0.02097		NI122
0.02384	0.02711	0.03063	0.03349	0.03593		NI123
0.03862	0.04116	0.04259	0.04052	0.03975		NI124
0.03480	0.03092	0.03040	0.	0.08900		NI125
0.01120	0.	0.	0.	0.		NI126
0.	0.	0.	0.	0.00228	0.00196	NI127
0.01953	0.01779	0.01279	0.01408	0.01643		NI128
0.01873	0.02136	0.02421	0.02655	0.02859		NI129
0.03084	0.03299	0.03427	0.03274	0.02660		NI130
0.02330	0.02050	0.02040	0.	0.06230		NI131
0.01960	0.	0.	0.	0.		NI132
0.	0.	0.	0.	0.	0.00123	NI133
0.04455	0.04049	0.02767	0.03026	0.03545	0.04059	NI134
0.04650	0.05293	0.05833	0.06313	0.06847	0.07368	NI135
0.07700	0.07402	0.03560	0.03120	0.02770	0.02725	NI136
0.	0.11000	0.07600	0.	0.	0.	NI137
0.	0.	0.	0.	0.	0.	NI138
0.	0.	0.	0.			NI139
0.04019	0.03636	0.02269	0.02448	0.02884	0.03321	NI140
0.03828	0.04386	0.04868	0.05306	0.05799	0.06291	NI141
0.06631	0.06432	0.01500	0.01313	0.01167	0.01149	NI142
0.	0.	0.12030	0.03370	0.	0.	NI143
0.	0.	0.	0.	0.	0.	NI144
0.	0.	0.	0.			NI145
0.03309	0.02966	0.01616	0.01708	0.02024	0.02345	NI146
0.02719	0.03136	0.03504	0.03848	0.04238	0.04635	NI147

0.04927	0.04822	0.00169	0.00148	0.00131	0.00129	NI148
0.	0.	0.06290	0.05470	0.07350	0.	NI149
0.	0.	0.	0.	0.	0.	NI150
0.	0.	0.	0.			NI151
0.02354	0.02052	0.00792	0.00810	0.00966	0.01126	NI152
0.01315	0.01528	0.01720	0.01904	0.02115	0.02334	NI153
0.02504	0.02475	0.	0.	0.	0.	NI154
0.	0.	0.	0.06160	0.01650	0.	NI155
0.	0.	0.	0.	0.	0.	NI156
0.	0.	0.	0.			NI157
2.70000	2.86000	2.98000	3.15000	3.30000	3.43000	NI158
3.57000	3.62000	3.69000	3.65000	3.59000	3.50000	NI159
3.45000	3.39000	3.35000	3.30000	3.27000	3.24000	NI160
3.20000	3.21000	3.22000	3.24000	3.26000	3.28000	NI161
3.30000	3.33000	3.37000	3.41000	3.46000	3.51000	NI162
3.60000	3.71000	3.85000	4.15000			NI163

NICKEL						NI164
3.9950	0.4950	0.	0.	0.01137	4.5000	NI165
4.5195	0.3705	0.	0.	0.01137	4.9000	NI166
5.2633	0.2267	0.	0.	0.01137	5.5000	NI167
6.8425	0.3465	0.	0.	0.01137	7.2000	NI168
8.1718	0.2162	0.	0.	0.01137	8.4000	NI169
10.7981	0.1889	0.	0.	0.01137	11.0000	NI170
12.8905	0.3955	0.	0.	0.01137	13.3000	NI171
13.8590	0.4250	0.	0.	0.01137	14.3000	NI172
14.5355	0.4455	0.	0.	0.01137	15.0000	NI173
15.0125	0.4605	0.	0.	0.01137	15.5000	NI174
16.4550	0.5050	0.	0.	0.01137	17.0000	NI175
16.5330	0.5080	0.	0.	0.01137	17.1000	NI176
16.6030	0.5100	0.	0.	0.01137	17.2000	NI177
16.7585	0.5145	0.	0.	0.01137	17.4000	NI178
16.7975	0.5155	0.	0.	0.01137	17.5000	NI179
17.5000	0.	0.	0.0337	0.01137	22.2000	NI180

D. 12 MOLYBDENUM

a. High-Energy Cross Sections

Total Cross Section: Measurements of the total cross section in molybdenum have been made by Nerenson and Darden,[134] Bratenahl, Peterson, and Stoering,[135] McCallum, Mani, and Ferguson,[136] and Weil and Jones.[137] Of these the first three appear to be mutually consistent and in agreement with Hughes and Schwartz[52] and Howerton.[101b] The Hughes and Schwartz values are used.

Nonelastic Cross Section: Values of the nonelastic cross section are given by Walt and Barshall[130] at 1 Mev, by Hans and Snowden[138] at 37 Mev, and by Lebedev[139] at 14 Mev. Howerton includes measured values from an unidentified source at 1 Mev and 2.5 Mev and proposes an interpolated curve consistent with all the measurements except that at 14 Mev. The Lebedev result appears to be a bit low compared with the sum of the several discrete cross sections involved. The Howerton curve is used, except near 14 Mev where the values are obtained by interpolation.

Elastic Cross Section: The elastic cross section is obtained at all energies as the difference between the total and the nonelastic cross sections.

Radiative-Capture Cross Section: The Diven and Terrell data[140] with suitable extrapolation at the higher energies is used.

Proton Emission Cross Sections: Values of the (n, p) and (n, pn) cross sections at 14 Mev are given for natural molybdenum and for separated isotopes by Allen,[32] Colli et al.,[33] Gardner,[141] and Paul and Clarke.[142] The sum of the Colli measurements of $\sigma_{n,p}$ and $\sigma_{n,pn}$ is in good agreement with the Allen result if it is assumed that the latter is a proton emission cross section. Below 14 Mev the assumption is made that the effective threshold for proton emission is ~6 Mev corresponding to a mean Coulomb barrier of 5 Mev and a reaction Q value for (n, p) of -1 Mev, and suitable excitation functions for the (n, p) and (n, pn) reactions are interpolated.

Inelastic and (n, 2n) Cross Sections: Benveniste[132] gives a value of the (n, 2n) cross section at 14 Mev for natural molybdenum in reasonable agreement with the difference between the Lebedev nonelastic result and the sum of the Colli data. Values for the pure neutron emission cross section are obtained as the difference between the nonelastic cross section and the sum of the other nonelastic processes. Distinction between (n, n') and (n, 2n) is made within the framework of the statistical model above the (n, 2n) threshold. The particular characteristics of the semi-magic Mo^{92} isotope are averaged into natural molybdenum.

b. Low-Energy Cross Sections

Total Cross Section: Taken directly from Hughes and Schwartz, except in the energy region in which calculated absorption cross sections are used. In this region the total cross section is the sum of the elastic and the calculated absorption cross sections.

Nonelastic Cross Section: The nonelastic cross section used above the resonance

region is the sum of the Howerton (n, n') cross section and the Diven and Terrell (n, γ) cross sections. In the resonance region the nonelastic cross section is the calculated resonance cross section.

Elastic Cross Section: Outside of the resonance region the elastic cross section is the difference between total and nonelastic cross sections. In the resonance region the elastic cross section used is that lying between resonances in the Hughes and Schwartz total cross-section plot. The thermal cross section is that of Hughes and Schwartz.

Radiative-Capture Cross Section: The Diven and Terrell results are used where available. Below 1 kev equivalent absorptions are calculated by using the Doppler-broadened molybdenum resonance parameters tabulated by Devaney.[143] In the intermediate range approximate capture cross sections were obtained by interpolation between the calculated results and Diven and Terrell's data. Surface resonance capture weights were calculated by using the Devaney tabulations when available. Above 1 kev surface absorption was ignored. The thermal cross section is that of Hughes and Schwartz.

Inelastic Scattering Cross Section: The values plotted by Howerton for (n, n') events were assigned to the 200-kev level in molybdenum and used as such.

c. Neutron Nonelastic Spectra

The following assumptions have been made.

1. Reactions of the forms (n, 2n) and (n, n') proceed via formation of a compound nucleus. Spectra are characterized by the Lang-LeCouteur formulation, as are the relative magnitudes of $\sigma_{n,n'}$ and $\sigma_{n,2n}$. Absolute magnitudes of the pure neutron emission cross sections are taken from direct measurement when available, or are inferred from the nonelastic cross section.

2. Reactions of the form (n, pn) proceed by direct interaction to emit the primary proton followed by compound nucleus emission of the secondary neutron. The primary protons are assumed to carry off a nominal 3 Mev in kinetic energy; the remaining ($E+Q_{n,p}-3$) Mev is available as excitation energy for neutron emission.

3. Reactions of the form (n, p) may proceed by direct interaction in those cases in which the residual energy is insufficient for secondary neutron emission, or by compound nucleus formation when, regardless of the incident energy, insufficient residual excitation energy is available for secondary neutron emission. It is assumed that each emergent proton carries off a nominal 5 Mev, a compromise between the estimated 7-Mev Coulomb barrier for compound nucleus reactions and the estimated 3-Mev barrier associated with direct interactions.

In the range between 1.6 Mev and 2.2 Mev the asymptotic empirical model is used. From 0.65 Mev to 1.6 Mev the truncated model is applicable.

Below 0.65 Mev all inelastic scattering is associated with excitation of the 0.204-kev level.

	σ_{nT}	$\sigma_{n,n}$	$\sigma_{n,X}$	$\sigma_{n,2n}$	$\sigma_{n,n'}$
01	3.9839	2.3100	1.6739	1.5331	0.0000
02	4.1429	2.4700	1.6729	1.5214	0.0200
03	4.1737	2.5500	1.6237	1.4552	0.0480
04	4.3300	2.6400	1.6900	1.1916	0.3984
05	4.3700	2.6700	1.7000	0.4667	1.1533
06	4.3115	2.6000	1.7115	0.0000	1.6615
07	4.1621	2.4200	1.7421	0.0000	1.7121
08	4.0429	2.2100	1.8329	0.0000	1.8229
09	3.9040	1.9200	1.9840	0.0000	1.9840
10	3.8753	1.7900	2.0853	0.0000	2.0853
11	3.8567	1.7300	2.1267	0.0000	2.1267
12	3.8385	1.6700	2.1685	0.0000	2.1685
13	3.8806	1.6700	2.2106	0.0000	2.2106
14	3.9230	1.7100	2.2130	0.0000	2.2130
15	4.0155	1.8100	2.2055	0.0000	2.2055
16	4.2034	2.0300	2.1734	0.0000	2.1684
17	4.4114	2.3000	2.1114	0.0000	2.1014
18	4.6596	2.6000	2.0596	0.0000	2.0446
19	4.8580	2.9400	1.9180	0.0000	1.8990
20	5.1180	3.2900	1.8280	0.0000	1.8060
21	5.3670	3.6300	1.7370	0.0000	1.7130
22	5.6850	4.0600	1.6250	0.0000	1.5990
23	5.9240	4.3900	1.5340	0.0000	1.5060
24	6.2060	4.7700	1.4360	0.0000	1.4060
25	6.4530	5.1800	1.2730	0.0000	1.2410
26	6.7780	5.6500	1.1280	0.0000	1.0940
27	6.9880	6.0200	0.9680	0.0000	0.9330
28	7.1680	6.3500	0.8180	0.0000	0.7810
29	7.4290	6.7300	0.6990	0.0000	0.6600
30	7.6100	7.0400	0.5700	0.0000	0.5300
31	7.7920	7.3300	0.4620	0.0000	0.4200
32	8.0240	7.6300	0.3940	0.0000	0.3500
33	8.2050	7.8900	0.3150	0.0000	0.2700
34	8.3570	8.1100	0.2470	0.0000	0.2000
35	8.8020	8.6300	0.1720	0.0000	0.1200
36	9.0850	9.0000	0.0850	0.0000	0.0300
37	9.0620	9.0000	0.0620	0.0000	0.0000
38	8.3980	8.3300	0.0680	0.0000	0.0000
39	7.6970	7.6200	0.0770	0.0000	0.0000
40	6.7830	6.6900	0.0930	0.0000	0.0000
41	5.5620	5.4500	0.1120	0.0000	0.0000
42	5.1300	5.0000	0.1300	0.0000	0.0000
43	4.7020	4.5500	0.1520	0.0000	0.0000
44	4.6750	4.5000	0.1750	0.0000	0.0000
45	5.2240	5.0000	0.2240	0.0000	0.0000
46	6.9140	6.7000	0.2140	0.0000	0.0000
47	6.6490	6.4000	0.2490	0.0000	0.0000
48	5.6420	5.4000	0.2420	0.0000	0.0000
49	5.5200	5.4000	0.1200	0.0000	0.0000
50	7.5000	4.8000	2.7000	0.0000	0.0000

TABLE D.21 FIFTY GROUP NEUTRON CROSS SECTIONS FOR MOLYBDENUM

	$\sigma_{n,p}$	$\sigma_{n,pn}$	$\sigma_{n,\gamma}$	Surface
01	0.0300	0.1108	0.0000	0.0000
02	0.0700	0.0615	0.0000	0.0000
03	0.1000	0.0205	0.0000	0.0000
04	0.1000	0.0000	0.0000	0.0000
05	0.0800	0.0000	0.0000	0.0000
06	0.0500	0.0000	0.0000	0.0000
07	0.0300	0.0000	0.0000	0.0000
08	0.0100	0.0000	0.0000	0.0000
09	0.0000	0.0000	0.0000	0.0000
10	0.0000	0.0000	0.0000	0.0000
11	0.0000	0.0000	0.0000	0.0000
12	0.0000	0.0000	0.0000	0.0000
13	0.0000	0.0000	0.0000	0.0000
14	0.0000	0.0000	0.0000	0.0000
15	0.0000	0.0000	0.0000	0.0000
16	0.0000	0.0000	0.0050	0.0000
17	0.0000	0.0000	0.0100	0.0000
18	0.0000	0.0000	0.0150	0.0000
19	0.0000	0.0000	0.0190	0.0000
20	0.0000	0.0000	0.0220	0.0000
21	0.0000	0.0000	0.0240	0.0000
22	0.0000	0.0000	0.0260	0.0000
23	0.0000	0.0000	0.0280	0.0000
24	0.0000	0.0000	0.0300	0.0000
25	0.0000	0.0000	0.0320	0.0000
26	0.0000	0.0000	0.0340	0.0000
27	0.0000	0.0000	0.0350	0.0000
28	0.0000	0.0000	0.0370	0.0000
29	0.0000	0.0000	0.0390	0.0000
30	0.0000	0.0000	0.0400	0.0000
31	0.0000	0.0000	0.0420	0.0000
32	0.0000	0.0000	0.0440	0.0000
33	0.0000	0.0000	0.0450	0.0000
34	0.0000	0.0000	0.0470	0.0000
35	0.0000	0.0000	0.0520	0.0000
36	0.0000	0.0000	0.0550	0.0000
37	0.0000	0.0000	0.0620	0.0000
38	0.0000	0.0000	0.0680	0.0000
39	0.0000	0.0000	0.0770	0.0000
40	0.0000	0.0000	0.0930	0.0000
41	0.0000	0.0000	0.1120	0.0000
42	0.0000	0.0000	0.1300	0.0000
43	0.0000	0.0000	0.1520	0.0000
44	0.0000	0.0000	0.1750	0.00675
45	0.0000	0.0000	0.2240	0.01210
46	0.0000	0.0000	0.2140	0.01624
47	0.0000	0.0000	0.2490	0.02970
48	0.0000	0.0000	0.2420	0.02900
49	0.0000	0.0000	0.1200	0.0000
50	0.0000	0.0000	2.7000	0.0000

TABLE D.21 (CONT.) FIFTY GROUP CROSS SECTIONS FOR MOLYBDENUM

MOLYBDENUM4						MO001
2.310	2.470	2.550	2.640	2.670	2.600	MO002
2.420	2.210	1.920	1.790	1.654	1.545	MO003
1.517	1.536	1.612	1.792	2.016	2.266	MO004
2.549	2.836	3.115	3.467	3.734	4.041	MO005
4.375	4.754	5.046	5.306	5.601	5.849	MO006
6.071	6.300	6.499	6.656			MO007
0.0	0.0	0.0	0.0	0.0	0.0	MO008
0.0	0.0	0.0	0.0	0.076	0.125	MO009
0.158	0.174	0.198	0.238	0.284	0.334	MO010
0.391	0.454	0.515	0.593	0.656	0.729	MO011
0.805	0.896	0.974	1.044	1.129	1.191	MO012
1.259	1.330	1.391	0.0			MO013
0.0	0.0	0.0	0.0	0.0	0.0	MO014
0.0	0.0	0.0	0.0	0.0	0.0	MO015
0.0	0.0	0.0	0.0	0.0	0.0	MO016
0.0	0.0	0.0	0.0	0.0	0.0	MO017
0.0	0.0	0.0	0.0	0.0	0.0	MO018
0.0	0.0	0.0	0.0			MO019
0.0	0.0	0.0	0.0	0.0	0.0	MO020
0.0	0.0	0.0	0.0	0.0	0.0	MO021
0.0	0.0	0.0	0.0	0.0	0.0	MO022
0.0	0.0	0.0	0.0	0.0	0.0	MO023
0.0	0.0	0.0	0.0	0.0	0.0	MO024
0.0	0.0	0.0	0.0			MO025
0.0	0.0	0.0	0.0	0.0	0.0	MO026
0.0	0.0	0.0	0.0	0.0	0.0	MO027
0.0	0.0	0.0	0.0	0.0	0.0	MO028
0.0	0.0	0.0	0.0	0.0	0.0	MO029
0.0	0.0	0.0	0.0	0.0	0.0	MO030
0.0	0.0	0.0	0.0			MO031
0.0	0.0	0.0	0.0	0.0	0.0	MO032
0.0	0.0	0.0	0.0	0.0	0.0	MO033
0.0	0.0	0.0	0.0	0.0	0.0	MO034
0.0	0.0	0.0	0.0	0.0	0.0	MO035
0.0	0.0	0.0	0.0	0.0	0.0	MO036

TABLE D.22 Molybdenum Nuclide Decks

0.0	0.0	0.0	1.454			MO037
1.0	1.0	1.0	1.0	1.0	1.0	MO038
1.0	1.0	1.0	1.0	0.775	0.620	MO039
0.535	0.485	0.445	0.405	0.375	0.350	MO040
0.325	0.300	0.280	0.260	0.240	0.225	MO041
0.210	0.195	0.180	0.165	0.150	0.140	MO042
0.130	0.115	0.105	0.100			MO043
0.10826	0.10115	0.09268	0.07891	0.05415		MO044
0.05599	0.05217	0.04964	0.04773	0.04379		MO045
0.03841	0.03322	0.02836	0.02343	0.01897		MO046
0.01490	0.09271	0.08542	0.07700	0.06444		MO047
0.04342	0.04449	0.04052	0.03765	0.03529		MO048
0.03153	0.02689	0.02257	0.01868	0.01494	0.01169	MO049
0.12089	0.11434	0.10633	0.09195	0.06415		MO050
0.06652	0.06326	0.06153	0.06052	0.05688		MO051
0.05120	0.04549	0.03996	0.03401	0.02842		MO052
0.02307	0.01814	0.08023	0.07273	0.06438		MO053
0.05286	0.03490	0.03517	0.03124	0.02826		MO054
0.02576	0.02235	0.01847	0.01500	0.01199	0.00924	MO055
0.13077	0.12496	0.11775	0.10327	0.07313		MO056
0.07558	0.07322	0.07261	0.07291	0.07003		MO057
0.06451	0.05873	0.05291	0.04626	0.03976		MO058
0.03325	0.02699	0.02167	0.06577	0.05852		MO059
0.05074	0.04077	0.02631	0.02586	0.02233		MO060
0.01960	0.01731	0.01452	0.01158	0.00906	0.00697	MO061
0.14022	0.13513	0.12886	0.11444	0.08213		MO062
0.08415	0.08288	0.08366	0.08559	0.08382		MO063
0.07883	0.07337	0.06764	0.06058	0.05341		MO064
0.04588	0.03832	0.03171	0.01470	0.05118		MO065
0.04459	0.03779	0.02964	0.01865	0.01771		MO066
0.01481	0.01258	0.01072	0.00867	0.00665	0.00499	MO067
0.14470	0.14041	0.13532	0.12154	0.08829		MO068
0.08923	0.08922	0.09149	0.09518	0.09486		MO069
0.09091	0.08630	0.08122	0.07434	0.06706		MO070
0.05902	0.05057	0.04300	0.06550	0.06280		MO071
0.03787	0.03223	0.02664	0.02035	0.01245		MO072
0.01130	0.00913	0.00747	0.00613	0.00476	0.00349	MO073

0.14943	0.14580	0.14183	0.12867	0.09449		MO074
0.09379	0.09505	0.09888	0.10442	0.10574		MO075
0.10305	0.09959	0.09548	0.08912	0.08207		MO076
0.07382	0.06474	0.05640	0.14510	0.13910		MO077
0.13680	0.02722	0.02257	0.01815	0.01346		MO078
0.00798	0.00686	0.00533	0.00419	0.00329	0.00244	MO079
0.14886	0.14591	0.14309	0.13097	0.09713		MO080
0.09432	0.09675	0.10195	0.10914	0.11219		MO081
0.11092	0.10893	0.10620	0.10089	0.09464		MO082
0.08682	0.07774	0.06924	0.22820	0.21820		MO083
0.21520	0.21800	0.01833	0.01477	0.01151		MO084
0.00826	0.00473	0.00380	0.00283	0.00212	0.00159	MO085
0.14851	0.14611	0.14427	0.13310	0.09958		MO086
0.09426	0.09775	0.10420	0.11291	0.11747		MO087
0.11784	0.11741	0.11619	0.11214	0.10698		MO088
0.09988	0.09113	0.08278	0.27850	0.26700		MO089
0.26230	0.26630	0.29000	0.01176	0.00917		MO090
0.00691	0.00478	0.00264	0.00195	0.00138	0.00099	MO091
0.14462	0.14276	0.14178	0.13169	0.09931		MO092
0.09134	0.09566	0.10304	0.11289	0.11881		MO093
0.12066	0.12179	0.12218	0.11962	0.11584		MO094
0.10988	0.10197	0.09430	0.27730	0.26580		MO095
0.26100	0.26470	0.28870	0.33450	0.00796		MO096
0.00531	0.00385	0.00256	0.00135	0.00090	0.00061	MO097
0.13900	0.13765	0.13734	0.12832	0.09746		MO098
0.08685	0.09177	0.09978	0.11040	0.11740		MO099
0.12055	0.12310	0.12501	0.12397	0.12168		MO100
0.11708	0.11031	0.10365	0.24380	0.23360		MO101
0.2300	0.2325	0.2540	0.2938	0.3400		MO102
0.00382	0.00276	0.00191	0.00122	0.00061	0.00036	MO103
0.13221	0.13136	0.13153	0.12350	0.09440		MO104
0.08131	0.08660	0.09495	0.10599	0.11376		MO105
0.11798	0.12174	0.12499	0.12537	0.12456		MO106
0.12139	0.11594	0.11052	0.19380	0.18570		MO107
0.1824	0.1851	0.2018	0.2332	0.2700		MO108
0.32800	0.00193	0.00133	0.00088	0.00053	0.00025	MO109
0.12685	0.12647	0.12697	0.11972	0.09204		MO110

0.07643	0.08199	0.09058	0.10193	0.11032		MO111
0.11544	0.12026	0.12469	0.12639	0.12695		MO112
0.12517	0.12102	0.11687	0.14400	0.13810		MO113
0.1356	0.1375	0.1500	0.1735	0.2008		MO114
0.24380	0.29700	0.00090	0.00059	0.00037	0.00021	MO115
0.11745	0.11756	0.11823	0.11187	0.08646		MO116
0.06906	0.07457	0.08294	0.09401	0.10253		MO117
0.10816	0.11365	0.11889	0.12164	0.12339		MO118
0.12294	0.12021	0.11745	0.10190	0.09750		MO119
0.0958	0.0972	0.1060	0.1227	0.1420		MO120
0.17230	0.21000	0.25800	0.00037	0.00023	0.00014	MO121
0.10828	0.10885	0.10957	0.10398	0.08073		MO122
0.06194	0.06726	0.07528	0.08588	0.09430		MO123
0.10020	0.10608	0.11187	0.11542	0.11812		MO124
0.11879	0.11731	0.11582	0.06920	0.06620		MO125
0.0651	0.0660	0.0721	0.0834	0.0965		MO126
0.11710	0.14270	0.17510	0.22070	0.00014	0.00008	MO127
0.09109	0.09198	0.09262	0.08809	0.06867		MO128
0.05061	0.05524	0.06215	0.07129	0.07874		MO129
0.08419	0.08973	0.09527	0.09901	0.10210		MO130
0.10351	0.10309	0.10271	0.04630	0.04430		MO131
0.0436	0.0443	0.0483	0.0557	0.0645		MO132
0.07840	0.09560	0.11730	0.14800	0.17880	0.00005	MO133
0.22169	0.22577	0.22727	0.21679	0.17004	0.11645	MO134
0.12806	0.14524	0.16803	0.18725	0.20211	0.21758	MO135
0.23344	0.24529	0.25590	0.26264	0.26502	0.26770	MO136
0.0620	0.0595	0.0584	0.0593	0.0646	0.0746	MO137
0.0865	0.1050	0.1278	0.1572	0.1980	0.2390	MO138
0.420	0.275	0.0	0.0			MO139
0.22127	0.22906	0.23009	0.22023	0.17423	0.10368	MO140
0.11524	0.13220	0.15477	0.17466	0.19106	0.20861	MO141
0.22715	0.24241	0.25707	0.26843	0.27590	0.28414	MO142
0.0261	0.0250	0.0246	0.0250	0.02721	0.0315	MO143
0.0364	0.0440	0.0539	0.0660	0.0834	0.1008	MO144
0.0	0.075	0.270	0.172			MO145
0.20539	0.21732	0.21783	0.20921	0.16695	0.07964	MO146
0.08948	0.10382	0.12301	0.14057	0.15584	0.17257	MO147

0.19070	0.20670	0.22281	0.23672	0.24782	0.26021	MO148
0.0029	0.0028	0.0027	0.0028	0.0029	0.0035	MO149
0.0040	0.0049	0.0060	0.0074	0.0094	0.0113	MO150
0.0	0.0	0.0	0.028			MO151
0.17508	0.18995	0.19211	0.18626	0.15005	0.04198	MO152
0.04773	0.05607	0.06731	0.07799	0.08774	0.09869	MO153
0.11084	0.12221	0.13413	0.14523	0.15515	0.16642	MO154
0.0	0.0	0.0	0.0	0.0	0.0	MO155
0.0	0.0	0.0	0.0	0.0	0.0	MO156
0.0	0.0	0.0	0.0			MO157
3.9839	4.1429	4.1737	4.3300	4.3700	4.3115	MO158
4.1621	4.0429	3.9040	3.8750	3.8567	3.8385	MO159
3.8806	3.9230	4.0155	4.2034	4.4114	4.6596	MO160
4.8580	5.1180	5.3670	5.6850	5.9240	6.2060	MO161
6.4530	6.7780	6.9880	7.1680	7.4290	7.6100	MO162
7.7920	8.0240	8.2050	8.3570			MO163

MOLYBDENUM MO164

8.026	0.724	0.0	0.0	0.006948	8.802	MO165
8.569	0.446	0.012	0.003	0.006948	9.085	MO166
8.764	0.236	0.0	0.0	0.006948	9.062	MO167
8.076	0.254	0.0	0.0	0.006948	8.398	MO168
7.495	0.125	0.0	0.0	0.006948	7.697	MO169
6.617	0.073	0.0	0.0	0.006948	6.783	MO170
5.347	0.103	0.0	0.0	0.006948	5.562	MO171
4.906	0.094	0.0	0.0	0.006948	5.130	MO172
4.465	0.085	0.0	0.0	0.006948	4.702	MO173
4.416	0.084	0.0	0.0	0.006948	4.675	MO174
4.906	0.094	0.0	0.0	0.006948	5.224	MO175
6.574	0.126	0.0	0.0	0.006948	6.914	MO176
6.280	0.120	0.0	0.0	0.006948	6.649	MO177
5.299	0.101	0.0	0.0	0.006948	5.642	MO178
5.299	0.101	0.0	0.0	0.006948	5.520	MO179
4.800	0.0	0.0	0.0209	0.006948	7.500	MO180
0.	0.	0.	0.			MO SR 1
0.	0.	0.	0.			MO SR 2
0.	0.00675	0.01210	0.01624			MO SR 3
0.02970	0.02900	0.	0.			MO SR 4

D. 13 LEAD

a. High-Energy Cross Sections

Total Cross Section: Plotted in the energy range of interest by Hughes and Schwartz,[52] and by Howerton[138] with good agreement. The plotted values at ~14 Mev are in agreement with the measurements of Khaletskii,[78] Coon et al.,[77] and Goodman.[144] The values plotted by Weil and Jones[137] in the range 4-8 Mev are consistently higher than those of Hughes and Schwartz and of Howerton. (The same condition was noted in connection with the molybdenum cross sections.) The value given by Walt and Barschall[130] at 1 Mev is somewhat lower than that given by Hughes and Schwartz and by Howerton.

Nonelastic Cross Section: Plots of the nonelastic cross section above threshold are given by Hughes and Schwartz,[52] and Howerton[138] with good agreement. Values tabulated by Levedev[139] at 14 Mev, and by Pasechnik[118] at 14 Mev and 4.1 Mev are in good agreement with the plotted curves. Values given for 2.5 Mev by Pasechnik[118] and by Strizhak[116] are in mutual agreement, but are appreciably higher than the values plotted by Hughes and Schwartz and by Howerton.

Elastic Cross Section: The elastic cross section at all energies of interest is taken to be the difference between the total and nonelastic cross sections. The value tabulated by Walt and Barschall[130] at 1 Mev appears to be low.

Radiative Capture Cross Section: Diven and Terrell[119] give a value of 4 mb for the (n, γ) cross section at 0.4 Mev. The value is small enough that the reaction can be ignored.

Charged-Particle Emission Cross Sections: No reactions of the general type (n, x), where x denotes a charged particle, have been observed in lead for neutrons at energies of interest. Since there appears to be no discrepancy between the nonelastic cross section and the sum of the (n, 2n) and (n, n') cross sections, all charged-particle emission cross sections are neglected.

(n, 2n) Cross Section: Values of the (n, 2n) cross section at 14 Mev are tabulated by Benveniste[132] and Ashby et al.[108] with very good agreement. Statistical-model predictions of the (n, 2n) cross section, normalized to the measured value at 14 Mev, are used at energies below 14 Mev.

Inelastic Cross Section: The (n, n') cross section is taken to be the difference between the nonelastic and (n, 2n) cross sections. Gamma-production cross sections in the energy region from threshold to ~3 Mev are plotted by Hughes and Schwartz.[52] Various gamma-production cross sections at 3.2 Mev are tabulated by Scherrer, Allison, and Faust.[133] Using the Hughes and Schwartz and Scherrer et al. results as reference points, and assuming Gaussian excitation functions corresponding to the known levels in the several lead isotopes, we find that the inelastic cross section is resolved into a set of approximate excitation functions for the various levels lying below ~3 Mev.

b. Low-Energy Cross Sections

Total Cross Section: Plotted by Hughes and Schwartz[52] and by Howerton[138] with good agreement. Of the two, the Hughes and Schwartz plot is the more easily read and is used.

Nonelastic Cross Section: The only nonelastic reaction permitted energetically in the lower energy region is the (n, γ) reaction. Hence, the nonelastic cross section is identically the radiative-capture cross section.

Elastic Cross Section: Taken to be the difference between the total and the nonelastic cross sections in the lower energy region.

Radiative-Capture Cross Section: Hughes and Schwartz[52] give for the (n, γ) cross section at 0.025 ev a value of 170 mb. Diven and Terrell[119] give at 400 kev a value of 4 mb. Tattersall et al.[133] measured an effective resonance integral for lead equal within the limits of accuracy of the experiment to that expected for a pure v^{-1} cross section, thereby indicating that resonance absorption is very weak. The cross section is assumed v^{-1} at low energies, and is extrapolated to agree with the measured value at 400 kev.

c. Neutron Nonelastic Spectra

For incident neutron energies above 3.7 Mev, the multiple-particle statistical model is used to calculate (n, n') and $(n, 2n)$ spectra. For energies in the range 1.8-3.7 Mev scattering from Pb^{206} nuclei is treated by the statistical model, scattering from Pb^{207} and Pb^{208} nuclei, for which estimates of the excitation functions are available, by the isolated level model. From threshold to 1.8 Mev the isolated-level model is used exclusively.

	σ_{nT}	$\sigma_{n,n}$	$\sigma_{n,X}$	$\sigma_{n,2n}$	$\sigma_{n,\gamma}$
01	5.4600	2.8600	2.6000	2.5500	0.0000
02	5.3200	2.6900	2.6300	1.9000	0.0000
03	5.1600	2.5100	2.6500	1.5900	0.0000
04	5.1400	2.4600	2.6800	1.0600	0.0000
05	5.2300	2.6700	2.6600	0.5800	0.0000
06	5.4000	2.8000	2.6000	0.2600	0.0000
07	5.6800	3.2100	2.4700	0.0000	0.0000
08	6.0800	3.6700	2.4100	0.0000	0.0000
09	6.5100	4.1700	2.3400	0.0000	0.0000
10	6.9600	4.6800	2.2800	0.0000	0.0000
11	7.3600	5.1000	2.2600	0.0000	0.0000
12	7.6100	5.5000	2.1100	0.0000	0.0000
13	7.6200	5.7200	1.9000	0.0000	0.0000
14	7.4400	5.8100	1.6300	0.0000	0.0000
15	7.0700	5.6900	1.3800	0.0000	0.0000
16	6.4900	5.3200	1.1700	0.0000	0.0000
17	6.0700	4.9800	1.0900	0.0000	0.0000
18	5.7700	4.7300	1.0400	0.0000	0.0000
19	5.5700	4.5900	0.9800	0.0000	0.0000
20	5.4300	4.5800	0.8500	0.0000	0.0000
21	5.3600	4.6300	0.7300	0.0000	0.0000
22	5.3000	4.6800	0.6200	0.0000	0.0000
23	5.3500	4.8300	0.5200	0.0000	0.0000
24	5.5000	5.0600	0.4400	0.0000	0.0000
25	5.5500	5.1800	0.3700	0.0000	0.0000
26	6.0000	5.7000	0.3000	0.0000	0.0000
27	5.9500	5.6900	0.2600	0.0000	0.0000
28	5.7700	5.6100	0.1600	0.0000	0.0000
29	5.4500	5.3500	0.1000	0.0000	0.0000
30	5.6000	5.6000	0.0000	0.0000	0.0000
31	5.4500	5.4500	0.0000	0.0000	0.0000
32	6.0000	6.0000	0.0000	0.0000	0.0000
33	4.5000	4.5000	0.0000	0.0000	0.0000
34	5.4000	5.4000	0.0000	0.0000	0.0000
35	6.6000	6.5970	0.0030	0.0000	0.0030
36	7.4000	7.3960	0.0040	0.0000	0.0040
37	9.4000	9.3960	0.0040	0.0000	0.0040
38	10.5000	10.4950	0.0050	0.0000	0.0050
39	10.6000	10.5940	0.0060	0.0000	0.0060
40	10.7000	10.6930	0.0070	0.0000	0.0070
41	10.9000	10.8920	0.0080	0.0000	0.0080
42	11.0000	10.9910	0.0090	0.0000	0.0090
43	11.0200	11.0110	0.0090	0.0000	0.0090
44	11.0400	11.0300	0.0100	0.0000	0.0100
45	11.0600	11.0490	0.0110	0.0000	0.0110
46	11.0800	11.0680	0.0120	0.0000	0.0120
47	11.1000	11.0860	0.0140	0.0000	0.0140
48	11.1200	11.1040	0.0160	0.0000	0.0160
49	11.1400	11.1220	0.0180	0.0000	0.0180
50	11.0000	10.8300	0.1700	0.0000	0.1700

TABLE D.23 FIFTY GROUP NEUTRON CROSS SECTIONS FOR LEAD

	$\sigma_{n,n'}$ (statistical)	$\sigma_{n,n'}$ (3.20)	$\sigma_{n,n'}$ (2.71)	$\sigma_{n,n'}$ (2.61)	$\sigma_{n,n'}$ (2.34)
01	2.6000	0.0000	0.0000	0.0000	0.0000
02	2.6300	0.0000	0.0000	0.0000	0.0000
03	2.6500	0.0000	0.0000	0.0000	0.0000
04	2.6800	0.0000	0.0000	0.0000	0.0000
05	2.6600	0.0000	0.0000	0.0000	0.0000
06	2.6000	0.0000	0.0000	0.0000	0.0000
07	2.4700	0.0000	0.0000	0.0000	0.0000
08	2.4100	0.0000	0.0000	0.0000	0.0000
09	2.3400	0.0000	0.0000	0.0000	0.0000
10	2.2800	0.0000	0.0000	0.0000	0.0000
11	2.2600	0.0000	0.0000	0.0000	0.0000
12	2.1100	0.0000	0.0000	0.0000	0.0000
13	1.9000	0.0000	0.0000	0.0000	0.0000
14	1.0500	0.1996	0.2000	0.2001	0.0000
15	0.9500	0.0000	0.1149	0.2002	0.1151
16	0.8500	0.0000	0.0000	0.0483	0.2763
17	0.7100	0.0000	0.0000	0.0000	0.0500
18	0.5700	0.0000	0.0000	0.0000	0.0000
19	0.5100	0.0000	0.0000	0.0000	0.0000
20	0.4700	0.0000	0.0000	0.0000	0.0000
21	0.0000	0.0000	0.0000	0.0000	0.0000
22	0.0000	0.0000	0.0000	0.0000	0.0000
23	0.0000	0.0000	0.0000	0.0000	0.0000
24	0.0000	0.0000	0.0000	0.0000	0.0000
25	0.0000	0.0000	0.0000	0.0000	0.0000
26	0.0000	0.0000	0.0000	0.0000	0.0000
27	0.0000	0.0000	0.0000	0.0000	0.0000
28	0.0000	0.0000	0.0000	0.0000	0.0000
29	0.0000	0.0000	0.0000	0.0000	0.0000
30	0.0000	0.0000	0.0000	0.0000	0.0000
31	0.0000	0.0000	0.0000	0.0000	0.0000
32	0.0000	0.0000	0.0000	0.0000	0.0000
33	0.0000	0.0000	0.0000	0.0000	0.0000
34	0.0000	0.0000	0.0000	0.0000	0.0000
35	0.0000	0.0000	0.0000	0.0000	0.0000
36	0.0000	0.0000	0.0000	0.0000	0.0000
37	0.0000	0.0000	0.0000	0.0000	0.0000
38	0.0000	0.0000	0.0000	0.0000	0.0000
39	0.0000	0.0000	0.0000	0.0000	0.0000
40	0.0000	0.0000	0.0000	0.0000	0.0000
41	0.0000	0.0000	0.0000	0.0000	0.0000
42	0.0000	0.0000	0.0000	0.0000	0.0000
43	0.0000	0.0000	0.0000	0.0000	0.0000
44	0.0000	0.0000	0.0000	0.0000	0.0000
45	0.0000	0.0000	0.0000	0.0000	0.0000
46	0.0000	0.0000	0.0000	0.0000	0.0000
47	0.0000	0.0000	0.0000	0.0000	0.0000
48	0.0000	0.0000	0.0000	0.0000	0.0000
49	0.0000	0.0000	0.0000	0.0000	0.0000
50	0.0000	0.0000	0.0000	0.0000	0.0000

TABLE D.23 (CONT.) FIFTY GROUP CROSS SECTIONS FOR LEAD

	$\sigma_{n,n'}$ (1.63)	$\sigma_{n,n'}$ (1.40)	$\sigma_{n,n'}$ (1.10)	$\sigma_{n,n'}$ (0.88)	$\sigma_{n,n'}$ (0.80)
01	0.0000	0.0000	0.0000	0.0000	0.0000
02	0.0000	0.0000	0.0000	0.0000	0.0000
03	0.0000	0.0000	0.0000	0.0000	0.0000
04	0.0000	0.0000	0.0000	0.0000	0.0000
05	0.0000	0.0000	0.0000	0.0000	0.0000
06	0.0000	0.0000	0.0000	0.0000	0.0000
07	0.0000	0.0000	0.0000	0.0000	0.0000
08	0.0000	0.0000	0.0000	0.0000	0.0000
09	0.0000	0.0000	0.0000	0.0000	0.0000
10	0.0000	0.0000	0.0000	0.0000	0.0000
11	0.0000	0.0000	0.0000	0.0000	0.0000
12	0.0000	0.0000	0.0000	0.0000	0.0000
13	0.0000	0.0000	0.0000	0.0000	0.0000
14	0.0000	0.0000	0.0000	0.0000	0.0000
15	0.0000	0.0000	0.0000	0.0000	0.0000
16	0.0000	0.0000	0.0000	0.0000	0.0000
17	0.3300	0.0000	0.0000	0.0000	0.0000
18	0.4701	0.0000	0.0000	0.0000	0.0000
19	0.5103	0.0000	0.0000	0.0000	0.0000
20	0.2902	0.0000	0.0000	0.0900	0.0000
21	0.0000	0.0950	0.1908	0.3511	0.0949
22	$\sigma_{n,n'}$ (0.57)	0.0000	0.1397	0.3389	0.1409
23	0.0703	0.0000	0.0606	0.2500	0.1400
24	0.1893	0.0000	0.0000	0.1300	0.1198
25	0.2076	0.0000	0.0000	0.0400	0.0500
26	0.3001	0.0000	0.0000	0.0000	0.0000
27	0.2600	0.0000	0.0000	0.0000	0.0000
28	0.1600	0.0000	0.0000	0.0000	0.0000
29	0.1000	0.0000	0.0000	0.0000	0.0000
30	0.0000	0.0000	0.0000	0.0000	0.0000
31	0.0000	0.0000	0.0000	0.0000	0.0000
32	0.0000	0.0000	0.0000	0.0000	0.0000
33	0.0000	0.0000	0.0000	0.0000	0.0000
34	0.0000	0.0000	0.0000	0.0000	0.0000
35	0.0000	0.0000	0.0000	0.0000	0.0000
36	0.0000	0.0000	0.0000	0.0000	0.0000
37	0.0000	0.0000	0.0000	0.0000	0.0000
38	0.0000	0.0000	0.0000	0.0000	0.0000
39	0.0000	0.0000	0.0000	0.0000	0.0000
40	0.0000	0.0000	0.0000	0.0000	0.0000
41	0.0000	0.0000	0.0000	0.0000	0.0000
42	0.0000	0.0000	0.0000	0.0000	0.0000
43	0.0000	0.0000	0.0000	0.0000	0.0000
44	0.0000	0.0000	0.0000	0.0000	0.0000
45	0.0000	0.0000	0.0000	0.0000	0.0000
46	0.0000	0.0000	0.0000	0.0000	0.0000
47	0.0000	0.0000	0.0000	0.0000	0.0000
48	0.0000	0.0000	0.0000	0.0000	0.0000
49	0.0000	0.0000	0.0000	0.0000	0.0000
50	0.0000	0.0000	0.0000	0.0000	0.0000

TABLE D.23 %CONT.% FIFTY GROUP CROSS SECTIONS FOR LEAD

LEAD						PB001
2.86	2.69	2.51	2.46	2.67	2.80	PB002
3.21	3.67	4.17	4.68	5.10	5.50	PB003
5.72	5.81	5.69	5.32	4.98	4.73	PB004
4.59	4.58	4.63	4.68	4.83	5.06	PB005
5.18	5.70	5.69	5.61	5.35	5.60	PB006
5.45	6.00	4.50	5.40			PB007
0.0	0.0	0.0	0.0	0.0	0.0	PB008
0.0	0.0	0.0	0.0	0.0	0.0	PB009
0.0	0.0	0.0	0.0	0.0	0.0	PB010
0.0	0.0	0.0	0.0	0.0	0.0	PB011
0.0	0.0	0.0	0.0	0.0	0.0	PB012
0.0	0.0	0.0	0.0			PB013
0.0	0.0	0.0	0.0	0.0	0.0	PB014
0.0	0.0	0.0	0.0	0.0	0.0	PB015
0.0	0.0	0.0	0.0	0.0	0.0	PB016
0.0	0.0	0.0	0.0	0.0	0.0	PB017
0.0	0.0	0.0	0.0	0.0	0.0	PB018
0.0	0.0	0.0	0.0			PB019
0.0	0.0	0.0	0.0	0.0	0.0	PB020
0.0	0.0	0.0	0.0	0.0	0.0	PB021
0.0	0.0	0.0	0.0	0.0	0.0	PB022
0.0	0.0	0.0	0.0	0.0	0.0	PB023
0.0	0.0	0.0	0.0	0.0	0.0	PB024
0.0	0.0	0.0	0.0			PB025
0.0	0.0	0.0	0.0	0.0	0.0	PB026
0.0	0.0	0.0	0.0	0.0	0.0	PB027
0.0	0.0	0.0	0.0	0.0	0.0	PB028
0.0	0.0	0.0	0.0	0.0	0.0	PB029
0.0	0.0	0.0	0.0	0.0	0.0	PB030
0.0	0.0	0.0	0.0			PB031
0.0	0.0	0.0	0.0	0.0	0.0	PB032
0.0	0.0	0.0	0.0	0.0	0.0	PB033
0.0	0.0	0.0	0.0	0.0	0.0	PB034
0.0	0.0	0.0	0.0	0.0	0.0	PB035
0.0	0.0	0.0	0.0	0.0	0.0	PB036

TABLE D.24 Lead Nuclide Decks

0.0	0.0	0.0	0.0			PB037
1.0	1.0	1.0	1.0	1.0	1.0	PB038
1.0	1.0	1.0	1.0	0.80	0.695	PB039
0.630	0.580	0.540	0.505	0.478	0.449	PB040
0.421	0.393	0.367	0.335	0.310	0.285	PB041
0.265	0.242	0.225	0.206	0.190	0.175	PB042
0.160	0.145	0.130	0.120			PB043
0.2270	0.2190	0.2060	0.1850	0.1500		PB044
0.1005	0.0974	0.0865	0.0772	0.0666		PB045
0.0589	0.0481	0.0375	0.01780	0.01337		PB046
0.01022	0.2100	0.2100	0.1880	0.1669		PB047
0.1325	0.0876	0.0800	0.0704	0.0609		PB048
0.0526	0.0452	0.0356	0.0259	0.01253	0.00909	PB049
0.2400	0.2320	0.2221	0.2035	0.1660		PB050
0.1119	0.1102	0.1012	0.0913	0.0821		PB051
0.0736	0.0620	0.0494	0.02405	0.01869		PB052
0.01451	0.01020	0.1901	0.1800	0.1650		PB053
0.1462	0.1120	0.0734	0.0642	0.0571		PB054
0.0468	0.0387	0.0324	0.0236	0.01837	0.00744	PB055
0.2460	0.2420	0.2342	0.2162	0.1779		PB056
0.1210	0.1230	0.1141	0.1059	0.0958		PB057
0.0866	0.0755	0.0619	0.0306	0.0244		PB058
0.01975	0.01394	0.00972	0.1710	0.1577		PB059
0.1438	0.1179	0.0978	0.0597	0.0496		PB060
0.0412	0.0336	0.0275	0.0223	0.01658	0.01171	PB061
0.2475	0.2460	0.2395	0.2238	0.1860		PB062
0.1280	0.1319	0.1244	0.1163	0.1087		PB063
0.1007	0.0890	0.0741	0.0375	0.0306		PB064
0.0250	0.01847	0.01320	0.01027	0.1450		PB065
0.1318	0.1186	0.0995	0.0775	0.0471		PB066
0.0358	0.02935	0.0234	0.01840	0.01437	0.01034	PB067
0.2465	0.2480	0.2430	0.2285	0.1921		PB068
0.1342	0.1380	0.1331	0.1263	0.1182		PB069
0.1130	0.0998	0.0854	0.0443	0.0366		PB070
0.0307	0.0232	0.01685	0.01345	0.01100		PB071
0.1191	0.1070	0.0932	0.0770	0.0570		PB072
0.0344	0.0242	0.01909	0.01463	0.01110	0.00845	PB073

0.2435	0.2460	0.2420	0.2305	0.1937		PB074
0.1367	0.1412	0.1370	0.1309	0.1267		PB075
0.1217	0.1095	0.0946	0.0841	0.0455		PB076
0.0360	0.1302	0.02065	0.01685	0.0365		PB077
0.0	0.0952	0.0831	0.0720	0.0583		PB078
0.0418	0.0249	0.01550	0.01170	0.00880	0.00645	PB079
0.2345	0.2380	0.2370	0.2280	0.1929		PB080
0.1370	0.1412	0.1383	0.1342	0.1294		PB081
0.1254	0.1175	0.1021	0.1398	0.0902		PB082
0.0406	0.1590	0.0242	0.02022	0.0652		PB083
0.0224	0.0	0.0718	0.0629	0.0522		PB084
0.0412	0.0293	0.01670	0.00919	0.00678	0.00479	PB085
0.2220	0.2280	0.2275	0.2193	0.1889		PB086
0.1352	0.1362	0.1352	0.1333	0.1297		PB087
0.1286	0.1196	0.1063	0.1696	0.0889		PB088
0.0441	0.1354	0.0271	0.0230	0.0390		PB089
0.1480	0.0	0.0148	0.0538	0.0444		PB090
0.0364	0.0274	0.01880	0.01061	0.00506	0.0035	PB091
0.2080	0.2120	0.2130	0.2070	0.1791		PB092
0.1289	0.1290	0.1282	0.1277	0.1261		PB093
0.1262	0.1189	0.1061	0.1574	0.0995		PB094
0.0460	0.0372	0.2024	0.0252	0.02205		PB095
0.1857	0.0376	0.0407	0.0	0.0367		PB096
0.0296	0.0240	0.01750	0.01162	0.00640	0.00252	PB097
0.1940	0.1998	0.2020	0.1975	0.1708		PB098
0.1232	0.1218	0.1220	0.1222	0.1219		PB099
0.1230	0.1182	0.1060	0.1044	0.0986		PB100
0.1145	0.0389	0.1870	0.0271	0.02415		PB101
0.0899	0.1640	0.0148	0.0485	0.0		PB102
0.0234	0.0193	0.01458	0.01033	0.00658	0.00344	PB103
0.1801	0.1870	0.1892	0.1858	0.1612		PB104
0.1180	0.1129	0.1146	0.1156	0.1159		PB105
0.1183	0.1130	0.1041	0.0827	0.0942		PB106
0.1481	0.0398	0.1729	0.0284	0.02565		PB107
0.0696	0.1808	0.0400	0.0993	0.0		PB108
0.0	0.01452	0.01118	0.00827	0.00565	0.00350	PB109
0.1674	0.1740	0.1773	0.1741	0.1523		PB110

0.1119	0.1041	0.1049	0.1078	0.1091		PB111
0.1122	0.1081	0.1005	0.0565	0.1121		PB112
0.1024	0.0399	0.0324	0.1611	0.0266		PB113
0.0631	0.0974	0.1280	0.0415	0.0770		PB114
0.0	0.0	0.00827	0.00608	0.00437	0.00288.	PB115
0.1522	0.1602	0.1647	0.1620	0.1417		PB116
0.1047	0.0947	0.0971	0.1013	0.1039		PB117
0.1043	0.1019	0.0948	0.0860	0.1047		PB118
0.0959	0.0392	0.0327	0.1485	0.0270		PB119
0.0571	0.0	0.1370	0.0	0.1330		PB120
0.0722	0.0	0.0	0.00442	0.00310	0.00214	PB121
0.1381	0.1452	0.1490	0.1478	0.1303		PB122
0.0958	0.0838	0.0867	0.0890	0.0917		PB123
0.0953	0.0934	0.0879	0.0790	0.0957		PB124
0.0881	0.0373	0.0308	0.1353	0.0264		PB125
0.0	0.0435	0.0850	0.0425	0.0676		PB126
0.1418	0.0	0.0	0.0	0.00210	0.00157	PB127
0.1249	0.1313	0.1348	0.1340	0.1222		PB128
0.0874	0.0741	0.0771	0.0794	0.0819		PB129
0.0854	0.0842	0.0798	0.0719	0.0552		PB130
0.0478	0.0349	0.0292	0.1225	0.0253		PB131
0.0	0.0390	0.0	0.0608	0.0		PB132
0.0861	0.0	0.0	0.0	0.0	0.000942	PB133
0.2705	0.287	0.295	0.296	0.261	0.1950	PB134
0.1551	0.1621	0.1680	0.1749	0.1848	0.1832	PB135
0.1754	0.1584	0.1339	0.1067	0.0976	0.0657	PB136
0.1195	0.1462	0.0475	0.0572	0.0191	0.1138	PB137
0.0250	0.0	0.260	0.0	0.0	0.0	PB138
0.0	0.0	0.0	0.0			PB139
0.2600	0.2775	0.2925	0.289	0.2575	0.1933	PB140
0.1355	0.1431	0.1499	0.1581	0.1688	0.1700	PB141
0.1643	0.1535	0.0945	0.1059	0.0968	0.0662	PB142
0.0655	0.2069	0.0475	0.0	0.0409	0.0127	PB143
0.0583	0.0	0.0	0.160	0.0	0.0	PB144
0.0	0.0	0.0	0.0			PB145
0.2340	0.252	0.262	0.266	0.236	0.1804	PB146
0.1026	0.1092	0.1159	0.1236	0.1329	0.1358	PB147

0.1330	0.0797	0.0787	0.0845	0.0821	0.0593	PB148
0.0575	0.1173	0.0	0.0	0.0	0.0	PB149
0.0067	0.0	0.0	0.0	0.100	0.0	PB150
0.0	0.0	0.0	0.0			PB151
0.1950	0.1780	0.1857	0.2275	0.206	0.1303	PB152
0.0534	0.0569	0.0613	0.0550	0.0727	0.0747	PB153
0.0746	0.0454	0.0453	0.0441	0.0411	0.0360	PB154
0.0357	0.0360	0.0	0.0	0.0	0.0	PB155
0.0	0.0	0.0	0.0	0.0	0.0	PB156
0.0	0.0	0.0	0.0			PB157
5.46	5.32	5.16	5.14	5.23	5.40	PB158
5.68	6.08	6.51	6.96	7.36	7.61	PB159
7.62	7.44	7.07	6.49	6.07	5.77	PB160
5.57	5.43	5.36	5.30	5.35	5.50	PB161
5.55	6.00	5.95	5.77	5.45	5.60	PB162
5.45	6.00	4.50	5.40			PB163

LEAD PB164

6.288	0.309	0.0	0.0	0.003218	6.600	PB165
7.158	0.238	0.0	0.0	0.003218	7.400	PB166
9.231	0.165	0.0	0.0	0.003218	9.400	PB167
10.281	0.214	0.0	0.0	0.003218	10.500	PB168
10.478	0.116	0.0	0.0	0.003218	10.600	PB169
10.615	0.078	0.0	0.0	0.003218	10.700	PB170
10.755	0.137	0.0	0.0	0.003218	10.900	PB171
10.852	0.139	0.0	0.0	0.003218	11.000	PB172
10.872	0.139	0.0	0.0	0.003218	11.020	PB173
10.891	0.139	0.0	0.0	0.003218	11.040	PB174
10.909	0.140	0.0	0.0	0.003218	11.060	PB175
10.928	0.140	0.0	0.0	0.003218	11.080	PB176
10.946	0.140	0.0	0.0	0.003218	11.100	PB177
10.963	0.141	0.0	0.0	0.003218	11.120	PB178
10.981	0.141	0.0	0.0	0.003218	11.140	PB179
11.000	0.0	0.0	0.0096	0.003218	11.170	PB180

Acknowledgment

The author wishes to acknowledge the contributions to this study made by Professors David J. Rose, Irving Kaplan, Kent F. Hansen, and Melville Clark, Jr. of the Department of Nuclear Engineering, M. I. T. Professor Rose conceived the need for an engineering evaluation of proposed fusion reactors and formulated the blanket problem. Professor Kaplan guided the nuclear calculations and, with Professor Rose, supervised the thesis research. Professors Hansen and Clark elucidated numerous points in neutron transport theory and numerical analysis.

Acknowledgment is due also to contributions of William G. Homeyer who pursued the parallel study of nuclear heating and heat removal in fusion reactor blankets and whose continued aid, guidance and support were major factors in the completion of this work. Laszlo N. Lontai contributed materially to this study through his analysis of the effects of fission in fusion blankets and his assistance in developing the resonance absorption model. Much benefit was also gained from extensive discussions of all aspects of the problem with other members of the Plasma Electronics Group of the Research Laboratory of Electronics, M. I. T.

Preliminary development of the computer codes was accomplished to a large extent through the cooperation of the Systems Laboratory of the Department of Civil Engineering, M. I. T. Final code preparation and production calculations were carried out at the Computation Center, M. I. T.

The author received support during the early stages of his research through the United States Atomic Energy Commission Fellowship Program.

References

1. W. G. Homeyer, Sc. D. Thesis, Department of Nuclear Engineering, Massachusetts Institute of Technology, 1963; see also Technical Report 435, Research Laboratory of Electronics, M. I. T., Cambridge, Mass., June 29, 1965.
2. P. Spangler, Sc. D. Thesis, Department of Nuclear Engineering, Massachusetts Institute of Technology, 1963; see also Technical Report 437, Research Laboratory of Electronics, M. I. T., Cambridge, Mass., July 13, 1965.
3. L. G. Barrett, KAPL-M-LGB-14 (1957).
4. P. Powell, LWS 24920 (1953).
5. L. N. Lontai, S. M. Thesis, Department of Nuclear Engineering, Massachusetts Institute of Technology, 1963; see also Technical Report 436, Research Laboratory of Electronics, M. I. T., Cambridge, Mass., July 6, 1965.
6. David J. Rose and Melville Clark, Jr., Plasmas and Controlled Fusion (The M. I. T. Press, Cambridge, Mass., and John Wiley and Sons, Inc., New York, 1961).
7. D. J. Rose, W. G. Homeyer, A. J. Impink, Jr., and P. S. Spangler (unpublished material, 1962).
8. R. F. Post, Paper CN-10/153, Third United Nations Conference on Peaceful Uses of Atomic Energy (Salzburg, 1961).
9. W. G. Homeyer, Sc. D. Thesis, Department of Nuclear Engineering, M. I. T., 1963.
10. W. G. Homeyer, A. J. Impink, Jr., D. J. Rose, and I. Kaplan, Quarterly Progress Report No. 62, Research Laboratory of Electronics, M. I. T., Cambridge, Mass., July 15, 1961, p. 64.
11. L. Spitzer, Jr., D. J. Grove, W. E. Johnson, L. Tonks, and W. G. Westendorp, NYO 6047 (1954).
12. E. P. Johnson, NYO 7900 (1957).
13. N. C. Christofilos, N. W. Cook, W. B. Myers, C. E. Taylor, and W. M. Wells, TID 7558, Suppl. 1 (1960), p. 18.
14. P. R. Bell, J. S. Luce, R. H. Makin, Jr., E. D. Shipley, and A. Simon (eds.), ORNL 2457 (1958), pp. 77-78.
15. Ibid., loc. cit.
16. W. G. Homeyer and A. J. Impink, Jr., Quarterly Progress Report No. 64, Research Laboratory of Electronics, M. I. T., Cambridge, Mass., January 15, 1962, p. 128.
17. W. G. Homeyer, A. J. Impink, Jr., and D. J. Rose, Quarterly Progress Report No. 66, Research Laboratory of Electronics, M. I. T., Cambridge, Mass., July 15, 1962, p. 142.
18. B. R. S. Buckingham, N. Parker, and E. D. Pendlebury, AWRE, O-28/60 (1960).
19. V. F. Weisskopf, Phys. Rev. 52, 295 (1937).
20. I. Frenkel, Soviet Phys. 9, 533 (1936).
21. V. F. Weisskopf and D. H. Ewing, Phys. Rev. 57, 472 (1940).
22. B. T. Feld, H. Feshbach, M. L. Goldberger, H. Goldstein, and V. F. Weisskopf, NYO-636 (1951).
23. K. J. LeCouteur, Proc. Phys. Soc. (London) A65, 718 (1952).
24. J. M. B. Lang and K. J. LeCouteur, Proc. Phys. Soc. (London) A67, 586 (1954).
25. J. M. B. Lang, Proc. Phys. Soc. (London) A65, 995 (1952).
26. E. R. Graves and L. Rosen, Phys. Rev. 89, 343 (1953).
27. Iu. S. Zamyatnin, E. K. Gutnihova, N. I. Ivanova, and I. N. Safina, Atomnaya Energiya 3, 540 (1957); J. Nucl. Energy II, 9, 41 (1959).

28. J. T. Prud'homme, I. L. Morgan, J. H. McCrary, J. B. Ashe, and O. M. Hudson, Jr., SWC-TR, 60-30 (1960).

29. P. C. Gugelot, Phys. Rev. 81, 51 (1951).

30. D. L. Allen, Nucl. Phys. 6, 464 (1958).

31. D. L. Allen, Proc. Phys. Soc. (London) A70, 195 (1957).

32. D. L. Allen, Nucl. Phys. 24, 274 (1961).

33. L. Colli, U. Facchine, J. Iori, M. G. Marcazzan, and A. M. Sona, Nuovo Cimento 13, 730 (1959).

34. E. Weigold and R. N. Glover, Nucl. Phys. 32, 106 (1962).

35. P. Strohal, N. Cindro, and B. Eman, Nucl. Phys. 30, 49 (1962).

36. J. Thomson and L. Cranberg, WASH 1028 (1960).

37. F. B. Hildebrand, Advanced Calculus for Engineers (McGraw-Hill Book Company, New York, 1961).

38. B. O. Peirce, A Short Table of Integrals (Ginn and Company, Boston, 1929).

39. D. J. Hughes and R. S. Carter, BNL 400 (1956).

40. H. A. Gerardo, XOC, 61-3-131 (1961).

41. F. Bjorklund and S. Fernbach, UCRL 4926T (1957).

42. F. Bjorklund and S. Fernbach, UCRL 4927T (1957).

43. B. Carlson, LA-1891 (1955).

44. R. S. Varga, WAPD-159 (1956); Trans. IRE on Nuclear Science 4 (1957).

45. G. G. Bilodeau, WAPD-TM-52 (1957).

46. P. G. Fischer, XDC 60-3-38 (1960).

47. P. G. Fischer, F. D. Wenstrup, and T. A. Hoffman, APEX 702 (1961).

48. L. V. Spencer and U. Fano, Phys. Rev. 81, 414L (1951).

49. L. V. Spencer and U. Fano, J. Research Nat. Bur. Standards 46, 446 (1951).

50. J. Certaine, In three parts: I-NYO 3081 (1954); II-NYO 6268 (1955); III-NYO 6270 (1956).

51. E. P. Wigner, E. Creutz, H. Jupnik, and T. Snyder, J. Appl. Phys. 26, 260 (1955).

52. D. J. Hughes and R. B. Schwartz, BNL-325 (Second edition, 1958).

53. H. Goldstein, Fundamental Aspects of Reactor Shielding (Addison-Wesley Press, Reading, Mass., 1959).

54. A. M. Weinberg and E. P. Wigner, The Physical Theory of Neutron Chain Reactors (University of Chicago Press, Chicago, Ill., 1958).

55. S. P. Belov, V. A. Dulin, Iu. A. Kazanskii, V. F. Kukhtevich, and S. G. Tsipin, Atomnaya Energiya 6, 663 (1959); J. Nucl. Energy, Part A, 13, 78 (1960).

56. D. L. Broder, A. A. Kutuzov, V. V. Levin, V. V. Orlov, and A. V. Turusova, Atomnaya Energiya 7, 313 (1959); J. Nucl. Energy, Part A, 13, 65 (1960).

57. A. T. G. Ferguson, US/UK Fast Reactor Data Conference, Harwell, September 26-27, 1960.

58. J. W. Weale, US/UK Fast Reactor Data Conference, Harwell, September 26-27, 1960.

59. J. W. Weale, H. Goodfellow, M. H. McTaggart, and M. L. Mullenden, J. Nucl. Energy, Part A, 14, 91 (1961).

60. Z. Dlougy, Atomnaya Energiya 9, 182 (1960).

61. R. S. Caswell, R. F. Gabbard, D. W. Padgett, and W. D. Doering, Nucl. Sci. Engr. 2, 143 (1957).

62. Iu. S. Zamyatnin, N. I. Ivanova, and J. N. Safina, Atomnaya Energiya 6, 466 (1959); J. Nucl. Energy 12, 83 (1960).
63. D. L. Allen, J. Nucl. Energy, Part A, 14, 100 (1961).
64. G. K. O'Neill, Phys. Rev. 95, 1235 (1954).
65. H. Goldstein, J. G. Sullivan, Jr., R. R. Coveyou, W. E. Kinney, and R. R. Bate, ORNL 2639 (1961).
66. W. B. Myers, W. N. Wells, and E. H. Canfield, UCID-4480 (May 22, 1962).
67. R. Shev and S. Moore, BNL-672 (1961), p. 5.
68. R. J. Howerton, UCRL 5351 (1958).
69. A. Prince, XDC 60-11-164 (1960).
70. V. M. Gorbachev and L. B. Poretsky, Atomnaya Energiya 4, 191 (1958); J. Nucl. Energy 9, 159 (1958).
71. L. Rosen and L. Stewart, LA-2643 (1956).
72. L. Armstrong, LA-1672 (1954).
73. F. Ajzenberg-Selove and T. Lauritsen, Nucl. Phys. 11, 1 (1959).
74. M. E. Battat and F. L. Ribe, Phys. Rev. 89, 80 (1953).
75. G. M. Frye, Phys. Rev. 93, 1086 (1954).
76. C. F. Cook and T. W. Bonner, Phys. Rev. 92, 651 (1954).
77. J. H. Coon, E. R. Graves, and H. H. Barschall, Phys. Rev. 88, 562 (1952).
78. M. M. Khaletshii, Soviet Phys. – Doklady 2, 129 (1957).
79. K. Parker, AWRE O-27/60 (1960).
80. D. B. Fossan, R. L. Walker, W. E. Wilson, and H. H. Barschall, Phys. Rev. 123, 209 (1961).
81. J. S. Levin and L. Cranberg, WASH 1028 (1960), p. 26; see also WASH 1029 (1960), p. 44.
82. J. B. Marion, J. S. Levin, and L. Cranberg, Phys. Rev. 114, 1524 (1959).
83. M. H. MacGregor, W. P. Ball, and R. Booth, Phys. Rev. 108, 726 (1957).
84. W. P. Ball, M. H. MacGregor, and R. Booth, Phys. Rev. 110, 1392 (1957).
85. L. Rosen and L. Stewart, Phys. Rev. 107, 824 (1957).
86. S. S. Vasil'ov, V. V. Komaron, and A. M. Popova, Soviet Phys. – Doklady 3, 354 (1958).
87. P. H. Stetson and E. C. Cambell, Phys. Rev. 106, 1252 (1957).
88. R. Baas, T. W. Bonner, and H. H. D. Haenni, Nuclear Phys. 23, 122 (1961).
89. H. C. Catron, M. D. Goldberg, R. W. Hill, J. M. Leblanc, J. T. Stoering, C. J. Taylor, and M. A. Williamson, Phys. Rev. 123, 218 (1961).
90. G. J. Fischer, Phys. Rev. 108, 99 (1957).
91. R. Shev and Sophie Moore, BNL-607 (1960), p. 178.
92. J. D. Anderson, C. C. Gardner, J. W. McClure, M. P. Nahada, and C. Wong, Phys. Rev. 111, 572 (1958).
93. F. Ajzenberg-Selove and T. Lauritsen, Nuclear Phys. 23, 122 (1961).
94. D. B. Fosson, R. L. Walter, W. E. Wilson, and H. H. Barschall, Phys. Rev. 123, 209 (1961).
95. G. M. Frye and J. H. Gammel, Phys. Rev 103, 328 (1956).
96. M. E. Wyman, E. M. Fryer, and M. M. Thorpe, Phys. Rev. 112, 1264 (1958).

97. R. Shev and S. Moore, BNL-607T (1960).
98. H. Eischel and T. W. Bonner, Phys. Rev. 108, 1025 (1957).
99. R. R. Day and M. Walt, Phys. Rev. 117, 1330 (1960).
100. M. H. MacGregor, W. P. Ball, and R. Booth, Phys. Rev. 108, 226 (1957).
101. R. J. Howerton, UCRL-5226 (1958); UCRL-5351 (1958).
102. W. P. Ball, M. H. MacGregor, and R. Booth, Phys. Rev. 110, 1342 (1952).
103. M. H. MacGregor, W. P. Ball, and R. Booth, Phys. Rev. 111, 1155 (1958).
104. M. H. MacGregor and R. Booth, Phys. Rev. 112, 486 (1958).
105. W. E. Kreger and B. D. Kern, Phys. Rev. 113, 890 (1959).
106. E. R. Graves and R. W. Davis, Phys. Rev. 97, 1205 (1955).
107. J. B. Marion and R. M. Brugger, Phys. Rev. 100, 69 (1955).
108. V. J. Ashby, H. C. Catron, L. I. Newkirk, and C. J. Taylor, Phys. Rev. 111, 616 (1958).
109. E. G. Paul and R. L. Clarke, Can. J. Phys. 31, 267 (1953).
110. L. A. Rayburn, Phys. Rev. 122, 168 (1961).
111. J. M. Freeman, Phys. Rev. 99, 1446 (1955).
112. R. B. Day, Phys. Rev. 102, 767 (1956).
113. L. Cranberg and J. S. Levin, Phys. Rev. 103, 343 (1956).
114. T. W. Bonner and J. C. Slattery, Phys. Rev. 113, 1088 (1959).
115. M. K. Machwe, D. W. Kent, and S. C. Snowdon, Phys. Rev. 114, 1563 (1959).
116. V. I. Strizhak, JETP (USSR) 4, 769 (1957).
117. J. R. Beyster, M. Walt, and P. Salm, Phys. Rev. 104, 1370 (1956).
118. M. V. Pasechnik, I. Geneva 3, 2 (1955).
119. J. Diven and J. Terrell, WASH-1021 (1959), p. 22.
120. M. H. MacGregor, W. P. Ball, and R. Booth, Phys. Rev. 108, 126 (1957).
121. R. N. Glover and E. Weigold, Nucl. Phys. 29, 309 (1962).
122. I. L. Preiss and R. W. Fink, Nucl. Phys. 15, 326 (1960).
123. R. N. Glover and K. H. Purser, Nucl. Phys. 24, 431 (1961).
124. I. Numabe and R. W. Fink, Nucl. Phys. 15, 316 (1960).
125. P. V. March and W. T. Morton, Phil. Mag. 3, 577 (1958).
126. J. J. Van Loef (see ref. 127).
127. L. Gonzalez, J. Rapaport, and J. J. Van Loef, Phys. Rev. 120, 1319 (1960).
128. R. M. Keihn and C. Goodman, Phys. Rev. 95, 989 (1954).
129. V. E. Scherrer, B. A. Allison, and W. R. Faust, Phys. Rev. 96, 386 (1954).
130. M. Walt and H. H. Barschall, Phys. Rev. 93, 1062 (1954).
131. B. P. Bayhurst and R. J. Prestwood, LA-2493 (1961).
132. J. Beneveniste, II Geneva (1958) (P. 2494).
133. P. B. Tattersall, H. Rose, S. U. Pattenden, and D. Jowitt, J. Nucl. Energy 12, 32 (1960).
134. N. Nerenson and S. E. Darden, Phys. Rev. 94, 1678 (1954).
135. A. Bratenahl, J. M. Peterson, and J. P. Stoering, Phys. Rev. 110, 927 (1958).
136. G. J. McCallum, G. S. Mani, and A. T. G. Ferguson, Nucl. Phys. 16, 313 (1960).

137. J. L. Weil and K. W. Jones, Phys. Rev. 110, 446 (1958).

138. H. S. Hans and S. C. Snowden, Phys. Rev. 108. 1028 (1957).

139. P. P. Lebedev, Iu. A. Zisin, Iu. S. Klintsov, and B. D. Stsiborski, J. Nucl. Energy 11, 39 (1959).

140. J. Diven and J. Terrell, WASH-1021 (1959), p. 22.

141. D. G. Gardner, Nucl. Phys. 29, 373 (1962).

142. E. B. Paul and R. L. Clarke, Can. J. Phys. 31, 267 (1953).

143. J. J. Devaney, D. Cowart, and R. E. Anderson, LA-2372 (1959).

144. L. S. Goodman, Phys. Rev. 88, 686 (1952).

JOINT SERVICES DISTRIBUTION LIST

Department of Defense

Defense Documentation Center
Attn: TISIA
Cameron Station, Bldg. 5
Alexandria, Virginia 22314

Director, National Security Agency
Attn: C3/TDL
Fort George G. Meade, Maryland 20755

Mr. Charles Yost, Director
For Materials Sciences
Advanced Research Projects Agency, DOD
Washington, D.C. 20301

Director
Advanced Research Projects Agency
Department of Defense
Washington, D.C. 20301

Dr. James A. Ward
Office of Deputy Director (Research
and Information Rm. 3D1037) DOD
The Pentagon
Washington, D.C. 20301

Dr. Edward M. Reilley
Asst. Director (Research)
Ofc of Defense Res. & Eng., DOD
Washington, D.C. 20301

Department of the Army

Librarian PTA130
United States Military Academy
West Point, New York 10996

Director
U.S. Army Electronics Laboratories
Fort Monmouth, New Jersey 07703
Attn: AMSEL-RD-ADT

	NP	SE
DR	NR	SR
FU#1	PE	SS
GF	PF	X
NE	PR	XC
NO	SA	XE
		XS

Commanding General
U.S. Army Electronics Command
Attn: AMSEL-SC
Fort Monmouth, New Jersey 07703

C.O., Harry Diamond Laboratories
Attn: Mr. Berthold Altman
Connecticut Ave. & Van Ness St. N.W.
Washington, D.C. 20438

The Walter Reed Institute of Research
Walter Reed Army Medical Center
Washington, D.C. 20012

Director
U.S. Army Electronics Laboratories
Attn: Mr. Robert O. Parker, Executive
Secretary, JSTAC (AMSEL-RD-X)
Fort Monmouth, New Jersey 07703

Director
U.S. Army Electronics Laboratories
Attn: Dr. S. Benedict Levin, Director
Institute of Exploratory Research
Fort Monmouth, New Jersey 07703

Commanding Officer
U.S. Army Research Office (Durham)
Attn: CRD-AA-IP (Richard O. Ulsh)
P.O. Box CM, Duke Station
Durham, North Carolina 27706

Commanding Officer
U.S. Army Medical Research Laboratory
Fort Knox, Kentucky

Commanding Officer
U.S. Army Personnel Research Office
Washington, D.C.

Dr. H. Robl, Deputy Director
U.S. Army Research Office (Durham)
P.O. Box CM, Duke Station
Durham, North Carolina 27706

Commandant
U.S. Command and General Staff College
Attn: Secretary
Fort Leavenworth, Kansas 66207

Director
U.S. Army Eng. Geodesy, Intell. and
Mapping
Research & Development Agcy.
Fort Belvoir, Virginia 22060

Commanding Officer
Human Engineering Laboratories
Aberdeen Proving Ground, Maryland 21005

Commanding Officer
U.S. Limited War Laboratory
Attn: Technical Director
Aberdeen Proving Ground, Maryland 21005

Commanding Officer
U.S. Army Security Agency
Arlington Hall, Arlington, Virginia 22212

C.O., Harry Diamond Laboratories
Attn: Dr. R. T. Young, Elec. Tubes Div.
Connecticut Ave. & Van Ness St., N.W.
Washington, D.C. 20438

U.S. Army Munitions Command
Attn: Technical Information Branch
Picatinney Arsenal
Dover, New Jersey 07801

Commanding General
Frankford Arsenal
Attn: SMUFA-1310 (Dr. Sidney Ross)
Philadelphia, Pennsylvania 19137

Commanding General
U.S. Army Missile Command
Attn: Technical Library
Redstone Arsenal, Alabama 35809

Commandant
U.S. Army Air Defense School
Attn: Missile Sciences Division, C&S Dept.
P.O. Box 9390
Fort Bliss, Texas 79916

Commanding Officer
U.S. Army Ballistics Research Lab.
Attn: V.W. Richards
Aberdeen Proving Ground
Aberdeen, Maryland 21005

Commanding Officer
U.S. Army Materials Research Agency
Watertown Arsenal
Watertown, Massachusetts 02172

Commanding General
U.S. Army Strategic Communications
Command
Washington, D.C. 20315

Commanding General
U.S. Army Materiel Command
Attn: AMCRD-RS-PE-E
Washington, D.C. 20315

Commanding Officer
Foreign Service & Technology Center
Arlington Hall
Arlington, Virginia

Research Plans Office
U.S. Army Research Office
3045 Columbia Pike
Arlington, Virginia 22204

Chief of Research and Development
Headquarters, Department of the Army
Attn: Physical Sciences Division P&E
Washington, D.C. 20310

Director
Human Resources Research Office
The George Washington University
300 N. Washington Street
Alexandria, Virginia 22314

Commanding Officer
U.S. Army Electronics R&D Activity
White Sands Missile Range
New Mexico 88002

Commanding Officer
U.S. Army Engineers R&D Laboratory
Attn: STINFO Branch
Fort Belvoir, Virginia 22060

Commanding Officer
U.S. Army Electronics R&D Activity
Fort Huachuca, Arizona 85163

Mr. Alvin D. Bedrosian
Room 26-131
Massachusetts Institute of Technology
Cambridge, Massachusetts 02139

Department of the Air Force

Battelle Memorial Inst.
Technical Library
505 King Avenue
Columbus, Ohio 43201

Goddard Space Flight Center
NASA
Greenbelt, Maryland 20771

Research and Tech. Div. (AFAPL)
Attn: APIE-2, Mr. Robert F. Cooper
Wright-Patterson AFB, Ohio 45433

Technical Library
White Sands Missile Range
New Mexico 88002

AFSC (Tech Library)
Andrews AFB
Washington, D.C. 20031

AUL-3T-9663
Maxwell AFB
Alabama 36112

DDR&E (Tech Library)
Rm. 3C 128
The Pentagon
Washington, D.C. 20301

Systems Engineering Group
Deputy for Systems Eng'g., SEPRR
Directorate of Tech. Pubs. & Specs.
Wright-Patterson AFB, Ohio 45433

APGC (PGBAP-1)
Eglin AFB
Florida 32542

RTD (Tech Library)
Bolling AFB
District of Columbia 20332

BSD (Tech Library)
Norton AFB
California 92409

ASD (Tech Library)
Wright-Patterson AFB
Ohio 45433

Industrial College of the Armed Forces
Attn: Library
Washington, D. C.

Southwest Research Institute
Library
8500 Culebra Road
San Antonio, Texas

Stanford Research Institute
Library
820 Mission St.
South Pasadena, Calif. 91030

Library
National Science Foundation
Washington 25, D.C.

Linda Hall Library
5109 Cherry St.
Kansas City, Mo.

Dr. H. Harrison
NASA (Code RRE)
Fourth and Independence Sts.
Washington, D.C. 20546

Mr. James Tippett
National Security Agency
Fort Meade, Maryland

Brig. Gen. J. T. Stewart
Director of Science & Technology
Deputy Chief of Staff (R&D)
USAF
Washington 25, D.C.

Dr. R. L. Sproull, Director
Advanced Research Projects Agency
Washington 25, D.C.

Lt. Col. Edwin M. Myers
Headquarters USAF (AFRDR)
Washington 25, D.C.

Dr. John M. Ide
Div. Director for Eng'g.
National Science Foundation
Washington 25, D.C.

Dr. Zohrab Kaprielian
University of Southern California
University Park
Los Angeles 7, California

Dr. Lowell M. Hollingsworth
AFCRL
L. G. Hanscom Field
Bedford, Massachusetts

Professor Nicholas George
California Institute of Technology
EE Department
Pasadena, California

Hon. Alexander H. Flax
Asst. Secretary of the Air Force
Office of the Secretary of the Air Force
(R&D)
Washington 25, D.C.

Prof. Arwin Dougal
University of Texas
EE Department
Austin, Texas

Mr. Roland Chase
National Aeronautics & Space Admin.
1512 H Street, N.W.
Washington 25, D.C.

AFAL (AVTE)
Wright-Patterson AFB
Ohio 45433

Systems Engineering Group (RTD)
Attn: SEPIR
Wright-Patterson AFB
Ohio 45433

JOINT SERVICES DISTRIBUTION LIST (Continued)

Commander
Space Systems Division (AFSC)
Office of the Scientific Director
Inglewood, California

Dr. G. E. Knausenberger
c/o Hq Co. Munich Post
APO 09407, New York, N. Y.

AVCO Research Lab, Library
2385 Revere Beach Parkway
Everett, Mass. 02149

California Institute of Technology
Aeronautics Library
1201 East California St.
Pasadena 4, Calif. 91102

Carnegie Institute of Technology
Science & Engineering Hunt Library
Schenley Park
Pittsburgh, Pa. 15213

Rand Corporation
1700 Main St.
Santa Monica, Calif. 90401

Aerospace Corp. (Tech Library)
P. O. Box 95085
Los Angeles, Calif. 90045

Lewis Research Center (NASA)
Technical Library
21000 Brookpark Road
Cleveland, Ohio

George C. Marshall Space Flight Center
(NASA)
Redstone Arsenal, Ala. 35808

High Speed Flight Center (NASA)
Technical Library
Edwards AFB, Calif. 93523

Ames Rsch. Center (NASA)
Technical Library
Moffett Field, Calif. 94035

CIA OCR/LY/IAS
IH 129 HQ
Washington, D.C. 20505

RADC (Tech Library)
Griffiss AFB, N. Y. 13442

AEDC (Tech Library)
Arnold AFS
Tennessee 37389

APGC (Tech Library)
Eglin AFB
Florida 32542

AFWL (WLIL, Technical Library)
Kirtland Air Force Base
New Mexico 87117

AFMDC (Tech Library)
Holloman AFB
New Mexico 88330

AFFTC (Tech Library)
Edwards AFB
California 93523

Space Systems Division
Los Angeles Air Force Station
Air Force Unit Post Office
Los Angeles, California 90045
Attn: SSSD

Churchill Research Range
Library
Fort Churchill
Manitoba, Canada

National Defense Library
Headquarters
Ottawa, Ontario, Canada

Director
National Aeronautical Establishment
Ottawa, Ontario, Canada

EDS (ESTI)
Laurence G. Hanscom Field
Bedford, Massachusetts 01731

Johns Hopkins University
Applied Physics Lab., Library
White Oak, Silver Spring, Maryland 20919

Los Alamos Scientific Lab
Attn: Technical Library
Los Alamos, New Mexico 87544

ARL (AROL)
Wright-Patterson AFB
Ohio 45433

Frank J. Seiler Rsch. Lab.
Library
USAF Academy, Colo. 80840

U. S. Atomic Energy Commission
Library
Gaithersburg, Maryland 20760

AFAPL (APIE-2, Lt. Barthelmey)
Wright-Patterson AFB, Ohio.45433

Rome Air Dev. Center (RAWL, H. Webb)
Griffiss Air Force Base, New York 13442

S. H. Sternick
Aerospace Com - Attn: ESNC
Waltham Federal Center
424 Trapelo Road
Waltham, Massachusetts 02154

AFCRL (CRFE-Dr. Nicholas Yannoni)
L. G. Hanscom Field
Bedford, Massachusetts

Mr. Rocco H. Urbano, Chief
AFCRL, Appl Math. Branch
Data Sciences Laboratory
Laurence G. Hanscom Field
Bedford, Massachusetts

AFCRL
Office of Aerospace Res., USAF
Bedford, Mass.
Attn: CRDA

Dr. Louis C. Block
AFCRL (CROO)
Laurence G. Hanscom Field
Bedford, Massachusetts 01731

Commander, AFCRL
Attn: C. P. Smith (CRBS)
L. G. Hanscom Field
Bedford, Massachusetts

AFETR (Tech Library MU-135)
Patrick AFB, Florida 32925

Mr. C. N. Hasert
Scientific Advisory Board
Hq. USAF
Washington 25, D.C.

Dr. Harvey E. Savely, SRL
Air Force Office of Sci. Res.
Office Aerospace Research, USAF
Washington 25, D.C.

Department of the Air Force
Headquarters, United States Air Force
Washington 25, D.C.
Attn: AFTAC/TD-1

John Crerar Library
35 West 33rd St.
Chicago, Ill.

LOOAR (Library)
AF Unit Post Office
Los Angeles, Calif. 90045

Office of Research Analyses
Library
Holloman AFB, New Mexico 88330

Office of Research Analyses
Attn: Col. K. W. Gallup
Holloman AFB, New Mexico 88330

ARL (ARD/Col. R. E. Fontana)
Wright-Patterson AFB
Ohio 45433

Brig. Gen. B. G. Holzman, USAF (Ret.)
National Aeronautics and Space Admin.
Code RS
Washington, D.C. 20546

AFRST (SC/EN)
Lt. Col. L. Stone
Room 4C 341
The Pentagon
Washington, D.C. 20301

Commander
Rome Air Development Center
AFSC
Office of the Scientific Director
Griffiss AFB, Rome, New York

Commander
Research & Technology Division (AFSC)
Office of the Scientific Director
Bolling AFB 25, D.C.

Commander
Air Force Systems Command
Office of the Chief Scientist
Andrews AFB, Maryland

Commander
Air Force Cambridge Research Lab.
Office of the Scientific Director
L. G. Hanscom Field
Bedford, Massachusetts

Commander
Aerospace Research Laboratories (OAR)
Office of the Scientific Director
Wright-Patterson AFB, Ohio

Commander, Aerospace Systems Division
AFSC
Office of the Scientific Director
Wright-Patterson AFB, Ohio

AFAL
AVR(L)
Wright-Patterson AFB
Ohio 45433

Air Force Cambridge Res. Lab.
L. G. Hanscom Field
Bedford, Massachusetts 01731
Attn: CRDM, Mr. Herskovitz

Commander
Air Force Office of Scientific Research
Washington 25, D.C.
Attn: SREE

Director
Air University Library
Maxwell A.F. Base, Alabama

NASA/AFSS/1 FOB6
Tech Library, Rm. 60084
Washington, D.C. 20546

USAFA (DLIB)
U.S. Air Force Academy
Colorado

ARPA
Tech Info Office
The Pentagon
Washington, D.C. 20301

AFCRL(CRXL)
L.G. Hanscom Field
Bedford, Mass. 01731

U.S. Regional Sci. Office (LAOAR)
U.S. Embassy
APO 676, New York, N.Y.

AEC
Div. of Tech Info. Ext.
P.O. Box 62
Oak Ridge, Tennessee

Dr. Hermann H. Kurzweg
Director of Research - OART
NASA
Washington, D.C. 20546

AFIT (MCLI)
Tech Library
Wright-Patterson AFB, Ohio 45433

Prof. W. H. Radford
Lincoln Laboratory, A-183
244 Wood Street
Lexington, Massachusetts

Department of the Navy

Chief of Naval Operations
Pentagon OP 07T
Washington, D.C.

Commanding Officer
Office of Naval Research Branch Office
Navy 100, Fleet P.O. Box 39
New York, New York

Library
U.S. Navy Electronics Lab.
San Diego, California 92152

Commander
U.S. Naval Air Development Center
Johnsville, Pennsylvania
Attn: NADC Library

Commanding Officer
Office of Naval Research Branch Office
495 Summer Street
Boston, Massachusetts 02110

Commanding Officer
U.S. Navy Underwater Sound Laboratory
Ft. Trumbull, New London, Connecticut

U.S. Navy Post Graduate School
Monterey, California
Attn: Electrical Engineering Department

Commander, Naval Ordnance Laboratory
White Oak, Maryland
Attn: Technical Library

Chief, Bureau of Ships, Attn: Code 680
Department of the Navy
Washington, D.C. 20360

Chief, Bureau of Weapons
Department of the Navy
Washington, D.C. 20360

Dr. Arnold Shostak, Code 427
Head, Electronics Branch
Physical Sciences Division
Office of Naval Research
Washington, D.C. 20360

Chief of Naval Research, Code 427
Department of the Navy
Washington, D.C. 20360

Director
Naval Research Laboratory
Washington, D.C. 20390